Design, Construction and Characterization of Holographic Optical Elements for Building-Integrated Concentrating Photovoltaics

Julia Marín Sáez

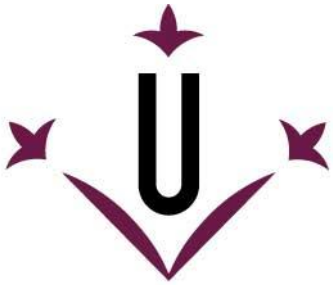

Universitat de Lleida

TESI DOCTORAL

Design, Construction and Characterization of Holographic Optical Elements for Building-Integrated Concentrating Photovoltaics

Julia Marín Sáez

Memòria presentada per optar al grau de Doctor per la Universitat de Lleida
Programa de Doctorat en Enginyeria i Tecnologies de la Informació

Director/a
Daniel Chemisana Villegas
Jesús Atencia Carrizo

Tutor/a
Daniel Chemisana Villegas

2019

Agradecimientos

Quiero agradecer a mis directores de tesis, Dani y Jesús, y a mi directora de tesis no oficial, Viqui, el haberme dado esta oportunidad y haberme enseñado tanto durante estos años.

Gracias a mi familia, en especial a mis padres y Ceci, por celebrar mis logros y por estar ahí cuando todo se hacía cuesta arriba.

Gracias a Pilar, Andrea, Elena, Izaskun, David, Ángel y Marta por su valiosa amistad.

Gracias a mis compañer@s de Zarpa por enseñarme que puedo marcar la diferencia.

Gracias a mis compañer@s de la UdL y Unizar por las charlas, comidas y cafés compartidos.

I would also like to thank Suzanne, Sanjay, and all my colleagues at DIT for welcoming me during my stay there and making me feel part of the group, letting me use all the facilities for my project.

Contents

Summary 1

Resumen 3

Resum 5

Chapter 1 Introduction 7

1.1 Objectives of this thesis 9

1.2 Methodology 10

Chapter 2 Fundamentals and state of the art of Holographic Optical Elements for Concentrating Photovoltaics 15

2.1. Introduction to Holographic Optical Elements for solar applications 15

2.2. Holographic recording 17

2.2.1. Wavefront recording and reconstruction in holography 17

2.2.2. Hologram types 18

2.2.3. Recording materials 19

2.3. State of the art 19

2.3.1. Literature review 20

2.3.1.1. Systems with one receptor 20

2.3.1.2. Systems with more than one receptor 21

2.3.1.2.1. Systems with transmission HOEs 21

2.3.1.2.2. Systems with reflection HOEs 24

2.3.2. Discussion of the theoretical treatment in the literature 26

Chapter 3 Theoretical modeling of Holographic Optical Elements for Concentrating Photovoltaics 31

Publication: P. Bañares-Palacios, S. Álvarez-Álvarez, J. Marín-Sáez, M.-V. Collados, D. Chemisana, and J. Atencia, "Broadband behavior of transmission volume holographic optical elements for solar concentration," Opt. Express 23, A671–A681 (2015) 33

Chapter 4 Simulations of a conceptual holographic Concentrating Photovoltaic-Thermal prototype to assess its adequacy 45

Publication: J. Marín-Sáez, D. Chemisana, Á. Moreno, A. Riverola, J. Atencia, and M.-V. Collados, "Energy Simulation of a Holographic PVT Concentrating System for Building Integration Applications," Energies 9, 577 (2016) 47

Chapter 5 Characterization of the photosensitive material for holographic recording 67

Publication: J. Marín-Sáez, J. Atencia, D. Chemisana, and M.-V. Collados, "Characterization of volume holographic optical elements recorded in Bayfol HX photopolymer for solar photovoltaic applications," Opt. Express 24, A720 (2016) 69

Chapter 6 Optimization of the design of Holographic Optical Elements for Concentrating Photovoltaics. Study of the transition regime 81

6.1. Theoretical background of the transition regime 82

Publication: J. Marín-Sáez, M. V. Collados, D. Chemisana, and J. Atencia, "Energy analysis of holographic lenses for solar concentration," in Proceedings of SPIE 10233, p. 1023317 (2017) 89

Publication: J. Marín-Sáez, J. Atencia, D. Chemisana, and M.-V. Collados, "Full modeling and experimental validation of cylindrical holographic lenses recorded in Bayfol HX photopolymer and partly operating in the transition regime for solar concentration," Opt. Express 26, A398 (2018) 101

Chapter 7 Evaluation of the performance of the Holographic Concentrating Photovoltaic system under real conditions 117

Publication: J. Marín-Sáez, D. Chemisana, J. Atencia, and M.-V. Collados, "Outdoor performance evaluation of a holographic solar concentrator optimized for building integration," (manuscript submitted to the journal Applied Energy in 2019) 119

Chapter 8 Global discussion of the results 139

8.1. Future work 144

Chapter 9 Conclusions 147

Summary

Building-integrated Photovoltaic (PV) systems enable the in-situ production of renewable energy. Concentrating Photovoltaic systems require a smaller PV cell surface, which can help reduce the economic and environmental cost of the system. Usually refractive or reflective optical elements are used for this purpose, but they present two main disadvantages: i) since they concentrate the whole solar spectrum, including spectral ranges that the PV cell is not sensitive to, they cause an increase of the temperature of the cell, that may worsen its performance; ii) they are not easily integrated in buildings.

Holographic Optical Elements (HOEs) are alternative concentrating elements. Their chromatic selectivity, the ability to efficiently diffract only a certain wavelength range, can be tuned with the solar spectrum and the spectral response curve of the PV cell to avoid undesired wavelengths. They are light-weight and versatile elements that can be more easily integrated in a building serving more than one purpose, for example as spectrum-splitters to redirect light towards two or more types of receivers (thanks to their selectivity and the dispersion that they introduce), or as illumination control elements of the interior of the building by letting only the diffuse radiation in.

The angular selectivity that HOEs also present has to be considered as well, because without tracking the sun's movement in two axes, the system would only be efficient for a short time of the day. When considering a holographic cylindrical lens tracking can be suppressed in the direction of low angular selectivity of the hologram. Furthermore, said lens can be integrated in the blinds of an automated shading louvre system of a building, in such a way that tracking is carried out in the direction of high angular selectivity.

The main objective of this thesis is the design, construction and characterization of a solar concentrating system formed by two cylindrical holographic lenses and a mono-crystalline Silicon PV cell with the aim of building façade integration. Theoretical and experimental work is carried out simultaneously during the course of the thesis.

A ray-tracing algorithm based on Coupled Wave Theory has been developed to locally and globally analyze holographic gratings, lenses and systems. Each ray is propagated through the system and its energetic contribution is taken into account on the receiver's plane. Simulations and experimental results have been compared and found in agreement; thus validating the ray-tracing algorithm, and proving its reliability as a design and modeling tool.

The suitability of the recording material, Bayfol HX photopolymer, has been tested by a laboratory characterization and by exposure to outdoor conditions. The holographic concentrating system has been recorded and assembled and also assessed both in the laboratory and outdoors with solar illumination.

The transition regime between the Bragg regime and Raman-Nath regime has also been studied, showing the promising advantages it offers for broadband spectrum illumination applications.

Resumen

Los sistemas fotovoltaicos (PV) para integración arquitectónica posibilitan la producción in-situ de energía renovable. Si se usan sistemas concentradores se requiere una superficie de célula fotovoltaica menor, que puede ayudar a reducir el coste económico y medioambiental del sistema. Normalmente para ello se emplean elementos ópticos refractivos o espejos, pero presentan dos principales inconvenientes: i) como concentran el espectro solar completo, incluyendo rangos espectrales a los que la célula PV no es sensible, causan un aumento de la temperatura de la célula que puede empeorar su rendimiento; ii) no se integran fácilmente en edificios.

Los elementos ópticos holográficos (HOEs) son elementos concentradores alternativos. Su selectividad cromática, la capacidad de difractar eficientemente sólo un determinado rango espectral, puede acoplarse con el espectro solar y la curva de respuesta espectral de la célula para evitar longitudes de onda no deseadas. Son elementos ligeros y versátiles que pueden integrarse de manera más sencilla en un edificio sirviendo más de un propósito, por ejemplo como divisores espectrales para redirigir luz hacia dos o más tipos de receptores (gracias a la selectividad y dispersión introducida), o como elementos de control de la iluminación dejando pasar al interior únicamente la radiación difusa.

También ha de considerarse la selectividad angular que presentan los HOEs, ya que sin seguimiento del movimiento del sol en dos ejes, el sistema sería eficiente durante un breve periodo al día únicamente. En el caso de una lente cilíndrica holográfica puede evitarse el seguimiento en la dirección de baja selectividad angular del holograma. Además, dicha lente puede integrarse en las lamas venecianas de un sistema automatizado de sombreo de un edificio, de manera que se realice seguimiento en la dirección de alta selectividad angular.

El principal objetivo de esta tesis es el diseño, construcción y caracterización de un sistema concentrador solar formado por dos lentes cilíndricas holográficas y una célula fotovoltaica de Silicio mono-cristalino para integración arquitectónica en fachadas. Durante el desarrollo de la tesis se ha realizado simultáneamente tanto trabajo teórico como experimental.

Se ha desarrollado un algoritmo de trazado de rayos basado en la Teoría de Ondas Acopladas para analizar local y globalmente redes, lentes y sistemas holográficos. Cada rayo se propaga a través del sistema y su contribución energética se tiene en cuenta en el plano del receptor. Se han comparado resultados experimentales y de simulaciones, encontrándose en concordancia, validando así el algoritmo de trazado de rayos y demostrando su fiabilidad como herramienta de diseño y modelización.

La idoneidad del material de registro, el fotopolímero Bayfol HX, se ha probado mediante caracterización en el laboratorio y exposición a condiciones exteriores. El sistema concentrador holográfico ha sido registrado, ensamblado y evaluado tanto en el laboratorio como al aire libre con iluminación solar.

También se ha estudiado el régimen de transición entre el régimen de Bragg y el de Raman-Nath, mostrando las ventajas prometedoras que ofrece para aplicaciones con iluminación con espectro ancho.

Resum

Els sistemes fotovoltaics (PV) per integració arquitectònica possibiliten la producció in-situ d'energia renovable. Si es fan servir sistemes concentradors es requereix una superfície de cèl·lula fotovoltaica menor, que pot ajudar a reduir el cost econòmic i mediambiental del sistema. Normalment per a això s'utilitzen elements òptics refractius o miralls, però presenten dos principals inconvenients: i) com concentren l'espectre solar complet, incloent rangs espectrals als quals la cèl·lula PV no és sensible, causen un augment de la temperatura de la cèl·lula que pot empitjorar el seu rendiment; ii) no s'integren fàcilment en edificis.

Els elements òptics hologràfics (HOEs) són elements concentradors alternatius. La seva selectivitat cromàtica, la capacitat de difractar eficientment només un determinat rang espectral, pot acoblar-se amb l'espectre solar i la corba de resposta espectral de la cèl·lula per evitar les longituds d'ona no desitjades. Són elements lleugers i versàtils que poden integrar-se de manera més senzilla en un edifici servint més d'un propòsit, per exemple com divisors espectrals per redirigir llum cap a dos o més tipus de receptors (gràcies a la selectivitat i dispersió introduïda), o com a elements de control de la il·luminació.

També ha de considerar-se la selectivitat angular que presenten els HOEs, ja que sense seguiment del moviment del sol en dos eixos, el sistema seria eficient durant un breu període al dia. En el cas dels elements cilíndrics pot evitar-se el seguiment en la direcció de baixa selectivitat angular de l'holograma (direcció de l'eix del cilindre). A més, si l'holograma es troba integrat en lames venecianes automatitzades el seguiment solar a la direcció d'alta selectivitat es satisfà, mentre que sobre l'altra direcció (baixa selectivitat a elements cilíndrics) el seguiment no ca.

El principal objectiu d'aquesta tesi és el disseny, construcció i caracterització d'un sistema concentrador solar format per dues lents cilíndriques hologràfiques i una cèl·lula fotovoltaica de silici mono-cristal·lí per integració arquitectònica en façanes. Durant el desenvolupament de la tesi s'ha realitzat simultàniament tant treball teòric com experimental.

S'ha desenvolupat un algoritme de traçat de raigs basat en la Teoria d'Ones Acoblades per analitzar local i globalment xarxes, lents i sistemes hologràfics. Cada raig es propaga a través del sistema i la seva contribució energètica es té en compte en el pla del receptor. S'han comparat resultats experimentals i de simulacions, trobant-se en concordança, validant així l'algoritme de traçat de raigs i demostrant la seva fiabilitat com a eina de disseny i modelització.

La idoneïtat del material de registre, el fotopolímer Bayfol HX, s'ha provat mitjançant caracterització al laboratori i exposició a condicions exteriors. El sistema concentrador hologràfic ha estat registrat, acoblat i avaluat tant al laboratori com a l'aire lliure amb il·luminació solar.

També s'ha estudiat el règim de transició entre el règim de Bragg i el de Raman-Nath, mostrant els avantatges prometedores que ofereix per a aplicacions amb il·luminació amb espectre ample.

Chapter 1

Introduction

The European Commission states that approximately 40% of the energy consumed in the EU and 36% of CO_2 produced is caused by buildings, and the reduction of these figures is one of the set goals [1]. It also states that by 2020 all new buildings should be nearly-zero energy buildings. A decrease of the energy used in buildings can be carried out by the integration of renewable energy generation systems, so that they contribute on-site to the electricity, cooling and heating demands.

One way of doing this is the placement of solar energy by placing photovoltaics (PVs) on the exterior of a building, in order to use the incident solar irradiance to produce an electric current which can be used inside the building. However, the manufacturing of said PVs is costly and not environmentally friendly [2,3], so quite often optical concentrating systems are used [4,5]. They redirect sun rays towards a smaller sized PV generator, in such a way that it generates the same electrical power as a larger PV device, ideally with the same surface as the optical concentrating system aperture area.

Refractive and reflective optical elements, such as lenses or mirrors, are usually placed as solar concentrators, and they can yield very high optical concentrations. However, when integrating concentrating photovoltaics (CPV) systems in buildings, especially on the façades, the concentrating factors that can be achieved are usually lower [6]. Different configurations of building-integrated (BI) CPV systems can be found in the literature, where CPV systems are placed on the rooftop of the building [7,8] or on the façade, especially on windows [9–13], where they also play the role of illumination control of the interior of the building.

Nevertheless, two main issues arise when using refractive and reflective elements for BICPV:

i. Low concentration systems are normally coupled to a single junction PV technology (most of them to Silicon). However, refractive and reflective optical elements focus the whole solar spectrum (although aberrations are present) on the PV cell surface and it is sensitive to only a spectral range, given by the band gap of the semiconductor it is composed by. This means that the PV cell receives rays that it will not transform into electricity, and that will cause an increase of the temperature of the cell [14]. Cooling systems are needed in order to control the temperature of the cell and avoid overheating [15], and they increase the size of the overall system, making it harder to be integrated in a building.
ii. If refractive optical elements are placed on windows the view through the window is largely affected, with no clear image available for the observer inside the building. On the other hand, standard reflective elements are opaque.

The use of Holographic Optical Elements (HOEs) as solar concentrators was a new technological system first proposed for this application by Ludman [16] and Bloss et al. [17] in 1982, which can overcome these two issues.

Holography is a two-step process in which periodic variations of a physical property (such as refractive index, thickness or absorption) are induced in a photosensitive material. This is achieved at the recording step by the interference of two coherent light waves within its volume, so that the periodic modulation of the intensity of the light turns into a periodic modulation of a certain physical property. These changes are then fixed in one way or another, depending on the type of material, to form the hologram. Holograms are diffractive optical elements, so when they are illuminated at the reconstruction or replay step the incident rays suffer diffraction, that is, they are deviated due to the encounter with an obstacle: the periodic variation of a physical property of the material. Several orders of diffraction, i.e., rays with different directions of propagation, emerge from this encounter, and the energy of the incident ray is distributed among them. The number of diffraction orders, the propagation direction of each one and the distribution of energy among them depend on the characteristics of the hologram and of the incident ray.

Volume holograms are a type of holograms in which only two diffraction orders appear: the 0^{th} or transmitted order and the 1^{st} or diffracted order. They are very commonly used because under certain conditions they provide 100% efficiency, that is, all the incident energy is transferred to the 1^{st} order of diffraction. When using volume HOEs for solar concentrating photovoltaics the system is very often designed so that only the diffracted order reaches the PV cell.

One of the reasons why holograms are a viable choice of optical elements for solar concentration is that they present chromatic selectivity, meaning that the efficiency depends on the incident wavelength. Therefore, if the HOE is well designed, it will be efficient for the spectral range that the PV cell is sensitive to, and not for the rest. Since HOEs are diffractive elements they also introduce chromatic dispersion, so rays with different wavelengths are diffracted with different directions. The system's layout can leverage these two effects so that the PV cell only receives the part of the spectrum that it can use. That way, overheating of the PV cell is avoided, with no cooling systems needed, solving the first of the issues listed above.

Another characteristic of holograms is the angular selectivity, i.e. the dependence of the efficiency with the angle of incidence of the incoming rays. If HOEs are placed on a window, the angular selectivity ensures that with a proper design, direct sun rays will be directed towards the PV cell and the diffuse light reaching the HOE with other incidence angles will be simply transmitted, since the HOE will not be efficient for them. This ensures clear vision through the window in different directions, the second issue stated above.

On the other hand, this characteristic of HOEs poses an important drawback for holographic solar concentrators because the Sun describes an apparent trajectory on the sky, which is different every day of the year and for each location. Therefore, the performance of the HOE will be different throughout the day and the year, and the optimal illumination conditions will only be met momentarily. A solution that is also applied to refractive optical systems, whose performance is affected by the angle of incidence as well, is the use of tracking devices to keep the incidence angle constant. However, it is not simple to integrate a tracking concentrating system in a building, especially if tracking is carried out in two axes to completely maintain the direction of incidence in the optical system.

Different types of HOEs have been proposed for solar concentrating photovoltaics: holographic gratings, cylindrical lenses and spherical lenses [18]. A literature review covering them can be found in chapter 3 of this dissertation. Tracking in one direction can be suppressed when using

holographic cylindrical lenses that concentrate sunlight onto a rectangular PV cell, at the cost of concentrating in one direction only. Holograms present higher angular selectivity when varying the incidence in one direction (which is the one that is being tracked in these type of system) and lower selectivity in the perpendicular direction. If the former direction matches the solar altitude movement and the latter direction matches the azimuth, a system that tracks the solar altitude movement is needed. This can be easily integrated in a building façade by taking advantage of shading systems placed on windows [19].

Although volume HOEs, or HOEs operating in the volume regime, are the most commonly used, the selectivity and dispersion that they present is rather high. This implies that the spectrum received by the PV cell is narrower than the optimal one and that when deviating from the optimal incidence conditions the system's overall efficiency will decrease quite rapidly. However, it has been found during the development of this thesis that HOEs operating in the transition regime are very advantageous for broadband spectrum applications, since they have lower selectivity and dispersion. This is at the expense of reaching lower efficiencies, so a compromise between these effects should be explored.

Several theories describe the behavior of holograms, but the most extended one is Coupled Wave Theory [20], which is applied in this thesis. A theoretical treatment of the diffraction of light by high-frequency sound waves was developed by Raman and Nath in 1935 and 1936 [21–25]. They demonstrated that the efficiency of the diffracted beams was given by a set of coupled differential equations, which, under certain conditions, had an analytical solution as Bessel functions. Kogelnik derived in 1969 a set of coupled differential equations from Maxwell's equations that had an analytical solution for other conditions, namely, when the hologram operates in the volume regime, when only the transmitted order and one diffracted order are found [26].

There are several types of recording materials for the construction of holograms. The one used in this thesis is Bayfol HX, a photopolymeric material manufactured by Covestro AG, formerly Bayer MaterialScience. As opposed to other types of materials widely used (e.g. dichromated gelatin), it needs no chemical or thermal post-processing, only photocuring. It also offers good light sensitivity and low shrinkage; therefore, imperceptible detuning [27].

1.1. Objectives of this thesis

The main objective of this thesis is the design, construction and characterization of a solar concentrating system formed by two cylindrical holographic lenses and a mono-crystalline Silicon PV cell for the scope of façade building integration.

The specific objectives are listed below:

- *Experimental characterization of the recording material, Bayfol HX photopolymer.* Three types of Bayfol HX photopolymer (Bayfol HX 104, Bayfol HX TP, Bayfol HX 200) will be used for the different steps of the thesis, depending on the availability of the material. An experimental characterization of the recording process and the material's response has to be carried out for a range of spatial frequencies, exposure intensities and exposure dosages.

- *Ray-tracing modeling of HOEs and holographic concentrating systems.* A ray-tracing algorithm that considers HOEs performing in the volume regime or in the general case (volume, transition, thin regimes) will be developed for this scope and implemented in Matlab. The energy associated with each ray will be calculated with Coupled Wave Theory, either by using Kogelnik's solution for volume HOEs or by numerically solving the coupled differential equations for the general case. Simulations of holographic concentrating systems will be carried out in order to determine the spectral irradiance received by the PV cell and the generated current under different illumination conditions. All these simulations must be validated with experimental results.
- *Analysis of the transition regime and its convenience for solar concentration.* The performance of HOEs in the transition regime will be considered, a novel approach for broadband reconstruction applications of holography.
- *Design of the holographic concentrating system.* A system formed by two identical cylindrical holographic lenses symmetrically placed and a mono-crystalline Si PV cell, with a total geometrical concentration of 11x will be proposed. The design of the HOEs will be optimized by the analysis of several effects with the help of the ray-tracing modeling, so that the generated current is maximal.
- *Construction of the holographic concentrating system.* The HOEs that constitute the concentrating system will be experimentally recorded and characterized and the whole system will be assembled.
- *Experimental analysis of the holographic concentrating system.* Measurements will be carried out with solar illumination on the HOEs, detecting the diffracted spectrum, and analyzing the output current of the PV cell.
- *Evaluation of the material's response under real conditions.* An analysis of the performance of HOEs recorded on Bayfol HX photopolymer will be conducted when varying the room temperature, since this application implies non controlled ambient conditions. Furthermore, an ageing study will be carried out, in which HOEs are exposed during the course of several weeks to high summer temperatures, varying humidity levels and solar irradiance.

1.2. Methodology

This dissertation is structured as follows:

- Chapter 2 covers the fundamentals of HOEs for concentrating photovoltaics. The most relevant characteristics of HOEs for this application are exposed and a brief explanation of the recording and reconstruction process of HOEs, different classifications of HOEs and recording material types are included. The state of the art is also presented, along with a discussion on the theoretical treatment of HOEs in the systems found in the literature, which shows the need of a more thorough study of HOEs for solar concentration.
- Chapter 3 presents the developed ray-tracing algorithm for volume holograms. The response of volume HOEs is addressed locally at each point in order to obtain its global performance and the energy distribution on the solar receiver. Some examples of the theoretical and the experimental performance are provided. The developed modeling tool, which is locally validated, allows the calculation of the optical concentration on the PV cell. A first analysis of two holographic concentrating system configurations

comprising a volume cylindrical holographic lens and a Silicon PV cell is included. This chapter comprises the following publication:

  - P. Bañares-Palacios, S. Álvarez-Álvarez, J. Marín-Sáez, M.-V. Collados, D. Chemisana, and J. Atencia, "Broadband behavior of transmission volume holographic optical elements for solar concentration," Opt. Express **23**, A671–A681 (2015).

- Chapter 4 exposes a theoretical study of a building-integrated volume holographic hybrid concentrating PVT system on the façade of a building. Simulations were carried out for the illumination and ambient temperature conditions of two locations throughout the year, taking into account the different energy demands. The validity of HOEs for BICPVT systems was demonstrated. It comprises the next publication:
  - J. Marín-Sáez, D. Chemisana, Á. Moreno, A. Riverola, J. Atencia, and M.-V. Collados, "Energy Simulation of a Holographic PVT Concentrating System for Building Integration Applications," Energies **9**, 577 (2016).
- Chapter 5 addresses an experimental characterization of the recording material, Bayfol HX, and its suitability for concentrating photovoltaics. There were no studies assessing its appropriateness for this application before the article included in this chapter:
  - J. Marín-Sáez, J. Atencia, D. Chemisana, and M.-V. Collados, "Characterization of volume holographic optical elements recorded in Bayfol HX photopolymer for solar photovoltaic applications," Opt. Express **24**, A720 (2016).
- Chapter 6 covers several studies of the design of cylindrical holographic lenses for the system proposed in chapter 4, with the aim of maximizing the generated electrical current. The possibility of using HOEs partly operating in the transition regime (therefore, not fulfilling the volume condition) in order to broaden the diffracted spectrum, thus enhancing the concentration of the system, was explored. This was a novel approach for broadband reconstruction applications. Two publications can be found in this chapter:
  - J. Marín-Sáez, M. V. Collados, D. Chemisana, and J. Atencia, "Energy analysis of holographic lenses for solar concentration," in *Proceedings of SPIE* **10233**, p. 1023317 (2017).
  - J. Marín-Sáez, J. Atencia, D. Chemisana, and M.-V. Collados, "Full modeling and experimental validation of cylindrical holographic lenses recorded in Bayfol HX photopolymer and partly operating in the transition regime for solar concentration," Opt. Express **26**, A398 (2018).
- Chapter 7 deals with the experimental performance of the designed holographic CPV system under real conditions and the verification of the global simulation method. The aging of the material is also studied. The following publication is included:
  - J. Marín-Sáez, D. Chemisana, J. Atencia, and M.-V. Collados, "Outdoor performance evaluation of a holographic solar concentrator optimized for building integration," (manuscript submitted to the journal Applied Energy in 2019).
- Chapter 8 is a global discussion of the results.
- Chapter 9 comprises the conclusions.

References

1. *Directive (EU) 2018/844 of the European Parliament and of the Council of 30 May 2018 Amending Directive 2010/31/EU on the Energy Performance of Buildings and Directive 2012/27/EU on Energy Efficiency* (European Parliament, Council of the European Union, 2018).

2. C. EPRI, Palo Alto, CA, and California Energy Commission, Sacramento, *Potential Health and Environmental Impacts Associated with the Manufacture and Use of Photovoltaic Cells* (2003).

3. V. M. Fthenakis and P. D. Moskowitz, "Photovoltaics: environmental, health and safety issues and perspectives," Prog. Photovoltaics Res. Appl. **8**, 27–38 (2000).

4. K. Menoufi, D. Chemisana, and J. I. Rosell, "Life Cycle Assessment of a Building Integrated Concentrated Photovoltaic scheme," Appl. Energy **111**, 505–514 (2013).

5. C. Lamnatou and D. Chemisana, "Photovoltaic/thermal (PVT) systems: A review with emphasis on environmental issues," Renew. Energy **105**, 270–287 (2017).

6. D. Chemisana, "Building integrated concentrating photovoltaics: A review," Renew. Sustain. Energy Rev. **15**, 603–611 (2011).

7. N. Vu and S. Shin, "Flat Concentrator Photovoltaic System with Lateral Displacement Tracking for Residential Rooftops," Energies **11**, 114 (2018).

8. H. Singh, M. Sabry, and D. A. G. Redpath, "Experimental investigations into low concentrating line axis solar concentrators for CPV applications," Sol. Energy **136**, 421–427 (2016).

9. K. Connelly, Y. Wu, X. Ma, and Y. Lei, "Transmittance and Reflectance Studies of Thermotropic Material for a Novel Building Integrated Concentrating Photovoltaic (BICPV) 'Smart Window' System," Energies **10**, 1889 (2017).

10. L. A. A. Bunthof, F. P. M. Kreuwel, A. Kaldenhoven, S. Kin, W. H. M. Corbeek, G. J. Bauhuis, E. Vlieg, and J. J. Schermer, "Impact of shading on a flat CPV system for façade integration," Sol. Energy **140**, 162–170 (2016).

11. Y. Wu, K. Connelly, Y. Liu, X. Gu, Y. Gao, and G. Z. Chen, "Smart solar concentrators for building integrated photovoltaic façades," Sol. Energy **133**, 111–118 (2016).

12. H. Baig, E. F. Fernández, and T. K. Mallick, "Influence of spectrum and latitude on the annual optical performance of a dielectric based BICPV system," Sol. Energy **124**, 268–277 (2016).

13. X. Liu, Y. Wu, X. Hou, and H. Liu, "Investigation of the Optical Performance of a Novel Planar Static PV Concentrator with Lambertian Rear Reflectors," Buildings **7**, 88 (2017).

14. E. Radziemska, "Thermal performance of Si and GaAs based solar cells and modules: a review," Prog. Energy Combust. Sci. **29**, 407–424 (2003).

15. X. Han, Y. Wang, and L. Zhu, "Electrical and thermal performance of silicon concentrator solar cells immersed in dielectric liquids," Appl. Energy **88**, 4481–4489 (2011).

16. J. E. Ludman, "Holographic solar concentrator," Appl. Opt. **21**, 3057–3058 (1982).

17. W. H. Bloss, M. Griesinger, and E. R. Reinhardt, "Dispersive concentrating systems

based on transmission phase holograms for solar applications," Appl. Opt. **21**, 3739 (1982).

18. M. V. Collados, D. Chemisana, and J. Atencia, "Holographic solar energy systems: The role of optical elements," Renew. Sustain. Energy Rev. **59**, 130–140 (2016).

19. D. Chemisana, M. V. Collados, M. Quintanilla, and J. Atencia, "Holographic lenses for building integrated concentrating photovoltaics," Appl. Energy **110**, 227–235 (2013).

20. R. R. A. Syms, "Vector Effects in Holographic Optical Elements," Opt. Acta Int. J. Opt. **32**, 1413–1425 (1985).

21. C. V. Raman and N. S. Nagendra Nathe, "The diffraction of light by high frequency sound waves: Part I.," Proc. Indian Acad. Sci. - Sect. A (1935).

22. C. V. Raman and N. S. Nagendra Nath, "The diffraction of light by sound waves of high frequency: Part II," Proc. Indian Acad. Sci. - Sect. A (1935).

23. C. V. Raman and N. S. Nagendra Nath, "The diffraction of light by high frequency sound waves: Part III - Doppler effect and coherence phenomena," Proc. Indian Acad. Sci. - Sect. A (1936).

24. C. V. Raman and N. S. Nagendra Nath, "The diffraction of light by high frequency sound waves: Part IV - Generalised theory," Proc. Indian Acad. Sci. - Sect. A (1936).

25. C. V. Raman and N. S. N. Nath, "The diffraction of light by high frequency sound waves. Part V. General considerations oblique incidence and amplitude changes," Proc. Indian Acad. Sci. - Sect. A (1936).

26. H. Kogelnik, "Coupled wave theory for thick hologram gratings," Bell Syst. Tech. J. **48**, 2909–2947 (1969).

27. H. Berneth, F.-K. Bruder, T. Fäcke, D. Jurbergs, R. Hagen, D. Hönel, T. Rölle, and G. Walze, "Bayfol HX photopolymer for full-color transmission volume Bragg gratings," SPIE Photonics West 2014-OPTO Optoelectron. Devices Mater. **9006**, 900602 (2014).

Chapter 2

Fundamentals and state of the art of Holographic Optical Elements for Concentrating Photovoltaics

This chapter provides a background of HOEs for solar concentration and it is divided in three sections. Section 2.1 exposes the basic characteristics and requirements of HOEs for concentrating photovoltaics, section 2.2 illustrates the bases of holographic recording, and the state of the art (including a critical discussion of the theoretical treatment of HOEs for concentrating photovoltaics found in the literature) is presented in section 2.3. Sections 2.1 and 2.2 are extracted from a book chapter [1], reprinted with permission from Nova Science Publishers, Inc.[1]

2.1. Introduction to Holographic Optical Elements for solar applications

Holographic optical elements (HOEs) have multiple applications in the solar energy field [2]. They include photovoltaic and thermal energy conversion, illumination and temperature control of buildings and initiation of photochemical reactions, among others. This is due to the numerous advantages that HOEs present, such as their versatility, possibility of multifunctionality, and they are light, thin and flat, in comparison with refractive elements. Besides, volume holograms can reach 100% of diffraction efficiency (defined as the ratio of the diffracted intensity and the sum of diffracted and transmitted intensity).

Holograms have angular selectivity, that is, their efficiency is different for each angle of incidence. For certain solar applications this implies that tracking of the sun needs to be carried out. However, the decrease of the efficiency when moving away from the optimal conditions depends on the direction of the change of angle. If the incident direction varies along the plane formed by the two recording beams, the HOE presents a high angular selectivity and the efficiency decreases rapidly. On the other hand, if the incidence angle is modified in the perpendicular direction, lower angular selectivity is revealed and the efficiency decreases slowly for a broad angle range.

The solar movement needs to be taken into consideration, since the angle of incidence has an influence on the efficiency of the hologram. The position of the sun in the sky from a certain location on Earth and at a given time depends on the longitude and latitude of that location and the time of the day and the year. Figure 2.1 shows three trajectories of the apparent movement of the sun on the sky (from a location in the North hemisphere), illustrating the difference between various days of the year. The position of the sun in the sky is determined at a certain

[1] Reprinted with permission from Nova Science Publishers, Inc from: *Advances in Energy Research* vol. 26, J. Marín-Sáez, M. V. Collados, J. Atencia, and D. Chemisana, "Optical and Energetic Performance of Volume Holographic Optical Elements for Solar Energy Applications", pp. 27-82, copyright (2017).

moment in a given location with two angles: the solar height and the azimuth (horizontal coordinates), represented in the figure.

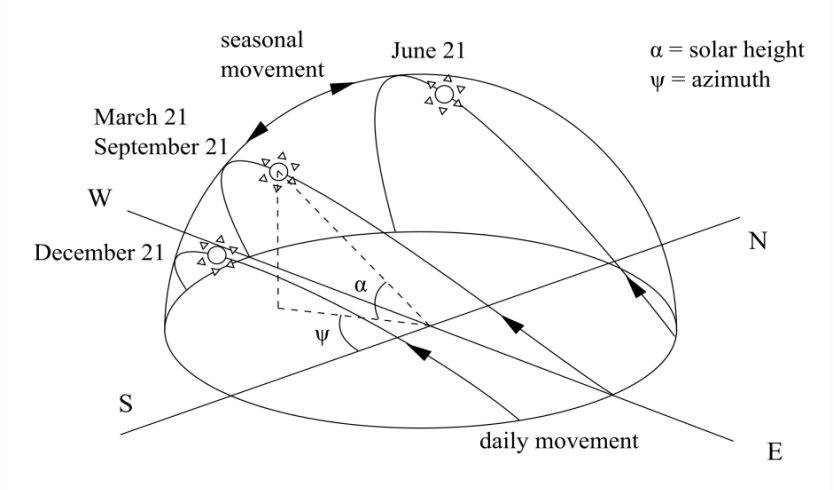

Figure 2.1. Daily and seasonal movement of the sun at a given location, determined at each moment with two angles: the solar height α and the azimuth ψ (horizontal coordinates).

Holograms also have chromatic selectivity, meaning that their behavior depends on the incident wavelength as well. The diffraction efficiency of a HOE is maximal for a selected wavelength and can be zero for another wavelength. This effect can turn into an advantage if a proper system design is utilized, to redirect incoming radiation towards one direction or another depending on their wavelength, and make use of it in different ways.

The design of a holographic solar concentration system should take into account the solar spectrum. The ASTM standard AM 1.5D solar spectrum normalized to 1000 W/m2 is depicted in Figure 2.2 with a solid line (left y-axis). Furthermore, if the system's receiver is a photovoltaic cell, the design should contemplate its spectral response as well. The spectral response of a mono-crystalline Si cell is illustrated in Figure 2.2 (dashed line, right y-axis). From this graph it can be stated that the optimal wavelength of a HOE that concentrates solar light onto a mono-crystalline Si cell should be between 500 and 950 nm in order to achieve higher cell electric current values.

Another effect that has to be taken into consideration is chromatic dispersion, since holograms work based on the principle of diffraction.

2.2. Holographic recording

2.2.1. Wavefront recording and reconstruction in holography

Holography is an optical technology based on the recording of the interference of two electromagnetic waves in a photosensitive medium. This is possible due to changes in the material corresponding to the difference of the recording intensity along the interference pattern.

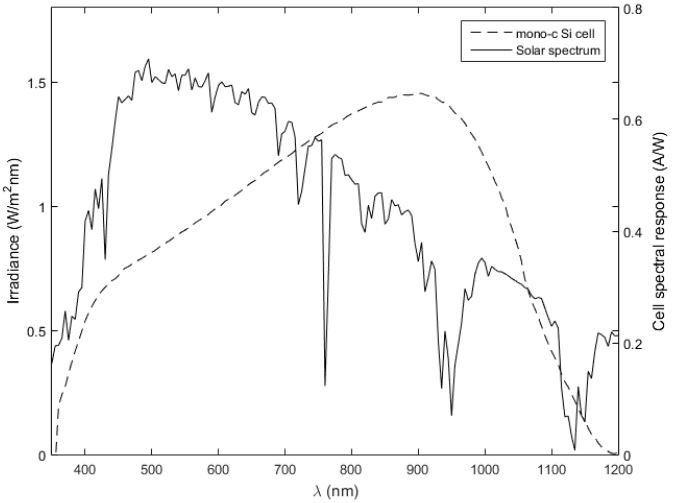

Figure 2.2. ASTM standard solar irradiance AM 1.5D, normalized to 1000 W/m^2 (solid line, left *y*-axis). Cell response of a mono-crystalline Si cell (dashed line, right *y*-axis).

Let's consider a hologram recorded with the interference of two coherent waves, Σ_1 and Σ_2, with respective complex amplitudes at each point of the hologram given by

$$\begin{aligned} \Sigma_1(x,y) &= A_1 e^{-i\varphi_1} \\ \Sigma_2(x,y) &= A_2 e^{-i\varphi_2} \end{aligned} \tag{2.1}$$

The intensity of the interference of both waves is

$$\begin{aligned} I(x,y) &= \left[\Sigma_1(x,y)+\Sigma_2(x,y)\right]\left[\Sigma_1(x,y)+\Sigma_2(x,y)\right]^* = \\ &= \Sigma_1\Sigma_1^* + \Sigma_2\Sigma_2^* + \Sigma_1\Sigma_2^* + \Sigma_1^*\Sigma_2 = \\ &= A_1^2 + A_2^2 + A_1A_2e^{-i(\varphi_1-\varphi_2)} + A_1A_2e^{i(\varphi_1-\varphi_2)} = \\ &= A_1^2 + A_2^2 + 2A_1A_2\cos(\varphi_1-\varphi_2) \end{aligned} \tag{2.2}$$

The intensity varies harmonically with the phase difference. This intensity pattern is recorded in a photosensitive medium, so its transmittance changes. Assuming that the intensity of the construction waves is uniform at the hologram plane and that it is linear with the recording exposure, the amplitude transmittance is

$$t_A(x,y) = t_b + \gamma\left[A_1A_2e^{-i(\varphi_1-\varphi_2)} + A_1A_2e^{i(\varphi_1-\varphi_2)}\right] \tag{2.3}$$

The constant term t_b is due to the uniform exposure of the construction waves. γ is proportional to the slope of the curve t_A as a function of the exposure, in the linear range.

When the hologram is illuminated with a coherent wave $U_0(x,y) = A_0e^{-i\varphi_0}$, several diffraction orders emerge:

$$\begin{aligned} U_0(x,y)t_A(x,y) &= t_bA_0e^{-i\varphi_0} + \gamma A_0A_1A_2e^{-i(\varphi_0+\varphi_1-\varphi_2)} + \gamma A_0A_1A_2e^{-i(\varphi_0-\varphi_1+\varphi_2)} = \\ &= U_1(x,y) + U_2(x,y) + U_3(x,y) \end{aligned} \tag{2.4}$$

Each of the addends can be considered as an independent wave, because of the linearity of Maxwell's equations. $U_1(x,y)$ is the beam transmitted by the hologram; it is a replica of the reconstruction wave $U_0(x,y)$ and corresponds to the 0 diffracted order. $U_2(x,y)$ corresponds to the -1 diffraction order and $U_3(x,y)$ corresponds to the +1 diffraction order. If the reconstruction wave is identical to $\Sigma_1(x,y) = A_1 e^{-i\varphi_1}$, then the diffracted wave corresponding to the third term becomes $U_3(x,y) = \gamma A_0 A_1 A_2 e^{-i\varphi_2}$, which is a replica of the wave $\Sigma_2(x,y)$.

2.2.2. Hologram types

Four hologram classifications must be taken into account to determine the best hologram type for solar concentration:

Absorption vs. phase hologram: An absorption hologram is one whose amplitude transmittance is proportional to the intensity recorded in the hologram. A phase hologram is one in which the interferential figure causes changes in the thickness or refractive index modulation along the material. The diffracted energy is higher for the phase holograms, since they do not present dissipation of energy along the material (associated with the absorption).

Thin vs. volume hologram: Thin holograms are those in which the thickness of the medium is much smaller than the recorded spatial period. The energy at a thin hologram output is distributed between the three waves (0, -1 and +1 orders) that appear in equation (2.4). Volume holograms (or thick) are those with thickness greater than the spatial period, and are characterized by presenting only the 0 order of diffraction, or transmitted order, and the +1 order of diffraction, given by U_1 and U_3 respectively in equation (2.4).

Transmission vs. reflection holograms: A transmission hologram is produced when at the recording step both waves arrive at the same face of the hologram so that in the reconstruction the light is transmitted; whereas in a reflection hologram the recording waves arrive to opposite sides of the plate, thus in the reconstruction the diffracted wave goes back to the same medium of incident wave.

Holographic lens vs. holographic grating: A holographic lens is a hologram recorded with two spherical waves, each one coming from a source point. For one of the waves, the source point can be at the infinity, in the case of a plane wave. The source can also be a line, if cylindrical lenses are considered. Holographic lenses can be used for image formation or for light concentration. When two plane waves are used in the recording, the result is named holographic grating. A holographic grating does not have optical power, so it only produces a detour of the incident wave.

For solar concentration, volume and phase holograms are used because they have more adequate characteristics for the application that occupies us (they allow to obtain a theoretical efficiency of 100% in the diffracted order +1 for a given wavelength and incidence direction). The following sections of this chapter will deal with transmission holograms; reflection holograms need a specific theoretical treatment and are of less widespread application in solar concentration.

2.2.3. Recording materials

Several kinds of photosensitive materials are used for holographic recording. When illuminated under proper conditions at the recording step, they present physical or chemical changes corresponding to the modulation of the incident intensity. Materials able to record phase holograms are more suitable for solar applications.

Another aspect to take into account is the spectral range that the material is sensitive to at the recording stage. This can limit the election of the recording wavelength, especially if the HOE is designed to perform efficiently at 800 nm, like in this study, since so far there are no photosensitive materials in that range.

High resolution is needed in order to record the desired spatial frequency of the intensity modulation. The recording material should also offer stability over time, so it is not affected by environmental conditions.

One of the most commonly used materials in holography is dichromated gelatin (DCG) [3–5]. During the recording, the Cr^{3+} ions (reduced from the dichromate ion $Cr_2O^{2-}_7$) cross-link the gelatin in the areas where high exposure is found. The hardness and solubility of these areas are modified and, after processing of the material, this turns into variations of the refractive index. The processing [6] includes thermal hardening, washing, swelling, dehydration and drying and is one of the inconveniences of DCG. Another drawback that this material presents is the sensitivity to humidity after the processing, so the HOE must be sealed in order to protect it.

On the other hand, DCG has important advantages, such as its high spatial resolution: for example, commercial Slavich PFG-04 gelatin plates have a resolving power greater than 5000 lines/mm [7]. The maximal index modulation obtained with these plates in a previous work [6] is 0.021, with a large linear dynamic range that allows the production of holographic gratings with high efficiency (close to 100%) when illuminated at 800 nm.

Photopolymers are another kind of recording materials that are also being used in solar applications [8–10]. During the recording stage, at the areas with high enough intensity, a photoinitiator starts a series of chemical reactions in which the monomers present in the material are combined and form photopolymers. The accumulation of molecules in those areas leads to modulation of the refractive index, without requiring chemical or thermal post-processing in some cases.

A photopolymeric material that has been characterized by the authors with a view to solar concentration application is Bayfol HX [11], manufactured by Covestro (formerly Bayer MaterialScience). It offers good light sensitivity, low shrinkage and detuning and no chemical or thermal post-processing is needed, only photocuring [12]. Efficiencies of almost 100% at 800 nm and a high dynamic range with an index modulation of 0.024 were obtained.

2.3. State of the art

Numerous holographic CPV systems can be found in the literature. A thorough review of holographic optical systems for solar applications up until 2015 can be found in [2]. The list of publications in this section comprises some of the systems described in [2], along with others not included in that publication. It is not an exhaustive list, but a description of some illustrative

examples of the types of holographic CPV systems found in the literature. Most of the studies are design proposals, and a theoretical assessment is included only in some of them. The system efficiencies are defined in different ways in each publication, which complicates a comparison of the different designs' performance, and few data are available. Building-integration is considered in some of them, being more feasible for those with lower tracking requirements. In most systems comprising holographic gratings or cylindrical lenses tracking can be suppressed in the direction of lower angular selectivity.

2.3.1. Literature review

The systems have been divided in two categories: systems with one receptor (a PV cell) and systems with more than one receptor (several PV cells or a PV cell and another type of collector).

2.3.1.1. Systems with one receptor

The simplest system configuration is a transmission holographic grating that diffracts incident sunlight towards a PV cell, as shown in figure 2.3(a). The cell also receives sunlight from the part of the aperture pupil without HOE, but concentration only occurs for the efficiently diffracted spectral range, so even though the PV cell receives the whole solar spectrum only the desired range is enhanced. This system can be designed so that diffracted rays that do not initially reach the PV cell may do so by being guided by total internal reflection, like in the system proposed by Zhang et al. [4] and Castro et al. [13]. In order to maintain the system's efficiency throughout the day, tracking would be needed in two directions, which would limit the possibilities of building-integration to the rooftop, which is the design placement of the system. If several gratings, each one designed for a certain angular range, are stacked on top of each other (as shown in figure 2.3(b)), tracking could be avoided in one axis, also studied in the same publications for different tilts of the system. A requirement for the correct operation of this type of systems is the absence of cross-coupling between the two gratings in the angular and spectral range of interest: rays diffracted by the first grating should be transmitted by the second one, not also efficiently diffracted.

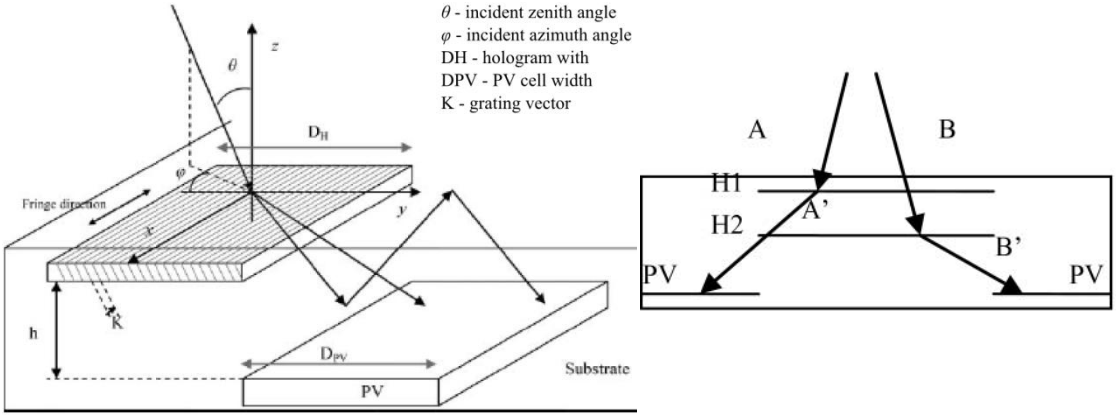

Figure 2.3. Systems formed by one or two stacked holographic transmission gratings and a PV cell [4,13].

In order to enhance the concentration ratio, a configuration with two or more gratings that redirect rays toward the same PV cell can be considered, as for example the one presented in figure 2.4 and proposed by Russo et al. [14]. It relies on total internal reflection to help redirect rays toward the PV cell, which is bifacial. In addition it could collect albedo and roof-reflected irradiance if it was placed on a rooftop. Rays with wavelengths that are diffracted with an angle not large enough to cause total internal reflection and transmitted rays do not reach the PV cell.

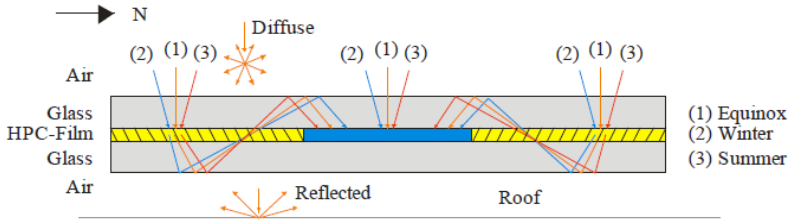

Figure 2.4. Systems formed by two holographic transmission gratings and one PV cell [14].

Another way of increasing the concentration ratio is by using holographic lenses, so that radiation incident on the entrance pupil is concentrated on a smaller surface, where the PV cell is placed, as carried out by Chemisana et al. with a holographic cylindrical lens [3] and shown in figure 2.5. An important advantage of this system is the suppression of the need of tracking in one direction. A possible integration on the shading system of a window is proposed.

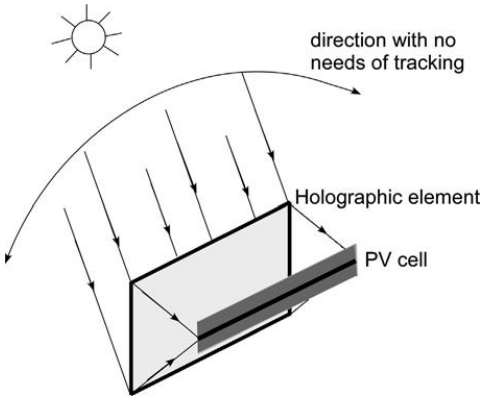

Figure 2.5. System formed by a holographic cylindrical lens and a PV cell [3].

Spherical lenses provide higher concentration since light is concentrated on a smaller area and the surface of the PV cell can be smaller than with holographic gratings or cylindrical lenses. Of course, combining two lenses (either both cylindrical or both spherical) in the same system will increase it even further, as Akbari et al. experimentally demonstrated [15]. The problem with spherical lenses is that in principle they require two-axes tracking.

2.3.1.2. Systems with more than one receptor

2.3.1.2.1. Systems with transmission HOEs

It is possible to take advantage of the chromatic dispersion introduced by transmission HOEs for spectrum-splitting configurations, in which two or more receivers use different parts of the solar spectrum.

Since the diffracted beam of holographic gratings is not focused, it is necessary to propagate it a certain distance in order to spatially separate the different spectral ranges and place different

receptors at their positions. Using a holographic lens facilitates this and in addition allows the use of smaller receptors, which is desirable for concentrating photovoltaics systems. Ludman et al. proposed a system where the diffracted beam of a cylindrical lens reached two or more different PV cells [16], depicted in figure 2.6(a).Vorndran et al. analyzed a system formed by a cylindrical holographic lens and two receivers: a PV cell and another receiver, which could be another PV cell, a thermal absorber or an algae biofuel system [17], illustrated in figure 2.6(b). They use a uniaxial lens, so its efficiency around its center is low. Whereas the first design could eliminate the need of tracking in one direction, two-axes tracking is required for the second one in order to maintain the efficiency if a holographic spherical lens is used, and one-axis tracking with a cylindrical lens.

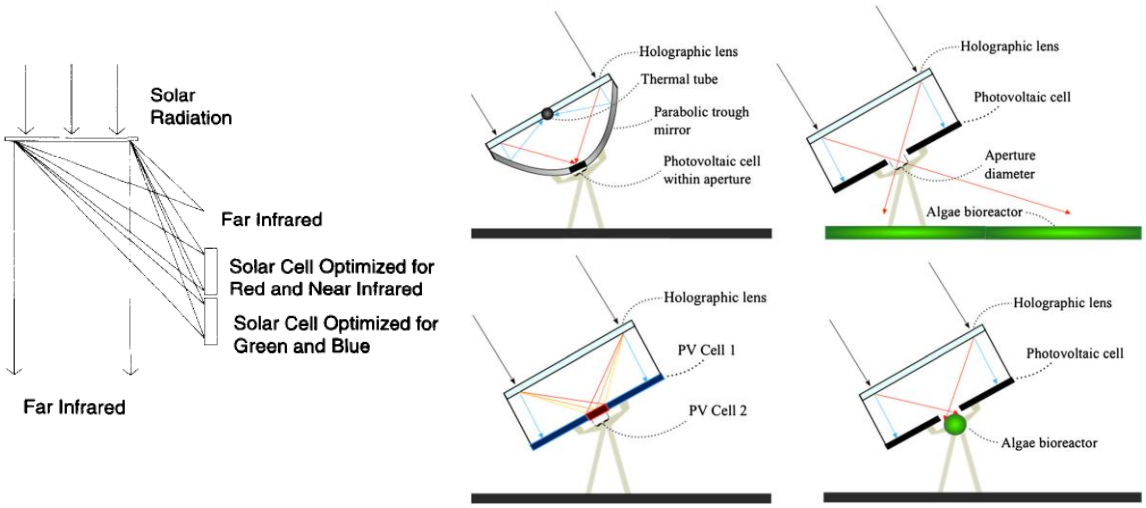

Figure 2.6. Spectrum-splitting systems formed by a holographic lens and two receivers [16,17].

Several lenses can be combined in the entrance pupil to redirect rays to several PV cells in the receiver plane, as shown by Gordon et al. [18] (figure 2.7(a)) and by Chrysler et al. [19] (figure 2.7(b)). Each holographic lens is efficient for a spectral range suitable for one PV cell type, so those rays are diffracted towards that cell. This allows precise spectrum-splitting across a wider entrance pupil. However, part of the spectral range that each PV cell cannot use (most of the infrared range) also reaches them, being either transmitted or diffracted. These geometries provide rather low concentration, which can be enhanced for one of the 2 PV cell types if its width is reduced.

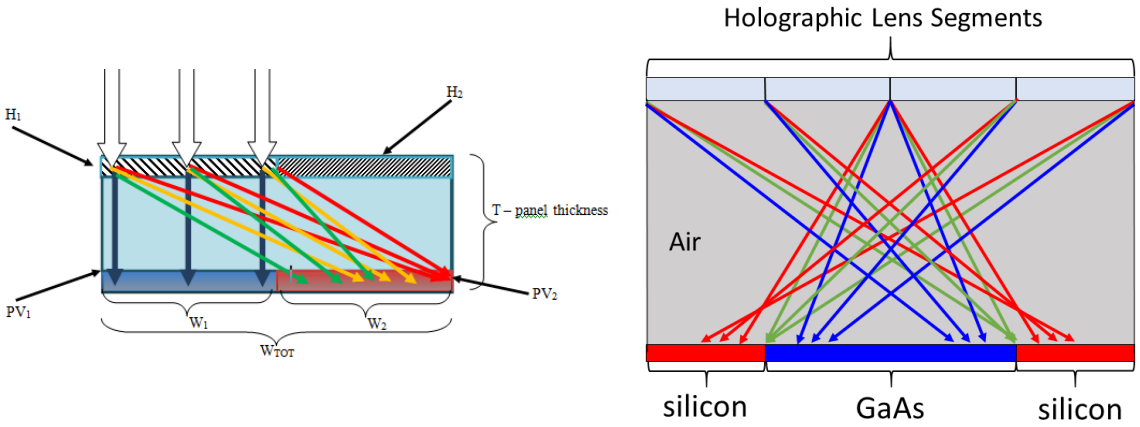

Figure 2.7. Spectrum-splitting systems with several holographic lenses and two types of PV cells [18,19].

Another way of introducing optical power in the system is to place a refractive lens after a holographic grating, as shown in figure 2.8 and studied by Wu et al. [20] and by Russo et al. [21]. The HOE introduces chromatic dispersion in the diffracted beam, so that the beam focused by the refractive lens is spectrally separated. In addition, the HOE can be designed to compensate the aberrations introduced by the refractive lens.

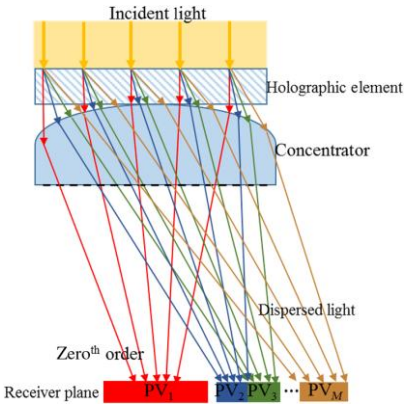

Figure 2.8. Spectrum-splitting systems formed by a holographic grating, a refractive lens and several PV cells. [20]

However, HOEs are efficient for a certain wavelength range only, so even if the system's geometry is properly designed so that the diffracted beam reaches the target receivers, the efficiency will not be high for the whole spectral range, thus part of the incident beam will be transmitted anyway for wavelengths in the range of interest. Stacking several HOEs, each one efficient for a different spectral range, can broaden the chromatic operation range. Wu et al. also considered stacking different transmission gratings in the previously mentioned publication [20] so that a broader spectral band could be efficiently diffracted towards the PV cell. The problem with this type of configuration is that in order to avoid cross-coupling the width of the chromatic selectivity curve of each HOE must be rather narrow or separated, so in principle the overall efficiency will not be greatly enhanced.

Another configuration with stacked transmission gratings is the one analyzed by Escarra et al. [22]. Four sets of three stacked gratings redirect different spectral bands toward four tandem dual-junction subcells, as shown in figure 2.9(a). Four beams (plus the low-efficiency cross-coupled beams) emerge from each set of HOEs: three diffracted beams (each one diffracted by one grating and transmitted by the rest, if no coupling is found at that wavelength range) and a beam transmitted by all three HOEs. Two compound parabolic concentrators (CPCs) allow the use of PV cells with a smaller surface than the one of the HOEs, as illustrated in figure 2.9(b).

An alternative to stacking HOEs is multiplexing. For this, several HOEs are recorded in the same volume, as theoretically studied by Ingersoll and Leger [23] with transmission gratings. As shown in figure 2.10, it offers the advantage of using only one element, but at the cost of having more coupled orders. This technique is limited by the recording material's dynamic range: high index modulation is needed [6].

Fröhlich et al. [24] analyzed a system with two stacked uniaxial lenses and two different PV cells, as shown in figure 2.11. Each uniaxial lens, in turn, is formed by two stacked HOEs: a transmission grating and a spherical lens.

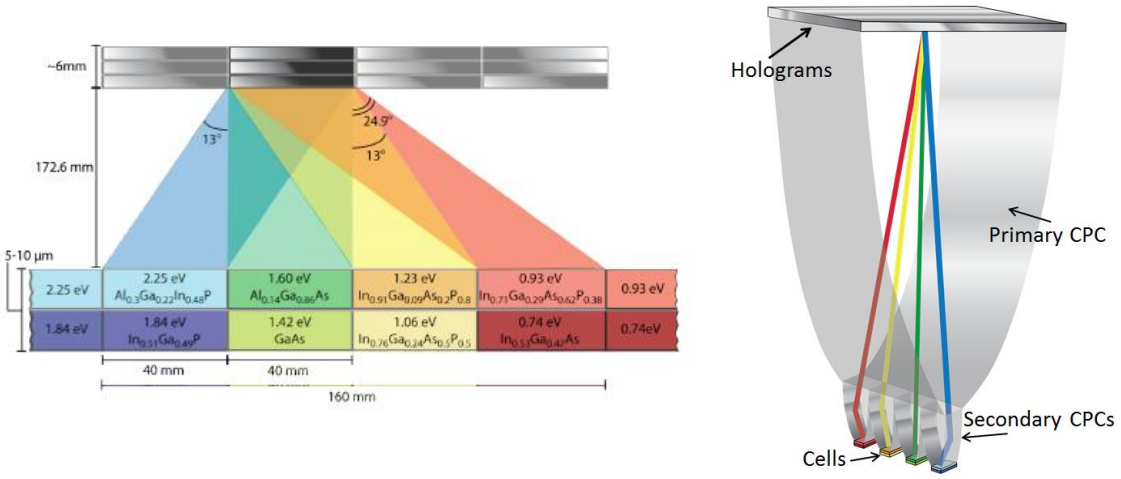

Figure 2.9. System of Escarra et al. [22].

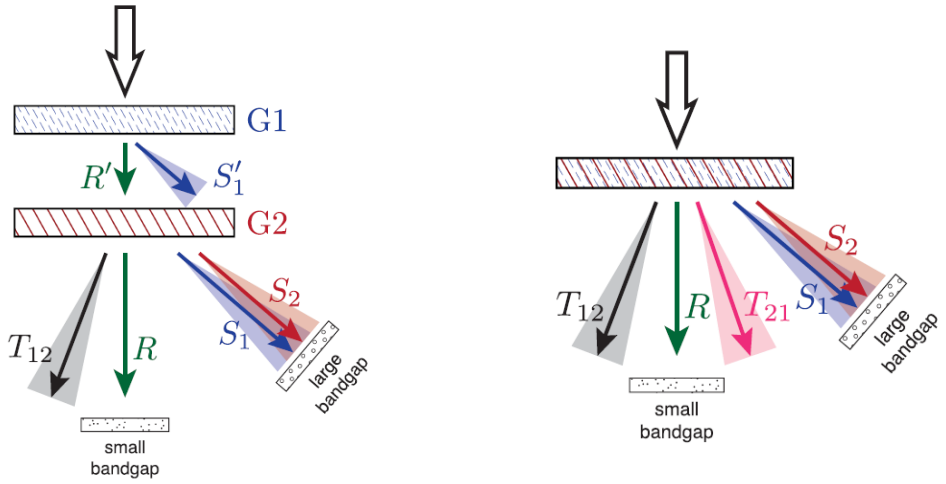

Figure 2.10. Systems of Ingersoll and Leger with stacked gratings (left) and multiplexed gratings (right) [23].

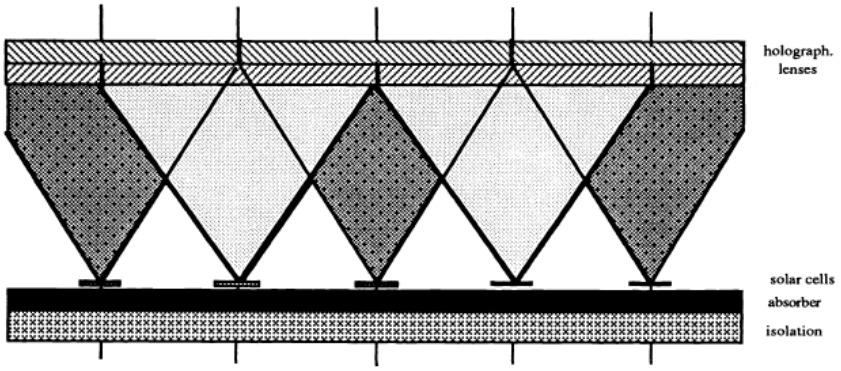

Figure 2.11. System of Fröhlich et al. with two stacked uniaxial lenses and two different PV cells [24].

2.3.1.2.2. Systems with reflection HOEs

Reflection HOEs provide another way of spectrum-splitting: since the diffracted beam is reflected, it is more easily separated from the transmitted beam.

The simplest configuration is shown in figure 2.12 and comprises only a reflection holographic grating. Zhang et al. studied a system of that type with a holographic reflection grating that

diffracted the wavelength range 875-1025 nm toward a Si PV cell and transmits the rest of the spectrum toward a GaAs PV cell [25].

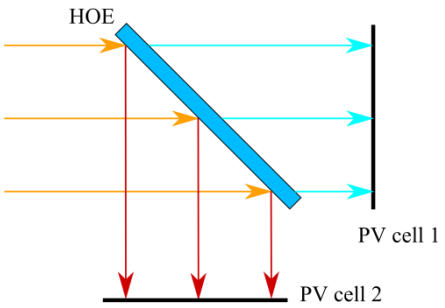

Figure 2.12. System formed by a holographic reflection grating a two PV cells.

Gordon et al. also proposed a system similar to the other one in their previously mentioned publication (that was shown in figure 2.7(a)) [18], with reflection instead of transmission HOEs, depicted in figure 2.13. However, the high chromatic selectivity of reflection HOEs causes a narrowing of the diffracted spectrum of each element.

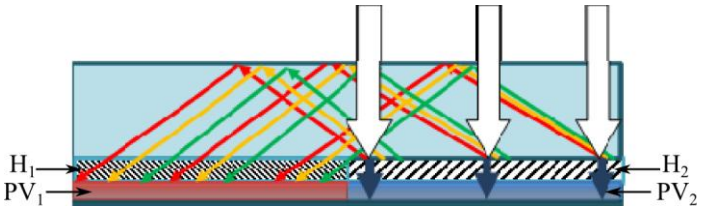

Figure 2.13. System formed by two reflection HOEs and two PV cells [18], similar to the one in figure 5(a) but with reflectionHOEs.

Stojanoff et al. proposed a Cassegrain concentrator where the secondary mirror was a reflection HOE pasted on a hyperbolic surface, presented in figure 2.14 [26]. Using a HOE instead of a second mirror allows spectrum-splitting, so that the diffracted light that reaches the PV cell (which can be a GaInP or a GaAs PV cell) belongs to its spectral response range, and transmitted light, a thermal absorber. This system would also require tracking.

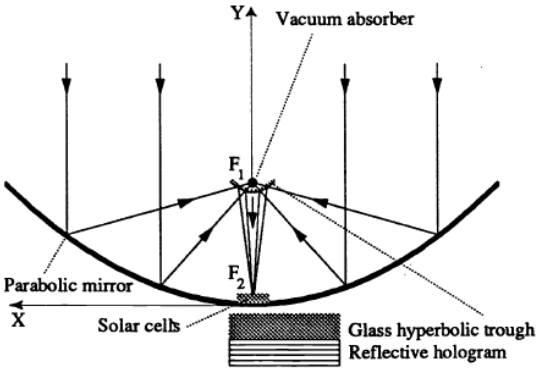

Figure 2.14. Holographic Cassegrain concentrator [26].

2.3.2. Discussion of the theoretical treatment in the literature

Many of the examples found in the literature only present design proposals and do not provide a thorough analysis of the concentrating system. Although many of them are experimentally constructed, most of them are characterized only vaguely and the behavior of the complete system is not compared to theoretical calculations. A comprehensive understanding is crucial to obtain efficient designs that take into account the operation conditions of the considered application.

Among the publications where a theoretical assessment of the concentrating holographic system is carried out, the ones authored by the researchers of the University of Arizona (Kostuk et al.) stand out. They consider systems both with volume holographic gratings and with volume holographic lenses.

When analyzing the first type (volume holographic transmission or reflection gratings) a local analysis of the HOE is enough, since the grating vector (and the index modulation if the recorded beams are assumed to be sufficiently expanded so that the Gaussian profile of the intensity of a laser beam is not noticeable at the exposed area) at each point of the HOE is the same. The efficiency can be determined with Coupled Wave Theory, and in the specific case of a volume hologram, Kogelnik's solution can be used [27]. This is applied in the publications of the researchers of the University of Arizona, either by using commercial software [20,21] or by performing the calculations themselves [4,13].

Another important aspect of the modeling of such systems is that for most configurations a ray-tracing analysis must be carried out in order to determine which rays, or what part of the diffracted beam, will reach the receiver. Assuming that the whole diffracted beam will reach the receiver is a wrong approach for the majority of system configurations. However, although in some of their publications a ray-tracing analysis is carried out (in [4] by performing the calculations themselves and in [21] with the help of a commercial software) in others the assumption of the whole diffracted beam reaching the receiver is made [13,20].

Of course, there are certain geometries where the whole diffracted beam will reach it (for example, the one proposed in [25] for the design incidence angle only, so tracking must be carried out in two axis if this assumption is made, which is not contemplated in the publication) and then it is not necessary.

Ray-tracing is also necessary in systems with stacked HOEs, as performed by Zhang et al. in [4], in order to determine the existence of coupling for each wavelength and angle of incidence.

This process (determining the direction of the diffracted rays, their energy and whether they reach the receiver or not) must be carried out for each angle of incidence of the sunrays and each wavelength of the solar spectrum.

However, when studying a concentrating system comprising a holographic lens, each point of the lens must be analyzed independently because of the different grating that is recorded at each point. Among the publications of this group regarding holographic lenses, this was carried out in [17] with the use of a commercial software to calculate the diffraction efficiency at each point of the lens. On the contrary, in other studies such as [18], the diffracted efficiency is averaged across the lens, obtaining only approximate values of the global performance.

Two more publications with rigorous global performance modeling of the holographic concentrating system have been found. Escarra et al. [22] use multiwave Coupled Wave Theory to calculate the irradiance that each PV cell of their spectrum-splitting system would receive, designing the holographic transmission gratings in order to maximize each spectral curve according to the sensitivity of the cells. Since the system they propose is based on stacked transmission gratings, they take into account the possible coupling among them by performing a ray-tracing calculation in which the output rays of the first grating are the incident rays on the second grating, and so on. Ingersoll and Leger [23] calculate the irradiance received by the PV cells in their spectrum-splitting system, using Kogelnik's solution for the system with stacked holographic gratings (and as Escarra et al., taking cross-coupling into account) and adapting the coupled differential equations as explained in [28] to consider all recorded gratings at the same time for the system with multiplexed holographic gratings.

Among the few publications by other authors where theoretical calculations are carried out, most of them only perform a local analysis of the HOE, which is sometimes validated with experimental results, but do not perform a global analysis of the system.

To summarize, although there are many design proposals, a great number of them are early-stage analyses. Among the studies that include a theoretical treatment, some of them are indeed based on a correct calculation procedure. The majority of these systems comprise holographic gratings, and only one comprising a cylindrical holographic lens (which requires a more complex analysis, that has been carried out with a commercial software) has been found [17].

As mentioned in chapter 1, one of the aims of this thesis is to obtain a reliable modeling tool that enables a correct analysis of holographic concentrating systems. This is necessary to accurately carry out theoretical studies of the system, as well as to optimize it for each design configuration. The algorithm of this modeling tool (determination of the direction of the diffracted rays by means of their cosine directors, their energy, whether they reach the receiver, the irradiance integration on the receiver and the generated electrical current) must be explained in detail.

Different definitions of the overall efficiency of the holographic CPV system can be found in the different publications, so a proper comparison of the performance of the existing designs is not straight-forward. A parameter that quantifies the operation of the system should be defined, in such a way that the performance of the optical elements and the PV cell with sunlight is addressed.

References:

1. J. Marín-Sáez, M. V. Collados, J. Atencia, and D. Chemisana, "Optical and Energetic Performance of Volume Holographic Optical Elements for Solar Energy Applications," in *Advances in Energy Research* (NOVA, 2017).

2. M. V. Collados, D. Chemisana, and J. Atencia, "Holographic solar energy systems: The role of optical elements," Renew. Sustain. Energy Rev. **59**, 130–140 (2016).

3. D. Chemisana, M. V. Collados, M. Quintanilla, and J. Atencia, "Holographic lenses for building integrated concentrating photovoltaics," Appl. Energy **110**, 227–235 (2013).

4. D. Zhang, J. M. Castro, and R. K. Kostuk, "One-axis tracking holographic planar

concentrator systems," J. Photonics Energy **1**, 015505 (2011).

5. C. G. Stojanoff, "A review of selected technological applications of DCG holograms," in *Proceedings of SPIE*, **7957** (2011), p. 79570L–79570L–15.

6. A. Villamarín, J. Atencia, M. V. Collados, and M. Quintanilla, "Characterization of transmission volume holographic gratings recorded in Slavich PFG04 dichromated gelatin plates.," Appl. Opt. **48**, 4348–4353 (2009).

7. *Geola Technical Product Specifications and Sales Information Brochure* (2001), http://www.geola.com.

8. S. T. L. Sam, A. P. T. Kumar, P. Predeep, M. Thakur, and M. K. R. Varma, "Design and Optimization of Photopolymer Based Holographic Solar Concentrators," in *Optics: Phenomena, Materials, Devices and Characterization (AIP Conference Proceedings)* (2011), pp. 248–250.

9. H. Akbari, I. Naydenova, and S. Martin, "Using acrylamide-based photopolymers for fabrication of holographic optical elements in solar energy applications," Appl. Opt. **53**, 1343 (2014).

10. G. Bianco, M. A. Ferrara, F. Borbone, A. Roviello, V. Pagliarulo, S. Grilli, P. Ferraro, V. Striano, and G. Coppola, "Multiplexed holographic lenses : realization and optical characterization," in *2015 Fotonica AEIT Italian Conference on Photonics Technologies* (Institution of Engineering and Technology, 2015), CP667.

11. J. Marín-Sáez, J. Atencia, D. Chemisana, and M.-V. Collados, "Characterization of volume holographic optical elements recorded in Bayfol HX photopolymer for solar photovoltaic applications," Opt. Express **24**, A720 (2016).

12. H. Berneth, F.-K. Bruder, T. Fäcke, D. Jurbergs, R. Hagen, D. Hönel, T. Rölle, and G. Walze, "Bayfol HX photopolymer for full-color transmission volume Bragg gratings," SPIE Photonics West 2014-OPTO Optoelectron. Devices Mater. **9006**, 900602 (2014).

13. J. M. Castro, D. Zhang, B. Myer, and R. K. Kostuk, "Energy collection efficiency of holographic planar solar concentrators," Appl. Opt. **49**, 858 (2010).

14. J. M. Russo, J. E. Castillo, E. D. Aspnes, R. K. Kostuk, and G. Rosenberg, "Daily and seasonal performance of angularly dependent fixed mount dual aperture holographic planar concentrator photovoltaic modules," in *Proceedings of SPIE*, **7769** (2010), p. 77690D.

15. H. Akbari, I. Naydenova, H. Ahmed, S. McCormack, and S. Martin, "Development and testing of low spatial frequency holographic concentrator elements for collection of solar energy," Sol. Energy **155**, 103–109 (2017).

16. J. E. Ludman, J. Riccobono, N. O. Reinhand, I. V. Semenova, J. Martín, W. Tai, X. Li, and G. Syphers, "Holographic solar concentrator for terrestrial photovoltaics," in *Proceedings of the 24th IEEE Photovoltaic Specialists Conference* (1994), pp. 1208–1211.

17. S. Vorndran, J. M. Russo, Y. Wu, M. Gordon, and R. Kostuk, "Holographic diffraction-through-aperture spectrum splitting for increased hybrid solar energy conversion efficiency," Int. J. Energy Res. **39**, 326–335 (2015).

18. M. Gordon, D. Zhang, S. Vorndran, J. M. Russo, C. K. Luscombe, S. E. Shaheen, and R. K. Kostuk, "Planar holographic spectrum-splitting PV module design," in *Proceedings of SPIE*, **8468** (2012), p. 846808.

19. B. D. Chrysler, Y. Wu, R. K. Kostuk, and Z. Yu, "Volume holographic lens spectrum-splitting photovoltaic system for high energy yield with direct and diffuse solar illumination," in *Proceedings of SPIE - Next Generation Technologies for Solar Energy Conversion VIII*, **10368** (SPIE, 2017), p. 12.

20. Y. Wu, B. Chrysler, and R. K. Kostuk, "Design and fabrication of cascaded dichromate gelatin holographic filters for spectrum-splitting PV systems," J. Photonics Energy **8**, 1 (2018).

21. J. M. Russo, D. Zhang, M. Gordon, S. D. Vorndran, Y. Wu, and R. K. Kostuk, "Grating-over-lens concentrating photovoltaic spectrum splitting systems with volume holographic optical elements," in *Proceedings of SPIE*, **8821** (2013), p. 882106.

22. M. D. Escarra, S. Darbe, E. C. Warmann, and H. A. Atwater, "Spectrum-splitting photovoltaics: Holographic spectrum splitting in eight-junction, ultra-high efficiency module," in *2013 IEEE 39th Photovoltaic Specialists Conference (PVSC)* (IEEE, 2013), pp. 1852–1855.

23. G. B. Ingersoll and J. R. Leger, "Optimization of multi-grating volume holographic spectrum splitters for photovoltaic applications," Appl. Opt. **55**, 5399 (2016).

24. K. Froehlich, E. U. Wagemann, H. Schulat, H. Schuette, and C. G. Stojanoff, "Fabrication and test of a holographic concentrator for two-color PV operation," in *Proceedings of SPIE*, **2255** (1994), pp. 812–821.

25. D. Zhang, M. Gordon, J. M. Russo, S. Vorndran, M. Escarra, H. Atwater, and R. K. Kostuk, "Reflection hologram solar spectrum-splitting filters," in *Proceedings of SPIE*, **8468** (2012), p. 846807.

26. C. G. Stojanoff, J. Schulat, and M. Eich, "Bandwidth- and angle-selective holographic films for solar energy applications," in *Proceedings of SPIE*, **3789** (1999), pp. 38–49.

27. H. Kogelnik, "Coupled wave theory for thick hologram gratings," Bell Syst. Tech. J. **48**, 2909–2947 (1969).

28. G. B. Ingersoll and J. R. Leger, "Spectral interference in multiplexed volume Bragg gratings: theoretical calculations and experimental verification," Appl. Opt. **53**, 5477 (2014).

Chapter 3

Theoretical modeling of Holographic Optical Elements for Concentrating Photovoltaics

A ray-tracing tool has been developed to analyze the behavior of volume HOEs. It integrates a geometrical and energetic modeling of the HOEs. The geometrical analysis is based on the directional cosines of the recording rays, which determine the direction of the reconstruction ones, for any angle of incidence [1]. The efficiency of the diffracted and transmitted orders is also determined with the directional cosines, using Kogelnik's analytical solution of the Coupled Wave Theory [2].

Although other authors had considered part of this approach in previous publications, it was not a consistent analysis addressing the global performance of the system, as exposed in chapter 2. The novelty of this work is that the energetic contribution of each ray that enters the entrance pupil is propagated through the rest of the system and then it is taken into account in the receiver's plane. The energy flux on the surface of the PV cell is calculated as the sum of the contribution of all rays that reach it. Therefore, it enables a local analysis of each point of the entrance pupil (the HOE) and a global analysis of the HOE, providing a detailed assessment of the whole concentrating system.

This work is presented in the publication included in this chapter [3]. The geometrical and energetic model of volume HOEs for solar concentration is exposed, along with simulations results and their experimental validation, showing the reliability of the ray-tracing algorithm and some of the possibilities it offers. The importance of the design of the HOE and its influence on the optical concentration are also shown with a comparison of the optical concentration yielded with two illustrative designs of cylindrical holographic lenses.

References:

1. J. N. Latta, "Computer-Based Analysis of Holography Using Ray Tracing," Appl. Opt. **10**, 2698 (1971).

2. H. Kogelnik, "Coupled wave theory for thick hologram gratings," Bell Syst. Tech. J. **48**, 2909–2947 (1969).

3. P. Bañares-Palacios, S. Álvarez-Álvarez, J. Marín-Sáez, M.-V. Collados, D. Chemisana, and J. Atencia, "Broadband behavior of transmission volume holographic optical elements for solar concentration," Opt. Express **23**, A671–A681 (2015).

Broadband behavior of transmission volume holographic optical elements for solar concentration

Paula Bañares-Palacios,[1] Samuel Álvarez-Álvarez,[1] Julia Marín-Sáez,[2] María-Victoria Collados,[1] Daniel Chemisana,[2] and Jesús Atencia[1,*]

[1]*Departamento de Física Aplicada, Instituto de Investigación en Ingeniería de Aragón (I3A), Universidad de Zaragoza, Facultad de Ciencias, Pedro Cerbuna 12, 50009 Zaragoza, Spain*
[2]*Departamento de Medio Ambiente (Sección de Física Aplicada), Universidad de Lleida, Escuela Politécnica Superior (INSPIRES), Jaume II 69, 25001 Lleida, Spain*
[*]*atencia@unizar.es*

Abstract: A ray tracing algorithm is developed to analyze the energy performance of transmission and phase volume holographic lenses that operate with broadband illumination. The agreement between the experimental data and the theoretical treatment has been tested. The model has been applied to analyze the optimum recording geometry for solar concentration applications.

OCIS codes: (090.2890) Holographic optical elements; (090.7330) Volume gratings; (220.4298) Nonimaging optics; (350.6050) Solar energy.

References and links

1. D. Zhang, J. M. Castro, and R. K. Kostuk, "One-axis tracking holographic planar concentrator systems," J. Photonics Energy **1**(1), 015505 (2011).
2. R. K. Kostuk and G. Rosenberg, "Analysis and design of holographic solar concentrators," Proc. SPIE **7043**, 70430I (2008).
3. D. Zhang, M. Gordon, J. M. Russo, S. Vorndran, and R. K. Kostuk, "Spectrum-splitting photovoltaic system using transmission holographic lenses," J. Photonics Energy **3**(1), 034597 (2013).
4. J. E. Ludman, "Holographic solar concentrator," Appl. Opt. **21**(17), 3057–3058 (1982).
5. K. Froehlich, E. U. Wagemann, H. Schulat, H. Schuette, and C. G. Stojanoff, "Fabrication and test of a holographic concentrator for two color PV-operation," Proc. SPIE **2255**, 812–821 (1994).
6. J. E. Ludman, J. Riccobono, I. V. Semenova, N. O. Reinhand, W. Tai, X. Li, G. Syphers, E. Rallis, G. Sliker, and J. Martin, "The optimization of a holographic system for solar power generation," Sol. Energy **60**(1), 1–9 (1997).
7. M. Gordon, D. Zhang, S. Vorndran, J. M. Russo, C. K. Luscombe, S. E. Shaheen, and R. K. Kostuk, "Planar holographic spectrum-splitting PV module design," Proc. SPIE **8468**, 846808 (2012).
8. D. Chemisana, M. V. Collados, M. Quintanilla, and J. Atencia, "Holographic lenses for building integrated concentrating photovoltaics," Appl. Energy **110**, 227–235 (2013).
9. J. M. Castro, D. Zhang, B. Myer, and R. K. Kostuk, "Energy collection efficiency of holographic planar solar concentrators," Appl. Opt. **49**(5), 858–870 (2010).
10. Y. W. Zhang, C. S. Ih, H. F. Yan, and M. J. Chang, "Photovoltaic concentrator using a holographic optical element," Appl. Opt. **27**(16), 3556–3560 (1988).
11. Y. Luo, J. Castro, J. K. Barton, R. K. Kostuk, and G. Barbastathis, "Simulations and experiments of aperiodic and multiplexed gratings in volume holographic imaging systems," Opt. Express **18**(18), 19273–19285 (2010).
12. H. Kogelnik, "Coupled wave theory for thick hologram gratings," Bell Syst. Tech. J. **48**(9), 2909–2947 (1969).
13. R. R. A. Syms, "Vector effects in holographic optical elements," Opt. Acta (Lond.) **32**(11), 1413–1425 (1985).
14. A. M. López, M. P. Arroyo, and M. Quintanilla, "Some polarization effects in holographic volume gratings," J. Opt. A, Pure Appl. Opt. **1**(3), 378–385 (1999).
15. J. N. Latta, "Computer-based analysis of holography using ray tracing," Appl. Opt. **10**(12), 2698–2710 (1971).
16. A. Villamarín, J. Atencia, M. V. Collados, and M. Quintanilla, "Characterization of transmission volume holographic gratings recorded in Slavich PFG04 dichromated gelatin plates," Appl. Opt. **48**(22), 4348–4353 (2009).
17. R. Leutz and A. Suzuki, *Nonimaging Fresnel Lenses. Design and Performance of Solar Concentrators* (Springer-Verlag 2001).

#234591 - $15.00 USD Received 17 Feb 2015; revised 17 Apr 2015; accepted 20 Apr 2015; published 18 May 2015

1 Jun 2015 | Vol. 23, No. 11 | DOI:10.1364/OE.23.00A671 | OPTICS EXPRESS A671

1. Introduction

During the last years, designs of devices with holographic optical elements have been proposed to be used as solar concentrators. These designs include volume transmission phase holograms [1,2], mainly spherical lenses [3–5] and cylindrical lenses [6–8]. Precisely, the last ones are the most commonly suggested to avoid tracking in one direction. This type of holograms is used due to its high efficiency and low cost; however, it has two special characteristics that can affect its performance as solar concentrator: angular selectivity and chromatic selectivity.

Due to the angular selectivity, volume holograms have high efficiency only for a range of incidence directions that depends on the holographic material thickness and the interbeam angle at the recording step. Angular selectivity is higher when the incidence direction varies in the plane formed by the two recording beams. This can be considered as a drawback, since the holograms need tracking if concentration is required during the whole day or the whole year, but it can be an advantage if the element operates only during a part of the day or over one season. If the incidence direction varies in the perpendicular plane, the angular selectivity is lower, so it is possible to eliminate tracking in this direction.

Due to chromatic selectivity, the efficiency of the volume hologram depends on the wavelength. It is high for a bandwidth centered at a wavelength that is determined by the value of refractive index modulation obtained in the recording step and the angle of incidence. If the chromatic selectivity region is tuned so the lens does not diffract infrared, the heating of the cell, one of the main problems of concentration refractive systems, is avoided. Lower cell temperature results in a higher conversion efficiency, and therefore lower cost/watt [8].

For a plane grating, the behavior is the same in all the points of the hologram. In the case of a holographic lens, the efficiency and its angular and chromatic selectivity vary at each point of the hologram. This has to be taken into account if the concentration factor or the distribution of the energy concentrated on the solar cell need to be calculated.

In previous works, a cylindrical holographic lens has been built and experimentally analyzed in terms of its performance as a solar concentrator [8] with tracking in only one direction. In the present study, the behavior of holographic cylindrical lenses as solar concentrators, for a general geometry of the recording beams, is theoretically evaluated. Some authors [9–11] calculate an average efficiency for all points of the hologram, and apply this efficiency to calculate the energy in the image plane. Since the efficiency does not vary linearly along the surface of the hologram, important information about the real energy distribution on the cell is lost in the mean value.

For this reason, a ray tracing algorithm is developed to simulate the performance across the full aperture of the lens that includes geometrical diffraction effects and efficiency calculation of local gratings. The novelty of the present work is the evaluation of the energy carried by each diffracted ray and the propagation of this energy to the plane of the PV cell, obtaining the real energy distribution on the cell.

2. Theoretical model

Kogelnik's Coupled Wave Theory [12] and the approximate scalar theory developed by Syms [13] are used in order to study the most general case of incidence lying outside of the recording plane. A comprehensive union of both models can be found in the work of Lopez *et al.* [14]. In [14], the diffraction efficiency of a pure phase transmission volume hologram for an incident wave with general wave propagation vector (conical diffraction) and a general polarization direction, as are described in the following paragraphs, are obtained.

In the present work, the equations of conical diffraction, calculating the efficiency and the direction of the diffracted light as a function of the directional cosines of the incident wavefront and the propagation vectors of the recording waves are utilized. The directions of

#234591 - $15.00 USD Received 17 Feb 2015; revised 17 Apr 2015; accepted 20 Apr 2015; published 18 May 2015

the rays diffracted by the hologram and its energy can be then calculated by means of ray tracing and thus, the energy distribution on the image plane can be estimated.

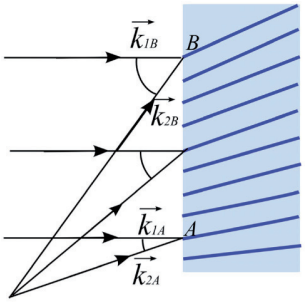

Fig. 1. Recording of a volume and transmission holographic lens.

For this analysis, it is considered that each point of the holographic lens acts as a plane grating ("local grating": Fig. 1). The recording plane of the local grating is defined as the plane that contains the two wave propagation vectors, $\vec{k}_1$ and $\vec{k}_2$, whose interference has created the hologram. The grating vector $\vec{K}$ is determined and it is given by:

$$\vec{K} = \vec{k}_1 \pm \vec{k}_2 \tag{1}$$

For simplicity, only the negative term option from Eq. (1) is considered. This is a good election for volume holograms. As it can be seen from Eq. (2) and (3), $\vec{k}_1$ and $\vec{k}_2$ can be written as a function of their directional cosines inside the material:

$$\vec{k}_1 = \frac{2\pi n}{\lambda_R}(l_1, m_1, n_1) \tag{2}$$

$$\vec{k}_2 = \frac{2\pi n}{\lambda_R}(l_2, m_2, n_2) \tag{3}$$

where n is the refraction index of the holographic material and λ_R is the recording wavelength.

If it is assumed that the hologram media index is sinusoidally modulated and the hologram is a volume one, when it is illuminated with a beam with propagation vector $\vec{k}_o$, there are only two waves that propagate inside the medium: zero order $\vec{k}_o$ and first diffraction order $\vec{k}_i$. The diffracted efficiency of the first order would be maximum when the Bragg condition is fulfilled [Fig. 2(a)]:

$$\vec{k}_i = \vec{k}_o - \vec{K} \tag{4}$$

The diffracted beam is given by the projection of $\vec{k}_i$, $\vec{k}_o$ and $\vec{K}$ on the hologram plane, $z = 0$ [Fig. 2(b)]:

$$\begin{cases} \vec{k}_i \cdot \vec{u}_x = (\vec{k}_o - \vec{K}) \cdot \vec{u}_x \\ \vec{k}_i \cdot \vec{u}_y = (\vec{k}_o - \vec{K}) \cdot \vec{u}_y \end{cases} \tag{5}$$

where $\vec{u}_x$ and $\vec{u}_y$ are the unitary vectors in x and y direction respectively.

#234591 - $15.00 USD Received 17 Feb 2015; revised 17 Apr 2015; accepted 20 Apr 2015; published 18 May 2015

1 Jun 2015 | Vol. 23, No. 11 | DOI:10.1364/OE.23.00A671 | OPTICS EXPRESS A673

Considering Eqs. (1) and (5), the direction cosines (l_i, m_i, n_i) of the diffracted beam $\vec{k}_i$ are given by the following equations [15]:

$$\begin{aligned} l_i &= l_o - \frac{\lambda_R}{\lambda_C}(l_1 - l_2) \\ m_i &= m_o - \frac{\lambda_R}{\lambda_C}(m_1 - m_2) \\ n_i &= \left(1 - l_i^2 - m_i^2\right)^{1/2} \end{aligned} \tag{6}$$

where (l_o, m_o, n_o) are directional cosines of $\vec{k}_o$.

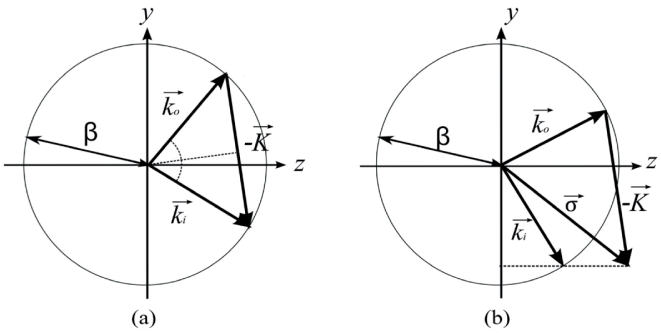

Fig. 2. The vector diagram when Bragg condition is fulfilled (a) or not (b).

The diffractive efficiency for two linear orthogonal polarizations, *N* and *M*, perpendicular and parallel respectively to the plane formed by $\vec{K}$ and $\vec{k}_o$, is given by [14]:

$$\eta_N = \frac{\sin^2\left[\left(\nu^2 + \xi^2\right)^{1/2}\right]}{1 + \frac{\xi^2}{\nu^2}} \tag{7}$$

$$\eta_M = \frac{\sin^2\left[\left(\nu_M^2 + \xi^2\right)^{1/2}\right]}{1 + \frac{\xi^2}{\nu_M^2}} \tag{8}$$

Since solar light is unpolarized, the total diffractive efficiency η_d as the mean of the two contributions η_N and η_M can be considered as:

$$\eta_d = \frac{1}{2}(\eta_N + \eta_M) \tag{9}$$

The parameters ν, ν_M and ξ depend on material characteristics and the deviation of Bragg condition,

$$\nu = \frac{\pi d \Delta n}{\lambda_C (n_o n_i)^{1/2}} \tag{10}$$

$$\nu_M = \nu\left(\vec{k}_o \cdot \vec{k}_i\right) \tag{11}$$

#234591 - $15.00 USD Received 17 Feb 2015; revised 17 Apr 2015; accepted 20 Apr 2015; published 18 May 2015

1 Jun 2015 | Vol. 23, No. 11 | DOI:10.1364/OE.23.00A671 | OPTICS EXPRESS A674

$$\xi = \frac{d\vartheta}{2n_i} \tag{12}$$

where Δn is the index modulation, d the thickness of the holographic medium and λ_C is the wavelength of the incident beam $\vec{k}_o$. Parameter ϑ represents the deviation of the Bragg condition, given by:

$$\vartheta = \frac{\beta^2 - |\vec{\sigma}|^2}{2\beta} \tag{13}$$

where $\beta = \frac{2\pi n}{\lambda_C}$. From Fig. 2(b), $\vec{\sigma} = \vec{k}_o - \vec{K}$; thus, ϑ can be written as a function of the directional cosines of $\vec{k}_o$ and $\vec{K}$:

$$\vartheta = \frac{1}{2}\beta\left(1 - \left[l_o - \frac{\lambda_C}{\lambda_R}(l_1 - l_2)\right]^2 - \left[m_o - \frac{\lambda_C}{\lambda_R}(m_1 - m_2)\right]^2 - \left[n_o - \frac{\lambda_C}{\lambda_R}(n_1 - n_2)\right]^2\right) \tag{14}$$

To reach $\eta_N = 1$, two conditions are necessary: first, Bragg condition must be fulfilled, so $\xi = 0$ $(\vartheta = 0)$; second, $\nu = \frac{\pi}{2}$. The second condition is only possible for a wavelength $\overline{\lambda_C}$ that matches $\Delta n = \frac{2\overline{\lambda_C}(n_o n_i)^{1/2}}{d}$. This value of Δn is determined by the exposure in the recording step, thus the hologram can be tuned to diffract with $\eta_N = 1$ for the desired wavelength [16].

For cylindrical lenses, in which a plane wave and a cylindrical wave interfere, the directional cosines l_1 and l_2 are zero.

3. Experimental measurements

A cylindrical holographic lens in dichromated gelatin emulsion PFG-04 is designed and constructed. The lens is designed for solar concentration applications [8]; thereby, the wavelength for which the efficiency will be maximum as a function of the cell sensitivity can be selected. Since a silicon cell is considered, the central wavelength at the reconstruction will be 800 nm.

The dimensions of the lens and the cell are determined by the desired geometrical concentration factor. In this case, the lens size is 5x5 cm and the cell size is 1x5 cm; thus, the concentration factor is 5 suns.

In Fig. 3, the recording and reconstruction geometry are shown. The recording wavelength is 532 nm and the exposure time is chosen to obtain an index modulation value adequate to give maximum efficiency at 800 nm at the reconstruction [16]. In this way, the chromatic selectivity of the hologram matches the spectral sensitivity curve of silicon PV cells. Given the fact that the central wavelength at the reconstruction is not the same with the recording wavelength, the cylindrical wavefront at the recording is not on axis.

#234591 - $15.00 USD Received 17 Feb 2015; revised 17 Apr 2015; accepted 20 Apr 2015; published 18 May 2015

1 Jun 2015 | Vol. 23, No. 11 | DOI:10.1364/OE.23.00A671 | OPTICS EXPRESS A675

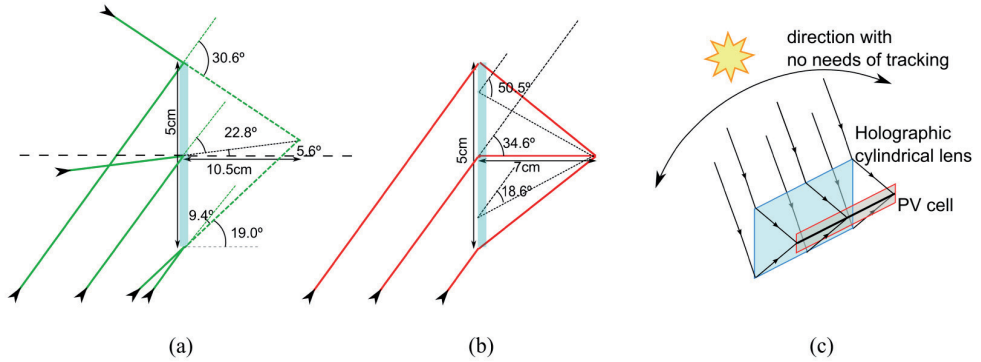

Fig. 3. (a) Recording geometry, (b) reconstruction geometry with monochromatic light and (c) reconstruction geometry with solar light for the cylindrical lens.

The recording interbeam angle has to be large enough to assure the volume condition in all points of the lens. Parameter Q is used to establish the limit of volume regime and it is defined as:

$$Q = \frac{2\pi\lambda_C d}{n\Lambda^2} \tag{15}$$

where Λ is the grating period. If $Q > 2\pi$, the hologram is considered as a volume hologram.

However, angular and chromatic selectivity increase when parameter Q increases; thereby, it is better to adopt a Q value as low as possible. The design criterion for the present work is to obtain efficiency higher than 50% for wavelengths larger than 575 nm at the point of the hologram in which the interbeam angle is lower. From this condition, the recording geometry shown in Fig. 3(a) is determined. The theoretical curve of efficiency, as a function of wavelength at the lower region of the lens depicted in Fig. 3(a), is illustrated in Fig. 4. For wavelengths higher than 575 nm, parameter Q is higher than 2π.

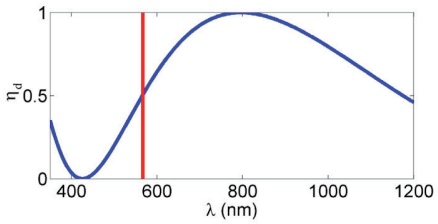

Fig. 4. The efficiency as a function of wavelength in the upper side of the lens shown in Fig. 3.

In Figs. 5(a) and 5(b) the angular selectivity curves in the center of the lens, measured at 800 nm, compared with the corresponding theoretical ones, are plotted. Coordinate θ denotes the variation of incidence direction contained in the recording plane while ϕ indicates the variation of incidence direction in the perpendicular plane. Experimental data have been corrected from reflection and absorption losses in the glass substrate and in the gelatin layer. The maximum diffraction efficiency obtained experimentally is around 95%, close to the theoretical value of 100% for 800 nm. This 5% difference is attributed to index modulation drop, which could be produced at the recording step due to instabilities; anyhow, the index modulation needed for 800 nm is high and the curve of index modulation against exposition saturates around this point [16].

The maximum efficiency peaks are located at 32.1° and –4.1°, instead of 34° and 0°, as it is shown in Fig. 3. This is due to a change of emulsion thickness (shrinkage) occurred during

#234591 - $15.00 USD Received 17 Feb 2015; revised 17 Apr 2015; accepted 20 Apr 2015; published 18 May 2015

1 Jun 2015 | Vol. 23, No. 11 | DOI:10.1364/OE.23.00A671 | OPTICS EXPRESS A676

the wet processing of dichromated gelatin, which changes the direction and module of the grating vector $\vec{K}$. These changes have been included in the theoretical model. The relative difference of FWHM with respect to the theoretical model is 7% and 2.7% in the case of peaks of Fig. 5(a) and 7.6% in the case of Fig. 5(b).

Figure 5(c) illustrates the chromatic selectivity when the hologram is illuminated with white light. The relative difference of FWHM in this case is 3.7%.

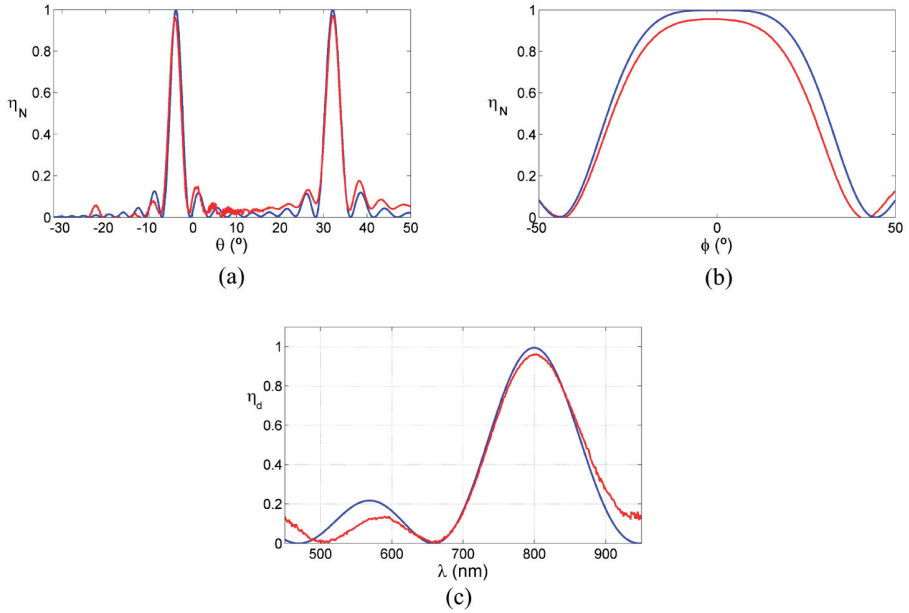

Fig. 5. Experimental (red) and theoretical (blue) curves of the efficiency at 800 nm as a function of (a) the incidence direction θ contained in the recording plane, (b) the incidence direction ϕ perpendicular to the recording plane. (c) Theoretical (blue) and experimental (red) efficiency as a function of wavelength.

4. Influence of recording geometry on the performance of cylindrical holographic lenses

The theoretical model is utilized to analyze the influence of the recording geometry on the angular and chromatic selectivity of holographic solar concentrators. To illustrate the usefulness of the developed algorithm, two typical recording geometries [6, 8] of cylindrical lenses are compared. The first one (lens 1) is the configuration shown in Fig. 3. The recording and reconstruction geometry of the second lens (lens 2) are illustrated in Fig. 6.

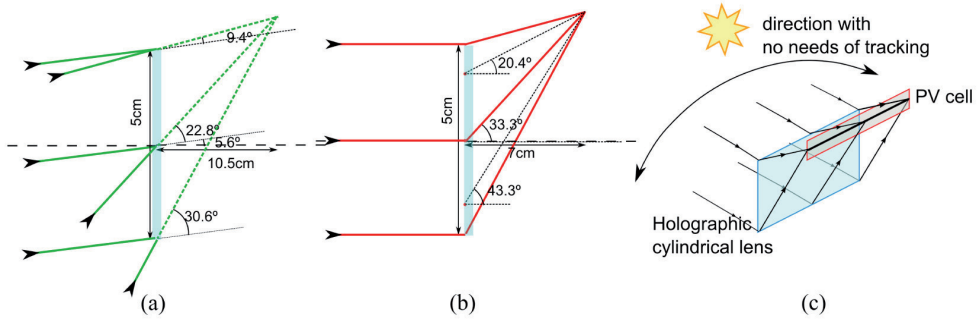

Fig. 6: (a) The recording geometry, (b) the reconstruction geometry with monochromatic light and (c) the reconstruction geometry with solar light of the cylindrical lens.

#234591 - $15.00 USD Received 17 Feb 2015; revised 17 Apr 2015; accepted 20 Apr 2015; published 18 May 2015

1 Jun 2015 | Vol. 23, No. 11 | DOI:10.1364/OE.23.00A671 | OPTICS EXPRESS A677

In lens 1 the cylindrical wavefront is reconstructed on-axis while in lens 2, the cylindrical wavefront is reconstructed off-axis. In the recording step, the interbeam angle at the center of the plate is the same for both lenses, but local gratings are not equal, so the lenses would have different chromatic and angular selectivity.

4.1 Local analysis

In Fig. 7, the monochromatic efficiency (at 800 nm) as a function of the incidence angle at three different points of each lens: at the upper side (+20 mm from the center), at the center and at the bottom (–20 mm from the center) is illustrated.

Lens 2 maintains better efficiency for a larger range of ϕ angles in comparison with lens 1; thereby, lens 2 is expected to have a better behavior if the tracking in ϕ direction is eliminated.

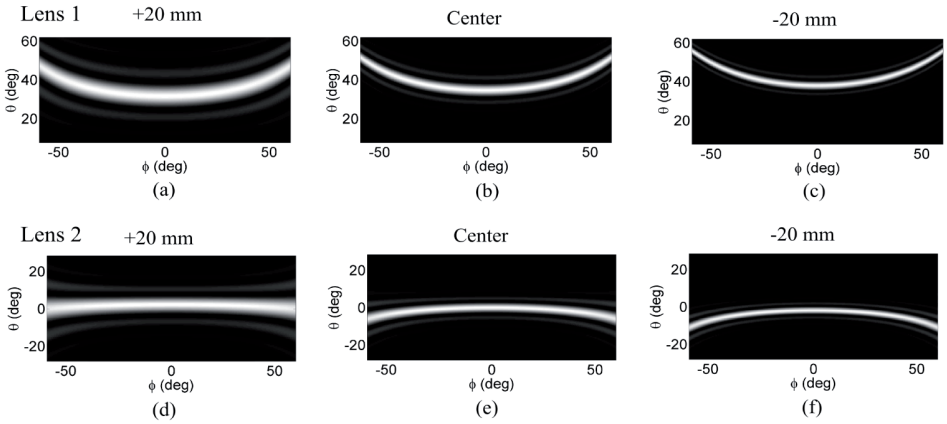

Fig. 7. The efficiency as a function of the incidence angle θ and ϕ in lens 1 and lens 2, calculated at three points of the lenses: at the center, (b) and (e); 20 mm above the center, (a) and (d); and 20 mm below the center, (c) and (f). Values range from black (η = 0) to white (η = 1).

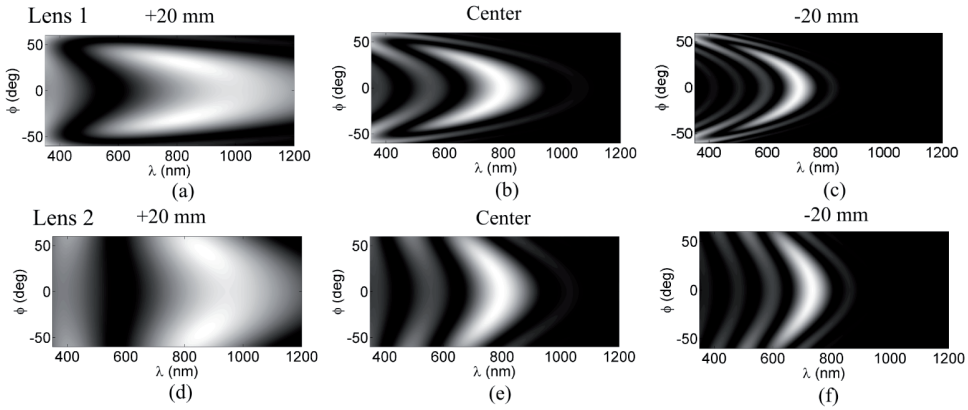

Fig. 8. The efficiency as a function of the incidence angle ϕ and λ in lens 1 and lens 2 calculated at three points of the lenses: at the center (b) and (e), 20 mm above the center (a) and (d), and 20 mm below the center (c) and (f). Values range from black (η = 0) to white (η = 1).

It should be taken into account the fact that these graphics are calculated for 800 nm; thus, although the efficiency drops in some points, for other wavelengths the efficiency would be

#234591 - $15.00 USD Received 17 Feb 2015; revised 17 Apr 2015; accepted 20 Apr 2015; published 18 May 2015

maximum. This effect can be observed in Fig. 8 where the efficiency as a function of wavelength and ϕ is presented. In the frame of attending the chromatic selectivity, both lenses are very similar.

4.2 Global analysis

As it has been demonstrated, the efficiency strongly depends on the point of the lens; thereby, it is necessary to make a global analysis taking into account the whole aperture.

By means of the present ray tracing calculation, the spot diagram considering the diffracted rays for each lens at the cell plane (Fig. 9) for three different wavelengths (700, 800 and 900 nm) is evaluated, when the direction of the incident beam fulfills the Bragg condition for 800 nm.

Both lenses present chromatic dispersion in y-direction (in the case of lens 2 the dispersion is higher than in lens 1); thereby not all the rays reach the cell area. This fact will reduce the theoretical geometrical concentration.

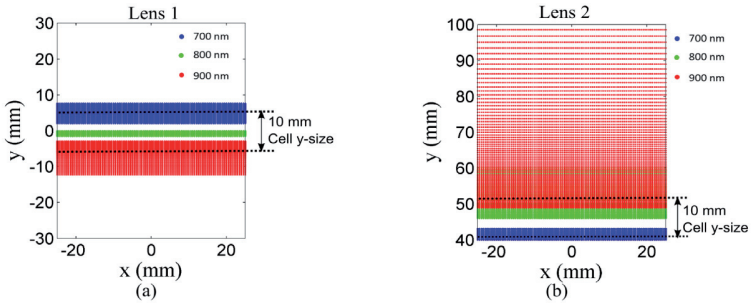

Fig. 9. Spot diagrams at the cell plane of lens 1 (a) and lens 2 (b) for 700, 800 and 900 nm.

Spot diagrams of Fig. 9 give information about the geometrical behavior of the lenses, but do not reveal the energy that reaches the cell, since each ray transports different energy depending on its wavelength and its incidence point on the lens.

Thus, to analyze the optical efficiency of the concentrator, it is necessary to calculate the light energy that reaches the cell area. From this energy, a set of optical concentration coefficients [17] are calculated as follows:

The cell area, A_c, is divided into small areas, ΔA_c. The local spectral optical concentration ratio, $\eta_{\lambda,y}$, in y-direction is given by:

$$\eta_{\lambda,y} = \frac{\Phi_{2,\lambda,y}}{\Phi_{1,\lambda}} \frac{A_L}{\Delta A_c} \tag{16}$$

where $\Phi_{1,\lambda}$ is the radiative spectral energy at the entrance pupil area, A_L, and $\Phi_{2,\lambda,y}$ is the radiative spectral energy that reaches ΔA_c.

Figure 10 shows the results obtained for both lenses.

#234591 - $15.00 USD Received 17 Feb 2015; revised 17 Apr 2015; accepted 20 Apr 2015; published 18 May 2015

1 Jun 2015 | Vol. 23, No. 11 | DOI:10.1364/OE.23.00A671 | OPTICS EXPRESS A679

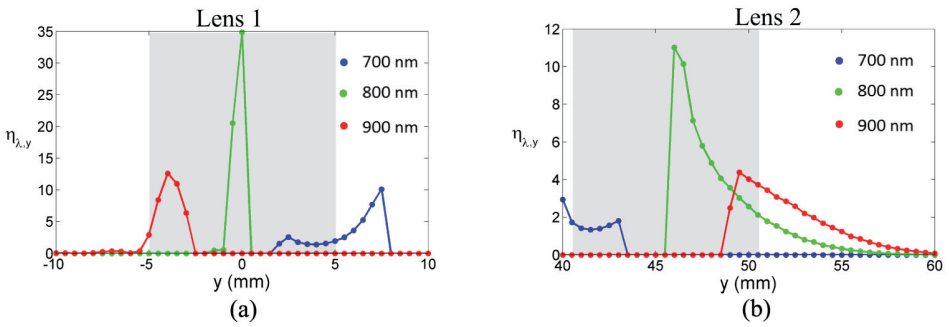

Fig. 10. Local spectral optical concentration ratio as a function of the *y*-coordinate in cell plane for (a) lens 1 and (b) lens 2.The shadow zone corresponds to cell width.

By focusing on the maximum values obtained in each lens, it can be observed that lens 1 concentrates more energy of the three wavelengths; nevertheless, in the case of lens 2, the energy is more distributed over the cell.

Integrating in a range of wavelengths, the local optical concentration ratio in y-direction, η_y, is given by:

$$\eta_y = \frac{\Phi_{2,y}}{\Phi_1}\frac{A_L}{\Delta A_c} \tag{17}$$

where Φ_1 is the radiative energy at the entrance pupil area and $\Phi_{2,y}$ is the radiative energy of the rays that reach ΔA_c in that range of wavelengths.

The results are shown in Fig. 11, for a range of wavelengths from 650 nm to 950 nm. This range is selected as a function of the sensitivity curve of the cell. It can be observed that lens 1 concentrates the light slightly more than lens 2.

In Figs. 10 and 11, it is considered that the energy associated with each ray at the entrance pupil does not depend on the wavelength and the reflection and absorption losses on the glass substrate are not taken into account.

For the full cell area, the optical concentration ratio is given by:

$$\eta = \frac{\Phi_2}{\Phi_1}\frac{A_L}{A_c} \tag{18}$$

where Φ_2 is the radiative energy at the cell area. The optical concentration ratio η is 1.94 for lens 1 and 1.67 for lens 2.

#234591 - $15.00 USD Received 17 Feb 2015; revised 17 Apr 2015; accepted 20 Apr 2015; published 18 May 2015

1 Jun 2015 | Vol. 23, No. 11 | DOI:10.1364/OE.23.00A671 | OPTICS EXPRESS A680

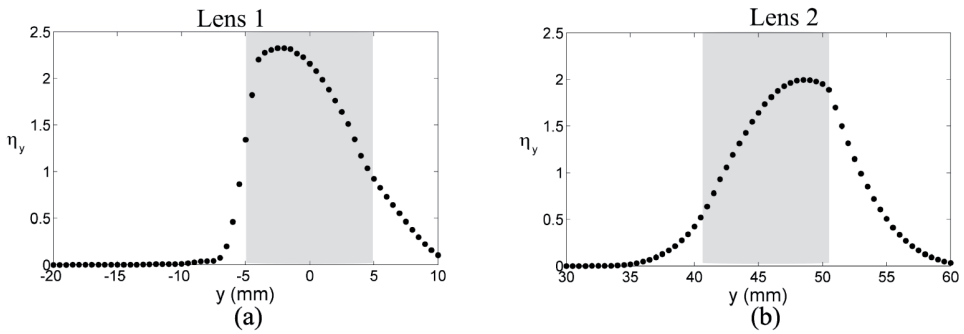

Fig. 11. Local optical concentration ratio as a function of the *y*-coordinate in cell plane for (a) lens 1 and (b) lens 2, considering wavelengths from 650 nm to 950 nm.The shadow zone corresponds to cell width.

Both lenses presents an optical efficiency lower than 40%, mainly due to chromatic dispersion, aberration effects and light diffracted in zero order. On the other hand, holographic concentrators have the advantage that the infrared radiation is not concentrated, avoiding cell overheating and enhancing the cell conversion efficiency. If the optical efficiency is improved by optimizing the recording geometry, holographic concentrators will be an attractive option to refractive concentrators.

5. Conclusions

A ray tracing algorithm has been developed in order to analyze the energy performance of volume and transmission holographic lenses as solar concentrators.

The algorithm is a powerful simulation tool that allows analyzing different designs of holographic concentrators, conducting a local analysis of angular and chromatic selectivity in different points of the lens, and performing a global analysis, by means of spots diagrams and energy integration onto cell, taking into account the whole aperture of the lens.

A holographic element was constructed in order to validate the model for a specific set of designed parameter. The comparison demonstrated very good agreement for both, chromatic and angular selectivity.

Two lens configurations with on-axis (lens 1) and off-axis (lens 2) cylindrical wave reconstructions are analyzed. Lens 2 has a better performance when the incident light goes out of the Bragg condition, as it can be seen in Fig. 7, but this lens presents a higher chromatic dispersion. An integration process of ray energy along the cell is conducted in order to obtain the optical concentration ratio when the incident beam fulfills the Bragg condition for 800 nm. Lens 1 shows an average concentration ratio of 1.94, which is 16.1% higher than in lens 2. A comparison of total concentration ratio when incident beam varies along the day will be necessary to determine the best configuration. As the theoretical model can be used to calculate the concentration ratio for any direction of the incident beam, this would be the purpose of future work.

Acknowledgments

This research has been supported by the Spanish Ministerio de Economía y Competitividad (grants FIS2012-35433 and ENE2013-48325-R), the Diputación General de Aragón (Grupo Consolidado TOL, T76) and the Generalitat de Catalunya (grant FI-DGR 2015).

In memoriam of Prof. Dr. Manuel Quintanilla.

#234591 - $15.00 USD Received 17 Feb 2015; revised 17 Apr 2015; accepted 20 Apr 2015; published 18 May 2015

Chapter 4

Simulations of a conceptual holographic Concentrating Photovoltaic-Thermal prototype to assess its adequacy

The developed ray-tracing algorithm has been presented in chapter 3, showing that it is a reliable tool that can be used to investigate holographic concentrating systems. As exposed in chapter 2, very few studies that rigorously analyze the behavior of HOEs for solar applications systems can be found in the literature.

The goal of this chapter is to evaluate whether holographic concentrating photovoltaic systems are feasible for building-integration. This can be theoretically assessed with the ray-tracing tool previously described. For this scope, one of the two cylindrical holographic lenses described in chapter 3 was chosen. It was the one designed for perpendicular reconstruction, referred to as "Lens 2" in the publication included in that chapter.

A building-integrated holographic concentrating system was designed, formed by two identical holographic lenses placed symmetrically and redirecting rays toward the receiver plane. This system was a hybrid photovoltaic-thermal (PVT) system with two receivers: a Si PV cell and a thermal absorber, which served a double purpose: make use of the infrared spectral range of the solar spectrum that the PV cell is not sensitive to, and at the same time help reduce the temperature of the cell. Therefore, both electrical and thermal energy were obtained.

This system would be placed on solar shading louvers on the South-oriented façade of a building in the Northern hemisphere (or a North-oriented façade in the Southern hemisphere). It takes advantage of the shading system, which tracks the solar altitude movement throughout the day. That way, tracking is carried out in one axis, and the HOEs are placed so that it matches the direction of high angular selectivity.

Two different locations are considered, which have different solar spectra throughout the day and the year, and different building energy demands. Simulations are carried out with the incident solar spectrum every minute, analyzing the performance of the holographic concentrating system, obtaining the irradiance received by the PV cell and the thermal absorbers and evaluating the ratio of the demanded electrical and thermal energy that was produced.

This study is presented in the publication included in this chapter [1]. Although other authors had evaluated year-round performance of holographic concentrating PV systems [2,3], the energy output had not been related to the specific building demands. To our knowledge, the publication presented in this chapter is the only study found in the literature where such a multidisciplinary analysis is carried out.

References:

1. J. Marín-Sáez, D. Chemisana, Á. Moreno, A. Riverola, J. Atencia, and M.-V. Collados, "Energy Simulation of a Holographic PVT Concentrating System for Building Integration Applications," Energies **9**, 577 (2016).

2. D. Zhang, J. M. Castro, and R. K. Kostuk, "One-axis tracking holographic planar concentrator systems," J. Photonics Energy **1**, 015505 (2011).

3. J. M. Castro, D. Zhang, B. Myer, and R. K. Kostuk, "Energy collection efficiency of holographic planar solar concentrators," Appl. Opt. **49**, 858 (2010).

energies

MDPI

Article

Energy Simulation of a Holographic PVT Concentrating System for Building Integration Applications

Julia Marín-Sáez [1], Daniel Chemisana [1,*], Álex Moreno [1], Alberto Riverola [1], Jesús Atencia [2] and María-Victoria Collados [2]

[1] Applied Physics Section of the Environmental Science Department, Polytechnic School, University of Lleida, Lleida 25001, Spain; jmarin@macs.udl.cat (J.M.-S.); alex.moreno@udl.cat (Á.M.); alberto.riverola@macs.udl.cat (A.R.)

[2] Applied Physics Department, Aragon Institute of Engineering Research (I3A), University of Zaragoza, Zaragoza 50009, Spain; atencia@unizar.es (J.A.); vcollado@unizar.es (M.-V.C.)

* Correspondence: daniel.chemisana@macs.udl.cat; Tel.: +34-973-003-711

Academic Editors: Francesco Calise and Massimo Dentice d'Accadia
Received: 1 June 2016; Accepted: 12 July 2016; Published: 25 July 2016

Abstract: A building integrated holographic concentrating photovoltaic-thermal system has been optically and energetically simulated. The system has been designed to be superimposed into a solar shading louvre; in this way the concentrating unit takes profit of the solar altitude tracking, which the shading blinds already have, to increase system performance. A dynamic energy simulation has been conducted in two different locations—Sde Boker (Israel) and Avignon (France)—both with adequate annual irradiances for solar applications, but with different weather and energy demand characteristics. The simulation engine utilized has been TRNSYS, coupled with MATLAB (where the ray-tracing algorithm to simulate the holographic optical performance has been implemented). The concentrator achieves annual mean optical efficiencies of 30.3% for Sde Boker and 43.0% for the case of Avignon. Regarding the energy production, in both locations the thermal energy produced meets almost 100% of the domestic hot water demand as this has been considered a priority in the system control. On the other hand, the space heating demands are covered by a percentage ranging from 15% (Avignon) to 20% (Sde Boker). Finally, the electricity produced in both places covers 7.4% of the electrical demand profile for Sde Boker and 9.1% for Avignon.

Keywords: solar energy; solar concentration; photovoltaics; PVT; holographic optical elements (HOE); building integration; energy dynamic simulation

1. Introduction

Energy consumption in the building sector represents 40% of the total energy consumed in the European Union. The European Commission, in order to decrease energy consumption, defined (considering buildings as a priority) the directive which states the "20-20-20" objectives: greenhouse gas emissions reductions (20%), the share of renewable energy (20%) and improvements in energy efficiency (20%) [1]. In this regard, building integrated solar hybrid Concentrating Photovoltaic-Thermal (CPVT) systems are a technology which perfectly addresses the objectives defined by the European Union, as may cover both the thermal and the electrical consumption needs.

CPV systems replace part of the cell area by cheaper and more environmentally friendly materials, the optical elements, which can lead to more cost-efficient systems from both, economic and environmental aspects [2]. On the contrary, when increasing the concentration ratio the percentage which is not converted into electricity becomes much higher in absolute terms. This could cause PV overheating and thus, problems related with efficiency reduction, stress of materials, etc. arise.

A strategy to profit the removal heat which negatively influences system performance is to use a hybrid Photovoltaic-Thermal (PVT) receptor. A PVT module controls PV temperature while simultaneously produces thermal energy. Another strategy to prevent the PV warming up is the spectral selection of the incident irradiance. A technology able to concentrate sunlight and at the same time to spectrally select irradiance is holography.

Among the different types of Holographic Optical Elements (HOEs), volume holograms have been studied as solar concentrators attending to some interesting properties as the high optical efficiency achieved (they can reach 100% efficiency for a selected wavelength). They may be utilized in different configurations [3]: plane gratings, that are not concentrating elements but as they operate directing light toward the same area the incident irradiance is concentrated [4–6] or concentrating optical elements (lenses) either cylindrical [7,8] or spherical [9–11].

HOEs present two main characteristics that affect their performance: angular and chromatic selectivity, in other words, their efficiency depends on the angle of incidence and the wavelength. Consequently, the solar spectrum and the spectral sensitivity range of the photovoltaic cell, among other parameters, need to be taken into account in the design of the HOE, in order to optimize its behavior for the wavelength range of interest. The chromatic selectivity of holograms provides an important advantage in comparison with refractive elements, since the concentration of undesired wavelengths on the photovoltaic cell is avoided. If the HOE is designed to diffract infrared wavelengths with very poor efficiency, the cell is prevented from overheating, which could cause a worsening on the cell's performance [12,13]. The chromatic selectivity also allows spectrum splitting, if a configuration with more than one kind of receiver (either different photovoltaic cells [8,9] or a hybrid photovoltaic-thermal receiver [10,14–16]) is chosen.

More specifically, regarding holographic PVT designs: Vorndran et al. [10] proposed a spectrum-splitting holographic system in which a holographic lens diffracts a narrow bandwidth towards a photovoltaic cell. The transmitted spectrum is reflected on a parabolic mirror towards a thermal tube. The solar concentrator described by Froehlich et al. [15] is formed by two stacked holographic lenses, each composed by a holographic grating to correct the incident direction and a holographic lens. Each holographic lens directs a different spectral range of the incoming light to a photovoltaic cell, sensitive to one of these two spectral bandwidths. The transmitted spectrum reaches a thermal absorber, which also refrigerates the PVs. Xia et al. [16] proposed a solar concentrator formed by a holographic grating, which would split the incident spectrum into visible and infrared range, and a Fresnel lens, which would concentrate the visible spectrum onto a set of PV cells and the IR spectrum onto a heat exchanger. Iurevych et al. [14] simulated the performance of a solar concentrator constituted by a reflection holographic grating. Incoming rays with wavelengths of a certain range are reflected by the HOE and the surfaces of the system, reaching a PV cell, whereas the rest are transmitted through the HOE and reach a thermal absorber.

Based on the previous studies found in the literature, it can be noted that even though there are some works conducting optical and energetic simulation of holographic concentrators, there is no research dealing with the energy simulation of the system performance considering more than the concentrating unit itself. In this regard, the present research aims at covering an important gap in the frame of Holographic Concentrating Photovoltaic-Thermal (HCPVT) solar generators, which is their dynamic energy simulation. For this purpose, a two-floor family house with an occupancy of three people is simulated for two different locations: Sde Boker (Israel) and Avignon (France), analyzing the thermal and electrical production under both climatic conditions and energy demand profiles.

2. System Description

The analyzed building integrated concentrating PVT system is designed to be superimposed on the blinds of a solar louvre shading system. In this manner, the concentrator is benefitted from the solar altitude tracking of the shading blinds and thus increasing the optical efficiency. Figure 1 illustrates the architectural configuration proposed, indicating in light blue the blind area where the

Energies **2016**, *9*, 577

concentrating system is placed (top-left). The blinds' size is 9 m long by 0.4 m wide and by 0.065 m high. The simulated building is considered to be 5.8 m height, starting the blinds at the ground floor window level (1 m height), therefore the number of blinds is 12. On the top-right, a schematic of a blind section shows the location of the holographic lenses and the PVT module, which is placed in the interior space. Both elements are assembled in a single unit forming a modular system with two parallel layers, the HOEs and the PVT module. At the bottom, a diagram of the cross section indicates the main dimensions of the module.

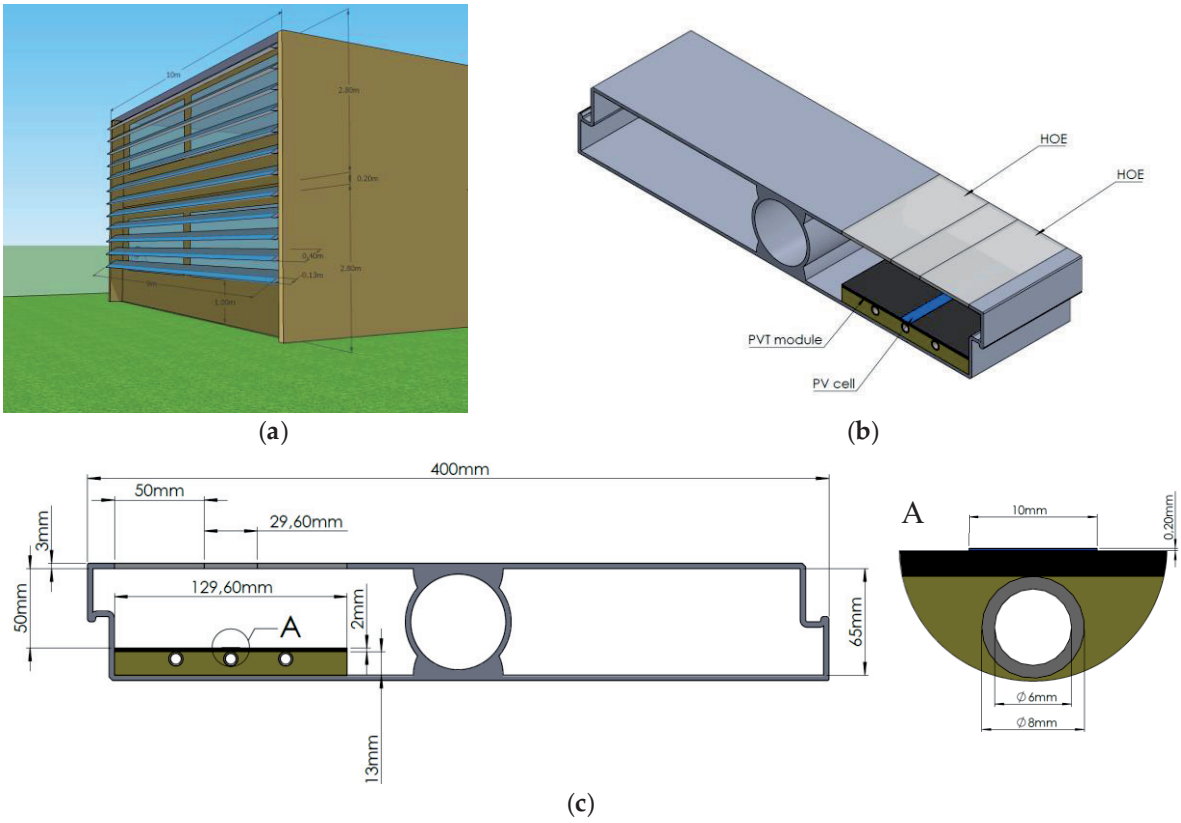

Figure 1. Architectural image of the building integrated concentrator (**a**), section of the blind where the PVT concentrator in placed (**b**) and cross-section and detail of the blind with the PVT concentrator (**c**).

The concentrating system consists of two holographic lenses that focus incident irradiance toward the PVT module. Both lenses are attached to the same glass substrate, which at the same time closes the space between them.

A diagram of the ray-tracing is represented in Figure 2. Three different wavelengths in the range of maximum spectral response of the Si PV cell are depicted to show the rays' spatial distribution at the *YZ* plane. On the right, a sketch illustrating the rays in the direction of the blind longitude represents the incidence along the x-axis (*XZ* plane), which corresponds to the solar azimuth movement. In this dimension, the length of the PVT receiver is slightly shorter than the length of the holographic lens to avoid vignetting effects. The azimuth angle translated to the entrance pupil's plane is named as φ. The maximum φ accepted by the concentrator is indicated in the figure.

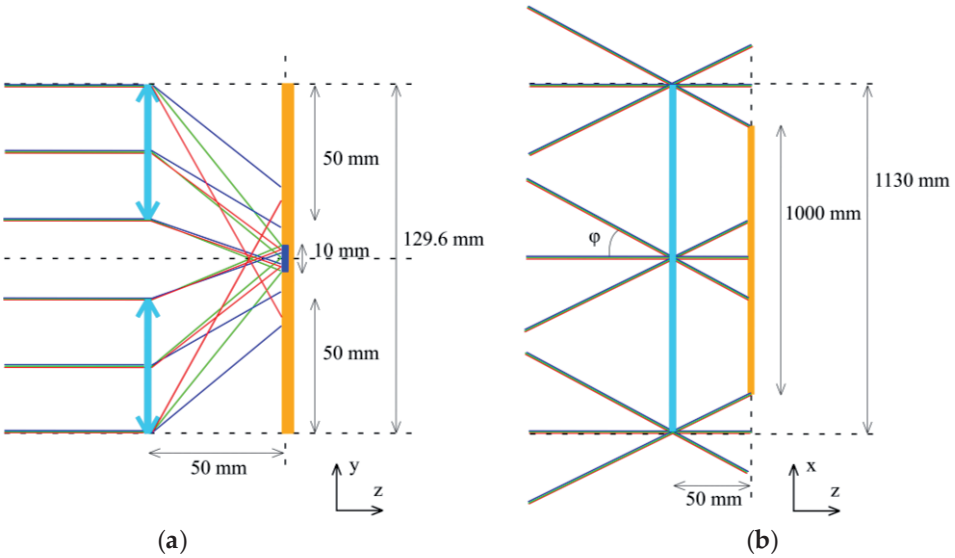

Figure 2. Schematic of the HCPVT generation unit, with ray-tracing for rays with three different wavelengths: 700 (depicted with blue lines), 800 (green lines) and 900 nm (red lines), at the *YZ*- (**a**) and *XZ*-plane (**b**).

2.1. Holographic Optical Element

A cylindrical holographic lens is chosen as a solar concentrator HOE. The recording of such lens is carried out by means of the interference of a plane wave and a cylindrical wave onto a photosensitive medium, as shown in Figure 3. This turns into variations of the refraction index along the material.

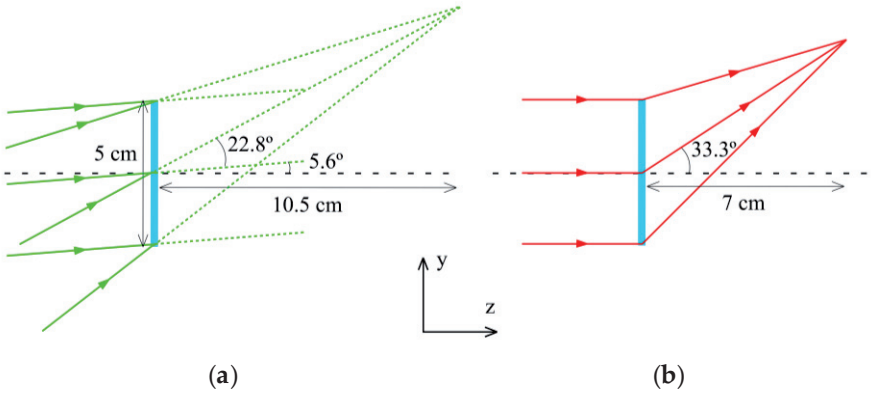

Figure 3. Sketch of the recording (**a**) at 532 nm, and reconstruction (**b**) at 800 nm schemes of the holographic cylindrical lens simulated in this study.

When illuminating a volume hologram at the reconstruction stage, only two waves are found at its output: the transmitted wave and the diffracted wave. With the adequate incident conditions (wavelength and angle), the efficiency of the diffracted beam is maximal, and it can reach 100% for a selected wavelength if the design is also optimum. When illuminating a holographic cylindrical lens with a plane wave, the resulting diffracted wave is a cylindrical one, as it is shown in Figure 3.

The reconstruction wavelength for which the HOE will be most efficient is set at 800 nm. This value results from a compromise between the incident solar spectrum (with maximal intensity at wavelengths around 500–800 nm most of the day) and the photovoltaic cell sensitivity (optimum around 700–1000 nm for mono-Si cells). Incident light at 800 nm will focus at a line parallel to the *x*-axis, 7 cm away from the HOE, as it is shown in Figure 3. However, the PVT module is placed at 5 cm away from

the HOE, in order to collect more energy of the desired wavelength range, since rays with different wavelengths are led towards different directions, as it is illustrated in Figure 2.

Holograms present higher angular selectivity when the incidence direction varies in the plane formed by the two recording beams, and lower in the perpendicular plane. Taking advantage of this effect, a cylindrical lens offers the possibility of suppressing tracking in one direction. Therefore, tracking is only necessary along the direction with higher angular selectivity.

The proposed recording material of the HOE is Bayfol HX, a photopolymer manufactured by Covestro AG (formerly Bayer MaterialScience) [17], adequate for holographic recording with solar photovoltaic applications [18].

In the configuration chosen for this study, two HOEs are placed separated in the same *XY*-plane, so that the spatial distributions of the diffracted beams are symmetrical. A glass plate located in this plane serves as a substrate for the photopolymer, covers the space between the two HOEs and is assumed to have the same refractive index as the photopolymer. The distance between the two lenses, and therefore, the position of the PV cell in the *y*-axis, was optimized so that it would receive more energy at the most favourable wavelength range for the cell. The ratio between the x dimension of the HOEs and the PV cell was chosen to avoid vignetting on the cell of its optimal wavelength range (700–1000 nm). Angles of incidence φ larger than the one depicted in Figure 2, when vignetting would occur for the optimal bandwidth, result in total internal reflection and prevent the former effect.

2.2. Hybrid Photovoltaic-Thermal Module

The PVT module units are considered to be 100 cm long by 12.96 cm wide; thus every shading blind of 9 m is composed of nine PVT modules. Every PVT module is formed by seven 14.29 cm long by 1 cm wide cells connected in series. The photovoltaic cells considered in the simulation are based on commercial mono-crystalline cells by Sunways [19], whose main electrical characteristics are summed up in Table 1. The characteristics of the thermal receiver are detailed in Section 3.2.

Table 1. Parameters of the PV cells, reprinted with permission from [19], copyright Sunways AG · Photovoltaic Technology · Max-Stromeyer-Str. 160 · D-78467 Konstanz. SD310912A version 03/13 EN.

V_{OC} (V)	J_{SC} (A/m^2)	*FF* (%)	γ (%/°C)	T_{NOCT} (°C)
0.635	377.6	78.4	−0.44	45

Notes: V_{OC} = Open circuit potential; J_{SC} = Short circuit current density; *FF* = Fill factor; γ = Power temperature dependence losses; T_{NOCT} = Nominal operating cell temperature.

3. Methodology

3.1. Spectra Simulation

The direct normal irradiance spectrum is calculated with the SMARTS radiative model [20], whose main atmospheric input parameters are (listed by order of importance): Air mass (*AM*), aerosol optical depth (τ), precipitable water (*PW*) and Ångström exponent (α).

Air mass is the parameter that normally affects more the spectrum. It is defined as the relative distance to the shortest vertical path length the sunrays traverse through the atmosphere before impacting the Earth's surface. SMARTS calculates the *AM* from the solar zenith angle (*Z*) for the location and time considered:

$$AM = \left[\cos Z + 0.45665 Z^{0.07} \left(96.4836 - Z\right)^{-1.7960}\right]^{-1} \quad (1)$$

τ refers to the quantity of aerosols in the vertical direction (urban haze, smoke particles, desert dust, sea salt ...) and characterizes its radiative strength. The τ at wavelength (λ) is linked to the Ångström exponent (α) by the Ångström law, where β (also called Ångström turbidity coefficient) is the aerosol optical depth at $\lambda = 1$ μm.

$$\tau = \beta\lambda^{-\alpha} \quad (2)$$

Values of α greater than 2 indicate the presence of fine particles (e.g., smoke particles or sulphates), whereas values close to zero are typically related to the presence of coarse particles, such as sea salt or desert dust [21].

Finally, *PW* is the total amount of condensed water (expressed in cm) corresponding to the total water vapour contained in a vertical atmospheric column above any location. Water vapour has strong absorption bands in the near infrared, which directly impacts the spectrum.

Measured values of *Z*, τ, *PW* and α, can be obtained from the Aerosol Robotic Network (AERONET) database [22]. For this study, only AERONET's level 2.0 data are used to guarantee the highest possible data quality (after cloud screening, calibration and degradation correction [23]).

τ at 500 nm and α (obtained between 440 and 870 nm) are retrieved. The latter provides both the α1 and α2 values required by SMARTS. This approach is considered because the single-α model is closer to the original Ångström definition and experimental errors associated with small-band determinations of the τ variation are decreased [24].

Detailed information on the sunlight spectrum for at least a complete year is required in order to accurately estimate the energy output of the PVT module. Therefore, a preliminary search on AERONET's database has been done to select only those locations and years with a high density of atmospheric retrievals. These retrievals are performed at least every 15 min for *AM* less than 5. Following the procedure described by Chan et al. [25], measurement gaps longer than 15 min are considered to be caused by extended cloudiness, not computing this time for the annual yield. In addition, the selected locations should be suitable for CPVT systems and have a high direct normal irradiance (DNI).

Two different locations have been selected according to three criteria: (i) they should be representative of different climatic conditions to provide not only differential spectral conditions, but also different electrical and thermal energy demands; (ii) they should provide high-quality data over an extended period of time (a constraint satisfied by only a small fraction of AERONET sites); and (iii) they should have co-located and simultaneous DNI measurements, in order to validate the simulated spectra. Based on the above criteria, Sde Boker, Israel, (2004) and Avignon, France, (2003) have been chosen (Table 2).

Table 2. Characteristic parameters for the selected locations.

Location	Simulated Year	Lat. (°)	Long. (°)	Elevation (m)	Mean Daily DNI (kWh/m^2/day) [26]	Annual Mean Atmospheric Parameters *AM* ǀ τ ǀ *PW* ǀ α
Sde Boker	2004	30.86	34.78	480	6–6.5	1.92 ǀ 0.18 ǀ 1.34 ǀ0.86
Avignon	2003	43.93	4.88	32	5–5.5	2.16 ǀ 0.25 ǀ1.76 ǀ 1.37

Figure 4 illustrates the monthly variation of the most representative atmospheric parameters obtained by AERONET at the selected locations. These graphs conveniently display the amplitude with which each variable varies throughout the simulation year.

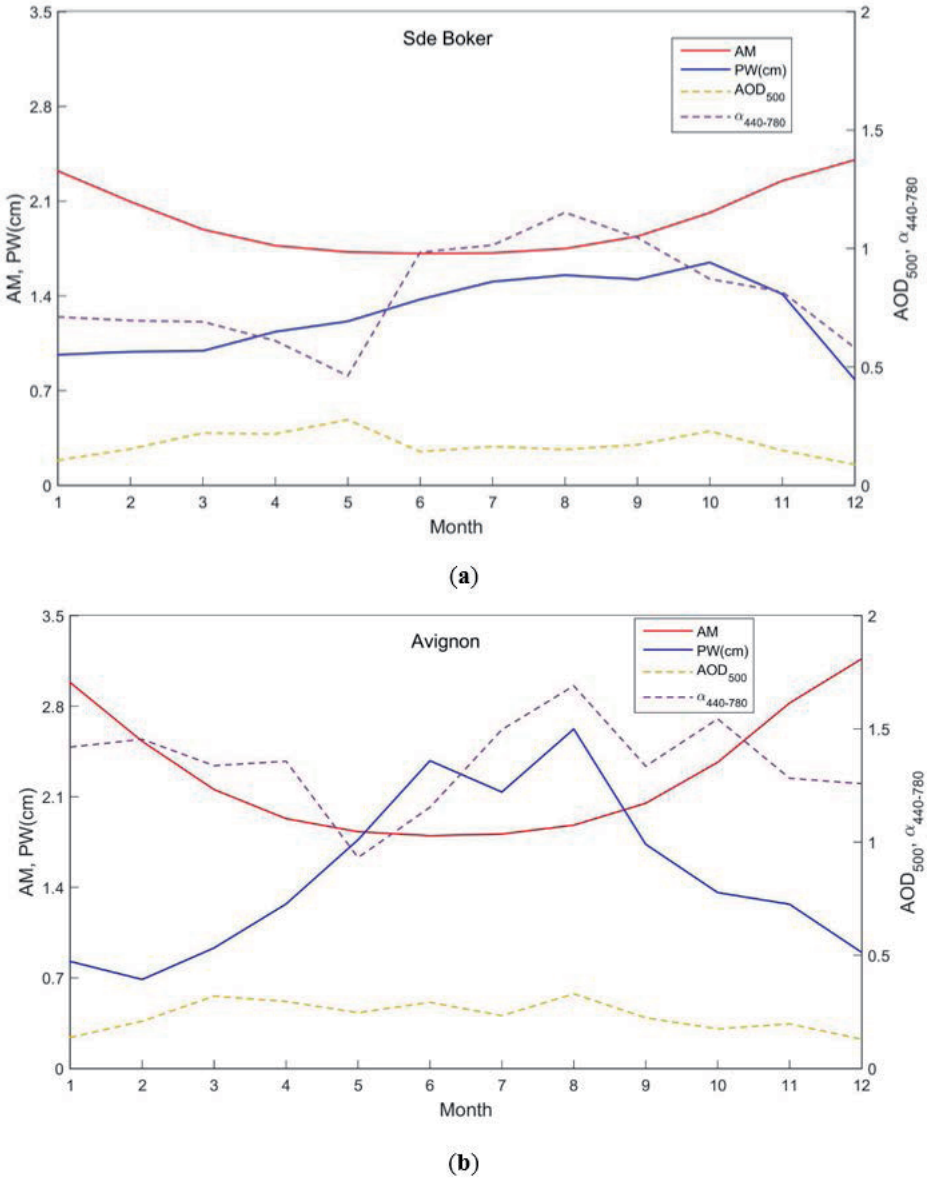

Figure 4. Monthly-average values of the main atmospheric variables for the simulated sites, obtained from AERONET. In the case of *AM*, the values are limited to $AM < 5$, in agreement with AERONET measurements. (**a**) Sde Boker and (**b**) Avignon.

Finally, the validation of the spectra generated by SMARTS is undertaken by comparing the calculated broadband DNI to reference irradiance measurements obtained from the Baseline Surface Radiation Network (BSRN) [27]. A good agreement is achieved between the simulated and the measured data, as depicted in Figure 5, showing the irradiance profiles for two different typical days in both locations. It should be stressed that the large drops in the measured data, due to clouds obscuring the sun, are not modelled in the simulations. In the case of Avignon, the validation has been conducted using DNI data from the BSRN station in Carpentras, located around 28 km away.

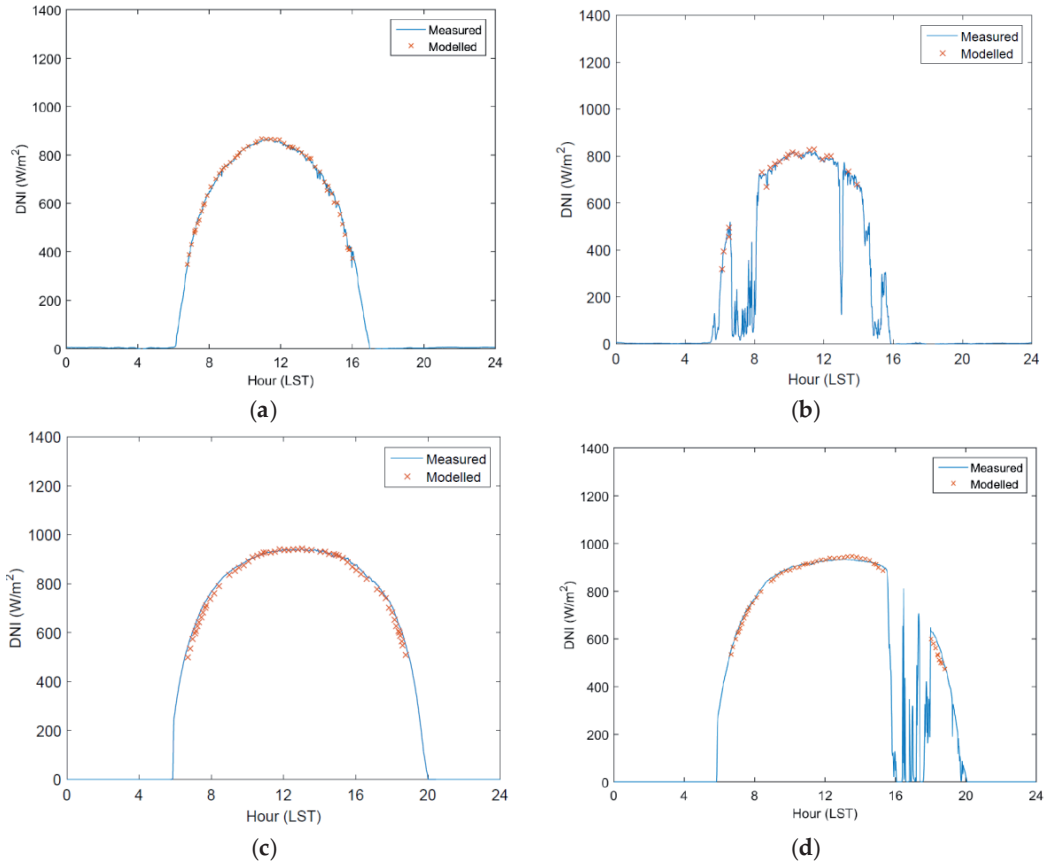

Figure 5. DNI data in Sde Boker under stable (**a**) and variable irradiance conditions (**b**) and in Avignon (**c**,**d**). The dates are respectively 19th of October, 20th of April, 1st of August and 30th of July in the selected simulated years. LST: Local standard time.

3.2. Optical Simulation

The performance analysis of the holographic lens is based on Kogelnik's Coupled Wave Theory [28] and the approximate scalar theory established by Syms [29]. A ray-tracing algorithm has been developed [30], which allows the calculation of the output directional cosines and the spectral energy associated with each ray, for the transmitted and the diffracted wave delivered to the PVT module.

The propagation wave vectors of the recording beams, $\vec{k}_1$ and $\vec{k}_2$, with modulus $k_1 = k_2 = 2\pi/\lambda_R$ (where λ_R is the recording wavelength), determine the grating vector $\vec{K} = \vec{k}_1 \pm \vec{k}_2$, illustrated in Figure 6.

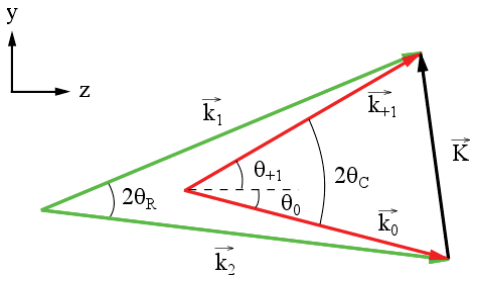

Figure 6. Sketch of the relation between the grating vector $\vec{K}$ and the wave vectors of the two recording beams, $\vec{k}_1$ and $\vec{k}_2$, and the transmitted and diffracted waves, $\vec{k}_0$ and $\vec{k}_{+1}$.

Since one of the recording beams is a cylindrical wave, its propagation wave vector has a different direction at each point along the y-direction, and the angle between beams is also different. Therefore, the vector $\vec{K}$, which is perpendicular to the planes with constant refractive index variation, is spatially dependant. Its modulus is $2\pi/\Lambda$, where Λ is the spatial period of a grating with vector $\vec{K}$, and also different at each point. Each point of the holographic lens behaves differently; thus, each point is treated as a local holographic grating.

When illuminating the HOE with a wave with vector $\vec{k}_0$ and a certain wavelength λ_C, the resulting diffracted wave has a vector $\vec{k}_{+1}$, which has the same modulus as $\vec{k}_0$ and direction determined with $\vec{k}_0$ and $\vec{K}$. This relation is shown in Figure 6. Thus, if the vector $\vec{K}$ along the hologram is known, the direction of the diffracted ray originated with each incident reconstruction ray at a certain point can be calculated.

The energy of the diffracted wave from each point is calculated with Equation (3):

$$\eta = \frac{\sin^2\left[\left(\nu^2 + \xi^2\right)^{1/2}\right]}{1 + \frac{\xi^2}{\nu^2}} \tag{3}$$

The parameters ν and ξ are given by:

$$\nu = \frac{\pi d \Delta n}{\lambda_C c_0 c_{+1}} \tag{4}$$

$$\xi = \frac{d\vartheta}{2c_{+1}} \tag{5}$$

where d is the thickness of the recording material, Δn is the refraction index modulation, λ_C is the reconstruction wavelength, and c_0 and c_{+1} are the directional cosines with respect to the z-axis of the reconstruction and diffracted wave, respectively. ϑ is a parameter that determines the variation from Bragg's law, that is, the condition of maximal efficiency. Bragg's law is met when the next equation is fulfilled:

$$2\Lambda \sin\theta_C = \lambda_C \tag{6}$$

where θ_c is the semiangle between the transmitted and the diffracted beam, shown in Figure 6. When Bragg's condition is not fulfilled the efficiency of the diffracted wave decreases, and the efficiency of the transmitted wave increases.

The energy of the transmitted wave is calculated as the remaining available energy that is not taken by the diffracted wave, at each point and for each reconstruction wavelength. The rays entering the system through the glass plate between the two HOEs are also considered.

The simulation considers the direct normal irradiance solar spectrum, generated by SMARTS, as the incident irradiance input parameter. Nevertheless, due to the implicit difficulty and computational time required, the solar semiangle and the diffuse irradiance fraction are not considered at this stage. Further research will be conducted to define the algorithm containing the particular angles of incidence and polarization constraints of the diffuse radiation, jointly with the implementation of the solar semiangle. Therefore, it should be taken into account that the irradiance delivered by the holographic concentrator is underestimated in a percentage proportional to the diffuse fraction at each simulated location. Losses due to Fresnel reflections on the surface and to total internal reflection [31] are taken into account in the simulations.

3.3. Energetic Simulation

The energetic simulation is conducted in TRNSYS, evaluating the HCPVT performance under the weather and energy demand conditions of Sde Boker and Avignon. Figure 7 charts the monthly

cumulated DNI values and the monthly average ambient temperatures in both locations. In Sde Boker the annual cumulated DNI is 2445 kWh/m^2 and the annual mean temperature is 18.3 °C, in Avignon these values are 1860 kWh/m^2 and 14.7 °C respectively. It should be noticed that, in agreement with AERONET criteria, values with $AM > 5$ (solar altitude below 11.5°) are not considered and, taking into consideration the optical efficiency limitations of the concentrating system, the direct beam irradiances accepted by the HCPVT module will be significantly lower than the DNI values. Results regarding optical efficiencies are included in Section 4.

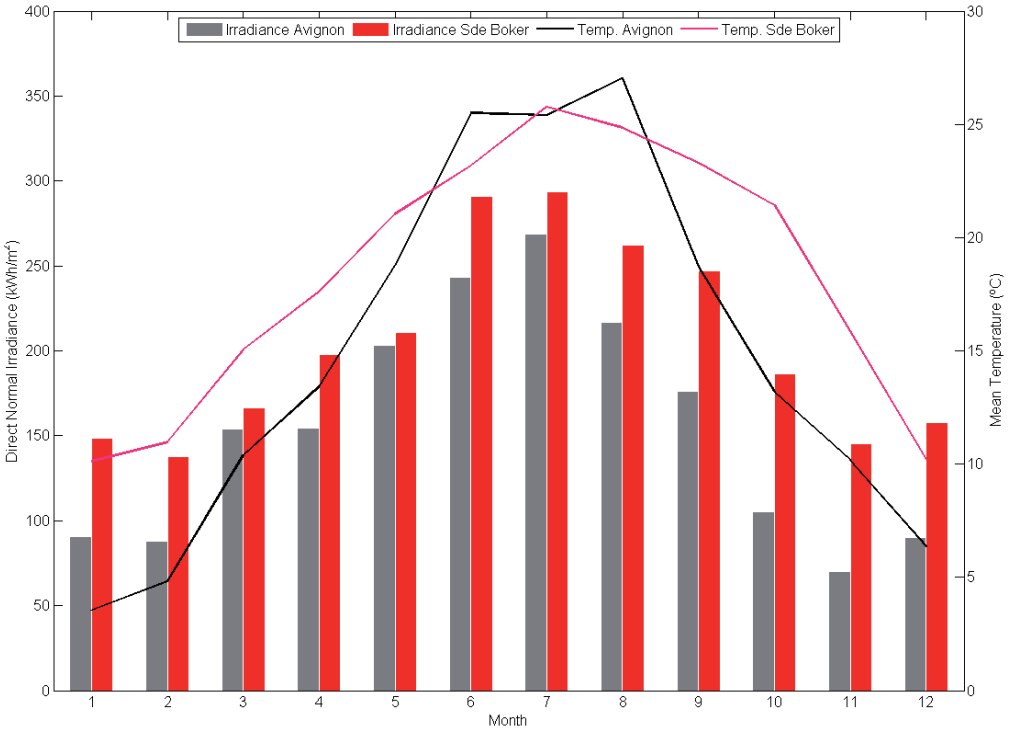

Figure 7. Monthly cumulated DNI and mean temperature values.

The energy demand considered corresponds to a three person individual family house with two floors of 80 m^2 each. The main façade, where the solar system is installed, is south-oriented. The thermal demand for space heating (SH) has been determined using the TRNBUILD tool considering the following thermal transmittance coefficients: 0.74 W/m$^2\cdot$ °C for the exterior walls, 0.5 W/m$^2\cdot$ °C for the roof and 2.1 W/m$^2\cdot$ °C for the windows. The space heating load is calculated to maintain the interior temperature at 20 °C. The domestic hot water (DHW) demand has been determined assuming a water consumption of 30 liters per person at 60 °C.

The electrical energy demand profiles have been estimated to reflect the importance of the air conditioning consumption during hot months, representing the highest load in Sde Boker, and a profile where the minimum of the curve is centered in summer (Avignon).

The cumulated annual energy demands for DHW, SH and electricity at Sde Boker and Avignon are listed in Table 3. As it can be appreciated, the DHW energy demand is 23% higher at Avignon than at Sde Boker due to its lower ambient temperatures. The same behavior is observed in the SH demand, whose value at Avignon is more than twice the one at Sde Boker, considering the colder climate during winter period. Conversely, in the case of the electrical energy demand the annual value at Sde Boker is quite bigger than at Avignon (24%) because of the air conditioning load during the hot months.

Energies **2016**, *9*, 577

Table 3. Energy demand cumulated annual values.

Location	DHW (kWh)	SH (kWh)	Electricity (kWh)
Sde Boker	1589	7813	4433
Avignon	1955	16624	3575

Once determined the energy demands for both places, the following system topology has been implemented in the simulation for both locations (Figure 8):

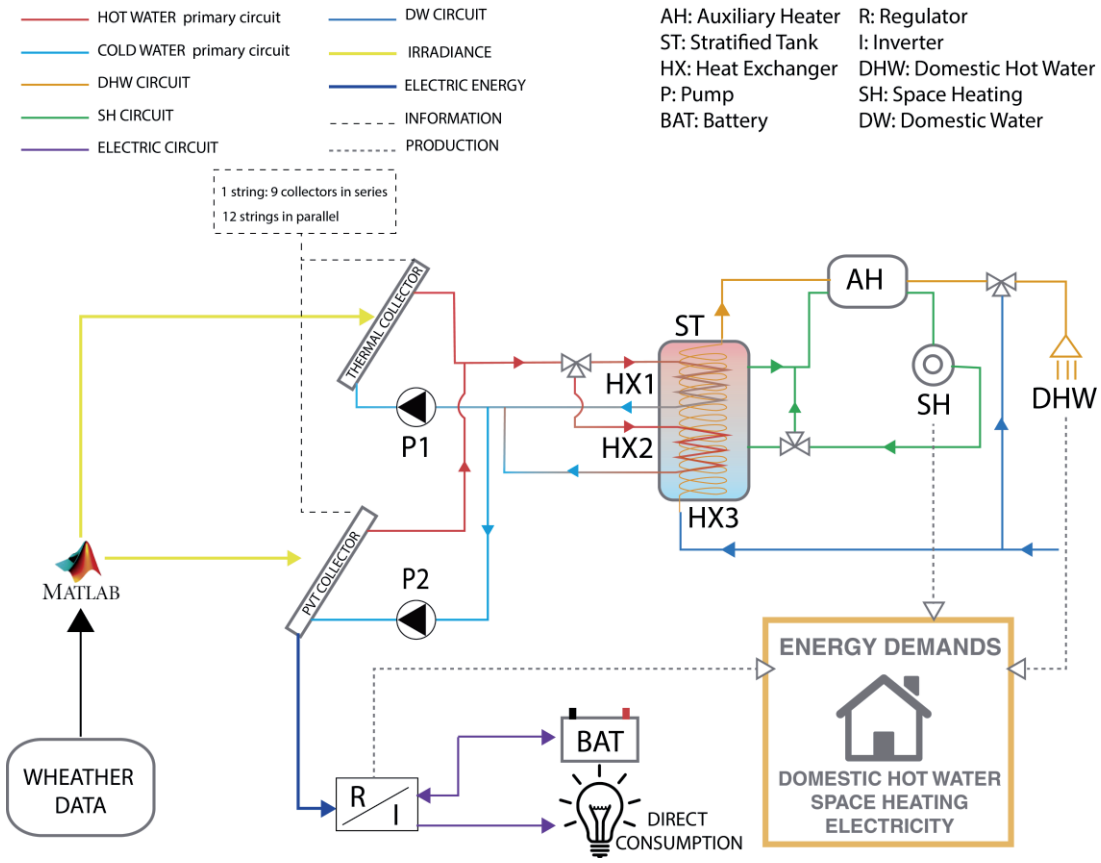

Figure 8. Simulated system topology.

The optical simulation program described in Section 3.2, which is programmed in MATLAB, is linked to TRNSYS delivering at every time step (1 min) the irradiance impacting on the PVT module, differentiating between the PV cell area where the irradiance is concentrated, named PVT collector, and the rest of the module, which is indicated in the system topology scheme as thermal collector (see Figure 8). From the irradiance received on the module, the thermal energy produced is calculated in two different ways: (i) for the receiver where there is no PV cell a standard *type 1b* has been used including the characteristics of a real commercial thermal module specified in Table 4; (ii) for the receiver where the PV is situated, strictly the PVT, a MATLAB code has been programmed which determines the electrical power (P'_{mpp}) coupled with the thermal generator *type 1b*, as a function of the solar cell electrical parameters and the cell temperature, calculated with the following Equation (7) [32]:

$$P'_{mpp} = P_{mpp}\left[1 + \gamma\left(T_{cell} - 25\right)\right] \quad (7)$$

where P_{mpp} is the electrical power generated by a PV cell without taking into account losses due to the temperature, γ is a temperature coefficient equal to $-0.44\%/^{\circ}C$ for the PV cells considered in this

study, and T_{cell} is the temperature of the cell in °C. The temperature of the cell of the PVT module is estimated with Equation (8) [33]:

$$T_{cell} = T_{in} + \frac{P_{th}}{F' U_L A} \left(1 - F'\right) \tag{8}$$

where T_{in} is the input temperature of the water circulating at each module, P_{th} is the power generated by the thermal absorber, F' is the collector efficiency factor, U_L is the overall convective heat loss coefficient of the collector and A is the surface of the collector. T_{in} and P_{th} values are obtained from the previous time step, considering the error to be minimum.

Table 4. Parameters of the thermal collector [34].

η_0 (%)	U_L (W/m^{2}K)	k_2 (W/m^{2}K^2)	F'	ε (%)	α (%)	τ (%)
79.9	3.97	0.016	0.913	5.0	95.5	91.6

η_0 = Efficiency; U_L, k_2 = Coefficients of heat loss; ε = Emission; α = Absorption; τ = Transmission and F' = Collector efficiency factor ($F' = \eta_0/\tau\alpha$).

The electrical power of the cell P_{mpp} without temperature effects is calculated with:

$$P_{mpp} = J_{SC} V_{OC} FF \tag{9}$$

The short circuit current, J_{SC} is calculated taking into account the spectral response curve of the mono-crystalline silicon solar cell manufacturer. The values of the open circuit voltage V_{OC} and the fill factor FF are assigned from the technical characteristics of the simulated solar cells (see Table 1).

4. Results

The optical efficiency of the concentrating holographic system is defined in Equation (10) as the ratio between the irradiance received at the generator surface, differentiated in the area where the PV is situated (A_{PV}) and the rest of the area where it is the thermal absorber (A_T), and the irradiance at the entrance pupil area of the system (A_E). The irradiances on the PV, thermal absorber and entrance pupil are respectively I_{PV}, I_T and I_E:

$$\eta_{opt} = \frac{I_{PV} A_{PV} + I_T A_T}{I_E A_E} \tag{10}$$

The average optical efficiency obtained each month with the solar irradiance of both locations is presented in Figure 9. The fact that the system works better during the winter months than the summer months may seem counterintuitive. However, it is due to the lack of tracking of the system in the azimuth direction, since the maximum optical efficiency is reached when the azimuth angle, φ, is zero (at solar midday), and decreases when the absolute value of this angle increases.

The azimuth angle reaches greater values in summer; therefore, the optimum incident angle range is found during less time each day, which results in lower optical efficiency, because of the angular selectivity of the HOEs. It should also be noticed that the performance of the optical system is better for Avignon than for Sde Boker, since the latter is located at lower latitude, and has larger values of φ along the year than Avignon. Moreover, the building integration imposes geometrical restrictions on the system: although it tracks the solar altitude movement of the sun, too large values of this parameter (which occur at solar midday in the summer months at Sde Boker) cause shading between blinds, and then the incident irradiance does not impact on the concentrator for those time periods.

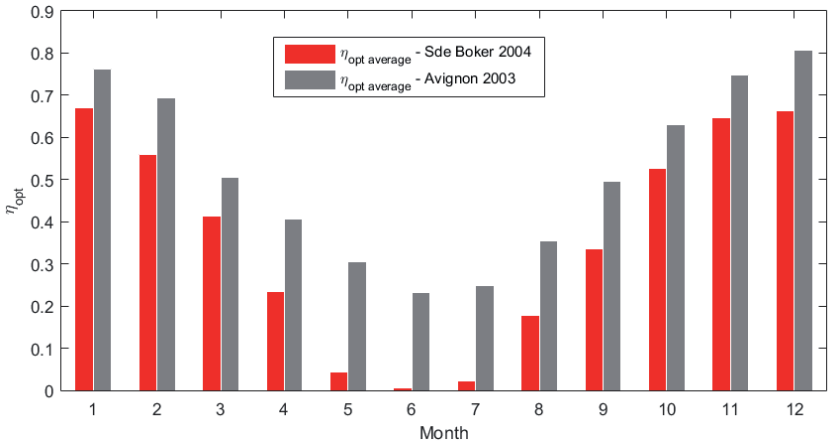

Figure 9. Average optical efficiency of the concentrating holographic system obtained each month with incident radiation of Sde Boker (2004) and Avignon (2003).

The incident mean annual spectral irradiance received at the surface of the PV cell and at the surface of the thermal absorber, determined by means of the optical simulation described in Section 3.2, is plotted in Figure 10, together with the incident solar spectral irradiance received at the entrance of the system. One of the most remarkable aspects of this graph is the shift of the peak wavelength of the spectrum that reaches the PV cell, compared to the solar spectrum. This effect is caused by the chromatic selectivity of the HOEs, which are designed to perform more efficiently around 800 nm. It is also clearly noticeable the difference between the spectra of Sde Boker and Avignon: due to the angular selectivity of the HOEs, the optical concentrator is more efficient at Avignon's latitude, although the incident irradiance is higher at Sde Boker. This results in a maximum incident irradiance value on the PV cell that doubles the maximum of the solar incident irradiance in Avignon. The shape of the spectral irradiance received by the thermal absorber is rather similar to the solar spectra of both locations, except for the optimum wavelength range of the PV cell. The irradiance received at Avignon is higher than the one received at Sde Boker, as expected.

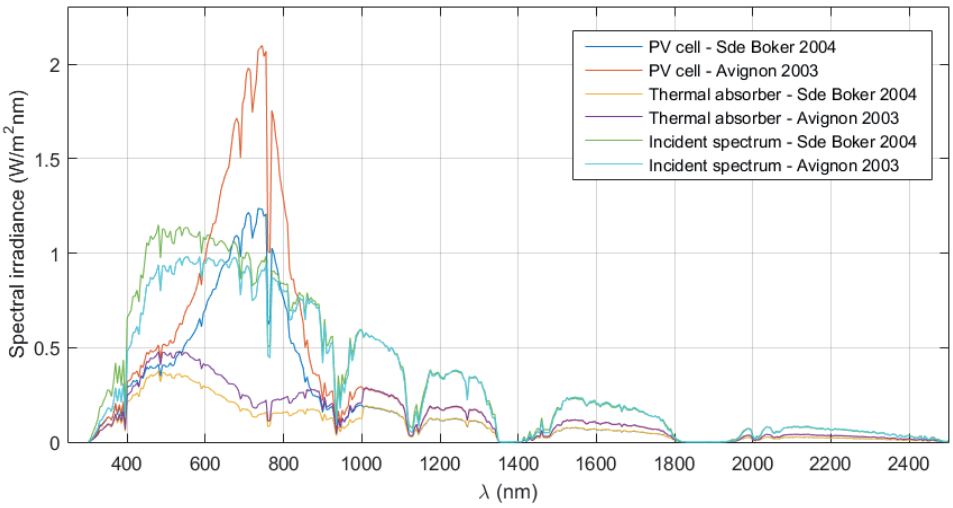

Figure 10. Average spectral irradiance at the entrance of the system, at the PV cell and at the thermal absorber at both locations.

The DHW energy demand is stated in the simulations to be satisfied prior to the SH demand. To evaluate the percentage of DHW demand that is covered by the HCPVT, the solar fraction is defined as:

$$SF_{DHW} = 100\left(1 - \frac{Consumption_{auxiliary,DHW}}{Demand\ DHW}\right) \quad (11)$$

In the case of Sde Boker, the solar thermal production covers well all the months except May, June and July. This happens because, as explained previously, the solar altitude is very high during these months and the system only accepts values lower than 71°. In the case of December, the values of production are not representative as only few days of atmospheric values are provided in AERONET. Following the tendency of the previous and next months a value of the solar fraction close to 100% should be expected (see Figure 11a). In Avignon, the HCPVT system accepts all the solar height angles, and in consequence the solar fraction takes a value of almost 100% in all the months. The annual solar production for DHW applications results in Sde Boker of 1218 kWh and in Avignon takes a value of 1869 kWh.

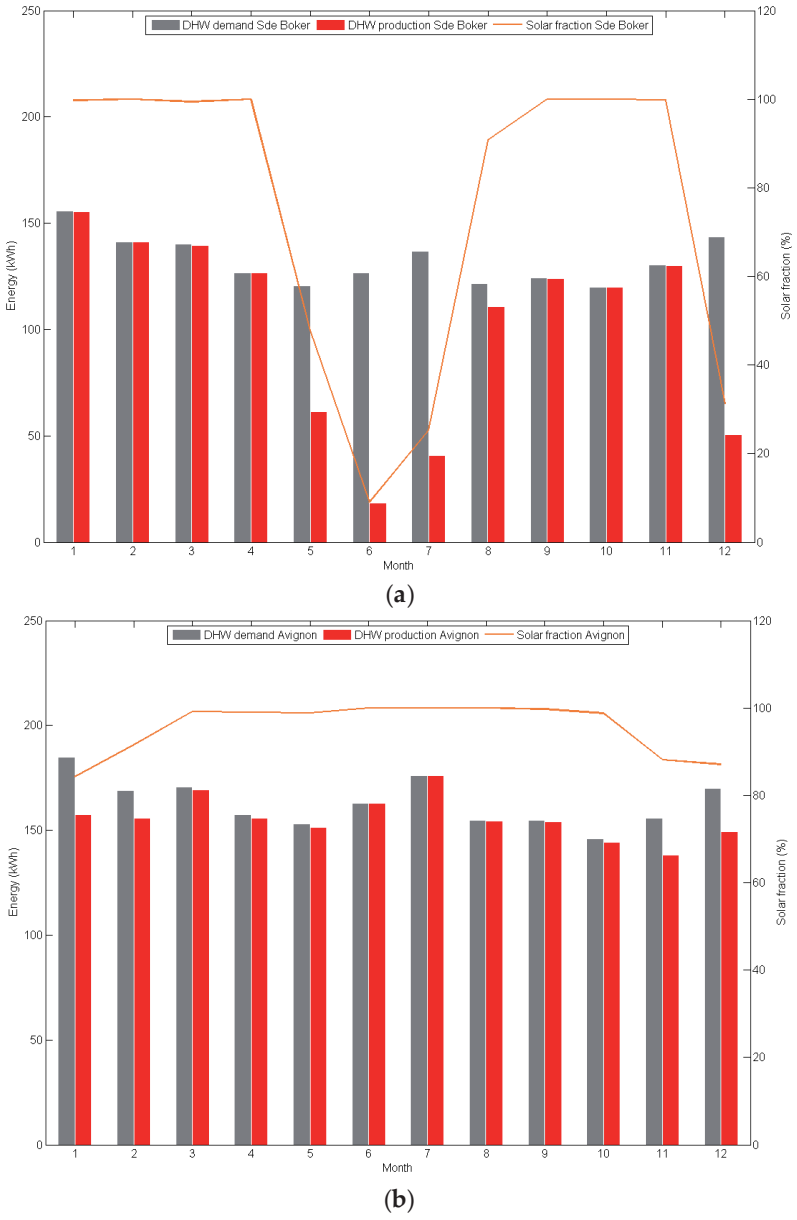

Figure 11. DHW energy demand, production and solar fraction in Sde Boker (**a**) and Avignon (**b**).

The solar production aims at partially covering the SH demand, taking into consideration that the collector total area is quite low, approximately 14 m^2. The heating system considered is a radiant floor which impulsion temperature is assumed to be 42 °C and the return one to be 34 °C. In an analogous manner than in the DHW, the solar fraction covering the SH demand is expressed as:

$$SF_{SH} = 100\left(1 - \frac{Consumption_{auxiliary,SH}}{Demand\,SH}\right) \quad (12)$$

Figure 12 plots the monthly SH demand and solar production, indicating that in Sde Boker there is no SH need during almost 6 complete months. In the rest of the months the solar fraction present values of around 20% (20.1%). On the contrary, Avignon is more demanding in SH energy, achieving in this case an average solar fraction of 15.8%.

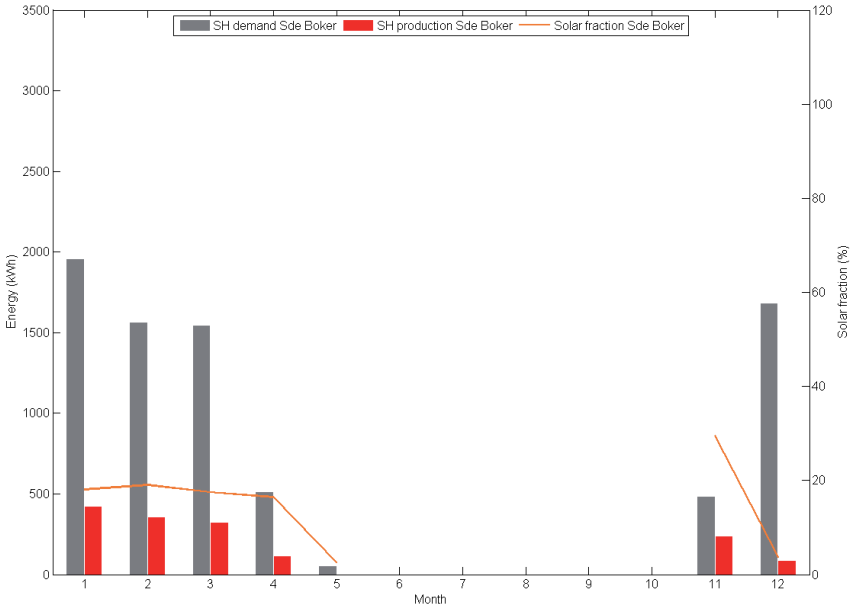

Figure 12. SH energy demand, production and solar fraction in Sde Boker (**a**) and Avignon (**b**).

The photovoltaic production results are included in Figure 13, where the solar fraction has been calculated with Equation (13). It can be seen that in both places the average solar fractions are near 10% (Sde Boker = 7.4% and Avignon = 9.1%), which is a very positive result considering that the PV net area is 1.08 m^2 and the electric demand values are important.

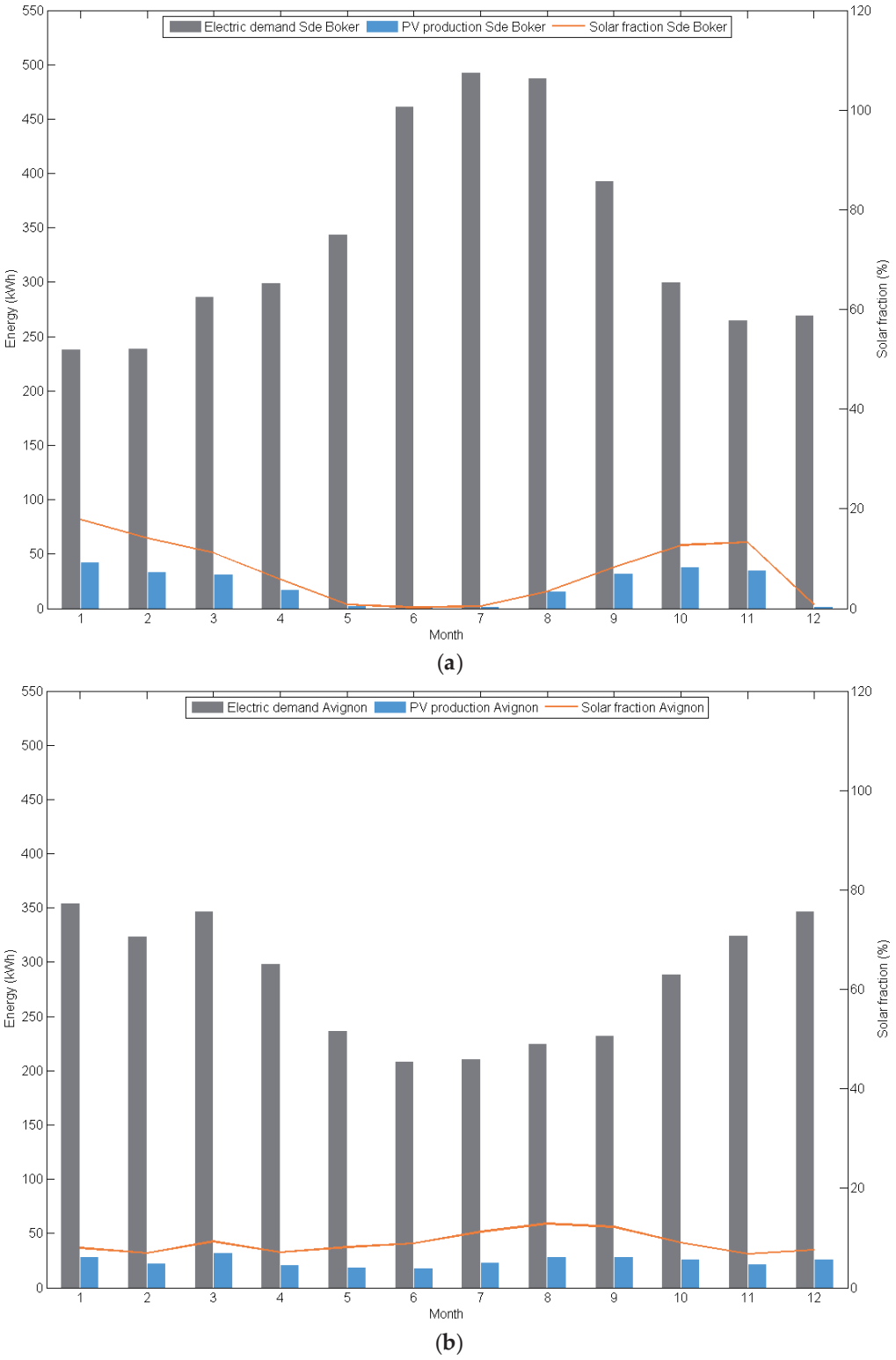

Figure 13. Electrical energy demand, production and solar fraction in Sde Boker (**a**) and Avignon (**b**).

This good performance is obtained due to the holographic optical element effect which concentrates on the cell only the bandwidth for which it is more sensitive and does not concentrated the infrared avoiding overheating. At the same time, the temperature of the cell is also controlled by the active cooling system incorporated in the PVT module (see Table 5):

$$SF_{PV} = 100 \left(\frac{Photovoltaic\ production}{Electric\ demand} \right) \quad (13)$$

Table 5. Summary of system efficiencies.

Month	Average Optical Efficiency (%)		Average Thermal Efficiency DHW (%)		Average Thermal Efficiency SH (%)		Average Electrical Efficiency (%)	
	Sde Boker	Avignon	Sde Boker	Avignon	Sde Boker	Avignon	Sde Boker	Avignon
January	67.1	76.3	11.9	19.7	28.2	22.0	22.4	16.6
February	56.1	69.5	12.5	21.7	27.7	19.2	27.7	15.2
March	41.4	50.5	13.1	16.8	26.6	23.9	23.5	17.0
April	23.3	40.6	17.2	20.3	14.2	20.9	29.9	14.3
May	4.3	30.4	45.8	23.0	1.0	15.0	22.6	15.8
June	0.7	23.1	56.3	27.2	0.0	5.7	23.1	16.8
July	2.2	24.8	51.5	23.4	0.0	0.0	24.4	16.8
August	17.8	35.5	18.9	17.0	0.0	0.0	19.7	16.8
September	33.5	49.6	11.4	17.2	0.0	9.9	23.7	16.5
October	52.6	63.1	10.0	16.2	0.0	21.2	21.9	14.7
November	64.7	74.9	11.6	23.1	18.5	20.1	19.7	16.9
December	66.2	80.6	17.5	22.0	28.9	20.5	17.6	17.3

Finally, in Table 5 the monthly average efficiencies of the main system components are presented. The optical efficiency values correspond to those plotted in Figure 9. It is important to highlight one of the most differential aspects of the present simulated system, which is the electrical efficiency values obtained. These values are high in comparison with standard PV installations, achieving in some months numbers above 25%. This performance is obtained, as mentioned previously, due to the proper combination of two factors: the active cooling and the spectrally selective concentration obtained by the HOEs.

5. Conclusions

A building-integrated holographic concentrating photovoltaic-thermal system has been designed and simulated. The module has been placed on the blinds of a solar louvre, which track the solar altitude movement of the sun along the day, on a south-oriented façade.

The direct normal irradiance solar spectra along one year have been calculated with the SMARTS radiative model, utilizing AERONET atmospheric parameters, for two locations (Sde Boker and Avignon), to test the concentrating system proposed under different conditions. These spectra have been verified with direct irradiance measurements obtained from the Baseline Surface Radiation Network (BSRN), which proved the high accuracy of the simulations.

The behavior of the holographic concentrator, based on two holographic cylindrical lenses, was simulated by means of a ray-tracing algorithm. It concentrates toward the cell mainly its optimal wavelength range and also distributes the rest of the spectral irradiance on the thermal absorber, reaching a total optical efficiency. The annual average optical efficiencies obtained for Sde Boker and for Avignon are 30.3% and 43.0%, respectively. A MATLAB-TRNSYS coupling was implemented to run simultaneously the optical, the thermal and the electrical simulation for the two locations weather data files.

The electrical energy generated by the PV cell aims at partially covering the electrical demand and the thermal energy produced by the module is managed to satisfy the domestic hot water energy (priority) and partially the space heating energy requirements, of a house of a three people family.

In the case of the domestic hot water energy demand, which was considered a priority, the average solar fractions found were 79.3% for Sde Boker and 95.5% for Avignon. On the other hand, the proposed system covered more than 15% of the space heating demand at both locations (Sde Boker = 20.1% and Avignon = 15.8%). Regarding the electrical energy produced, more stable values were obtained in the case of Avignon throughout the year; however, at both locations the mean annual values were quite satisfactory, near the 10% (Sde Boker = 7.4% and Avignon = 9.1%). A future work of the present study is the construction and experimental characterization for the system performance validation.

Acknowledgments: This research was supported by 'Ministerio de Economía y Competitividad' of Spain for the funding (grants ENE2013-48325-R and BES-2014-069596), the Generalitat de Catalunya (grant 2016 FI_B1 00019), the UdL-Santander Bank (UdL-Impuls grant) and the Diputación General de Aragón-Fondo Social Europeo (TOL research group, T76).

Author Contributions: The research team works in a collaborative manner and all the authors have contributed in all the sections of the present manuscript.

Conflicts of Interest: The authors declare no conflict of interest.

References

1. Directive 2010/31/EU of the European Parliament and of the Council of 19 May 2010 on the Energy Performance of Buildings. European Parliament: Strasbourg, France, 2010.
2. Menoufi, K.; Chemisana, D.; Rosell, J.I. Life Cycle Assessment of a Building Integrated Concentrated Photovoltaic scheme. *Appl. Energy* **2013**, *111*, 505–514. [CrossRef]
3. Collados, M.V.; Chemisana, D.; Atencia, J. Holographic solar energy systems: The role of optical elements. *Renew. Sustain. Energy Rev.* **2016**, *59*, 130–140. [CrossRef]
4. Zhang, D.; Castro, J.M.; Kostuk, R.K. One-axis tracking holographic planar concentrator systems. *J. Photonics Energy* **2011**, *1*. [CrossRef]
5. Castillo, J.E. Thermal effects of the extended holographic regions for holographic planar concentrator. *J. Photonics Energy* **2011**, *1*. [CrossRef]
6. Castro, J.M.; Zhang, D.; Myer, B.; Kostuk, R.K. Energy collection efficiency of holographic planar solar concentrators. *Appl. Opt.* **2010**, *49*. [CrossRef] [PubMed]
7. Chemisana, D.; Collados, M.V.; Quintanilla, M.; Atencia, J. Holographic lenses for building integrated concentrating photovoltaics. *Appl. Energy* **2013**, *110*, 227–235. [CrossRef]
8. Ludman, J.E.; Riccobono, J.; Semenova, I.V.; Reinhand, N.O.; Tai, W.; Li, X.; Syphers, G.; Rallis, E.; Sliker, G.; Martín, J. The optimization of a holographic system for solar power generation. *Sol. Energy* **1997**, *60*, 1–9. [CrossRef]
9. Zhang, D.; Gordon, M.; Russo, J.M.; Vorndran, S.; Kostuk, R.K. Spectrum-splitting photovoltaic system using transmission holographic lenses. *J. Photonics Energy* **2013**, *3*. [CrossRef]
10. Vorndran, S.; Russo, J.M.; Wu, Y.; Gordon, M.; Kostuk, R. Holographic diffraction-through-aperture spectrum splitting for increased hybrid solar energy conversion efficiency. *Int. J. Energy Res.* **2015**, *39*, 326–335. [CrossRef]
11. Ludman, J.E. Holographic solar concentrator. *Appl. Opt.* **1982**, *21*, 3057–3058. [CrossRef] [PubMed]
12. Xiao, C.; Yu, X.; Yang, D.; Que, D. Impact of solar irradiance intensity and temperature on the performance of compensated crystalline silicon solar cells. *Sol. Energy Mater. Sol. Cells* **2014**, *128*, 427–434. [CrossRef]
13. Chander, S.; Purohit, A.; Sharma, A.; Nehra, S.P.; Dhaka, M.S. A study on photovoltaic parameters of mono-crystalline silicon solar cell with cell temperature. *Energy Rep.* **2015**, *1*, 104–109. [CrossRef]
14. Iurevych, O.; Gubin, S.; Dudeck, M. Combined receiver of solar radiation with holographic planar concentrator. *IOP Conf. Ser. Mater. Sci. Eng.* **2012**, *29*. [CrossRef]
15. Froehlich, K.; Wagemann, E.U.; Frohn, B.; Schulat, J.; Stojanoff, C.G. Development and fabrication of a hybrid holographic solar concentrator for concurrent generation of electricity and thermal utilization. In Proceedings of SPIE, San Diego, CA, USA, 13–14 July 1993; pp. 311–319.

16. Xia, X.W.; Parfenov, A.V.; Aye, T.M.; Shih, M.-Y. Efficient hybrid electric and thermal energy generation. In Proceedings of SPIE, San Diego, CA, USA, 22–24 August 2011.
17. Berneth, H.; Bruder, F.-K.; Fäcke, T.; Jurbergs, D.; Hagen, R.; Hönel, D.; Rölle, T.; Walze, G. Bayfol HX photopolymer for full-color transmission volume Bragg gratings. SPIE Photonics West 2014-OPTO Optoelectron. *Devices Mater.* **2014**, *9006*. [CrossRef]
18. Marín-Sáez, J.; Atencia, J.; Chemisana, D.; Collados, M.-V. Characterization of volume holographic optical elements recorded in Bayfol HX photopolymer for solar photovoltaic applications. *Opt. Express* **2016**, *24*, A720. [CrossRef] [PubMed]
19. Sunways. Copyright: Sunways AG · Photovoltaic Technology · Max-Stromeyer-Str. 160 · D-78467 Konstanz. SD310912A version 03/13 EN. Available online: http://www.sunways.eu (accessed on 22 May 2013).
20. Gueymard, C.A. Parameterized transmittance model for direct beam and circumsolar spectral irradiance. *Sol. Energy* **2001**, *71*, 325–346. [CrossRef]
21. Eck, T.F.; Holben, B.N.; Reid, J.S.; Dubovik, O.; Smirnov, A.; O'Neill, N.T.; Slutsker, I.; Kinne, S. Wavelength dependence of the optical depth of biomass burning, urban, and desert dust aerosols. *J. Geophys. Res. Atmos.* **1999**, *104*, 31333–31349. [CrossRef]
22. Aerosol Robotic Network (AERONET). Available online: http://aeronet.gsfc.nasa.gov/ (accessed on 14 October 2015).
23. Holben, B.N.; Eck, T.F.; Slutsker, I.; Tanré, D.; Buis, J.P.; Setzer, A.; Vermote, E.; Reagan, J.A.; Kaufman, Y.J.; Nakajima, T.; et al. AERONET—A Federated Instrument Network and Data Archive for Aerosol Characterization. *Remote Sens. Environ.* **1998**, *66*, 1–16. [CrossRef]
24. Jaus, J.; Gueymard, C.A. Generalized spectral performance evaluation of multijunction solar cells using a multicore, parallelized version of SMARTS. In Proceedings of the AIP Conference, Toledo, Spain, 16–18 April 2012; Volume 1477, pp. 122–126.
25. Chan, N.L.A.; Brindley, H.E.; Ekins-Daukes, N.J. Impact of individual atmospheric parameters on CPV system power, energy yield and cost of energy. *Prog. Photovoltaics Res. Appl.* **2014**, *22*, 1080–1095. [CrossRef]
26. Solar and Wind Energy Resource Assessment (SWERA). Available online: https://maps.nrel.gov/swera (accessed on 27 May 2016).
27. World Radiation Monitoring Center—Baseline Surface Radiation Network Homepage. Available online: http://bsrn.awi.de/ (accessed on 27 May 2016).
28. Kogelnik, H. Coupled wave theory for thick hologram gratings. *Bell Syst. Tech. J.* **1969**, *48*, 2909–2947. [CrossRef]
29. Syms, R.R.A. Vector Effects in Holographic Optical Elements. *Opt. Acta Int. J. Opt.* **1985**, *32*, 1413–1425. [CrossRef]
30. Bañares-Palacios, P.; Álvarez-Álvarez, S.; Marín-Sáez, J.; Collados, M.-V.; Chemisana, D.; Atencia, J. Broadband behavior of transmission volume holographic optical elements for solar concentration. *Opt. Express* **2015**, *23*, A671–A681. [CrossRef] [PubMed]
31. Hecht, E. *Optics*; Addison Wesley: Reading, UK, 1998.
32. Marion, B. A method for modeling the current-voltage curve of a PV module for outdoor conditions. *Prog. Photovoltaics Res. Appl.* **2002**, *10*, 205–214. [CrossRef]
33. Amrizal, N.; Chemisana, D.; Rosell, J.I. Hybrid photovoltaic–thermal solar collectors dynamic modeling. *Appl. Energy* **2013**, *101*, 797–807. [CrossRef]
34. Schüco. Available online: https://www.schueco.com (accessed on 27 May 2016).

Chapter 5

Characterization of the photosensitive material for holographic recording

Chapter 4 showed the adequacy of a holographic concentrating system for building-integrated photovoltaic and thermal energy production. In order to consider a PV generator instead of a hybrid PVT one, higher optical efficiencies need to be obtained with the HOEs. Therefore, their optical design has to be optimized. The recording material where the optimized HOEs will be recorded is Bayfol HX [1], a photopolymeric material developed by Covestro AG (formerly Bayer MaterialScience). It was chosen because the features it offers (good light sensitivity, low shrinkage; thus negligible detuning) are similar to the ones of dichromated gelatin, the recording material used in chapter 3, with an added advantage: no chemical or thermal processing is necessary after the recording, only photocuring, which is less cumbersome and more adequate for mass-production of HOEs.

As explained in chapter 2, HOEs used for concentrating photovoltaics should efficiently diffract part of the solar spectrum that the PV cell is sensitive to, ideally reaching a compromise between the solar spectrum and the spectral response curve of the cell. When using a Si PV cell, a good choice could be to optimize the HOE for a target wavelength of 800 nm. This has to be achieved with relatively low spatial frequencies, in order to reach low values of parameter Q to obtain angular and chromatic selectivities as low as possible, as detailed in chapter 3. Additionally, the bleaching process should ensure that absorption on the material when illuminating it with sunlight is minimal.

To investigate whether these conditions can be met with Bayfol HX and to obtain the dependency of the desired properties of HOEs with the recording parameters, a characterization of the material is needed before the optimization of the design of the HOEs. This is carried out in the publication included in this chapter [2]. It was one of the first studies about the response and possibilities of this material, at the time still under testing and optimization processes by the manufacturing company.

References:

1. H. Berneth, F.-K. Bruder, T. Fäcke, D. Jurbergs, R. Hagen, D. Hönel, T. Rölle, and G. Walze, "Bayfol HX photopolymer for full-color transmission volume Bragg gratings," SPIE Photonics West 2014-OPTO Optoelectron. Devices Mater. **9006**, 900602 (2014).

2. J. Marín-Sáez, J. Atencia, D. Chemisana, and M.-V. Collados, "Characterization of volume holographic optical elements recorded in Bayfol HX photopolymer for solar photovoltaic applications," Opt. Express **24**, A720 (2016).

Characterization of volume holographic optical elements recorded in Bayfol HX photopolymer for solar photovoltaic applications

Julia Marín-Sáez,[1] Jesús Atencia,[2,*] Daniel Chemisana,[1] and María-Victoria Collados[2]

[1]*Departamento de Medio Ambiente (Sección de Física Aplicada), Universidad de Lleida, Escuela Politécnica Superior (INSPIRES), Jaume II 69, 25001 Lleida, Spain*

[2]*Departamento de Física Aplicada, Instituto de Investigación en Ingeniería de Aragón (I3A), Universidad de Zaragoza, Facultad de Ciencias, Pedro Cerbuna 12, 50009 Zaragoza, Spain*

[*]*atencia@unizar.es*

Abstract: Volume Holographic Optical Elements (HOEs) present interesting characteristics for photovoltaic applications as they can select spectrum for concentrating the target bandwidth and avoiding non-desired wavelengths, which can cause the decrease of the performance on the cell, for instance by overheating it. Volume HOEs have been recorded on Bayfol HX photopolymer to test the suitability of this material for solar concentrating photovoltaic systems. The HOEs were recorded at 532 nm and provided a dynamic range, reaching close to 100% efficiency at 800 nm. The diffracted spectrum had a FWHM of 230 nm when illuminating at Bragg angle. These characteristics prove HOEs recorded on Bayfol HX photopolymer are suitable for concentrating solar light onto photovoltaic cells sensitive to that wavelength range.

OCIS codes: (350.6050) Solar energy; (090.2890) Holographic optical elements; (090.7330) Volume gratings; (160.5335) Photosensitive materials.

References and links

1. M. V. Collados, D. Chemisana, and J. Atencia, "Holographic solar energy systems: the role of optical elements," Renew. Sustain. Energy Rev. **59**, 130–140 (2016).
2. H. Field, "Solar cell spectral response measurement errors related to spectral band width and chopped light waveform," in Conference Record of the Twenty Sixth IEEE Photovoltaic Specialists Conference - 1997 (IEEE, 1997), pp. 471–474.
3. C. Xiao, X. Yu, D. Yang, and D. Que, "Impact of solar irradiance intensity and temperature on the performance of compensated crystalline silicon solar cells," Sol. Energy Mater. Sol. Cells **128**, 427–434 (2014).
4. S. Chander, A. Purohit, A. Sharma, S. P. Nehra, and M. S. Dhaka, "A study on photovoltaic parameters of mono-crystalline silicon solar cell with cell temperature," Energy Reports **1**, 104–109 (2015).
5. D. Chemisana, M. V. Collados, M. Quintanilla, and J. Atencia, "Holographic lenses for building integrated concentrating photovoltaics," Appl. Energy **110**, 227–235 (2013).
6. J. E. Ludman, J. Riccobono, I. V. Semenova, N. O. Reinhand, W. Tai, X. Li, G. Syphers, E. Rallis, G. Sliker, and J. Martín, "The optimization of a holographic system for solar power generation," Sol. Energy **60**(1), 1–9 (1997).
7. A. Villamarín, J. Atencia, M. V. Collados, and M. Quintanilla, "Characterization of transmission volume holographic gratings recorded in Slavich PFG04 dichromated gelatin plates," Appl. Opt. **48**(22), 4348–4353 (2009).
8. P. Bañares-Palacios, S. Álvarez-Álvarez, J. Marín-Sáez, M.-V. Collados, D. Chemisana, and J. Atencia, "Broadband behavior of transmission volume holographic optical elements for solar concentration," Opt. Express **23**(11), A671–A681 (2015).
9. D. Zhang, J. M. Castro, and R. K. Kostuk, "One-axis tracking holographic planar concentrator systems," J. Photonics Energy **1**(1), 015505 (2011).
10. J. M. Castro, D. Zhang, B. Myer, and R. K. Kostuk, "Energy collection efficiency of holographic planar solar concentrators," Appl. Opt. **49**(5), 858–870 (2010).
11. C. G. Stojanoff, "A review of selected technological applications of DCG holograms," Proc. SPIE **7957**, 79570 (2011).
12. S. T. L. Sam, A. P. T. Kumar, P. Predeep, M. Thakur, and M. K. R. Varma, "Design and Optimization of Photopolymer Based Holographic Solar Concentrators," in *Optics: Phenomena, Materials, Devices and Characterization*, (AIP Conference Proceedings, 2011), pp. 248–250.
13. H. Akbari, I. Naydenova, and S. Martin, "Using acrylamide-based photopolymers for fabrication of holographic optical elements in solar energy applications," Appl. Opt. **53**(7), 1343–1353 (2014).

#258926 Received 3 Feb 2016; revised 10 Mar 2016; accepted 12 Mar 2016; published 18 Mar 2016

14. G. Bianco, M. A. Ferrara, F. Borbone, A. Roviello, V. Pagliarulo, S. Grilli, P. Ferraro, V. Striano, and G. Coppola, "Multiplexed holographic lenses : realization and optical characterization," in *2015 Fotonica AEIT Italian Conference on Photonics Technologies* (IET, 2015), pp. 1–3.
15. H. Berneth, F.-K. Bruder, T. Fäcke, D. Jurbergs, R. Hagen, D. Hönel, T. Rölle, and G. Walze, "Bayfol HX photopolymer for full-color transmission volume Bragg gratings," Proc. SPIE **9006**, 900602 (2014).
16. M. R. Gleeson, J. T. Sheridan, F.-K. Bruder, T. Rölle, H. Berneth, M.-S. Weiser, and T. Fäcke, "Comparison of a new self developing photopolymer with AA/PVA based photopolymer utilizing the NPDD model," Opt. Express **19**(27), 26325–26342 (2011).
17. A. Zanutta, E. Orselli, T. Fäcke, and A. Bianco, "Photopolymeric films with highly tunable refractive index modulation for high precision diffractive optics," Opt. Mater. Express **6**(1), 252 (2016).
18. A. Zanutta, A. Bianco, M. Insausti, and F. Garzón, "Volume phase holographic gratings for astronomy based on solid photopolymers," Proc. SPIE **9151**, 91515 (2014).
19. M.-L. Piao, K.-C. Kwon, H.-J. Kang, K.-Y. Lee, and N. Kim, "Full-color holographic diffuser using time-scheduled iterative exposure," Appl. Opt. **54**(16), 5252–5259 (2015).
20. Y. S. Hwang, F.-K. Bruder, T. Fäcke, S.-C. Kim, G. Walze, R. Hagen, and E.-S. Kim, "Time-sequential autostereoscopic 3-D display with a novel directional backlight system based on volume-holographic optical elements," Opt. Express **22**(8), 9820–9838 (2014).
21. P. Vojtíšek and M. Květoň, "Impact of overmodulation on spectral response in high efficient transmission gratings," Proc. SPIE **9442**, 94421H (2015).
22. H. Kogelnik, "Coupled wave theory for thick hologram gratings," Bell Syst. Tech. J. **48**(9), 2909–2947 (1969).
23. E. Hecht, *Optics* (Addison-Wesley, 1998).
24. M. V. Collados, I. Arias, A. García, J. Atencia, and M. Quintanilla, "Silver halide sensitized gelatin process effects in holographic lenses recorded on Slavich PFG-01 plates," Appl. Opt. **42**(5), 805–810 (2003).
25. F.-K. Bruder, T. Fäcke, R. Hagen, D. Hönel, E. Orselli, C. Rewitz, T. Rölle, G. Walze, and B. Wewer, "Second harmonics HOE recording in Bayfol HX," Proc. SPIE **9508**, 95080G (2015).

1. Introduction

Volume Holographic Optical Elements (HOEs) can operate as solar concentrators [1]. For their design two main characteristics should be taken into consideration: chromatic and angular selectivity. Since holograms are wavelength-selective optical elements they can be designed to efficiently diffract the bandwidth for which the photovoltaic cell will work best. In the case of a Si or a CIGS cell the range is approximately from 700 to 1050 nm, and for a GaAs, from 500 to 850 nm [2], as it can be seen in Fig. 1. To operate as a solar concentrator, a HOE should diffract a broad spectrum and the design should also take into account the solar spectrum (Fig. 1). An advantage of the chromatic selectivity that holograms offer is the possibility of eliminating the non-desired wavelengths, such as infrared, by diffracting that range with a very poor efficiency. This prevents the photovoltaic cell from overheating, which causes a performance decrease on the cell [3,4].

Volume HOEs present angular selectivity, i.e., they efficiently diffract light for a range of incident directions. This is an important aspect to take into account, since the position of the sun varies over the day and the year. When varying the incident direction along the plane formed by the two recording beams, this efficient angular range is rather small, so the HOE has a high angular selectivity. On the other hand, in the perpendicular plane, low angular selectivity is achieved. One can take advantage of this effect by using cylindrical holographic lenses which allow the use of single-axis solar tracking devices [5].

Moreover, the efficiency depends on additional parameters: composition and thickness of the photosensitive material, recording geometry and spatial frequency, among others. The chromatic dispersion of the holographic lens should also be taken into account. Each wavelength is focused on a different point, which could be a drawback, since the wavelength range of interest should focus on the photovoltaic cell, or an advantage, if several photovoltaic cells, each one sensitive to a different wavelength range, are used [6].

#258926 Received 3 Feb 2016; revised 10 Mar 2016; accepted 12 Mar 2016; published 18 Mar 2016

21 Mar 2016 | Vol. 24, No. 6 | DOI:10.1364/OE.24.00A720 | OPTICS EXPRESS A721

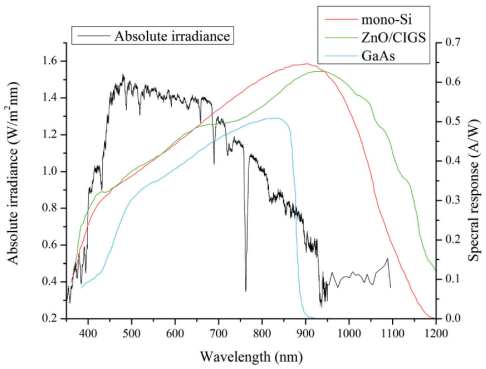

Fig. 1. Absolute irradiance of the sun (black curve, left y-axis) and spectral response of several photovoltaic cells [2] (red, green, and blue curves, right y-axis).

The material dynamic range of index modulation is a decisive parameter because it limits the value of the highest wavelength which can be efficiently diffracted. In addition, a large dynamic range is required to multiplex several holograms with different incident recording directions [7], to overcome the high angular selectivity and therefore, eliminating or reducing the need of tracking.

Two kinds of photosensitive materials proven to be suitable for the recording of holographic lenses as solar concentrators are dichromated gelatin (DCG) [5,8–11] and photopolymers [12–14]. Both of these materials can be self-produced or acquired from manufacturing companies and provide high efficiency, resolution, index modulation and transparency. However, DCG requires wet and thermal post-processing, whereas some photopolymers are self-developing materials.

Both types of materials have been studied and characterized for reconstruction with a broad spectrum. Even though many researchers have adopted DCG for solar applications, only a few propose solar concentrators based on photopolymers. Sam et al. [12] used HoloMer 6A photopolymer, produced by Light Logics Holography and Optics, to record a holographic lens. Akbari et al. [13] utilized self-produced acrylamide-based photopolymers for HOE recording in the frame of solar energy applications. They stacked together a combination of HOEs to achieve a broad angle range. All the gratings were recorded on thin layers and had low spatial frequency to obtain a larger angular and chromatic working range of the optical component. Bianco et al. [14] recorded multiplexed cylindrical lenses in a sol-gel photopolymer also to increase the angle range.

A new acrylate based photopolymer, Bayfol HX, developed by Covestro AG (formerly Bayer MaterialScience), is the material studied in this work with emphasis on a solar application, due to its advantageous characteristics such as good light sensitivity, low shrinkage and detuning and specially no chemical or thermal processing needed, only photocuring [15]. Its index modulation has been studied in comparison with a well-known acrylamide/polyvinylalcohol (AA/PVA) based photopolymer material, and it was concluded that Bayfol photopolymer can achieve a significantly higher refractive index modulation [16]. Some initial tests of this new photopolymer material for the recording of vHOEs are reported in the literature. Zanutta et al. [17,18] investigated holograms in order to utilize them as an optical dispersing element for an astronomical spectrograph. Piao et al. [19] evaluated multiplexed holograms with three different wavelengths to be used as a holographic diffuser. Hwang et al. [20] stacked three holograms recorded each with a different wavelength to obtain a autostereoscopic display system. Vojtíšek et al. [21] analyzed the over-modulation of transmission gratings recorded on this material.

Taking into account the studies which are available in the literature, the goal of the present study is to characterize Bayfol HX and to prove its suitability as a recording material for holographic solar photovoltaic concentrators. Since each point of a holographic lens acts as a

#258926 Received 3 Feb 2016; revised 10 Mar 2016; accepted 12 Mar 2016; published 18 Mar 2016

21 Mar 2016 | Vol. 24, No. 6 | DOI:10.1364/OE.24.00A720 | OPTICS EXPRESS A722

plane grating ("local grating" treatment) [8], it is necessary to study first the performance of volume gratings recorded on this material. In order to achieve a compromise between solar irradiance and cell optimum wavelength ranges, depicted in Fig. 1, 800 nm is established as the desired wavelength with maximum efficiency in the reconstruction.

2. Theoretical background

The analysis of holographic gratings is based on Kogelnik's Coupled Wave Theory [22]. A holographic grating is recorded with the interference of two beams with wave propagation vectors $\vec{k}_1$ and $\vec{k}_2$, with modulus $k_1 = k_2 = \frac{2\pi}{\lambda_R}$, where λ_R is the recording wavelength. The grating vector $\vec{K}$, is determined by means of

$$\vec{K} = \vec{k}_1 \pm \vec{k}_2 \tag{1}$$

For simplicity, only the negative term in Eq. (1) is considered, as shown in Fig. 2. The vector $\vec{K}$ is perpendicular to the constant interference planes and has a modulus of $\frac{2\pi}{\Lambda}$, where Λ is the grating period.

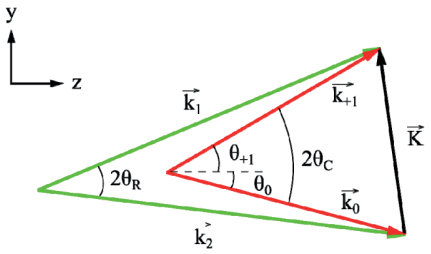

Fig. 2. Relation between the grating vector $\vec{K}$, the recording wave propagation vectors $\vec{k}_1$ and $\vec{k}_2$ and the reconstruction wave propagation vectors $\vec{k}_0$ and $\vec{k}_{+1}$ when Bragg condition is met. Z-axis is chosen perpendicular to the holographic film plane.

In volume phase holograms, it is assumed that the refractive index is sinusoidally modulated along the material, in the form $n(\vec{r}) = n_0 + n_1 \cos(\vec{K} \cdot \vec{r})$, where n_0 is the average material index and n_1 is the index modulation. When illuminating with a beam with wave vector $\vec{k}_0$ only two waves are diffracted: zero order $\vec{k}_0$ and first diffraction order $\vec{k}_{+1}$, with modulus $k_0 = k_{+1} = \frac{2\pi}{\lambda_C}$, where λ_C is the reconstruction wavelength.

The diffractive efficiency of the grating is defined with

$$\eta = \frac{I_{+1}}{I_0 + I_{+1}} \tag{2}$$

where I_0 is the intensity of the transmitted beam and I_{+1} is the intensity of the diffracted beam.

The efficiency will be maximal when Bragg condition is fulfilled (Fig. 2),

$$2\Lambda \sin\theta_C = \lambda_C \tag{3}$$

and it is given by

#258926 Received 3 Feb 2016; revised 10 Mar 2016; accepted 12 Mar 2016; published 18 Mar 2016

21 Mar 2016 | Vol. 24, No. 6 | DOI:10.1364/OE.24.00A720 | OPTICS EXPRESS A723

$$\eta = \sin^2\left(\frac{\pi n_1 d}{\lambda_C \sqrt{\cos\theta_0 \cos\theta_{+1}}}\right) \quad (4)$$

where d is the material thickness, and θ_0 and θ_{+1} are depicted in Fig. 2. With an appropriate value of n_1, determined with the recording exposure, the efficiency can reach $\eta = 1$.

3. Experimental method and results

Two non-commercial photosensitive materials manufactured by Covestro AG (formerly Bayer MaterialScience) have been tested in the present study: Bayfol HX 104, green-sensitive and an early-stage material Bayfol HX TP, RGB-sensitive. Each sample is a film formed by two layers: a substrate made of polycarbonate in the first case and made of polyamide in the second one, and a photopolymer film. The refractive index of each layer was measured by means of an Abbe refractometer and the thickness was then obtained from the transmission spectrum measured by a spectrophotometer (Varian Cary 500) when illuminating with a broadband light source. The interference pattern of multiple reflections provided the product $n \cdot d$ (refractive index and thickness, respectively). In Table 1, the results and the values provided by Covestro AG are shown.

Table 1. Comparison of the provided and measured values of refraction index and thickness of the photopolymer and substrate of Bayfol HX 104 and HX TP.

	Measured				Provided by Covestro AG			
	n_{phot}	d_{phot} (μm)	n_{subs}	d_{subs} (μm)	n_{phot}	d_{phot} (μm)	n_{subs}	d_{subs} (μm)
Bayfol HX 104	1.49	16.3	1.59	128.7	1.485 1.492	16	1.58	125
Bayfol HX TP	1.45	15.2	1.53	60.7	-	16	-	60

It should be noted that no chemical or thermal processing is needed after the recording. However, photocuring is required to stop the polymerization process and bleach the remaining dye of the sample. In this way, absorption is reduced and higher absolute efficiencies (ratio of diffracted and incident intensity) can be reached. The manufacturer recommends bleaching with a mercury arc lamp (commercially discontinued), that emits visible and UV light, with a dosage of 5-10 J/cm^2. Tests with a metal halide lamp (Philips HPA 400 SD), with a similar spectrum, and with a 50 W white LED flood light have been performed. They revealed that the most comfortable and less agresive option is photocuring with white LED, since to achieve analogous results the metal halide lamp had to be placed close to the photopolymer sample, which caused a temperature increase above the material's tolerance.

The white LED provided an intensity -on the holographic film- of 160 mW/cm^2 (measured with Ophir 50(150)A-BB-26 power sensor) and the spectral intensity presented in Fig. 3. A dosage of 240 J/cm^2 was used to bleach the samples, much higher than the dosage recommended by the manufacturer. However, the transmission spectrum increases up to 3% around 550 nm when performing a second photocuring step with the metal halide lamp (placed further from the sample to avoid the temperature increase) with a UV-A intensity -on the holographic film- of 30.4 mW/cm^2 (measured with UV-Design Radiometer Black Standard UV-A) and a dosage of 60 J/cm^2.

#258926 Received 3 Feb 2016; revised 10 Mar 2016; accepted 12 Mar 2016; published 18 Mar 2016

21 Mar 2016 | Vol. 24, No. 6 | DOI:10.1364/OE.24.00A720 | OPTICS EXPRESS A724

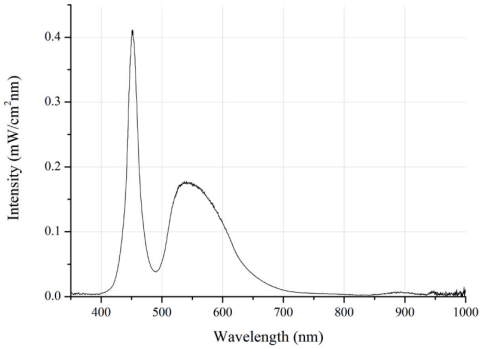

Fig. 3. Intensity on the sample provided by the white LED used for photocuring as a funcion of the wavelength.

Given the fact that the present study focuses on solar-concentration applications, it would not be necessary to perform the second step, since sun radiation would act as the visible and UV light source, giving similar results. In Fig. 4(a) and (b), the transmission spectra of unrecorded photopolymer before and after two-step bleaching (visible LED and metal halide lamp, or visible LED and sun radiation) are shown. It should also be mentioned that reflection losses on all surfaces have been substracted with Fresnel's expressions [23]. The spectra look rather wavy because of the interference of multiple reflections into the material.

Bayfol HX absorbs radiation with wavelengths under 300 nm [18], both before and after bleaching. This high absorption (close to 100%) is likely due to the substrate (made of polyamide or polycarbonate), rather than the dye. This is not critical in solar application, since the types of solar cells this work was proposed for (mono-Si, ZNO/CIGS, GaAs) have no sensitivity at wavelengths under 300 nm (Fig. 1) [2].

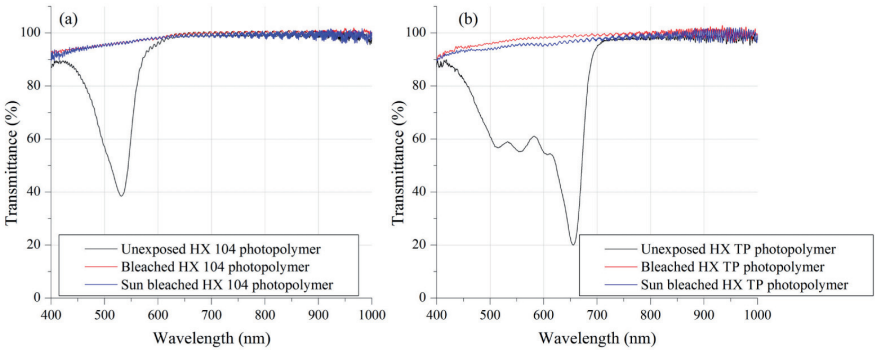

Fig. 4. Transmission spectra of unexposed (black curve) and bleached with visible LED and a metal halide lamp (red curve) and with visible LED and the sun radiation (blue curve) Bayfol HX 104 (a) and Bayfol HX TP (b) photopolymer. The reflection losses on all surfaces have been eliminated.

A slanted grating has been recorded on each sample in order to calibrate material holographic properties. Slanted gratings are of great interest, since variations in the diffracted beams directions from those given by theory (Eq. (3)) indicate a variation of the material thickness after the recording and processing.

In all the cases, the recording wavelength was 532 nm (Coherent Verdi V6 laser with variable output power from 10 mW to 6 W) and the target reconstruction wavelength was 800 nm. The chosen angle between the reference and the object beam (25° in air, with one beam normal to the holographic film) and therefore, the spatial frequency (820 lines/mm, the inverse of the spatial period), ensure that the hologram operates in the volume regime for 800 nm, to achieve high efficiency, but diffracting a broad spectrum.

#258926 Received 3 Feb 2016; revised 10 Mar 2016; accepted 12 Mar 2016; published 18 Mar 2016

21 Mar 2016 | Vol. 24, No. 6 | DOI:10.1364/OE.24.00A720 | OPTICS EXPRESS A725

After the bleaching treatment, the efficiency η of each grating was determined based on Eq. (2). The intensity of the diffracted orders was measured (with Newport Power Meter Model 1815-C with detector Model 818-SL, with an uncertainty of 5 μW) by illuminating at Bragg angle with a laser, emitting either at 800 nm (ThorLabs Laser Diode CPS808A, emitting 4.4 mW) or at 532 nm, as illustrated in Fig. 5. The index modulation n_1 was calculated by means of Eq. (4).

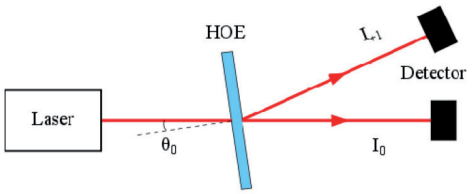

Fig. 5. Schematic of the geometry used for the measurement of the transmitted and diffracted beams intensity to calculate the efficiency. The detector could be placed on either beam.

Figures 6 and 7 show the dependency of the efficiency with the exposure for gratings recorded with an incident intensity (equal to the sum of the intensities of both reference and object beam) of 0.275 mW/cm^2 for Bayfol HX 104 and 1.17 mW/cm^2 for Bayfol HX TP. In the case of efficiency curves at 532 nm, overmodulation effect can be noticed with a clear efficiency reduction from exposure energies around 3.5 mJ/cm^2, for Bayfol HX 104, and around 12 mJ/cm^2, for Bayfol HX TP. However, for 800 nm, saturation of index modulation gives a maximum constant 100% efficiency value, so, with the 820 lines/mm gratings recorded, it cannot be possible to obtain 100% efficiency for λ_C >800 nm with neither Bayfol material, as Eq. (4) indicates.

The optimum exposure energy is different for each material, with Bayfol HX TP requiring higher recording energies than Bayfol HX 104. When increasing the exposure energy, index modulation saturation was achieved in all cases, which can cause nonlinear effects, turning into a non-sinusoidal index modulation and higher harmonics generation, as it will be later shown.

Values of the index modulation up to 0.024 are obtained for both materials at the saturation range, as shown in Fig. 8. The optical path modulation obtained, $n_1 \cdot d$ = 0.3912 μm for HX 104 and $n_1 \cdot d$ = 0.3648 μm for HX TP, is similar to that obtained by DCG investigated by the authors [7]. The thickness of the DCG emulsion in [7] was 30 μm, around the double of photopolymer thickness, and the index modulation was the half: 0.012.

Zanutta et al. [17,18] stated that the maximum reachable index modulation can be selected varying the recording intensity. In order to determine the optimal intensity for this work (with a target wavelength of 800 nm), several recording intensities were used. For each intensity several samples were recorded using different exposure energies, to obtain the index modulation n_1 for each one (as in Fig. 8). The maximal index modulation for each intensity was then identified and plotted in Fig. 9. The conducted measurements demonstrate that if too low intensity is used no hologram is recorded for any exposure value, whereas if too high intensity is adopted, gratings with lower index modulation than the maximum one are obtained. This is in accordance with data provided by the manufacturer for non-slanted transmission holograms. Higher intensity and exposure (3-4x) was required for HX TP than for HX 104. Figures 6-8 show data of volume gratings recorded with incident intensities belonging to the optimum range illustrated in Fig. 9.

#258926 Received 3 Feb 2016; revised 10 Mar 2016; accepted 12 Mar 2016; published 18 Mar 2016

21 Mar 2016 | Vol. 24, No. 6 | DOI:10.1364/OE.24.00A720 | OPTICS EXPRESS A726

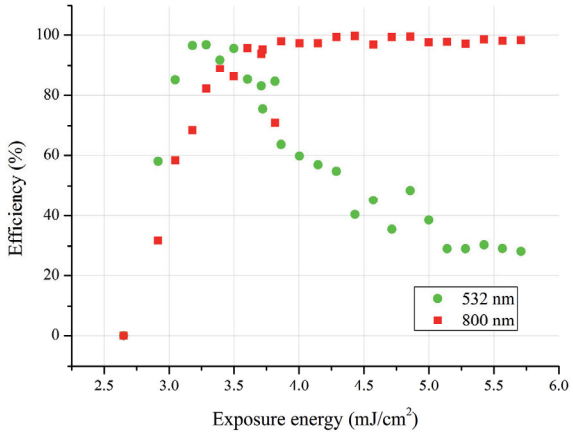

Fig. 6. Efficiency versus exposure energy of gratings recorded in Bayfol HX 104 with 0.275 mW/cm^2 of intensity and measured with a laser emitting at 532 nm (green circles) and one at 800 nm (red squares).

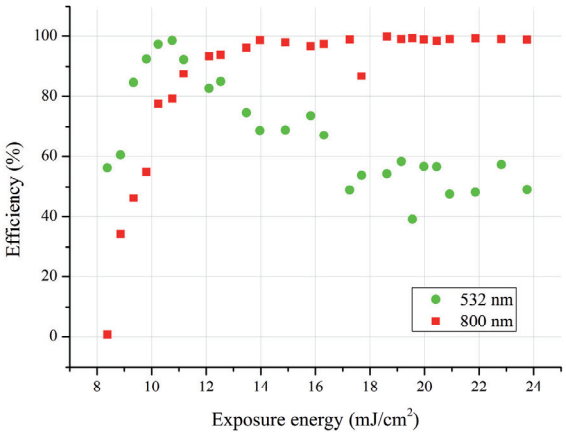

Fig. 7. Efficiency versus exposure energy of gratings recorded in Bayfol HX TP with 1.17 mW/cm^2 of intensity and measured with a laser emitting at 532 nm (green circles) and one at 800 nm (red squares).

#258926 Received 3 Feb 2016; revised 10 Mar 2016; accepted 12 Mar 2016; published 18 Mar 2016

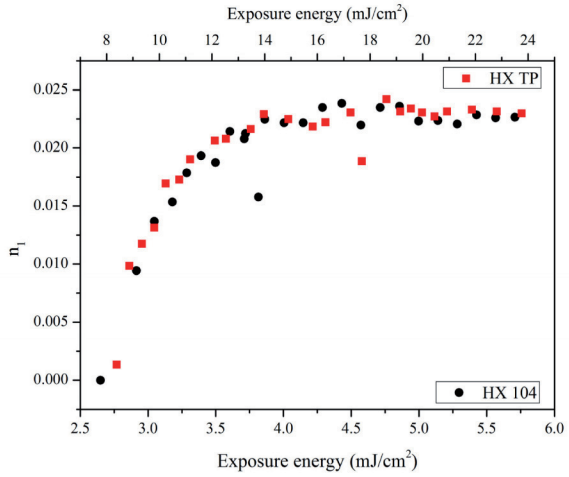

Fig. 8. Refractive index modulation of gratings recorded in Bayfol HX 104 (black circles, bottom x-axis) with 0.275 mW/cm^2 of intensity, and Bayfol HX TP (red squares, top x-axis) with 1.17 mW/cm^2 of intensity.

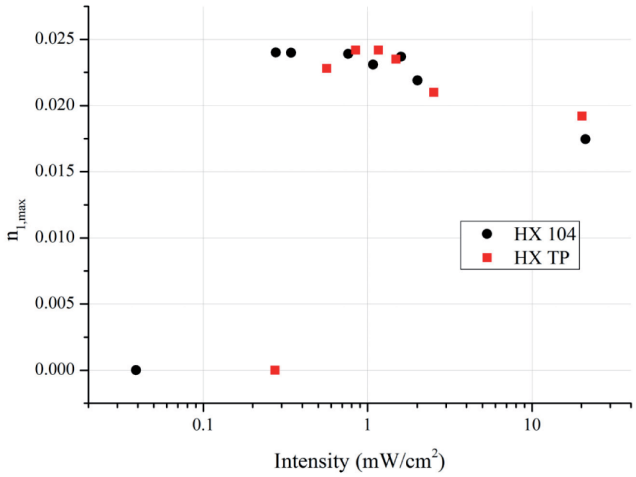

Fig. 9. Maximum refraction index modulation obtained by different recording intensities with Bayfol HX 104 (black circles) and Bayfol HX TP (red squares). The x-axis corresponds with the sum of the intensity of the reference beam and the object beam.

The efficiency as a function of the angle of incidence of the gratings corresponding to the points with exposure energy 4.43 mJ/cm^2 for HX 104 (illustrated in Fig. 6) and 19.56 mJ/cm^2 for HX TP (presented in Fig. 7) was also measured at 800 nm. A detector was placed to measure the efficiency of the 0th order. Black curves in Figs. 10(a) and 10(b) show the angular selectivity when varying the incident direction along the plane formed by the two recording beams. Reflection losses have been suppressed with Fresnel's expressions. Since the recorded gratings are volume holograms, minimums in the 0th order of diffraction correspond to maximums in the 1st order. The angles, at which the diffracted efficiency is maximal (that fulfill Bragg condition), –6.3°and 31.9°, are in agreement with the values obtained with the theoretical curves predicted by Kogelnik's theory with the initial thickness (green curves). Therefore, there is no noticeable variation in thickness of the photopolymer after recording and processing [24]. The curve for HX 104 has a FWHM of approximately 6° and HX TP of 7°.

#258926 Received 3 Feb 2016; revised 10 Mar 2016; accepted 12 Mar 2016; published 18 Mar 2016

21 Mar 2016 | Vol. 24, No. 6 | DOI:10.1364/OE.24.00A720 | OPTICS EXPRESS A728

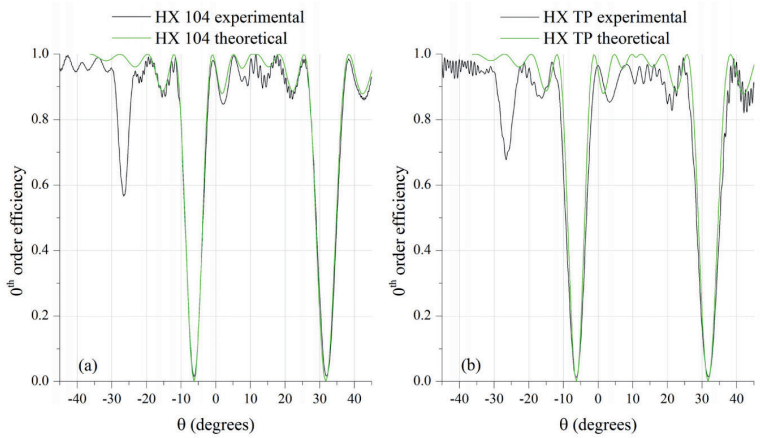

Fig. 10. Comparison of theoretical (green curves) and experimental (black curves) angular selectivity of a grating recorded with 4.43 mJ/cm^2 in Bayfol HX 104 (a) and a grating recorded with 19.56 mJ/cm^2 in Bayfol HX TP (b), measured with a laser emmiting at 800 nm and varying the incident direction along the plane formed by the two recording beams. Reflection losses have been suppressed.

The peak at $\theta = -26.1°$ of Figs. 10(a) and 10(b) corresponds to a grating with grating vector $2\vec{K}$. This occurs due to the fact that the index modulation is saturated (Fig. 8); thus, the recorded grating is not sinusoidally modulated and higher order harmonics appear [25]. This effect does not seem to affect the behavior of the recorded grating.

Figure 11 shows the angular selectivity when varying the incident direction along the plane perpendicular to the two recording beams. Reflection losses have also been suppressed with Fresnel's expressions. The curves have a FWHM slightly bigger than 80°. This characteristic will allow the design of HOEs for solar concentration with one-axis tracking [5].

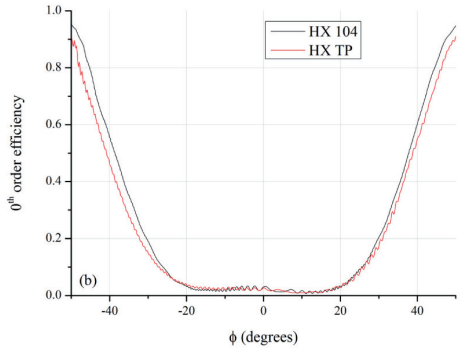

Fig. 11. Angular selectivity of a grating recorded with 4.43 mJ/cm^2 in Bayfol HX 104 (black curve) and a grating recorded with 19.56 mJ/cm^2 in Bayfol HX TP (red curve), measured with a laser emmiting at 800 nm and varying the incident direction along the plane perpendicular to the two recording beams. Reflection losses have been suppressed.

In order to analyze the chromatic selectivity (the dependence of the efficiency with the wavelength), the HOE is illuminated at Bragg angle with a white light source (Ocean Optics LS-1) and the transmitted light is measured with a spectrometer (Ocean Optics USB2000). In Fig. 12, the efficiency of the 0th order of the previous gratings versus the wavelength, when illuminating in a direction that fulfills Bragg condition for 800 nm, is shown. Reflection losses have also been suppressed with Fresnel's expressions. The maximum around 800 nm has a FWHM of approximately 200 nm for the HX 104 sample and 230 nm for the HX TP

#258926 Received 3 Feb 2016; revised 10 Mar 2016; accepted 12 Mar 2016; published 18 Mar 2016

21 Mar 2016 | Vol. 24, No. 6 | DOI:10.1364/OE.24.00A720 | OPTICS EXPRESS A729

sample. A peak corresponding to the second harmonic (grating vector $2\vec{K}$) is seen at 400 nm, as it is expected. In Figs. 10-12, it can be noticed that the broadest curve corresponds to the material with the smallest thickness, HX TP, as stated by Kogelnik's Coupled Wave theory [22].

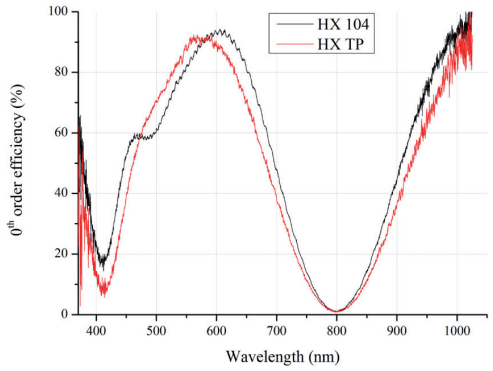

Fig. 12. Chromatic selectivity of a grating recorded with 4.43 mJ/cm^2 in Bayfol HX 104 (black curve) and a grating recorded with 19.56 mJ/cm^2 in Bayfol HX TP (red curve), measured at Bragg angle for 800 nm. Reflection losses have been suppressed.

4. Conclusions

Two acrylate-based photopolymer materials, Bayfol HX 104 and Bayfol HX TP, have been calibrated by means of recording 820 lines/mm volume gratings at 532 nm. High efficiency for a broad spectrum has been obtained and the high dynamic range with an index modulation of 0.024 allowed 100% efficient diffraction at 800 nm with a FWHM greater than 200 nm, which matches the maximal spectral response region of a set of solar cells. Therefore, it has been concluded that these photopolymer materials are suitable for solar concentration applications and future work will include the recording of holographic lenses for this aim. Nonetheless, given the high angular selectivity, tracking along one axis is necessary.

Some minor differences in the behavior of the two photopolymeric materials have been observed. The exposure energy required for the recording of the holograms is higher for Bayfol HX TP.

The optical path modulation of the HOEs obtained are similar to those obtained with DCG, as studied by the authors [7]. However, this photopolymer material is more convenient since there is no need of wet or thermal processing, especially when considering the application of industrial production of solar concentrators.

Further analysis of this material is needed in order to study multiplexing different gratings in the same sample, which could eliminate completely the need of tracking. For other photovoltaic cells with different working spectral range, the HOE would be designed in accordance to that range. If the target reconstruction wavelength is lower or equal to 800 nm the same material can be used; however, if it is higher than 800 nm another material, which could provide a higher optical path modulation $n_1 \cdot d$, should be utilized.

Acknowledgments

The authors would like to thank Covestro AG (formerly Bayer Material Science) for providing the photopolymer samples and to Dr. Enrico Orselli (Covestro AG) and Dr. Carlos Sánchez Somolinos (Instituto de Ciencia de Materiales de Aragón) for their helpful discussions. This research has been supported by the Spanish Ministerio de Economía y Competitividad (grants ENE2013-48325-R and FIS2012-35433), the Diputación General de Aragón-Fondo Social Europeo (TOL research group, T76) and the Generalitat de Catalunya (grant 2015 FI_B 00328).

#258926 Received 3 Feb 2016; revised 10 Mar 2016; accepted 12 Mar 2016; published 18 Mar 2016

21 Mar 2016 | Vol. 24, No. 6 | DOI:10.1364/OE.24.00A720 | OPTICS EXPRESS A730

Chapter 6

Optimization of the design of Holographic Optical Elements for Concentrating Photovoltaics. Study of the transition regime.

Chapter 4 showed the validity of cylindrical holographic lenses for building-integrated concentrating photovoltaics and chapter 5 the suitability of Bayfol HX photopolymer as recording material. The next step was to study different aspects that affect the design of HOEs recorded on Bayfol HX, in order to optimize it and achieve higher electrical current values on the PV cell than the ones presented in chapter 4.

First, a theoretical analysis (based on a ray-tracing algorithm) of the overall system performance with cylindrical holographic lenses recorded at different wavelengths is carried out in one of the publications included in this chapter [1]. This is an indirect way of analyzing the effect of chromatic and monochromatic aberrations that arise when the reconstruction wavelength differs from the recording wavelength. In applications with broadband and continuous spectrum reconstruction, such as solar concentration, aberrations are present but analytically studying them would be complex. Besides, an improvement for one wavelength would imply a worsening for others, and the angular and chromatic selectivity would also need to be considered. However, holographic concentrators are anidolic systems, so the quality of the image is not an important issue. Due to these reasons, no aberrations study is performed.

A comparison of three lenses (with identical behavior under the paraxial approximation) recorded at three different wavelengths is carried out. Two of them are typical laser wavelengths, 532 nm and 632.8 nm, and the other one is 800 nm, the target wavelength. The aim of this analysis is to determine the global effect of the recording wavelength on the irradiance received by the PV cell. It is purely an illustrative study, since to our knowledge no suitable recording materials are sensitive to 800 nm.

The next step was the consideration of the transition regime, which is the intermediate situation between the volume or Bragg regime and the thin or Raman-Nath regime. Volume holograms have traditionally been used for the majority of the applications due to their many advantages for monochromatic reconstruction; however, as pointed out in chapter 3, HOEs with low Q values, near the limit of the volume regime, are more desirable for solar concentration [2]. Therefore, the convenience of using HOEs partly performing in the transition regime for this application needs to be explored, to determine whether there is a favorable compromise between the related advantages (lower chromatic and angular selectivity) and disadvantages (lower efficiency). To our knowledge, the inclusion of the transition regime had not been considered before for broadband spectrum applications of holography.

Since the geometrical and energetic model in chapter 3 only covered volume HOEs, a section has been included in this chapter to provide the necessary background of the transition regime.

6.1. Theoretical background of the transition regime

As mentioned in chapter 3, parameter Q, given by

$$Q = \frac{2\pi\lambda d}{n\Lambda^2} \ , \tag{6.1}$$

is often used to determine the operation regime of a HOE.

Large values of Q (usually Q >10 or Q >2π) are associated with the volume or Bragg regime and small values of Q with the thin or Raman-Nath regime. This parameter expresses the relation among the geometrical magnitudes of the grating (thickness d, spatial period Λ) and the replay wavelength. However, it does not include the index modulation and some authors [3–5] had stated the need of this parameter to be included in the determination of the regime, since it had been experimentally observed that it also affected the number of diffraction orders. Moharam et al. published in 1980 an alternative criterion to determine whether a HOE performs in the Bragg (or volume) regime, in the Raman-Nath (or thin) regime, or in the transition or intermediate regime [6,7].

According to this criterion, a HOE is considered to operate in the volume regime when all the following conditions are met:

- The efficiency of the +1 order of diffraction wave is given by Kogelnik's solution for volume holograms within a specified error limit:

$$\left| \eta_{+1} - \frac{\sin^2\left(\sqrt{\nu^2 + \xi^2}\right)}{1 + \frac{\xi^2}{\nu^2}} \right| \leq \varepsilon \tag{6.2}$$

- The efficiency of the transmitted order is given by the function that is complementary to the efficiency of the +1 order, also within an error limit:

$$\left| \eta_0 - \frac{\frac{\xi^2}{\nu^2} + \cos^2\left(\sqrt{\nu^2 + \xi^2}\right)}{1 + \frac{\xi^2}{\nu^2}} \right| \leq \varepsilon \tag{6.3}$$

- Only the 0^{th} and 1^{st} orders of diffraction exist, i.e. the sum of the efficiencies of the rest of orders is smaller than a certain absolute error value:

$$\sum_{i \neq 0,+1} \eta_i \leq \varepsilon \tag{6.4}$$

On the other hand, the HOE is considered to operate in the thin or Raman-Nath regime if the efficiency of each order of diffraction i of a HOE is given by integer order ordinary Bessel functions of the first kind within an error limit:

$$\left| \eta_i - J_i^2(2\nu) \right| \leq \varepsilon \tag{6.5}$$

The set of conditions for the Bragg regime and the condition for the Raman-Nath regime were evaluated by Moharam et al. [6,7]. For this, several HOEs comprising a wide range of parameter ν, defined in chapter 3 by

$$\nu = \frac{\pi d n_1}{\lambda \sqrt{c'_{0z}\, c'_{+1z}}} \tag{6.6}$$

and parameter Q', given by

$$Q' = \frac{Q}{\sqrt{c'_{0z}\, c'_{+1z}}} = \frac{2\pi\lambda d}{n\Lambda^2} \frac{1}{\sqrt{c'_{0z}\, c'_{+1z}}} \tag{6.7}$$

were considered so that virtually all practical physical cases were covered. The efficiency of each diffraction order was calculated with the general multiwave coupled wave theory. The set of values of parameters ν and Q' that simultaneously fulfill equalities (6.2) to (6.4) for an absolute error value of ε = 0.01 are plotted in figure 6.1 with orange markers. They indicate the limit of the volume regime so that HOEs with coordinates ν and Q' on the right side of this boundary operate in said regime. The same process was conducted for equality (6.5), obtaining the blue markers in figure 6.1, which show the limit of the thin regime. HOEs with coordinates ν and Q' on the left side of this boundary operate in said regime. Similar results are obtained with smaller error values. The dependency of ν with Q' for each boundary can be approximated to $Q'\nu = constant$ for the Raman-Nath regime and $Q'/\nu = constant$ for the Bragg regime.

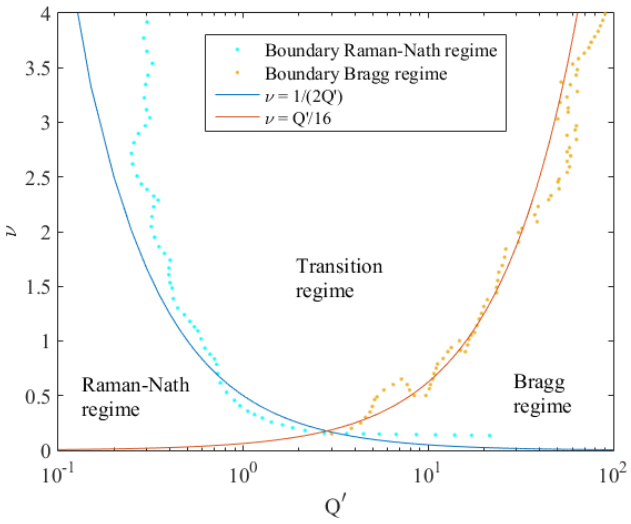

Figure 6.1. Moharam et al.'s criterion for the determination of the operation regime of holograms [6,7].

If neither set of conditions is met then the HOE operates in the intermediate or transition regime. The number of diffraction orders that can emerge from a hologram under certain reconstruction conditions (wavelength and angle of incidence) in this regime can be determined from Ewald sphere, shown in figure 6.2 in the YZ plane (with ϕ =0). The *x*- and *y*-components of the wave vector of each diffracted order must fulfill the so called beta-closure, already used in chapter 3 for the +1 diffraction order.

As opposed to the Raman-Nath regime and the Bragg regime, there is no analytical expression of the efficiency in the transition regime, so the coupled differential equations of each diffraction order L [5,8],

$$c'_{Lz} \frac{dA_L}{dz} + j\vartheta_L A_L + j\kappa\left[A_{L+1}\left(\vec{p}_{L+1}\cdot\vec{p}_L\right) + A_{L-1}\left(\vec{p}_{L-1}\cdot\vec{p}_L\right)\right] = 0, \tag{6.8}$$

must be solved numerically.

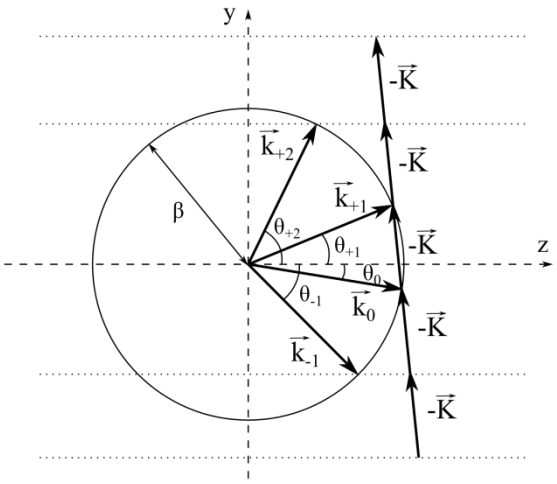

Figure 6.2: Ewald sphere.

Moharam et al.'s criterion to distinguish the regime a HOE operates at under certain conditions is more accurate than the Q criterion explained in chapter 3, especially when the HOE is near the limit of the volume regime. In order to illustrate this, simulations of the efficiency of some HOEs under different recording or reconstruction conditions are carried out.

For example, a holographic grating recorded at 532 nm with angles inside the medium 19.66º and 2.53º (which provide a spatial frequency of 840 lines/mm if the photosensitive medium has a refractive index of 1.5), thickness 16 μm and index modulation 0.033 is considered. When reconstructing at 800 nm with an angle of incidence in air θ = -2.76º (fulfilling Bragg condition), the HOE operates as a volume hologram. The chromatic selectivity curves with that reconstruction incidence in figure 6.3(a) show that at 800 nm only orders +1 and 0 have non negligible efficiency. The point determined by ν and Q' parameters is situated on the right side of the boundary of Bragg regime, as shown in figure 6.3(b), and Q = 37.8. However, when reconstructing with the same angle of incidence and wavelengths shorter than approximately 700 nm more orders of diffraction appear (as shown in the chromatic selectivity in figure 6.3(a)). This is in agreement with Moharam et al.'s criteria, since the HOE is now performing in the transition regime, as indicated in figure 6.3(b), although Q is still higher than 10.

Furthermore, the index modulation does indeed play an important role in determining which diffraction orders exist and with what efficiency; thus which regime it is. Figure 6.4(a) shows the growth curve, that is, the dependency of the efficiency of each diffraction order with the index modulation, of a grating with 495 lines/mm reconstructing with 800 nm at Bragg angle. At low values of the index modulation only diffraction orders 0 and +1 are present, but when increasing this parameter the efficiency of the orders +2 and -1 starts to grow. Since the only parameter that changes is the index modulation, the value of Q' remains constant, as marked in figure 6.4(b). It can be clearly observed that the increase in index modulation implies a change from the volume regime to the transition regime.

In spite of these efficiencies being rather low, they cause a difference in the distribution of efficiency between orders 0 and +1 from the one that would be found if only those two diffraction orders were considered, as demonstrated by Markovski et al. [9].

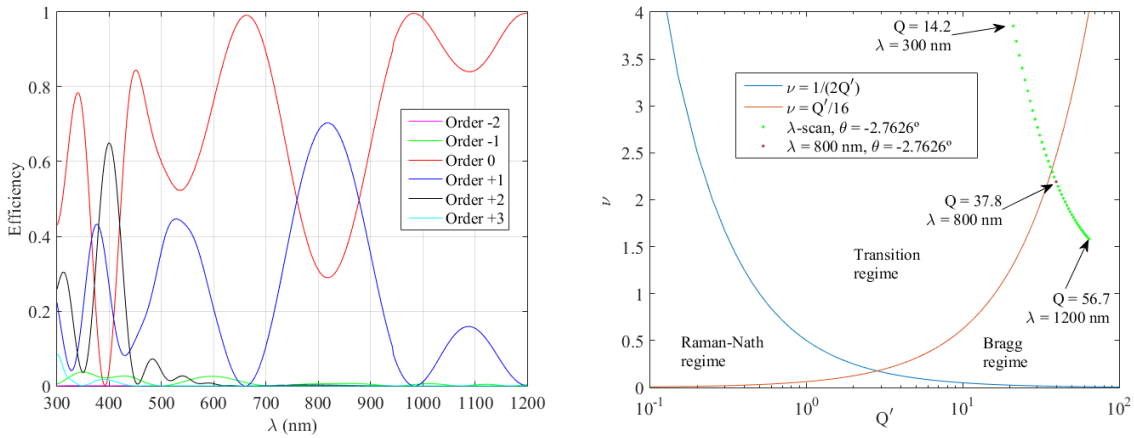

(a) (b)

Figure 6.3: Chromatic selectivity (a) and corresponding points in the Q' ν diagram (b).

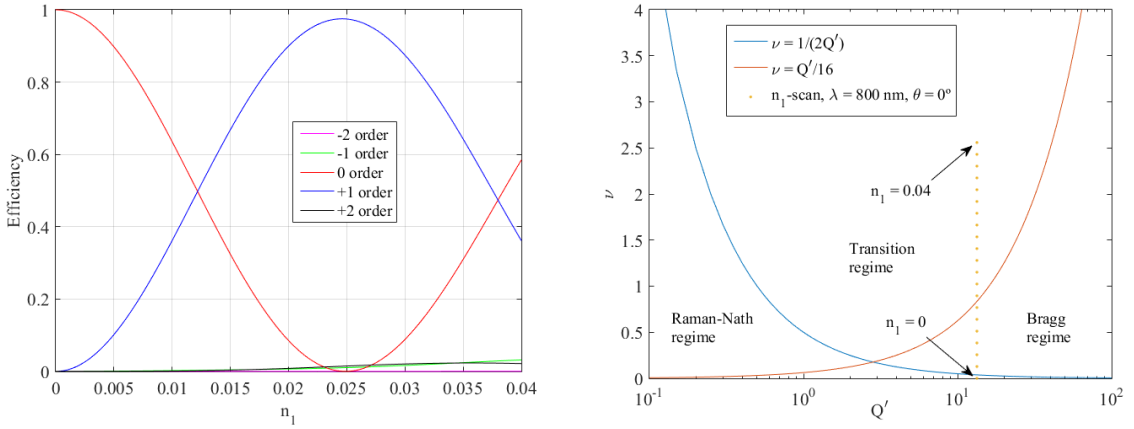

(a) (b)

Figure 6.4: Growth curve (a) and corresponding points in the Q' ν diagram (b).

A correct modeling of the behavior of HOEs in the transition regime is essential to obtain a reliable tool that can be used for any reconstruction conditions. The procedure used in this chapter and the following one for the determination of the energetic performance of HOEs is to numerically solve the set of coupled differential equations (6.8) for the number of diffraction orders that exist for each reconstruction wavelength and angle of incidence, as shown above. It is valid in all three regimes and no assumptions about which one the HOE operates in need to be made.

The convenience of using volume HOEs with low Q values [2], low spatial frequencies [10] and low thicknesses [11] for solar concentration applications had been previously stated. All three approaches (although originally contemplated for volume HOEs in the cited publications, as stated by their authors) point towards the extension to the transition regime. Nevertheless, to our knowledge, deliberately including the transition regime was a novel approach not found in the literature for broadband applications.

The advantages of including the transition regime are the lower angular and chromatic selectivity of the +1 diffraction order, which in principle imply higher energy received by the PV cell. They also present lower chromatic dispersion, so rays from a wider wavelength range

will reach the PV cell, which is desirable as long as it does not exceed its sensitivity range. Besides, other diffraction orders apart from the +1 may reach the PV cell and also contribute to the generation of electricity.

On the other hand, the incident energy on the HOE must be distributed among more diffraction orders than in the volume regime, so the +1 order cannot reach 100% efficiency.

An optimal design is needed in which a compromise among these aspects is reached.

A theoretical and experimental analysis of HOEs partly operating in the transition regime is carried out in the publications included in this chapter, [1,14]. Holographic gratings performing in the different regimes are recorded on Bayfol HX photopolymer and experimentally characterized. This allows the determination of the dependency of the index modulation with the spatial frequency, needed for the description of holographic lenses. The ray-tracing algorithm used in previous chapters is adapted in order to include the transition regime with the multiwave coupled wave theory. Resulting simulations are validated with the experimental characterization of recorded cylindrical holographic lenses partly performing in the transition regime.

The optical concentration and the electrical current concentration of three different lenses are compared. The latter parameter includes the response of the PV cell, in addition to the performance of the HOEs and the incident spectrum, thus allowing a more accurate comparison of the systems.

References:

1. J. Marín-Sáez, M. V. Collados, D. Chemisana, and J. Atencia, "Energy analysis of holographic lenses for solar concentration," in *Proceedings of SPIE* (2017), **10233** p. 1023317.
2. P. Bañares-Palacios, S. Álvarez-Álvarez, J. Marín-Sáez, M.-V. Collados, D. Chemisana, and J. Atencia, "Broadband behavior of transmission volume holographic optical elements for solar concentration," Opt. Express **23**, A671–A681 (2015).
3. R. Alferness, "Analysis of propagation at the second-order Bragg angle of a thick holographic grating," J. Opt. Soc. Am. **66**, 353 (1976).
4. F. G. Kaspar, "Diffraction by thick, periodically stratified gratings with complex dielectric constant," J. Opt. Soc. Am. **63**, 37 (1973).
5. R. Magnusson and T. K. Gaylord, "Analysis of multiwave diffraction of thick gratings," J. Opt. Soc. Am. **67**, 1165 (1977).
6. M. G. Moharam, T. K. Gaylord, and R. Magnusson, "Criteria for Bragg regime diffraction by phase gratings," Opt. Commun. **32**, 14–18 (1980).
7. M. G. Moharam, T. K. Gaylord, and R. Magnusson, "Criteria for Raman-Nath regime diffraction by phase gratings," Opt. Commun. **32**, 19–23 (1980).
8. R. Syms, *Practical Volume Holography* (Oxford University Press, 1990).
9. P. Markovski, N. Koleva, and T. Todorov, "Some characteristics of phase holographic gratings in the intermediate regime of diffraction," Opt. Quantum Electron. **13**, 515–518 (1981).
10. H. Akbari, I. Naydenova, H. Ahmed, S. McCormack, and S. Martin, "Development and

testing of low spatial frequency holographic concentrator elements for collection of solar energy," Sol. Energy **155**, 103–109 (2017).

11. R. Ranjan, A. Ghosh, and H. L. Yadav, "Dependence of angular selectivity of thick phase transmission hologram recorded in dichromated gelatin film on processing parameters," J. Opt. **41**, 65–69 (2012).

12. A. Ghosh, A. K. Nirala, and H. L. Yadav, "Optical design and characterization of holographic solar concentrators for photovoltaic applications," Optik (Stuttg). **168**, 625–649 (2018).

13. A. Villamarín, J. Atencia, M. V. Collados, and M. Quintanilla, "Characterization of transmission volume holographic gratings recorded in Slavich PFG04 dichromated gelatin plates.," Appl. Opt. **48**, 4348–4353 (2009).

14. J. Marín-Sáez, J. Atencia, D. Chemisana, and M.-V. Collados, "Full modeling and experimental validation of cylindrical holographic lenses recorded in Bayfol HX photopolymer and partly operating in the transition regime for solar concentration," Opt. Express **26**, A398 (2018).

Energy analysis of holographic lenses for solar concentration

Julia Marín-Sáez[a], M. Victoria Collados[b], Daniel Chemisana[a], Jesús Atencia*[b]
[a]Applied Physics Section of the Environmental Science Department, Polytechnic School, University of Lleida, E-25001 Lleida, Spain;
[b]Applied Physics Department, Aragon Institute of Engineering Research (I3A), University of Zaragoza, E-50009 Zaragoza, Spain

ABSTRACT

The use of volume and phase holographic elements in the design of photovoltaic solar concentrators has become very popular as an alternative solution to refractive systems, due to their high efficiency, low cost and possibilities of building integration. Angular and chromatic selectivity of volume holograms can affect their behavior as solar concentrators. In holographic lenses, angular and chromatic selectivity varies along the lens plane. Besides, considering that the holographic materials are not sensitive to the wavelengths for which the solar cells are most efficient, the reconstruction wavelength is usually different from the recording one. As a consequence, not all points of the lens work at Bragg condition for a defined incident direction or wavelength. A software tool that calculates the direction and efficiency of solar rays at the output of a volume holographic element has been developed in this study. It allows the analysis of the total energy that reaches the solar cell, taking into account the sun movement, the solar spectrum and the sensitivity of the solar cell. The dependence of the recording wavelength on the collected energy is studied with this software. As the recording angle is different along a holographic lens, some zones of the lens could not act as a volume hologram. The efficiency at the transition zones between volume and thin behavior in lenses recorded in Bayfol HX is experimentally analyzed in order to decide if the energy of generated higher diffraction orders has to be included in the simulation.

Keywords: Holographic lenses, solar concentration, volume holograms, photovoltaics

1. INTRODUCTION

Holographic Optical Elements (HOEs) are a versatile technology that has multiple applications. One of them is solar concentration, for which different configurations have been studied[1]. With the adequate design, both holographic gratings and cylindrical and spherical lenses can act as solar concentrators.

The efficiency of HOEs reaches its maximal values for certain conditions depending, among other parameters, on the incidence angle and wavelength, that is, they present angular and chromatic selectivity.

HOEs can be designed so that their efficiency reaches high values for a particular wavelength range, which in solar concentration applications needs to take into account the incident solar spectrum and also the kind of receiver the solar radiation will be directed to. Figure 1 shows the ASTM standard solar spectrum AM 1.5D, normalized to 1000 W/m^2 over the wavelength range 350-1200 nm, depicted with a blue line and left *y*-axis. The spectral response curve of a mono-crystalline Si photovoltaic cell is plotted as well, with a red line and right *y*-axis. The spectral range a HOE should diffract more efficiently towards this type of PV cell may be determined with a compromise between these two curves, and would be then centered at 800 nm, which will be referred to as the target wavelength.

*atencia@unizar.es

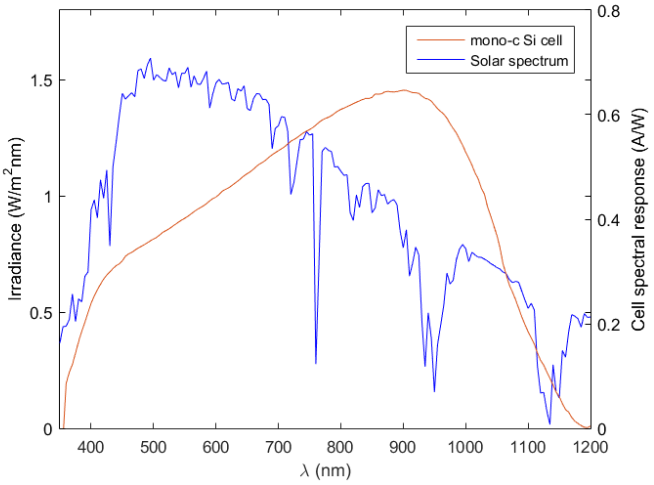

Figure 1. ASTM standard solar spectrum AM 1.5D, normalized to 1000 W/m^2 over the wavelength range 350-1200 nm (blue curve, left *y*-axis). Cell response of a mono-crystalline Si cell (red curve, right *y*-axis).

Regarding the angular selectivity, since the apparent position of the Sun in the sky changes along the day and the year, tracking of its movement may be required in order to avoid the efficiency loss that occurs when the incident angle is too different from the optimal conditions. When the incidence angle varies along one direction, that lies on the plane defined by the wavevectors of the recording beams, the efficiency decreases promptly (direction of high angular selectivity); whereas if it varies along the perpendicular direction, the efficiency decreases slowly (direction of low angular selectivity). Cylindrical holographic lenses are a rather suitable option for solar concentration, because if they are placed in such a way that the direction of low angular selectivity matches the daily solar movement direction[2,3], tracking is only needed in one axis, simplifying the final system design.

Volume HOEs can achieve 100% efficiency, which is desired in most applications. However, their chromatic and angular selectivity are also very high. HOEs operating at the limit of the volume regime or even in the transition regime achieve very high efficiency as well, whereas enlarging the acceptance angular and spectral range. Holographic cylindrical lenses for solar concentration may benefit from that, since a broad spectrum is desired to be diffracted.

Among the different photosensitive materials for holographic recording, photopolymers have been frequently used for the recording of holographic lenses[4–6] or gratings[7]. Bayfol HX, a photopolymeric recording material developed by Covestro AG[8], offers very interesting advantages, such as the lack of requirement of a wet processing after the recording; a simple photocuring process is needed instead. It can also provide the dynamic range necessary for recording HOEs that are highly efficient at 800 nm[9].

Holographic cylindrical lenses have been studied in certain systems designed to concentrate solar irradiance onto one or more photovoltaic cells. Gordon et al.'s design[10] is based on a system formed by two different holographic cylindrical lenses, each diffracting more efficiently a spectral range towards a different PV cell, so a broader part of the incident spectrum can be used. Ludman's configuration[11,12] also includes several PV cells but its geometry presents an important characteristic: the transmitted order (which includes the infrared that may cause overheating of the PV cell and a worsening of its performance) does not reach any PV cell, thus avoiding this problem. With that scope in mind, some concentrating holographic systems have been proposed by the authors[2,13], comprising volume cylindrical holographic lenses.

This work studies the effect of two different aspects of the design of cylindrical holographic lenses on the overall system performance and the collected irradiance on a PV cell. Section 2 covers a brief theoretical background on holographic recording, concentration coefficients used on solar applications and the developed software tool used for the theoretical calculations. The influence of the recording wavelength on the behavior of a holographic cylindrical lens is analyzed in section 3. Section 4 presents a preliminary analysis of a holographic cylindrical lens operating in the transition regime for a reconstruction wavelength of 800 nm.

2. THEORETICAL BACKGROUND

2.1 Basis of holographic recording

Holograms are recorded on a photosensitive medium with the interference of two coherent waves. A cylindrical holographic lens can be recorded with a cylindrical wave and a plane wave, with wave propagation vectors $\vec{k_c}$ and $\vec{k_p}$, respectively. The incidence angle of the cylindrical beam at the medium's surface is different along a direction, thus $\vec{k_c} = \vec{k_c}(\vec{r})$, which can be set to match the *y*-axis. Therefore, the interference pattern of the recording waves has a different frequency along *y*-direction, whereas in a plane grating this frequency is constant, since the angle between the recording beams does not vary. The grating vector, defined with equation (1), has a different direction and modulus at each point of the *y*-axis of a cylindrical holographic lens.

$$\vec{K} = \vec{k_p} - \vec{k_c} \tag{1}$$

The modulus of the grating vector is given by

$$K = \frac{2\pi}{\Lambda} \tag{2}$$

where Λ is the period of the interference fringes of the recording waves. In phase holograms, these variations of the intensity along the photosensitive material may be recorded on it by means of variations of the refractive index, so it can be written as

$$n = n_0 + n_1 \sin\left(\vec{K}\cdot\vec{r}\right) \tag{3}$$

where n_0 is the average refractive index and n_1 is the index modulation. Since the grating vector $\vec{K}$ is different along *y*-direction, the period and frequency of the variations of the refractive index are different as well.

After the refractive index variations have been made permanent in the photosensitive medium, if the resulting hologram is a volume HOE, when it is illuminated two diffraction orders emerge at the output: the transmitted order (or 0 order of diffraction) and the first diffracted order (or +1 order). The efficiency of the diffracted order is maximal (and the one of the transmitted order minimal) when Bragg condition is met, defined with equation (4), where θ_1 and θ_2 are the angles of incidence of the transmitted and the diffracted wave.

$$2n_0\Lambda \sin\left(\frac{\theta_1 - \theta_2}{2}\right) = \lambda \tag{4}$$

If the hologram is not a volume one, more diffraction orders emerge, and the efficiency of the +1 diffracted order is consequently lower than in the previous case.

2.2 Concentration coefficients for solar applications

In solar concentration applications, a parameter called concentration coefficient is defined[3], with equation (5):

$$CC = \frac{\Phi_C}{\Phi_L}\frac{A_L}{A_C} = \frac{\sum_\lambda \Phi_{C,\lambda}\Delta\lambda}{\sum_\lambda \Phi_{L,\lambda}\Delta\lambda}\frac{A_L}{A_C} \tag{5}$$

It is the ratio of the irradiance received by the photovoltaic cell (which is the quotient between the optical flux received, Φ_C, and the surface of the cell, A_C) and the irradiance at the entrance pupil of the system (the quotient between the incident optical flux, Φ_L, and the surface of the entrance pupil, that is, the surface of the lens A_L). The flux can also be

expressed as the sum of the spectral flux corresponding to each wavelength, multiplied by the wavelength step ($\sum_{\lambda}\Phi_{C,\lambda}\Delta\lambda$ for the flux on the cell and $\sum_{\lambda}\Phi_{L,\lambda}\Delta\lambda$ at the entrance pupil of the system).

For solar concentration purposes, it is necessary not only to calculate the concentration coefficient defined in equation (5) as the ratio of irradiances, but also the ratio of current intensities generated by the PV cell with and without the holographic concentrator, in order to take into account the spectral response of the cell. It is defined in equation (6), where SR_{λ} is the spectral response of the cell (the current intensity generated due to the optical flux that reaches the cell).

$$CC_{current\,intensity} = \frac{\sum_{\lambda}\Phi_{C,\lambda}SR_{\lambda}\Delta\lambda}{\sum_{\lambda}\Phi_{L,\lambda}SR_{\lambda}\Delta\lambda}\frac{A_L}{A_C} \tag{6}$$

2.3 Software tool

A software tool has been developed in Matlab in order to study the performance of HOEs[3,14]. It is based on a ray tracing algorithm, so the behavior of each point of the HOE is examined independently. This is based on the assumption that it can be considered that for each point of a cylindrical holographic lens the recording waves are two plane waves, that is, each point of the HOE can be treated as a local grating.

The efficiency of each ray that reaches the HOE is calculated based on the coupled wave differential equations, either solving them applying Kogelnik's Coupled Wave Theory[15] when it is a volume hologram, or solving them numerically when it is not[16].

The algorithm takes into account Fresnel reflection losses[17] at both the entrance and output interfaces, and the AM 1.5D solar spectrum can be considered to be the incident spectrum. Since sunlight is depolarized, the efficiencies are calculated for both polarizations and then averaged to obtain the final efficiency.

3. ANALYSIS OF THE INFLUENCE OF THE RECORDING WAVELENGTH ON THE COLLECTED ENERGY

Three recording wavelengths have been chosen for this analysis: two typical laser wavelengths (532 and 632.8 nm) and the target wavelength (800 nm). One may assume beforehand that the best results would be achieved when the recording wavelength matches the target wavelength, since less aberration effects would appear at the reconstruction. However, the reconstructed image quality is not a critical factor in solar concentration applications. Instead, the total energy belonging to a certain spectral range that reaches the receiver is desired to be optimum, and it is not necessary that the rays converge to a point, but a small area.

The three lenses were designed so that Bragg condition would be met at the center of the lens when replaying with $\theta_0 = 0°$ and $\lambda = 800$ nm. The angle with *z*-axis (defined perpendicular to the HOE, so that the *YZ*-plane is the recording plane) of the diffracted wave at that point under those conditions is $\theta_{+1} = 45°$ for all three lenses, so the spatial period is the same at the center and varies similarly along the lens. The paraxial image at the reconstruction is located in the same *Z*-plane, 70 mm away from the HOE.

The angles of incidence of the two recording waves are presented in Table 1. They ensure that the whole HOEs operate at the volume regime when reconstructing with $\lambda = 800$ nm.

A global analysis of the performance of each lens has been carried out by means of the software tool mentioned in section 2. The direction of the diffracted rays with incidence angle $\theta_0 = 0°$ and wavelengths from 350 to 1200 nm was calculated, as well as their efficiency. As expected when the recording wavelength does not match the reconstruction wavelength, the efficiency of the 800 nm rays that impact the center of each lens is maximal, and it decreases when moving away towards positive or negative values of y, as shown in Figure 2. That is not the case of the lens recorded

with λ_R = 800 nm, where Bragg condition is met at every point of the lens when reconstructing with θ_0 = 0° and λ = 800 nm. The efficiency of two other sample wavelengths near the target wavelength, 700 and 900 nm, is also represented in Figure 2 for each lens. Since both polarizations are taken into account in the calculations and the efficiency of the 800 nm rays is 100 % at the center for one of them, but not for the other one, the final efficiency does not reach 100 % in any case.

Table 1. Angles of incidence in air θ_p (of the plane wave) and θ_c (of the cylindrical wave, at the center of the lens) of the recording waves of the considered holographic lenses.

	λ_R = 532 nm	λ_R = 632.8 nm	λ_R = 800 nm
θ_p (°)	7.2	4.5	0
θ_c (°)	36.5	39.7	45

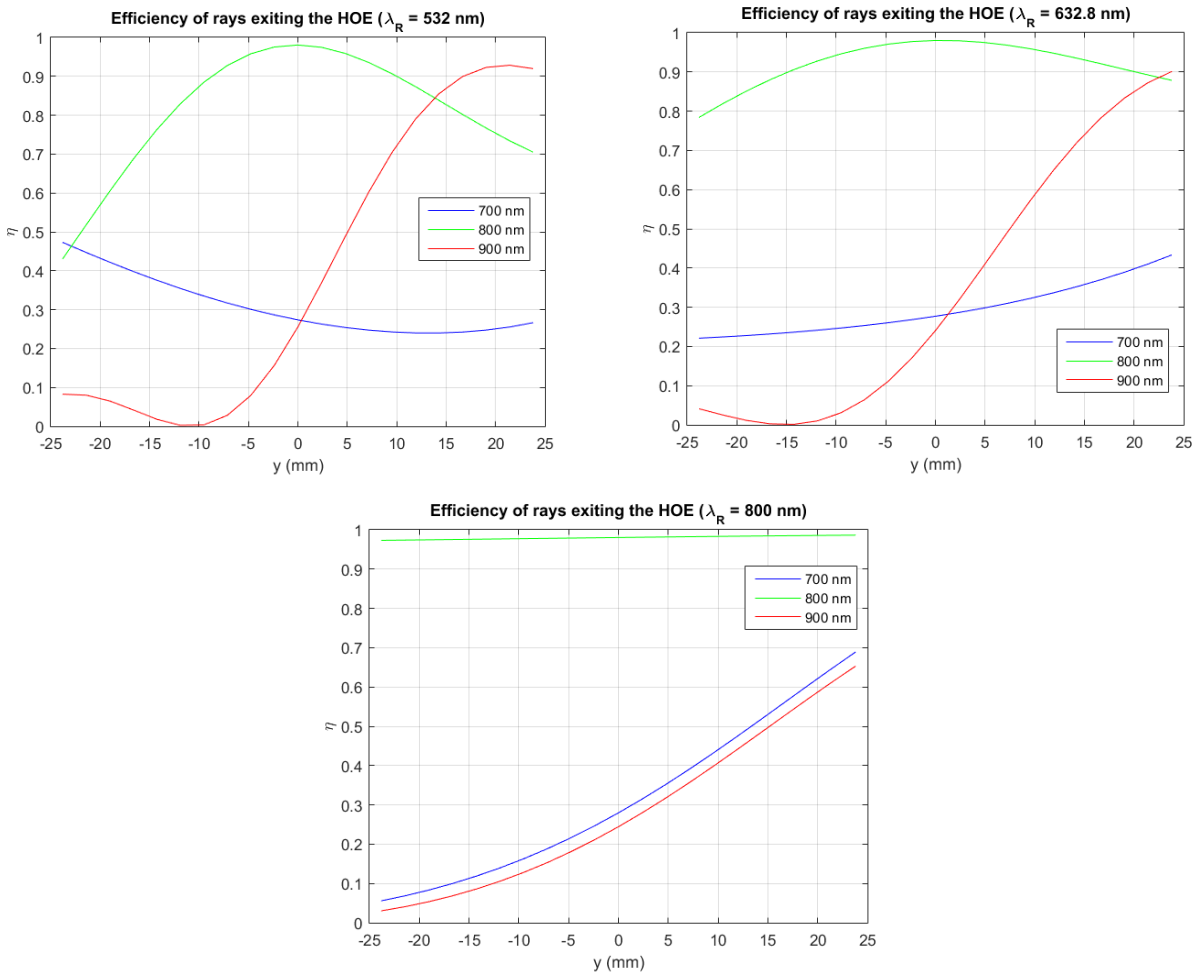

Figure 2. Efficiency of 700 (blue curves), 800 (green curves) and 900 nm (red curves) rays when reconstructing with θ = 0° at the output of lenses recorded at 532 (top left), 632.8 (top right) and 800 nm (bottom).

Not only is the efficiency of each ray relevant for this analysis, but also its direction, to determine if they would be collected by the PV cell. The calculated ray tracing for those three wavelengths is plotted in Figure 3. The presence of aberrations in the 800 nm rays diffracted by the lenses recorded with 532 and 632.8 nm can be clearly noticed, as well as the lack of them in the lens recorded with 800 nm. The black line at around z = 40 mm in the first two cases and z = 60 mm in the third one represents the PV cell located at a position, in which all 800 nm rays are collected and the final concentration coefficient is optimized. The spectral irradiance received by the cell with each of the three lenses when considering the AM 1.5D solar spectrum normalized to 1000 W/m^2 over the range 350-1200 nm is shown in Figure 4. Fresnel reflection losses[17] on the entrance and output interfaces are also taken into account in the calculations.

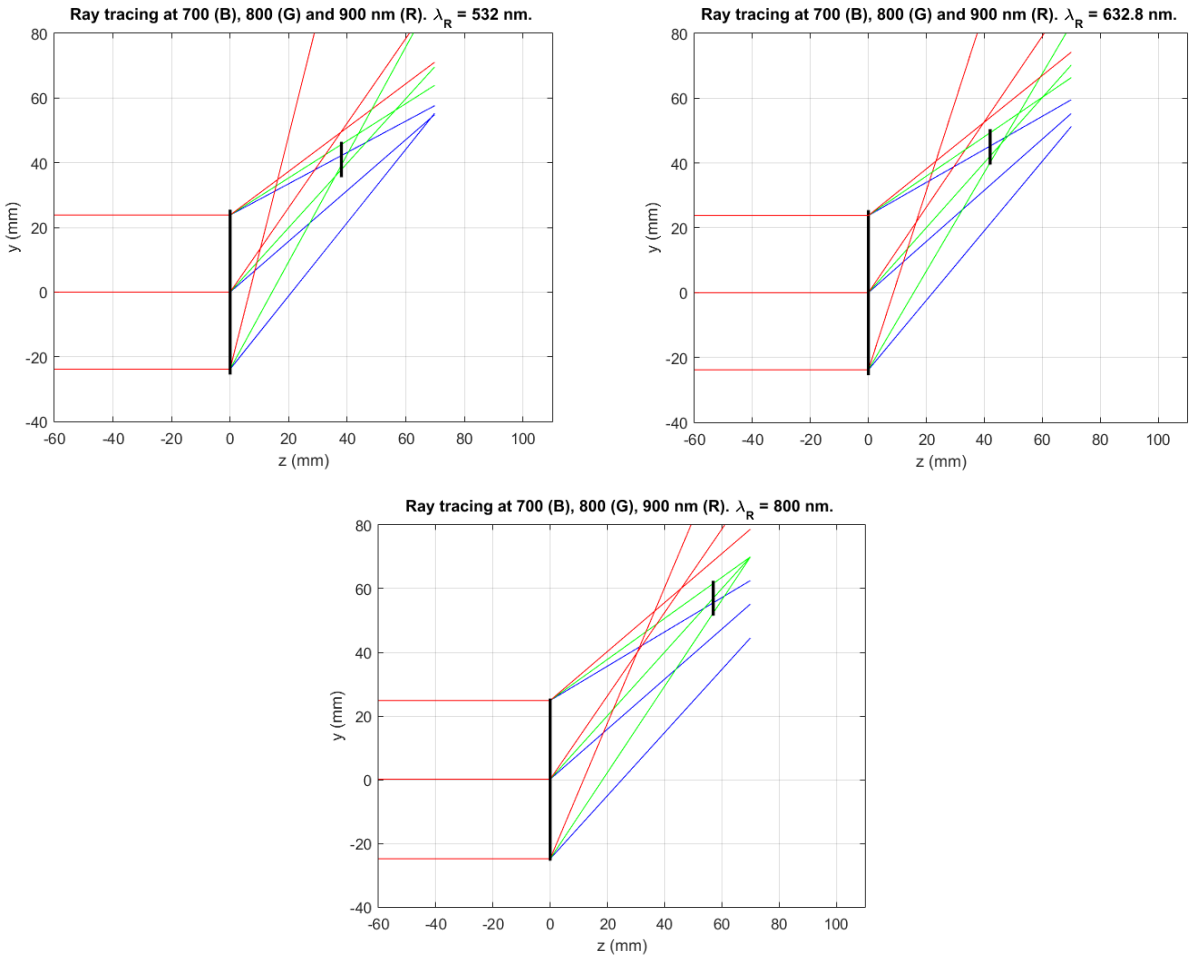

Figure 3. Ray tracing of rays of 700 (blue lines), 800 (green lines) and 900 nm (red lines) at the reconstruction stage of lenses recorded at 532 (top left), 632.8 (top right) and 800 nm (bottom), with θ = 0°. The black lines around z = 40 and 60 mm are possible placements of the PV cell.

The resulting optical and current intensity concentration coefficients, defined with equations (5) and (6), are presented in Table 2. They may seem low values, but it has to be taken into account that the concentrated spectrum belongs only to the wavelength range for which the PV cell has a spectral response, and no irradiance outside that wavelength range will cause an increase of the temperature of the PV cell, so its performance would not decline. Besides, more lenses could be included in the system to contribute with more irradiance corresponding to the diffracted or even the transmitted order to the same PV cell without an excessive increase of the temperature, such as the geometry described and analyzed in another work by the authors[13].

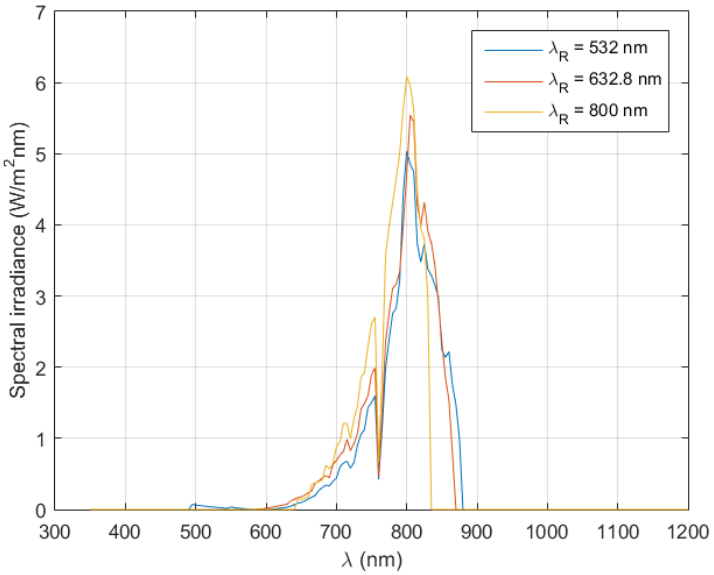

Figure 4. Spectral irradiance received by the PV cell when it is located at its optimum placement, with the lens recorded with 532 nm (blue curve), 632.8 nm (orange curve) and 800 nm (yellow curve). The entrance spectrum is the AM 1.5D solar spectrum normalized to 1000 W/m^2 over the range 350-1200 nm and Fresnel reflection losses at the entrance and output interfaces are considered.

Table 2. Concentration coefficients obtained with the optimum PV cell placement for each lens.

	λ_R = 532 nm	λ_R = 632.8 nm	λ_R = 800 nm
CC	0.41	0.44	0.43
$CC_{current\,intensity}$	0.57	0.60	0.57

Recording the holographic cylindrical lens with the same wavelength as the target wavelength does not result in higher concentration coefficients than in the other cases. Furthermore, since no 800 nm photosensitive material adequate for this application has been found, it is not convenient to continue a thorough study with this recording wavelength. It is observed that the change in the concentration coefficients when recording a cylindrical lens with any of the other two wavelengths is not too big when the same design criterions are applied in order to obtain similar reconstruction conditions. Therefore, the election of the recording wavelength may be based on the laboratory equipment.

4. HOLOGRAPHIC CYLINDRICAL LENSES OPERATING IN THE TRANSITION REGIME

The high angular selectivity of holographic lenses operating in the volume regime may be a drawback in solar concentration applications, even if tracking in the direction of highest selectivity is carried out. Since the incidence angle of the cylindrical beam at the recording is different at each point of the lens along *y*-direction, the angle of incidence that fulfills Bragg condition at each point when reconstructing at 800 nm is also different from the one of the center of the lens. This difference is greater the further away from the center the considered point is. As a consequence, the efficiency of the 800 nm rays when reconstructing at Bragg angle for the center of the lens (which is, in principle, the reconstruction incidence direction that would be maintained with the tracking system) depends on the point of the lens

that the rays impact, being maximum at the center and decreasing when moving away from it. This effect is emphasized the more into the volume regime the HOE operates at 800 nm, since the angular selectivity is higher.

Therefore, holographic cylindrical lenses that operate at the limit of the volume regime or even at the transition regime between Bragg regime and Raman-Nath regime for the target wavelength and a small spectral range around it are of special interest for solar concentration applications. This way, a small deviation of the incident reconstruction direction from Bragg angle does not imply a big decrease of the efficiency.

The analytical solution of Kogelnik's Coupled Wave Theory can only be applied to volume HOEs, in which solely the transmitted and first order diffracted wave appear. In order to include higher diffraction orders, the coupled differential equations need to be solved numerically, which adds time to calculations, so it is not convenient unless it is necessary.

A holographic cylindrical lens has been recorded on Bayfol HX photopolymer at 532 nm with the recording geometry shown in Figure 5. The center of the lens fulfills Bragg condition when reconstructing with $\theta_0 = 0°$ and $\lambda = 800$ nm. Part of the HOE operates in the volume regime and part of it in the transition regime when reconstructing with this wavelength.

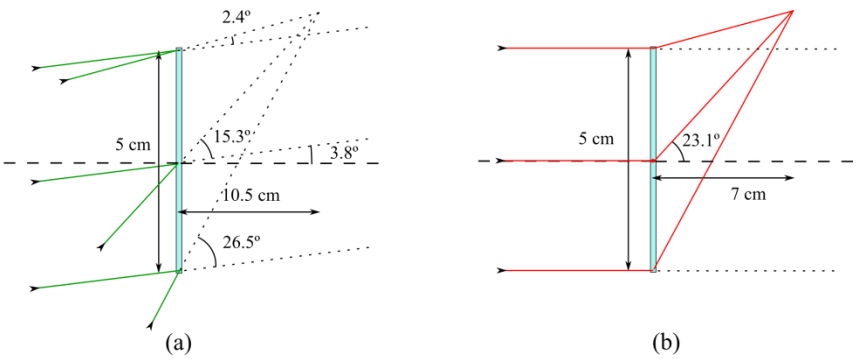

Figure 5. Recording geometry of the considered holographic cylindrical lens at 532 nm (left) and expected ray tracing at the reconstruction with $\theta = 0°$ and 800 nm.

After the recording process, photocuring was carried out as previously described[9]. The intensity of each diffracted ray was then measured (with Newport Power Meter Model 1815-C with detector Model 818-SL, with an uncertainty of 5 μW) when illuminating a point of the HOE with a laser emitting at 800 nm (ThorLabs Laser Diode CPS808A, emitting 4.4 mW) and at $\theta_0 = 0°$. The relative efficiency of each order of diffraction at each point was calculated with equation (7):

$$\eta_i = \frac{I_i}{\sum_j I_j} \tag{7}$$

where I_i is the measured intensity of the i-diffracted order. The resulting efficiencies are plotted in Figure 6 with filled circles. It can be noticed that for $y \leq$ -10 mm only the first diffracted order (+1) and the transmitted order can be found, whereas when $y >$ -10 mm more diffraction orders emerge, achieving non negligible efficiencies. At the edge of the HOE where the angle between the recording beams was the smallest (y = +25 mm), the efficiency of the -1 order of diffraction even reaches the value of the efficiency of the +1 order.

The efficiency of each diffraction order with 800 nm at the output of the lens has been calculated by a numerical resolution of the coupled differential equations. An estimated value of the index modulation, n_1, was assigned to each point of the lens according to its spatial frequency. The obtained theoretical efficiencies are shown in Figure 6 as well. Good agreement between theoretical and experimental results has been observed.

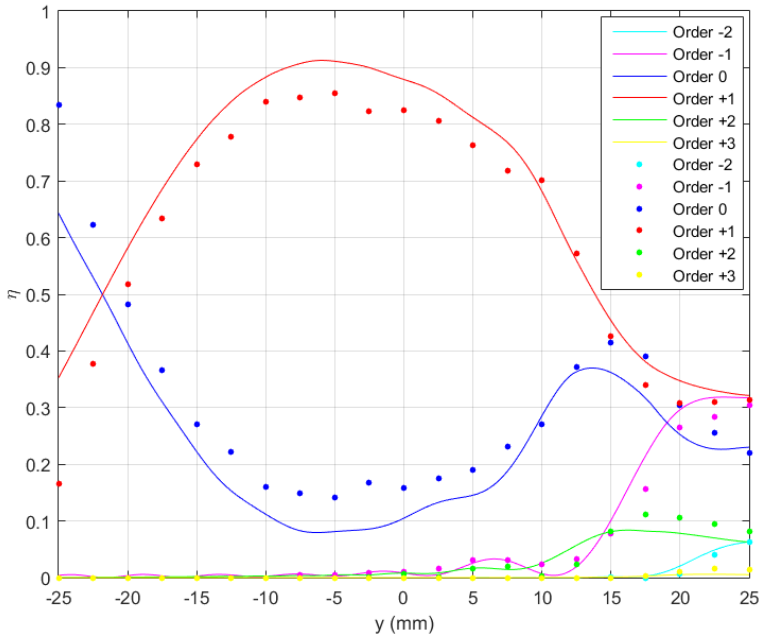

Figure 6. Experimental (filled circles) and theoretical (lines) efficiencies of every order of diffraction observed at each point of the considered holographic cylindrical lens when reconstructing with $\theta = 0°$ and $\lambda = 800$ nm.

The direction of every ray was also calculated with the software. Figure 7 illustrates the ray tracing of all diffraction orders observed (-2, -1, 0, +1, +2 and +3 orders, depicted with cyan (C), magenta (M), blue (B), red (R), green (G) and yellow (Y) lines, respectively) that emerge from the center and the edges of the lens when reconstruction is carried out at 800 nm and $\theta_0 = 0°$.

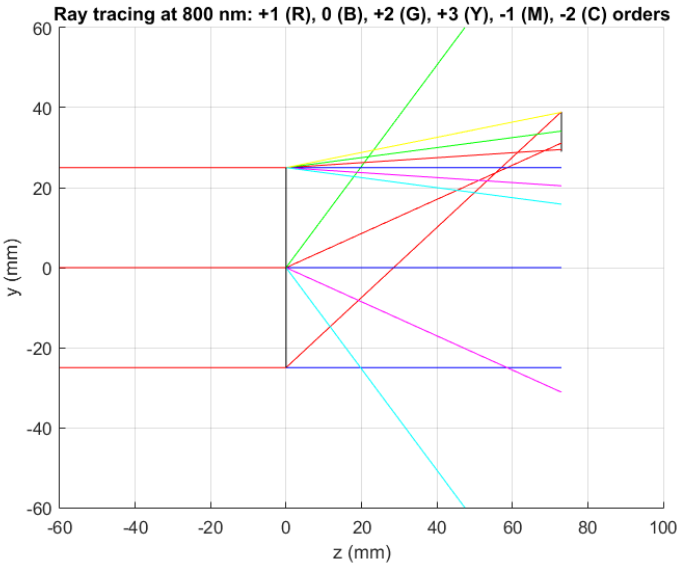

Figure 7. Ray tracing of rays corresponding to all diffraction orders (-2, -1, 0, +1, +2 and +3 orders, depicted with cyan, magenta, blue, red, green and yellow lines, respectively) observed at the considered lens output when reconstructing with 800 nm and $\theta = 0°$. The black line at $z = 73$ mm represents a possible placement of the PV cell, where all 800 nm rays corresponding to the +1 diffracted order are collected.

Simulations of the energetic performance of the lens and different placements of the 10 mm wide photovoltaic cell have been carried out. Solar movement tracking in the direction of highest angular selectivity is assumed, so the reconstruction angle is $\theta_0 = 0°$, and the incident irradiance corresponds to the standard AM 1.5D solar spectrum normalized to 1000 W/m^2 over the range 350-1200 nm. Fresnel reflection losses[17] at the entrance and output interfaces have been taken into account. One of the optimum placements is the one depicted in Figure 7, collecting all +1 order of diffraction rays of 800 nm. The spectral irradiance received by the whole surface of the PV cell due to all diffraction orders is shown in Figure 8. As expected, the maximal spectral irradiance is concentrated around 800 nm, and although this curve reaches values of irradiance lower than the ones obtained with the volume HOEs studied in the previous section, it is wider, so the total area under the curve is bigger and therefore, more energy is collected. Besides, the +2 order of diffraction rays with wavelengths around 450 nm, and to a lesser extent the +3 order of diffraction, despite having lower irradiance, also reach the PV cell and contribute to the generation of current intensity.

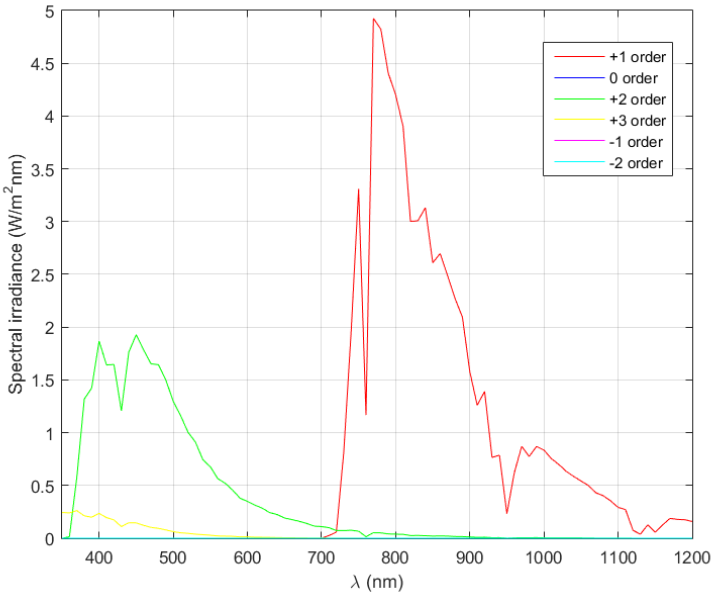

Figure 8. Spectral irradiance received by the PV cell placed according to Figure 7, with incoming standard AM 1.5D solar spectrum normalized to 1000 W/m^2 over the range 350-1200 nm and $\theta = 0°$, due to all orders of diffraction (-2, -1, 0, +1, +2 and +3 orders, depicted with cyan, magenta, blue, red, green and yellow lines, respectively).

A total optical concentration coefficient (defined with equation (5)) of 1.01 was achieved, which is higher than the ones obtained in the previous section. It is roughly the same value that would be obtained with no optical concentration system, however, it has to be remembered that the concentrated spectral range corresponds mainly to the optimal wavelength range of the PV cell, so the generated current intensity would be higher than with no concentration system. In fact, if the spectral response of the cell is taken into account, a total current intensity concentration coefficient (defined with equation (6)) of 1.14 is obtained, which is a promising result.

Other factors also need to be noted. The spectral irradiance from the largest considered wavelengths that reaches the cell is not significantly higher than the corresponding values of the solar spectrum. That means that the temperature of the cell due to solar radiation will not be increased because of it.

Furthermore, similarly to the discussion on the previous section, this geometry allows the use of more than one holographic concentrator leading sun rays to the same PV cell, so the total irradiance received in the optimum spectral range and the generated current intensity would increase.

Higher orders of diffraction need to be taken into account in the calculations when the HOE operates in the transition regime, because if not, the efficiency of the +1 diffracted order would be overestimated. Besides, depending on the placement of the PV cell, the rays corresponding to higher orders of diffraction might reach it as well and contribute to the generation of electricity and also to its increase of temperature.

5. CONCLUSION

Some energetic aspects of the behavior of holographic cylindrical lenses have been studied in this work by means of a developed ray tracing algorithm. On the one hand, a theoretical analysis of the effect of the recording wavelength on the efficiency of the diffracted beam has proved that it is not critical for this application, since the image quality of the reconstruction wave is not relevant. On the other hand, a holographic cylindrical lens operating both in the volume regime and the transition regime has been recorded, and the measured efficiency of every diffracted order that emerges is in good agreement with the calculated values obtained with the algorithm. The spectral irradiance that a PV cell at a certain location would collect has been calculated, providing higher concentration coefficients than the volume holographic cylindrical lenses considered. This shows that HOEs operating in the transition regime should be considered for solar concentration applications, where a broadband diffracted spectrum is desired.

Future work includes further analysis of holographic cylindrical lenses operating in the transition regime. A more thorough analysis of the coupling between the concentrating holographic system and the PV cell is also needed, in which the whole solar spectrum is considered, and not only the spectral range 350-1200 nm, in order to study the direction and energy of the rays with higher wavelengths. Applying a model of the behavior of the PV cell, an estimation of the cell temperature and the corresponding decrease of the current intensity can be made.

AKNOWLEDGEMENTS

This research was supported by the Ministerio de Economía y Competitividad of Spain with funding (grant ENE2013-48325-R), the Generalitat de Catalunya (grant 2016 FI_B1 00019) and the Diputación General de Aragón-Fondo Social Europeo (TOL research group, T76).

REFERENCES

[1] Collados, M. V., Chemisana, D., Atencia, J., "Holographic solar energy systems: The role of optical elements," Renew. Sustain. Energy Rev. **59**, 130–140 (2016).

[2] Chemisana, D., Collados, M. V., Quintanilla, M., Atencia, J., "Holographic lenses for building integrated concentrating photovoltaics," Appl. Energy **110**, 227–235 (2013).

[3] Bañares-Palacios, P., Álvarez-Álvarez, S., Marín-Sáez, J., Collados, M.-V., Chemisana, D., Atencia, J., "Broadband behavior of transmission volume holographic optical elements for solar concentration," Opt. Express **23**(11), A671–A681 (2015).

[4] Fernández, R., Gallego, S., Márquez, A., Francés, J., Navarro-Fuster, V., Pascual, I., "Diffractive lenses recorded in absorbent photopolymers," Opt. Express **24**(2), 1559 (2016).

[5] Sam, S. T. L., Kumar, A. P. T., Predeep, P., Thakur, M., Varma, M. K. R., "Design and Optimization of Photopolymer Based Holographic Solar Concentrators," Opt. Phenomena, Mater. Devices Charact. (AIP Conf. Proceedings), 248–250 (2011).

[6] Bianco, G., Ferrara, M. A., Borbone, F., Roviello, A., Pagliarulo, V., Grilli, S., Ferraro, P., Striano, V., Coppola, G., "Multiplexed holographic lenses : realization and optical characterization," 2015 Fotonica AEIT Ital. Conf. Photonics Technol., Institution of Engineering and Technology (2015).

[7] Akbari, H., Naydenova, I., Martin, S., "Using acrylamide-based photopolymers for fabrication of holographic optical elements in solar energy applications," Appl. Opt. **53**(7), 1343 (2014).

[8] Berneth, H., Bruder, F.-K., Fäcke, T., Jurbergs, D., Hagen, R., Hönel, D., Rölle, T., Walze, G., "Bayfol HX photopolymer for full-color transmission volume Bragg gratings," Proc. SPIE. **9006**, 900602 (2014).
[9] Marín-Sáez, J., Atencia, J., Chemisana, D., Collados, M.-V., "Characterization of volume holographic optical elements recorded in Bayfol HX photopolymer for solar photovoltaic applications," Opt. Express **24**(6), A720 (2016).
[10] Gordon, M., Zhang, D., Vorndran, S., Russo, J. M., Luscombe, C. K., Shaheen, S. E., Kostuk, R. K., "Planar holographic spectrum-splitting PV module design," Proc. SPIE, 846808 (2012).
[11] Ludman, J. E., Riccobono, J., Reinhand, N. O., Semenova, I. V., Martín, J., Tai, W., Li, X., Syphers, G., "Holographic solar concentrator for terrestrial photovoltaics," Proc. 24th IEEE Photovolt. Spec. Conf., 1208–1211 (1994).
[12] Ludman, J. E., Riccobono, J., Semenova, I. V., Reinhand, N. O., Tai, W., Li, X., Syphers, G., Rallis, E., Sliker, G., et al., "The optimization of a holographic system for solar power generation," Sol. Energy **60**(1), 1–9, Elsevier Science Ltd (1997).
[13] Marín-Sáez, J., Chemisana, D., Moreno, Á., Riverola, A., Atencia, J., Collados, M.-V., "Energy Simulation of a Holographic PVT Concentrating System for Building Integration Applications," Energies **9**(8), 577 (2016).
[14] Marín-Sáez, J., Collados, M. V., Atencia, J., Chemisana, D., "Optical and Energetic Performance of Volume Holographic Optical Elements for Solar Energy Applications." (in press).
[15] Kogelnik, H., "Coupled wave theory for thick hologram gratings," Bell Syst. Tech. J. **48**(9), 2909–2947 (1969).
[16] Syms, R., Practical Volume Holography, Oxford University Press (1990).
[17] Hecht, E., Optics, Addison Wesley (1998).

Research Article | Vol. 26, No. 10 | 14 May 2018 | OPTICS EXPRESS A398

Optics EXPRESS

Full modeling and experimental validation of cylindrical holographic lenses recorded in Bayfol HX photopolymer and partly operating in the transition regime for solar concentration

JULIA MARÍN-SÁEZ,[1] JESÚS ATENCIA,[2,*] DANIEL CHEMISANA,[1] AND MARÍA-VICTORIA COLLADOS[2]

[1]*Applied Physics Section of the Environmental Science Department, Polytechnic School, University of Lleida, Jaume II 69, 25001 Lleida, Spain*
[2]*Applied Physics Department, Aragon Institute of Engineering Research (I3A), Faculty of Science, University of Zaragoza, Pedro Cerbuna 12, 50009 Zaragoza, Spain*
atencia@unizar.es

Abstract: Concentrating photovoltaics for building integration can be successfully carried out with Holographic Optical Elements (HOEs) because of their behavior analogous to refractive optical elements and their tuning ability to the spectral range that the photovoltaic (PV) cell is sensitive to. That way, concentration of spectral ranges that would cause overheating of the cell is avoided. Volume HOEs are usually chosen because they provide high efficiencies. However, their chromatic selectivity is also very high, and only a small part of the desired spectral range reaches the PV cell. A novel approach is theoretically and experimentally explored to overcome this problem: the use of HOEs operating in the transition regime, which yield lower chromatic selectivity while keeping rather high efficiencies. A model that considers the recording material's response, by determining the index modulation reached for each spatial frequency and exposure dosage, has been developed. It has been validated with experimental measurements of three cylindrical holographic lenses with different spatial frequency ranges recorded in Bayfol HX photopolymer. Simulations of systems comprising two lenses and a mono-c Si PV cell are carried out with the standard AM 1.5D solar spectrum. Promising results are obtained when using the system with lower spatial frequencies lenses: a total current intensity equal to 3.72 times the one that would be reached without the concentrator.

OCIS codes: (090.0090) Holography; (090.1970) Diffractive optics; (090.2890) Holographic optical elements; (350.6050) Solar energy; (050.1965) Diffractive lenses.

References and links

1. D. Chemisana, "Building integrated concentrating photovoltaics: A review," Renew. Sustain. Energy Rev. **15**(1), 603–611 (2011).
2. H. Baig, N. Sarmah, D. Chemisana, J. Rosell, and T. K. Mallick, "Enhancing performance of a linear dielectric based concentrating photovoltaic system using a reflective film along the edge," Energy **73**, 177–191 (2014).
3. D. Chemisana and M. Ibáñez, "Linear Fresnel concentrators for building integrated applications," Energy Convers. Manage. **51**(7), 1476–1480 (2010).
4. G. Li, G. Pei, M. Yang, J. Ji, and Y. Su, "Optical evaluation of a novel static incorporated compound parabolic concentrator with photovoltaic/thermal system and preliminary experiment," Energy Convers. Manage. **85**, 204–211 (2014).
5. N. Yamada, K. Kanno, K. Hayashi, and T. Tokimitsu, "Performance of see-through prism CPV module for window integrated photovoltaics," Opt. Express **19**(S4 Suppl 4), A649–A656 (2011).
6. M. V. Collados, D. Chemisana, and J. Atencia, "Holographic solar energy systems: The role of optical elements," Renew. Sustain. Energy Rev. **59**, 130–140 (2016).
7. American Society for Testing and Materials, "Standard tables for reference solar spectral irradiances: direct normal and hemispherical on 37° tilted surface," in *Book of Standards Volume: 14.04* (2004).
8. R. K. Kostuk and G. Rosenberg, "Analysis and design of holographic solar concentrators," Proc. SPIE **7043**,

#319983 https://doi.org/10.1364/OE.26.00A398
Journal © 2018 Received 18 Jan 2018; revised 16 Mar 2018; accepted 17 Mar 2018; published 28 Mar 2018

Research Article | Vol. 26, No. 10 | 14 May 2018 | OPTICS EXPRESS A399

Optics EXPRESS

70430I (2008).
9. J. M. Castro, D. Zhang, B. Myer, and R. K. Kostuk, "Energy collection efficiency of holographic planar solar concentrators," Appl. Opt. **49**(5), 858–870 (2010).
10. H. Akbari, I. Naydenova, and S. Martin, "Using acrylamide-based photopolymers for fabrication of holographic optical elements in solar energy applications," Appl. Opt. **53**(7), 1343–1353 (2014).
11. J. E. Ludman, J. Riccobono, N. O. Reinhand, I. V. Semenova, J. Martín, W. Tai, X. Li, and G. Syphers, "Holographic solar concentrator for terrestrial photovoltaics," in *Proceedings of the 24th IEEE Photovoltaic Specialists Conference* (1994), pp. 1208–1211.
12. J. E. Ludman, J. Riccobono, I. V. Semenova, N. O. Reinhand, W. Tai, X. Li, G. Syphers, E. Rallis, G. Sliker, and J. Martín, "The optimization of a holographic system for solar power generation," Sol. Energy **60**(1), 1–9 (1997).
13. K. Froehlich, E. U. Wagemann, H. Schulat, H. Schuette, and C. G. Stojanoff, "Fabrication and test of a holographic concentrator for two-color PV operation," Proc. SPIE **2255**, 812–821 (1994).
14. D. Zhang, M. Gordon, J. M. Russo, S. Vorndran, and R. K. Kostuk, "Spectrum-splitting photovoltaic system using transmission holographic lenses," J. Photonics Energy **3**(1), 34597 (2013).
15. S. Vorndran, J. M. Russo, Y. Wu, M. Gordon, and R. Kostuk, "Holographic diffraction-through-aperture spectrum splitting for increased hybrid solar energy conversion efficiency," Int. J. Energy Res. **39**(3), 326–335 (2015).
16. H. Akbari, I. Naydenova, H. Ahmed, S. McCormack, and S. Martin, "Development and testing of low spatial frequency holographic concentrator elements for collection of solar energy," Sol. Energy **155**, 103–109 (2017).
17. D. Chemisana, M. V. Collados, M. Quintanilla, and J. Atencia, "Holographic lenses for building integrated concentrating photovoltaics," Appl. Energy **110**, 227–235 (2013).
18. P. Bañares-Palacios, S. Álvarez-Álvarez, J. Marín-Sáez, M.-V. Collados, D. Chemisana, and J. Atencia, "Broadband behavior of transmission volume holographic optical elements for solar concentration," Opt. Express **23**(11), A671–A681 (2015).
19. J. Marín-Sáez, D. Chemisana, Á. Moreno, A. Riverola, J. Atencia, and M.-V. Collados, "Energy Simulation of a Holographic PVT Concentrating System for Building Integration Applications," Energies **9**(8), 577 (2016).
20. M. G. Moharam, T. K. Gaylord, and R. Magnusson, "Criteria for Bragg regime diffraction by phase gratings," Opt. Commun. **32**(1), 14–18 (1980).
21. M. G. Moharam, T. K. Gaylord, and R. Magnusson, "Criteria for Raman-Nath regime diffraction by phase gratings," Opt. Commun. **32**(1), 19–23 (1980).
22. W. H. Bloss, M. Griesinger, and E. R. Reinhardt, "Dispersive concentrating systems based on transmission phase holograms for solar applications," Appl. Opt. **21**(20), 3739–3742 (1982).
23. C. Bainier, C. Hernandez, and D. Courjon, "Solar concentrating systems using holographic lenses," Solar Wind Technol. **5**(4), 395–404 (1988).
24. G. B. Ingersoll and J. R. Leger, "Optimization of multi-grating volume holographic spectrum splitters for photovoltaic applications," Appl. Opt. **55**(20), 5399–5407 (2016).
25. A. Villamarín, J. Atencia, M. V. Collados, and M. Quintanilla, "Characterization of transmission volume holographic gratings recorded in Slavich PFG04 dichromated gelatin plates," Appl. Opt. **48**(22), 4348–4353 (2009).
26. R. Syms, *Practical Volume Holography* (Oxford University Press, 1990).
27. W. R. Klein and B. D. Cook, "Unified Approach to Ultrasonic Light Diffraction," IEEE Trans. Sonics Ultrason. **14**(3), 123–134 (1967).
28. H. Kogelnik, "Coupled wave theory for thick hologram gratings," Bell Syst. Tech. J. **48**(9), 2909–2947 (1969).
29. F.-K. Bruder, T. Fäcke, and T. Rölle, "The Chemistry and Physics of Bayfol HX Film Holographic Photopolymer," Polymers (Basel) **9**(12), 472 (2017).
30. J. Marín-Sáez, J. Atencia, D. Chemisana, and M.-V. Collados, "Characterization of volume holographic optical elements recorded in Bayfol HX photopolymer for solar photovoltaic applications," Opt. Express **24**(6), A720–A730 (2016).
31. J. Marín-Sáez, M. V. Collados, D. Chemisana, and J. Atencia, "Energy analysis of holographic lenses for solar concentration," Proc. SPIE **10233**, 1023317 (2017).
32. Covestro Deutschland AG, *Bayfol HX200 Datasheet* (2016).
33. P. Markovski, N. Koleva, and T. Todorov, "Some characteristics of phase holographic gratings in the intermediate regime of diffraction," Opt. Quantum Electron. **13**(6), 515–518 (1981).
34. J. Marín-Sáez, M. V. Collados, J. Atencia, and D. Chemisana, "Optical and Energetic Performance of Volume Holographic Optical Elements for Solar Energy Applications," in *Advances in Energy Research* (NOVA, 2017).
35. N. Uchida, "Calculation of diffraction efficiency in hologram gratings attenuated along the direction perpendicular to the grating vector," J. Opt. Soc. Am. **63**(3), 280 (1973).
36. M. Prijatelj, J. Klepp, Y. Tomita, and M. Fally, "Far-off-Bragg reconstruction of volume holographic gratings: A comparison of experiment and theories," Phys. Rev. A **87**(6), 63810 (2013).
37. E. Hecht, *Optics* (Addison Wesley, 1998).
38. F.-K. Bruder, F. Deuber, T. Fäcke, R. Hagen, D. Hönel, D. Jurbergs, T. Rölle, and M.-S. Weiser, "Reaction-diffusion model applied to high resolution Bayfol HX photopolymer," Proc. SPIE **7619**, 76190I (2010).

Research Article | Vol. 26, No. 10 | 14 May 2018 | OPTICS EXPRESS A400
Optics EXPRESS

1. Introduction

Concentrating photovoltaics for building integration has been commonly carried out with optical refractive reflective elements [1–5]. It allows the reduction of the necessary PV cell surface while obtaining the same electrical energy. However, the concentration of the solar spectrum on the PV cell causes an increase of its temperature, which may lead to a worsening of its performance. For that reason, concentrating photovoltaics for building integration is one of the numerous fields in which the use of Holographic Optical Elements (HOEs) provides important advantages [6]. This is because the chromatic selectivity of holograms allows the concentration on the PV cell of only the spectral range of the solar radiation that will be more efficiently converted into electricity; thus avoiding wavelengths that would only contribute to overheating of the cell. If a mono-crystalline Si cell is used, with the spectral response curve shown in Fig. 1, a good design possibility would be utilizing a HOE that performs most efficiently for wavelengths around 800 nm, in order to couple the aforementioned spectral response with the solar spectrum, also plotted in Fig. 1 [7]. This wavelength will be later referred to as target wavelength.

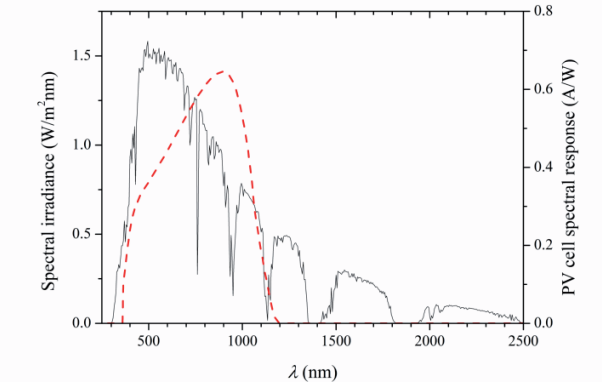

Fig. 1. Standard AM 1.5D solar spectrum [7] (solid black line, left *y*-axis). Monocrystalline Si PV cell response curve (dashed red line, right *y*-axis).

Redirection and concentration of light can be carried out either with non-concentrating HOEs (such as gratings) [8–10] or with concentrating HOEs (such as spherical or cylindrical lenses) [11–19]. Due to the angular selectivity of holograms, tracking of the apparent movement of the sun in the sky is often required in order to keep the reconstruction direction of incidence constant. However, if a holographic cylindrical lens is placed in such a way that its direction of low angular selectivity matches either the direction of solar altitude or azimuth, tracking can be suppressed in one axis [17,18].

Holograms can operate in three different regimes: the volume or Bragg regime, the transition regime, and the thin or Raman-Nath regime, depending on the recording and reconstruction conditions [20,21]. At the output of a volume hologram, i.e. a hologram operating in the volume regime, only two beams emerge: the one corresponding to the transmitted order and the one corresponding to the first order of diffraction. Under certain recording conditions and for a specific reconstruction wavelength and angle of incidence, all the energy can be transferred to the diffracted beam, thus having 100% efficiency. Volume holograms are very often used because of this characteristic.

However, volume holograms present very high chromatic selectivity. They also have high chromatic dispersion, so rays of different wavelengths emerge from the hologram with different directions and only some of them will reach the position where the PV cell would be located. These effects are accentuated the more into the volume regime the HOE performs. Although in principle they are advantages because concentration of less efficient bandwidths on the PV cell is prevented, they can be counter-productive in applications with broadband

Research Article | Vol. 26, No. 10 | 14 May 2018 | OPTICS EXPRESS A401
Optics EXPRESS

spectrum reconstruction, such as solar concentration. This is because very high chromatic selectivity and dispersion involves a narrow spectral range collected by the cell, which can be narrower than its spectral sensitivity.

One way to address this issue is to multiplex [22–24], that is, to record several holograms in the same sample to enhance the wavelength acceptance. A recording material that provides very high index modulation is needed to obtain high efficiency with all the holograms [25], and the recording geometry should avoid cross-coupling among the different HOEs. To the authors' knowledge, this procedure has not been successfully carried out for solar concentration applications.

A novel approach to overcome the problem of volume holograms' high selectivity is explored in this research: the use of HOEs that operate in the transition regime for the target wavelength. This type of holograms had not been previously used in solar concentration applications. They still provide reasonably high efficiencies and have lower angular and chromatic selectivities than holograms operating further into the volume regime [26,27]. This would imply an enhancement of the spectral irradiance that is collected by the PV cell without concentrating the non-desired parts of the solar spectrum, producing higher current intensities than with volume holographic concentrators and lower cell temperatures than with refractive optical concentrators.

Three different cylindrical holographic lenses (one of them performing entirely in the volume regime for 800 nm and the other two, partly in the transition regime) were theoretical and experimentally analyzed in this study. The index modulation reached at each point of each HOE was modeled as a function of the spatial frequency and the recording exposure to include the response of the material. This was needed to solve the coupled differential equations of Coupled Wave Theory [28], which explain the behavior of HOEs.

The index modulation modeling was validated with the comparison with experimental results. Finally, the model was applied to the simulation of three holographic concentration systems with the aim of determining whether the inclusion of the transition regime is suitable for solar concentration applications.

This paper is structured as follows. The experimental recording of HOEs is described in subsection 2.1; the experimental approach carried out in this study to obtain the index modulation at each point of the HOE is explained in subsection 2.2; and the simulation of the three global systems, in subsection 2.3. The results corresponding to the determination of the index modulation are presented in subsection 3.1, the ones corresponding to the simulations of cylindrical holographic lenses and their validation with experimental recordings, in subsection 3.2, and the global system simulations, in subsection 3.3.

2. Materials and Methods

2.1. Holographic recording

The photosensitive material on which all transmission phase holograms in this work have been recorded is Bayfol HX TP photopolymer, manufactured by Covestro Deutschland AG [29]. This material had been previously tested and it was found that the needed index modulation to obtain 100% efficiency with an 800 lines/mm grating when reconstructing with 800 nm could be reached [30]. In all cases the thickness of the photopolymer layer was 16 μm. No recording materials sensitive to 800 nm exist, and since it was determined in [31] that the election of the recording wavelength did not affect significantly the resulting spectra received by the PV cell and therefore could be based on the laboratory equipment availability, the recording wavelength was 532 nm (Coherent Verdi V6 laser). The photopolymer material is laminated onto a glass slide by applying pressure, as indicated in the technical characteristics document from the manufacturers [32]. No index-matching is necessary, since the surface tension prevents the existence of air between the photopolymer and the glass. The back side of the glass slide is blackened to avoid undesired holograms recorded due to

Research Article | Vol. 26, No. 10 | 14 May 2018 | OPTICS EXPRESS A402
Optics EXPRESS

reflections. After the recording, a two-step photocuring process with incoherent light was carried out, described elsewhere [30].

Holographic gratings were recorded with two plane waves, whereas holographic cylindrical lenses were recorded with a plane wave and a cylindrical wave. Figure 2 shows the recording setup of a cylindrical holographic lens. In order to record a grating, the cylindrical lens would be removed. Z-Direction is defined as the normal to the photopolymer plane; y-direction as parallel to its surface and is contained in the plane of incidence and x-direction is perpendicular to the plane of incidence. Parameter z_0 is the distance from the holographic plate to the focal point at 532 nm, parallel to *z*-axis.

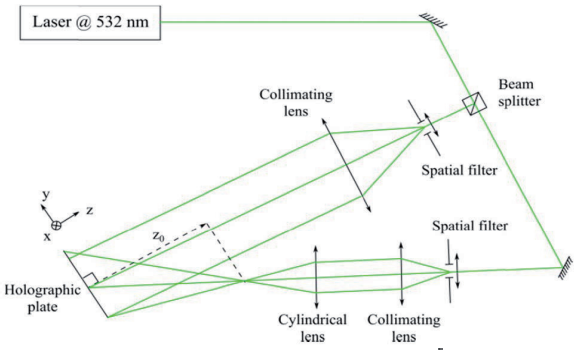

Fig. 2. Recording setup of a cylindrical holographic lens.

2.2. Experimental determination of the index modulation

The index modulation n_1 achieved during the recording of a phase hologram depends on several factors: the physical and chemical properties of the photosensitive material, the angle between beams and the recording intensity and time.

Since the angle between the recording beams of a holographic cylindrical lens is different at each position of the HOE (and thus, its spatial frequency), the index modulation reached at each point is also different. In order to find out this dependence, several slanted transmission gratings were recorded with different spatial frequencies, ranging from 70 to 1200 lines/mm. The recording intensity was kept approximately equal in all cases (around 1.4 mW/cm^2), while varying the exposure time to obtain different exposure dosages. Each hologram was then illuminated at the reconstruction stage with an 800 nm laser (ThorLabs Laser Diode CPS808A, emitting 4.4 mW) at Bragg angle and polarization perpendicular to the incidence plane.

Depending on which regime each hologram operated in for the reconstruction wavelength, the number of diffraction orders that emerged from it was different, being two for volume holograms (0 and + 1 order) and higher for holograms operating in the transition regime or the Raman-Nath regime.

The intensity of every order of diffraction that was found at the output of each hologram was measured (with Newport Power Meter Model 1815-C with detector Model 818-SL, with an uncertainty of 1 μW) and the relative efficiency of each diffraction order was calculated with

$$\eta_L = \frac{I_L}{\sum_L I_L} \tag{1}$$

where I_L is the intensity of the L diffraction order.

Research Article | Vol. 26, No. 10 | 14 May 2018 | OPTICS EXPRESS A403
Optics EXPRESS

Several criteria are defined in [20] in order to determine whether a hologram operates in the volume regime: only two orders of diffraction exist (0 and + 1 orders), the efficiency of the + 1 order when Bragg condition is met is given by Kogelnik's solution [28],

$$\eta = \sin^2\left(\frac{\pi d n_1}{\lambda\sqrt{c'_{0z}c'_{+1z}}}\right) \tag{2}$$

and the efficiency of the 0 order is given by the complementary cosine function. The parameters that appear in Eq. (2) are: d, the thickness of the photopolymer layer; λ, the reconstruction wavelength and c'_{0z} and c'_{+1z}, the directional cosines inside the medium in z-direction of the transmitted and diffracted beam, respectively.

If the considered holographic grating is a volume hologram (for the reconstruction wavelength 800 nm) then the index modulation is calculated by simply substituting the efficiency in Eq. (2) when Bragg condition is met.

However, if the considered holographic grating is not a volume hologram for this wavelength, then Kogelnik's solution cannot be applied [33] and the coupled wave equations need to be solved numerically. The coupled wave equation corresponding to diffraction order L is [26,28]

$$c'_{Lz}\frac{dA_L}{dz} + j\vartheta_L A_L + j\kappa\left[A_{L+1}\left(\vec{p}_{L+1}\cdot\vec{p}_L\right) + A_{L-1}\left(\vec{p}_{L-1}\cdot\vec{p}_L\right)\right] = 0 \tag{3}$$

where A_L is the amplitude of the L order wave, c'_{Lz} is its directional cosine in z-direction, ϑ_L is the dephasing parameter, $\vec{p}_L$ is its polarization direction and κ is the coupling parameter, given by

$$\kappa = \frac{\pi n_1}{\lambda} \tag{4}$$

where the index modulation appears.

These equations were solved for each spatial frequency and for a series of index modulation values, and the value of the index modulation was determined as the one that provided diffraction efficiencies that were the closest to the previously obtained experimental ones. Afterwards, the set of index modulation data for each spatial frequency was fitted to an exponential dependency with the exposure dosage, since for exposure dosages higher than a certain value, saturation occurs. This would later allow the determination of n_1 for a specific exposure dosage.

Another aspect that affects the index modulation that can be reached, and that needs to be taken in consideration when modeling the index modulation, is the recording intensity throughout the HOE. Since laser beams present a Gaussian profile, in principle the intensity along each beam is not uniform. However, the recording beams are sufficiently expanded so that only the central part of the beams is used for the recording; therefore the intensity variation due to this effect is rather small.

When recording a holographic cylindrical lens one of the recording beams is a cylindrical beam, as shown in Fig. 2. Thus, the wavefront that reaches each point of the holographic plate is different, and so is the intensity associated with each one. Nevertheless, it has also been verified that these variations are rather small as well and correspond to a negligible change in index modulation (for the intensity and exposure dosage values later used to record holographic cylindrical lenses).

To summarize, it has been assumed that the achieved value of index modulation at each point will only be affected by the variation of spatial frequency throughout the holographic cylindrical lens.

Research Article | Vol. 26, No. 10 | 14 May 2018 | OPTICS EXPRESS A404
Optics EXPRESS

2.3. Algorithm for simulations of cylindrical holographic lenses as solar concentrators

A geometrical and energetic analysis of the HOEs is carried out. A ray tracing algorithm was previously developed [34] in a MATLAB environment, which calculates the direction of propagation and the efficiency of the diffracted order in volume holograms, for any given wavelength and direction of incidence (whether or not Bragg condition is met). It can analyze both holographic gratings (in which all points behave equally) and other HOEs, such as cylindrical holographic lenses, in which the grating vector $\vec{K}$ is different at each point. Thus, each point of the holographic lenses is analyzed independently under the assumption that each one can be modeled as a distinct holographic grating ("local-grating").

This algorithm was improved so that the higher orders of diffraction that appear in non-volume holograms were considered as well. The number of diffraction orders that emerge at each point inside the medium at the reconstruction step and their direction of propagation are determined with the help of the so-called beta-value closure [26,34–36]

$$\vec{k}_L{}' \cdot \vec{u}_y = \left(\vec{k}_0{}' - L\vec{K}\right) \cdot \vec{u}_y \tag{5}$$

The y-component of the wave vector of the L order inside the medium, $\vec{k}_L{}' \cdot \vec{u}_y$, is given by the wave vector of the 0th order, $\vec{k}_0{}'$, and the grating vector $\vec{K}$. The z-component is then calculated so that the modulus of the vector $\vec{k}_L{}'$ is the same as that of $\vec{k}_0{}'$. Of course, only orders of diffraction with $\vec{k}_L{}' \cdot \vec{u}_y \le \left|\vec{k}_0{}'\right|$ are generated.

The index modulation of each point was assigned by means of its dependence with the spatial frequency determined in subsection 3.1. Then the efficiency of each order of diffraction was calculated by a numerical resolution of the coupled wave equations (as explained in subsection 2.2) for each point of the HOEs and each reconstruction wavelength and angle of incidence.

The system in Fig. 3, previously proposed in [19], is considered in this study. It comprises two identical and symmetrically placed cylindrical holographic lenses that redirect sunrays to a mono-crystalline Si PV cell. Sunlight that goes through the space between the HOEs also reaches the PV cell. It can easily be integrated on a building façade by superimposing it on the blinds of a solar louvre shading system, which tracks the solar altitude by rotating around *x*-axis.

When carrying out simulations of this specific system, the standard AM 1.5D solar spectrum is considered. Since sunlight is unpolarized the coupled wave equations are solved for two polarizations (parallel and perpendicular to the incidence plane), and the final efficiency of each ray and each wavelength is the average of the ones corresponding to each polarization. Fresnel reflection losses [37], which are different for each polarization, are also taken into account. The irradiance that is found at the surface of the PV cell, placed at a specific location, is calculated by integrating the power associated with each ray that reaches it and dividing by the surface. The product of the spectral irradiance and the spectral response of the PV cell gives the peak current intensity that is generated by the PV cell, when no temperature effects are considered. These procedures are explained in detail in a previous publication [34].

Research Article | Vol. 26, No. 10 | 14 May 2018 | OPTICS EXPRESS A405
Optics EXPRESS

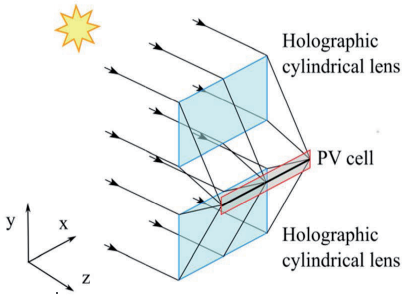

Fig. 3. Schematic of the system considered: each cylindrical holographic lens redirects sun rays towards a PV cell.

The *y*- and *z*-position of the PV cell for each specific system (and therefore, the *y*-distance between the two HOEs) is optimized with the following criteria:

- When reconstructing with perpendicular incidence all rays corresponding to the + 1 order of diffraction and 800 nm must reach the PV cell. Moreover, none of the rays of the 0 order of diffraction should reach it, in order to avoid the incidence of infrared.
- The current intensity generated by the PV cell when reconstructing with the range of the solar spectrum optimum for its coupling with the PV cell (in this work, 700-900 nm) must be maximal.

3. Results and Discussion

3.1 Determination of the index modulation

Several slanted gratings with spatial frequencies within 70-1200 lines/mm were recorded on Bayfol HX photopolymer with the same recording intensity and different exposure dosages, as explained in subsection 2.2. Table 1 shows the angle between the recording beams and the spatial frequency of each grating. When reconstructing at 800 nm a different number of diffraction orders were found at the output of the gratings, as indicated in Table 1. The appearance of higher orders of diffraction and the observed distribution of intensity among them clearly illustrates the gradual shift from Bragg regime to the transition regime and to Raman-Nath regime, also stated in Table 1.

Table 1. Characteristics of the recorded holographic gratings.

$\Delta\theta_{recording,\,air}$ (°)	SF (lines/mm)	Number of diffraction orders @ 800 nm	Regime @ 800 nm
37.2	1199	2	Volume
30.9	1001	2	Volume
25.0	814	2	Volume
19.0	620	2	Volume
15.5	507	4	Transition
12.5	409	4	Transition
9.0	295	4	Transition
6.0	197	6	Transition
3.0	98	9	Transition
2.1	70	9	Thin

The index modulation (calculated as described in subsection 2.2) obtained for each grating when varying the recording time, and thus, the exposure dosage, is plotted with markers in Fig. 4.

Research Article | Vol. 26, No. 10 | 14 May 2018 | OPTICS EXPRESS A406
Optics EXPRESS

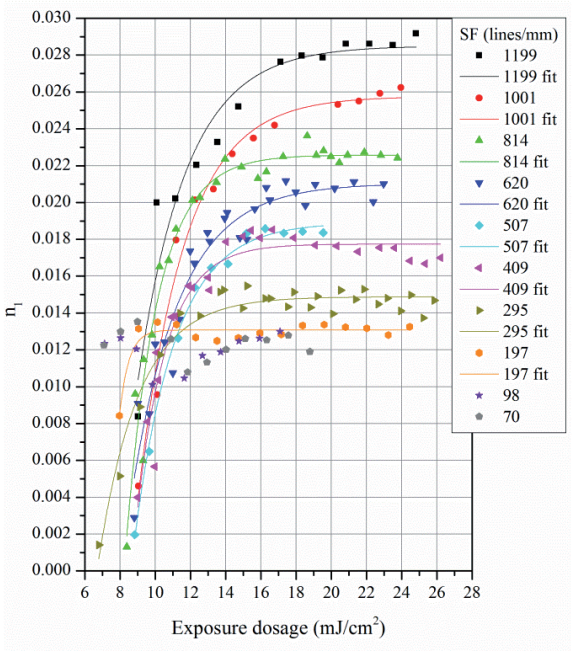

Fig. 4. Index modulation experimental values as a function of the exposure dosage for several spatial frequencies.

The index modulation obtained with each spatial frequency (using the same recording intensity) for a certain exposure dosage is different, and it decreases with the angle between the recording beams. This is in agreement with other studies on photopolymers for holographic recording [38]. Therefore, it cannot be assumed that the index modulation achieved at each point of a holographic lens with spatial frequencies varying in the range shown in Fig. 4 is the same.

Each set of index modulation data for a given spatial frequency is fitted to an exponential dependency with the exposure dosage. The resulting index modulation values at 16 mJ/cm^2 are plotted in Fig. 5. This exposure dosage was selected because it would later be used to record the cylindrical holographic lenses. It shows a linear dependency, $n_1 = (1.31 \pm 0.04)\cdot 10^{-5}\, SF + (0.0114 \pm 0.0003)$, where the spatial frequency, SF, is expressed in lines/mm. This allows the estimation of the index modulation at each point of a holographic lens recorded with this exposure dosage.

3.2 Experimental validation of the index modulation modeling with cylindrical holographic lenses

Three holographic cylindrical lenses (later referred to as A, B and C) were considered, each with a different range of spatial frequencies, shown in Fig. 6. The white, light grey and dark grey areas denote Bragg, transition and Raman-Nath regimes, respectively, when reconstructing the designed lenses (with the calculated index modulations) with 800 nm. All points in lens A operate in Bragg regime for this wavelength, roughly two thirds of the points in lens B (with $y \leq 10$ mm approximately) operate in Bragg regime and the rest in the transition regime, and roughly one third of the points in lens C (with $y \leq -10$ mm approximately) operate in Bragg regime, with the rest operating in the transition regime except for the point with $y = 25$ mm, which operates in Raman-Nath regime.

Research Article | Vol. 26, No. 10 | 14 May 2018 | OPTICS EXPRESS A407
Optics EXPRESS

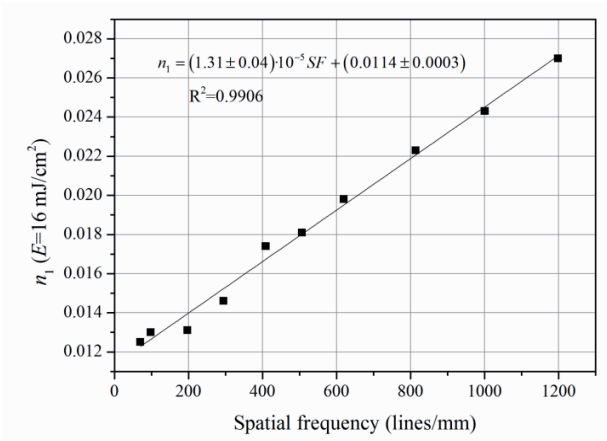

Fig. 5. Linear fit of the obtained values of the index modulation with a recording exposure dosage of 16 mJ/cm^2 versus the spatial frequency.

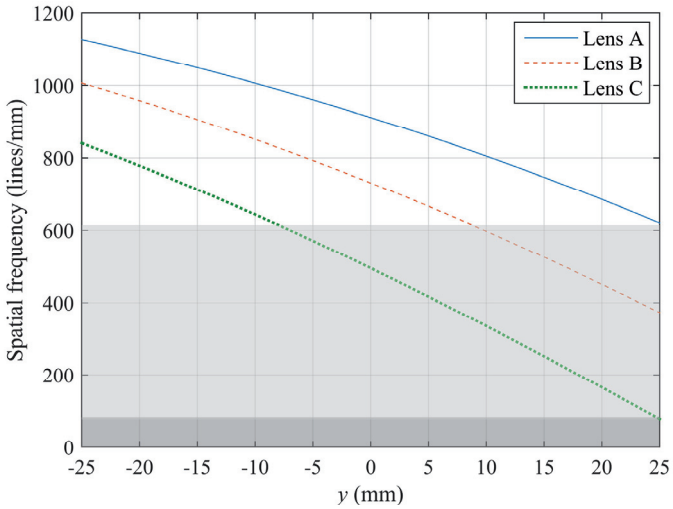

Fig. 6. Spatial frequency along y-direction of all three lenses. The white, light grey and dark grey areas denote Bragg, transition and Raman-Nath regime, respectively, when reconstructing with 800 nm.

The recording angles are presented in Table 2, where θ_p is the angle of the plane wave and $\theta_{c,center}$ is the angle of the cylindrical wave at the center of the hologram, in air. These angles ensured that Bragg condition was met at the center of the lens when illuminating with 800 nm and perpendicular incidence at the reconstruction stage. The angle of the recording plane waves is not zero because of the difference between the recording and the target wavelength. The distance from the holographic plate to the focal point at 532 nm, parallel to z-axis, marked as z_0 in Fig. 2, is the same for all three lenses, 105 mm. This provides a focal point at 800 nm that is 70 mm away from the holographic plate, measured in the direction of z-axis.

Research Article | Vol. 26, No. 10 | 14 May 2018 | OPTICS EXPRESS A408
Optics EXPRESS

Table 2. Recording angles of the three cylindrical holographic lenses considered

	Lens A	Lens B	Lens C
θ_p (°)	7.2	5.7	3.8
$\theta_{c,center}$ (°)	36.5	28.7	19.1

The diameter of the recorded holographic lenses was slightly bigger than 50 mm. The exposure dosage at the center of all lenses was 16 mJ/cm^2, which provides the necessary index modulation to obtain 100% efficiency at the center of lens A when reconstructing perpendicularly with 800 nm.

After the recording and photocuring, all three HOEs were reconstructed with an 800 nm laser beam (with an approximate diameter of 0.5 mm and perpendicular polarization, with the model specified in the previous subsection) that illuminated with normal incidence a point of the HOE, every 2.5 mm. The intensity of each detectable diffraction order was measured and the efficiency was calculated with Eq. (1) as explained in subsection 2.2. The experimental data are plotted in Fig. 7 with filled circles of various colors (each color corresponds to a different order of diffraction). The solid lines are the theoretical curves obtained by numerically solving the coupled wave equations, with index modulation values assigned to each point based on Fig. 5, as detailed in subsections 2.2 and 2.3. A good agreement between the experimental and theoretical results is observed, validating the index modulation determination throughout the lenses.

The number of diffraction orders that appear at the output of each lens is consistent with the expected operating regimes in Fig. 6: only two in the volume regime and more in the rest. At y = 25 mm of Lens C, the theoretical and experimental efficiencies of the diffraction orders pairs + 1 and −1, and + 2 and −2 are nearly the same, corroborating the operation in Raman-Nath regime.

When reconstructing perpendicularly at 800 nm only the central points of each lens with y = 0 mm fulfill Bragg condition, since the recording wavelength was 532 nm. However, only the central point of lens A reaches 100%, not the one of lens B or C. This is because the index modulation achieved at y = 0 mm in lens A is the one that provides 100% efficiency for its spatial frequency when reconstructing with 800 nm at perpendicular incidence. Although Bragg condition is also met with that wavelength and angle of incidence at the central point of the other two lenses, the index modulation needed to obtain 100% efficiency is different from the one reached with the recording intensity and exposure dosage considered.

When moving away from the center of the lenses towards negative y, the efficiency of the + 1 diffraction order decreases faster than towards y positive, as expected due to the higher angular selectivity of HOEs with higher spatial frequency and therefore, that are deeper into the volume regime.

3.3 Simulations of cylindrical holographic lenses as solar photovoltaic concentrators

Three global systems (systems A, B and C) like the one represented in Fig. 3 were considered. Each one comprises two identical cylindrical holographic lenses (lenses A, B or C) with index modulations calculated in subsection 3.1 corresponding to a recording exposure dosage of 16 mJ/cm^2. They are placed in a symmetrical configuration so that they redirect sunrays impacting with perpendicular incidence towards the same PV cell: a mono-crystalline Si PV cell, with the spectral response curve of Fig. 1. Its y-dimension is 10 mm and the x-dimension is the same as the HOE's. The space between the two HOEs allows sunrays to go through and reach the PV cell, so the geometrical concentration of the global system is x11. This configuration was explored in a previous publication [19] and can easily be integrated on a building façade. The position of the PV cell was optimized with the criteria explained in subsection 2.3, and the coordinates are given in Table 3 (the center of the lower holographic lens has coordinates y = 0 mm, z = 0 mm in all three cases).

Research Article | Vol. 26, No. 10 | 14 May 2018 | OPTICS EXPRESS A409
Optics EXPRESS

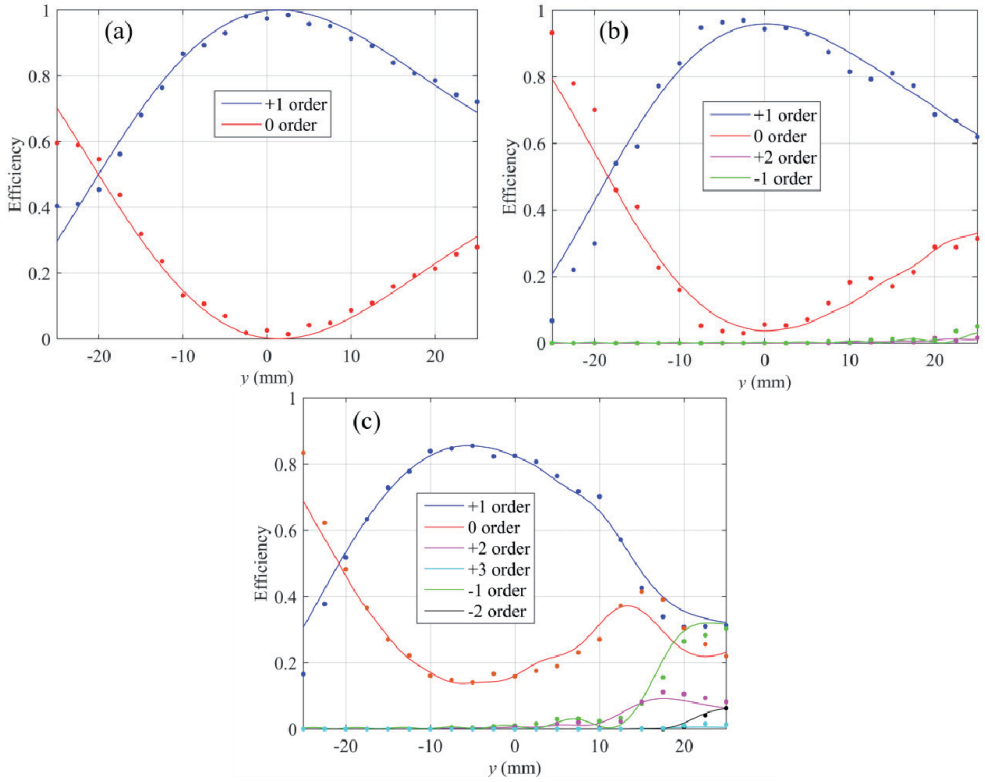

Fig. 7. Experimental (filled circles) and theoretical (solid lines) efficiencies of each order of diffraction found at the output of cylindrical holographic lenses A (a), B (b) and C (c).

Table 3. Position of the PV cell and current concentration coefficients for each one of the three systems considered.

	Lens A	Lens B	Lens C
z_{cell} (mm)	40	52	68
$y_{cell,\,center}$ (mm)	44	38	30
$CC_{current,\,1\,HOE}$	0.61	1.01	1.36
$CC_{current,\,global\,sist}$	2.22	3.02	3.72

Simulations of the three global systems were carried out when reconstructing with perpendicular incidence. In order to obtain results as realistic as possible, the unpolarized standard AM 1.5D solar spectrum [2] was considered, as well as reflection Fresnel losses in all three interfaces (air-photopolymer, photopolymer-substrate, substrate-air).

The spectral irradiance received by the whole surface of the PV cell with only one of the two lenses of systems A, B and C is plotted in Fig. 8. The different colors correspond to different orders of diffraction that reach the PV cell (diffraction orders 0, −1 and −2 of all lenses and order + 3 of lens A do not reach it and are not included in the graphs). The standard AM 1.5D solar spectrum [7] and spectral response curve of the mono-crystalline Si PV cell from Fig. 1 have been included in the graph for comparison. In all three cases the received spectrum comprises wavelengths around 800 nm, as expected, so the solar spectrum is enhanced in a range that the PV cell performs more efficiently.

Research Article | Vol. 26, No. 10 | 14 May 2018 | OPTICS EXPRESS A410
Optics EXPRESS

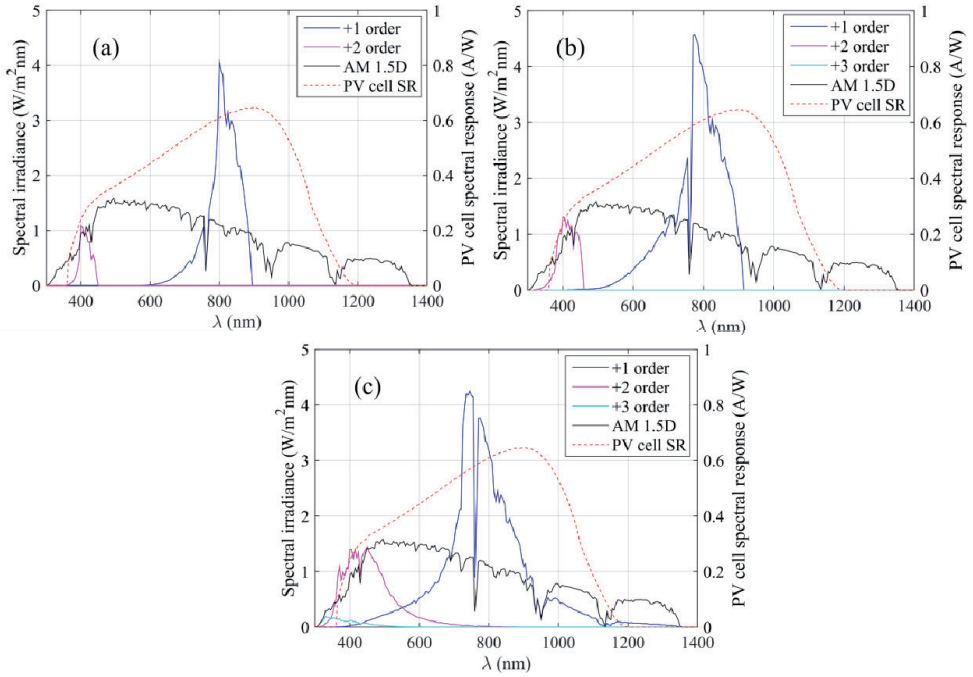

Fig. 8. Spectral irradiance received by the PV cell with lens A (a), B (b) and C (c) (colored solid lines, left *y*-axis). Only orders of diffraction that reach the PV cell are included. Standard AM 1.5D solar spectrum [7] (black solid line, left *y*-axis), and mono-crystalline Si PV cell spectral response curve (red dashed line, right *y*-axis) included for comparison.

It is clearly observed in Fig. 8 that the received spectrum corresponding to the + 1 order of diffraction belongs to a broader spectrum for lens C than lens B and than lens A. In other words, the more into the transition regime the lens operates; a broader irradiance spectrum is collected by the PV cell. This is due to the lower chromatic selectivity and dispersion of HOEs in the transition regime: more rays and with higher energy reach the PV cell.

Besides, when the transition regime is included, higher orders of diffraction (+ 2 in lens A and + 2 and + 3 in lenses B and C) reach the PV cell. Despite the fact that lens A operates entirely in the volume regime at 800 nm, when the reconstruction wavelength is shorter part of the lens operates in the transition regime, so higher orders of diffraction appear. Likewise, order + 3 emerges lens B with shorter reconstruction wavelengths, although its irradiance at the PV cell is negligible. The spectral ranges of orders + 2 and + 3 at the cell in all cases correspond to wavelengths around 400 nm, which the PV cell will also transform into electrical current, although with a lower response than that of the optimal range. The irradiance associated with order + 2 with lens C is higher than that of lenses A and B, illustrating its lower chromatic selectivity and dispersion.

The maximal spectral irradiance received with lens A is found at 800 nm, as expected. However, that is not the case with lens B or C. This is due to the index modulation reached at each point of the lenses. As mentioned in the previous subsection, the recording exposure dosage (and therefore, the index modulation) was optimized for 800 nm only for lens A, and then the same recording intensities and exposure dosages were used for lens B and C. Then the efficiency of 800 nm rays exiting the HOEs is lower than that of rays with wavelengths slightly shorter than 800 nm, and due to the lower chromatic dispersion most of them reach the PV cell as well.

The results in Fig. 8 confirm that these HOEs do not concentrate the infrared part of the solar spectrum that the PV cell cannot use: there is a cutoff in the received irradiance in Figs.

Research Article | Vol. 26, No. 10 | 14 May 2018 | OPTICS EXPRESS A411
Optics EXPRESS

8(a) and 8(b) at approximately 900 nm, and lens C (Fig. 8(c)) only redirects towards the cell a negligible percentage of the solar irradiance of wavelengths longer than 1100 nm. The ray tracing analysis has demonstrated that due to several effects (chromatic dispersion, total internal reflection and the nonexistence of the + 1 diffracted order for long wavelengths) no irradiance with wavelengths longer than 1400 nm reaches the cell. Thus, the increase of the cell temperature would be reduced, so that it would not cause a worsening of its performance.

In order to calculate the spectral irradiance when considering the whole system, the curves in Fig. 8 have to be doubled, since both lenses in each system are identical and symmetrically placed, and the solar spectrum from Fig. 1 needs to be added, which corresponds to light that goes through the space between the lenses. Although this means that the PV cell will receive infrared radiation that it cannot convert into electricity, it will not be concentrated, unlike with refractive concentrating elements, and therefore, the increase in temperature will be rather low. The maximal optical efficiency obtained with system A is 76%; with system B, 79% and with system C, 72%.

The generated current intensity depends on the irradiance associated with each wavelength, as indicated by the spectral response curve of the mono-crystalline Si cell of Fig. 1. The current concentration coefficient, $CC_{current}$, defined in [34], is the ratio between the total current intensity obtained with the holographic concentrator and the current intensity that would be obtained without the HOE. The resulting values when considering one lens of each system, $CC_{current,1\,HOE}$, and the whole system, $CC_{current,\,global\,syst}$, are included in Table 3. They demonstrate the advantage of using HOEs operating in the transition regime rather than the volume regime for the target wavelength in solar concentration applications, since the current concentration obtained with lens C, 1.36, doubles the value with lens A and is also higher than the one with lens B. Although these values may seem low, it has to be remembered that it is not the whole solar spectrum what is being concentrated, but a small range of it, which corresponds to the most efficient spectral range that the chosen PV cell can transform into electricity, without being affected by temperature effects.

Another aspect that needs to be analyzed is the spatial distribution of the irradiance received by the cell, or more precisely, of the current generated. Due to the chromatic dispersion of holograms the spectral irradiance received at each point of the cell is different, which causes the peak current intensity at each point to be different as well. The current intensity should be as homogeneous as possible throughout the cell, since the lowest value will limit the resulting current intensity.

Figure 9 shows the current concentration coefficient along *y*-dimension of the PV cell with one lens of each system (a) and with each whole system (b). Although the variations of this coefficient for lens A and B are relatively small, the current distribution for lens C is rather inhomogeneous. Nevertheless, this problem is reduced when considering the whole system C, since the part of the PV cell with lower current concentration due to one HOE would correspond to higher current concentration due to the other HOE, and vice versa, and the resulting current concentration is more homogeneous.

These simulations have been carried out for perpendicular incidence only, that is, with two-axes tracking. However, this system would only track the solar altitude movement [19], so the azimuth angle variation along the day would correspond to the direction of low angular selectivity of the HOEs (which in Fig. 3 corresponds to directions of incidence contained in plane *XZ*). Except at solar midday, incidence will not be perpendicular and this will cause a change in the direction of the output rays, not reaching the PV cell. The use of HOEs operating in the transition regime is also advantageous when considering this effect, since this change is smaller, and because they have lower angular selectivity.

Research Article | Vol. 26, No. 10 | 14 May 2018 | OPTICS EXPRESS A412
Optics EXPRESS

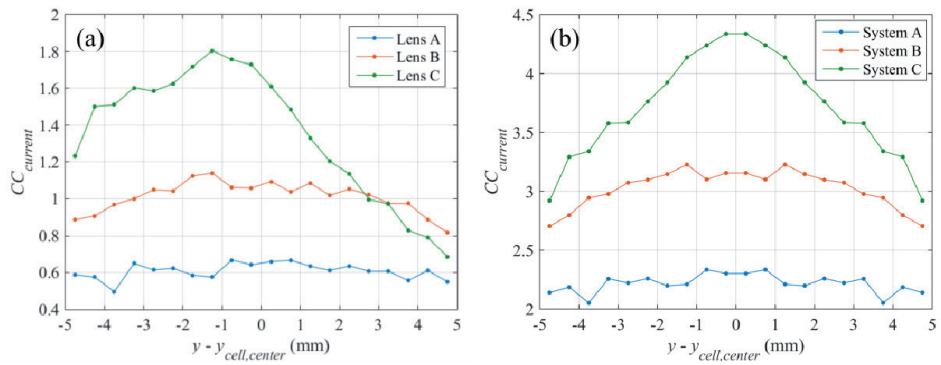

Fig. 9. Current intensity concentration throughout the PV cell with one lens (a) and with the whole system (b) A (blue curve), B (orange curve) and C (green curve).

4. Conclusions

This study focuses on HOEs partly operating in the transition regime between the Bragg and Raman-Nath regimes with the scope of analyzing the performance of cylindrical holographic lenses for solar concentration for building integration. This is a novel approach that, to our knowledge, had not been considered in broadband reconstruction spectrum applications. The change in index modulation throughout the HOEs due to the variation of the spatial frequency has been considered, in order to include the material's response. The index modulation of gratings recorded in Bayfol HX photopolymer with various spatial frequencies was determined, revealing a linear dependence for the recording intensity and exposure utilized. The index modulation values were needed to solve the coupled differential equations corresponding to each point of three different holographic lenses operating in the transition regime, where Kogelnik's solution [28] cannot be applied.

Future work must include experimental tests of the PV cell with these holographic concentrators and a study of the temperature of the cell.

Funding

Generalitat de Catalunya (2017FI_B2_00127); Ministerio de Economía y Competitividad of Spain (ENE2013-48325-R, ENE2016-81040-R); Diputación General de Aragón - Fondo Social Europeo (TOL research group, T76); Universidad de Zaragoza (UZ2017-CIE-02).

Acknowledgements

The authors would like to thank Dr. Enrico Orselli (Covestro Deutschland AG) for supplying the recording photopolymer material.

Chapter 7

Evaluation of the performance of the Holographic Concentrating Photovoltaic system under real conditions

After showing the feasibility of holographic concentrating photovoltaic systems for building-integration in chapter 4, the suitability of Bayfol HX photopolymer as recording material of HOEs for solar concentration in chapter 5 and the design of said HOEs was optimized for CPV in chapter 6, the final step of this thesis was the analysis of the performance of the system under outdoor conditions and solar illumination. This can be divided in the following objectives:

- design and construction of the holographic concentrating photovoltaic system
- evaluation of its response with solar illumination
- validation of the ray-tracing algorithm for the global analysis of the HOEs and the system
- assessment of outdoor conditions that may influence the system's performance, such as the ambient temperature
- study of the ageing of the HOEs due to the exposure to environmental conditions

This analysis is presented in the publication included in this chapter [1].

References

1. J. Marín-Sáez, D. Chemisana, J. Atencia and M. V. Collados, "Outdoor performance evaluation of a holographic solar concentrator optimized for building integration," submitted to Applied Energy Journal in 2019.

Outdoor performance evaluation of a holographic solar concentrator optimized for building integration

Julia Marín-Sáez,[1,2] Daniel Chemisana,[1,*] Jesús Atencia,[2] María-Victoria Collados[2].

[1]*Applied Physics Section of the Environmental Science Department, Polytechnic School, University of Lleida, Jaume II 69, 25001 Lleida, Spain*
[2]*Applied Physics Department, Aragon Institute of Engineering Research (I3A), Faculty of Science,University of Zaragoza, Pedro Cerbuna 12, 50009 Zaragoza, Spain*
* daniel.chemisana@macs.udl.cat

Abstract:

A holographic solar concentrating system with a Silicon photovoltaic (PV) cell is designed, constructed and characterized. The design is based on a previous system and is further optimized. The cylindrical holographic lenses forming the concentrating system are modeled with a ray-tracing algorithm based on Coupled Wave Theory and are recorded on Bayfol® HX photopolymer. Measurements are carried out outdoors with solar illumination and provide a current density of 146 mA/cm^2 with a current concentration factor of 3.48, validating the theoretical simulations results (172 mA/cm^2 and 3.81, respectively). The effect of the temperature on the performance of the Holographic Optical Elements (HOEs) is studied and taking it into account by assuming a 1.3º tilt of the fringes of the hologram caused by thermal expansion (which is reversible if the HOEs are encapsulated and sealed) provides simulation results closer to the experimental ones (a current density value of 155 mA/cm^2 and current concentration of 3.43). The ageing of HOEs recorded in Bayfol® HX photopolymer due to the outdoor environmental conditions is also analyzed, revealing the need of encapsulation and sealing.

Keywords: Building Integrated Photovoltaics, Solar Concentration, Holographic Concentrators, Holographic Optical Elements.

Glossary

HOE	Holographic Optical Element
PV	Photovoltaic
CPV	Concentrating Photovoltaic
θ	Angle that the projection of the incident sun rays on the YZ plane forms with *z*-axis
ϕ	Angle that the projection of the incident sun rays on the XZ plane forms with *z*-axis
c'_{Lz}	Directional cosine in *z*-direction of the L -diffraction order
A_L	Amplitude of the L -diffraction order wave
ϑ_L	Dephasing parameter of the L -order
n_1	Index modulation
λ	Reconstruction wavelength
$\vec{p}_L$	Polarization vector of the L -order
$CC_{current,\lambda}$	Concentration of generated electrical current for each wavelength

$I_{SC,\,HOEs,\,\lambda}$	Electrical current generated with the concentrating system for each wavelength
$I_{SC,\,no\ HOEs,\,\lambda}$	Electrical current generated without the concentrating system for each wavelength
$CC_{current}$	Concentration of generated electrical current
$I_{SC,\,HOEs}$	Electrical current generated with the concentrating system
$I_{SC,\,no\ HOEs}$	Electrical current generated without the concentrating system
J_{SC}	Electrical current density generated at short circuit

1. Introduction

The integration of solar photovoltaic systems in buildings represents a potential way of reducing their energy consumption. In addition, since the energy is generated on-site, costs and losses associated to transmission and distribution of electricity are minimized and thus the system efficiency is enhanced. On the other hand, by incorporating a concentrating element the size of photovoltaic (PV) cells is decreased and related environmental impact and economic issues are improved, leading to a more cost-effective and green technology [1]. Among solar concentrators for building-integrated photovoltaics, Holographic Optical Elements (HOEs) are positioned as advantageous option due to two main factors [2]. The first is related to the chromatic selectivity and dispersion that enable the coupling of the spectral response curve of the PV cell with the solar spectrum so that wavelengths outside the spectral response of the PV cell are not concentrated. This implies the avoidance of overheating without having to use cooling systems, which can be a drawback in building-integrated systems. The second is in regard with the diffraction efficiency due to the angular selectivity of the hologram, which makes it totally see-through and improves building integration features with respect to conventional refractive or reflective optical elements.

There are currently several publications where HOEs are proposed as solar concentrators for photovoltaics systems. In most studies they are only characterized in the laboratory with monochromatic light sources. Among the existing publications where the holographic concentrator is illuminated with white light and measurements with a PV cell are performed [3–6], no modeling of the irradiance that reaches the PV cell is carried out. This is an important aspect of the study of HOEs, since it allows the optimization of the system for each configuration and the understanding of its behavior. The experimental study of other authors shows current concentration factors (the ratio of the generated electrical current with and without the concentrating system) of 1.23 [3], 1.27 [6], 1.80 [4], and 1.93 [5].

A holographic concentrator was previously proposed by the authors, modeled with a ray-tracing algorithm and experimentally characterized locally in the laboratory by illuminating the HOEs with an 800 nm laser, thus validating the calculations [7–9]. In reference [7] a volume cylindrical holographic lens was considered in order to evaluate the suitability of a holographic solar concentrator for a building-integrated hybrid photovoltaic-thermal system. Year-round simulations were carried out for two different locations in the Northern hemisphere, with positive results. In [8,9] three different designs of the holographic lenses were studied, each one comprising a different range of spatial frequencies and index modulations. It was determined that using HOEs partly operating in the transition regime was very advantageous for solar applications. HOEs have been recorded in the photosensitive material Bayfol® HX photopolymer, manufactured by Covestro Deutschland AG [10]. It was determined that it can

reach the required range of index modulation values to operate adequately in the bandwidth where silicon PV cells are more efficient [11]. This material was chosen due to the advantages it offers, including the lack of requirement of a thermal or chemical post-processing (as opposed to the other commonly used recording material, dichromated gelatin), allowing a future mass production of HOEs [12].

Furthermore, the environmental conditions need to be considered when analyzing the performance of HOEs for solar applications, because they cannot be controlled as in other indoors applications. The performance of a HOE in the laboratory (e.g. with set room temperature and humidity) differs from its performance outdoors, with varying ambient conditions throughout the day and the year and depending on the location. This is because the photosensitive material where the HOE is recorded may also be sensitive to these factors [13–17]; in fact they may be used as sensors [13,14]. Some authors have investigated the response of HOEs recorded on Bayfol® HX photopolymer while being at cryogenic temperatures [18], but there is no research analyzing the behavior of the hologram at temperatures that could be achieved outdoors.

Another important aspect in the evaluation of HOEs for this application is the degradation that they may suffer due to the prolonged exposure to the aforementioned outdoor conditions. Some authors have studied this with different photopolymer recording materials, reporting changes [19] such as efficiency loss [5,6]. Regarding HOEs recorded in Bayfol® HX photopolymer, Zanutta et al. [18] noted slight changes after being exposed to cycles of one week of duration at 40ºC. However, Chrysler et al. [20] attached sealed HOEs recorded in Bayfol® HX 102 photopolymer to a Silicon PV panel placed outdoors and took measurements every four weeks, noticing substantial changes in the gratings and the material itself already after the first four weeks (but do not provide the temperatures that the HOEs are exposed to although they state that typical PV cell temperatures reach 80ºC in summer). Nevertheless, in most solar applications the HOEs are not placed directly attached to the PV cells but at a certain distance, and then the HOEs temperature will not increase that much. Therefore, further investigation about ageing should be carried out in general and specially for each considered configuration.

Based on the references presented above, it can be seen that albeit the big potential of holographic concentrators for building-integrated solar applications there are few rigorous studies dealing with the topic and more research is needed for better comprehension of their performance and reliability under real operating conditions. In order to fill this gap, the present study describes a holographic concentrator that doubles the concentration ratio of those found in the literature, leading to a higher cost-effectiveness. The system, which had been optimized considering both the solar spectrum and the spectral response of the PV cell, is fabricated and assessed outdoors determining optical and electrical performances under real conditions of operation, namely solar illumination and outdoor summer temperatures. The obtained results are compared with theoretical calculations, in order to validate the global performance that is modeled. In addition, temperature and ageing effects on the HOEs are also addressed to analyze their suitability for solar applications.

This article is structured as follows: the holographic concentrating system is described in section 2, comprising the optical design (subsection 2.1) and the fabrication of the HOEs (subsection 2.2) and the results are presented in section 3, which is divided in three parts. Subsection 3.1 covers the experimental study of the performance of the holographic concentrating system under sunlight illumination and its comparison with the theoretical simulations. An analysis of the

response of the HOEs under different temperatures of operation is included in subsection 3.2. An ageing study of the HOEs at summer outdoor conditions can be found in subsection 3.3. Finally, the conclusions are presented in section 4.

2. Description of the Holographic Concentrating System

A solar concentrating photovoltaic system formed by two identical HOEs and a conventional mono-crystalline Si PV cell, shown in figure 1(a), is studied in this work. The two HOEs are cylindrical lenses and are placed symmetrically at the same XY-plane so that sunlight incident on each one of them is diffracted towards the same PV cell. There is a separation between the two HOEs, where light is simply transmitted. Figure 1(c) shows the way the system would be integrated in the solar shading louvers in a South-oriented façade of a building in the Northern hemisphere (or a North-oriented façade in the Southern hemisphere). The blinds track the solar altitude movement, and that means that θ (the angle that the projection of the incident sun rays on the YZ plane forms with *z*-axis) is kept equal to zero at every moment and ϕ (the angle that the projection of the incident sun rays on the XZ plane forms with *z*-axis) is allowed to vary. The system is placed in such a way that the direction with tracking matches the direction of high angular selectivity of the HOEs and the direction without tracking matches the direction of low angular selectivity, as depicted in Figure 1(b). This configuration was already proposed in previous publications [7–9] by the authors, where the HOEs and the system's dimensions were at earlier design stages.

2.1. Optical design

The holographic cylindrical lenses are recorded by interfering a plane wave with a cylindrical wave, so when illuminating them with a plane wave a cylindrical wave is obtained at its output. This cylindrical wave will focalize at a different locus for each illumination wavelength. Since solar light can be assumed to have a plane wavefront, it is concentrated onto a linear spot.

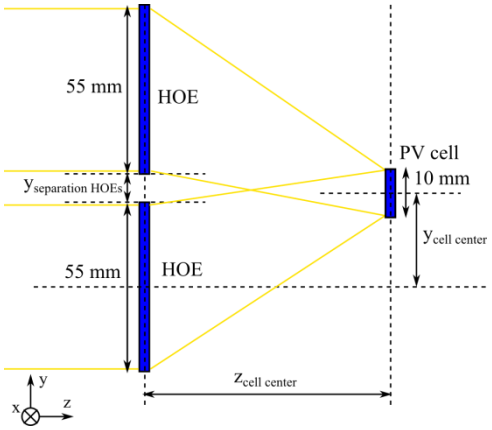

(a)

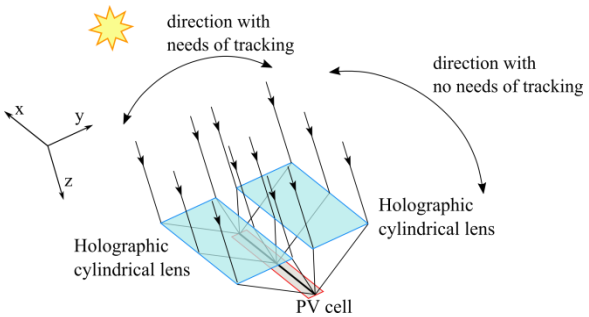

(b)

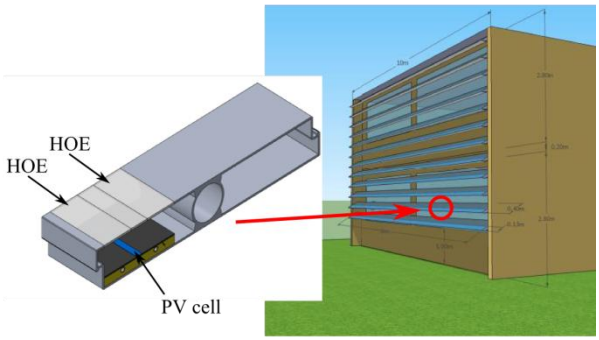

(c)

Figure 1. (a) Holographic concentrating system: two cylindrical holographic lenses redirect sunrays towards the PV cell; (b) Directions with and without need of tracking; (c) Integration of the system in the solar shading louvers of a building façade [7].

In the case of a volume hologram (a hologram operating in the volume regime), only two beams are found: the transmitted beam or 0th order, and the diffracted beam, or 1st order of diffraction. However, in the general case of holograms not operating in the volume regime, more diffraction orders emerge, and the incident energy is distributed among them. It was found in a previous study[8] that HOEs partly performing in the transition regime are more suitable for solar concentration than HOEs operating entirely in the volume regime. This is due to several factors, including the lower angular and chromatic selectivity and dispersion of HOEs in the transition regime. Based on the authors' previous findings, the present hologram is designed partly operating in the transition regime and is optimized under the solar spectrum illumination to maximize PV electrical output.

The design and associated model is performed with a ray-tracing algorithm with an energetic modeling based on Coupled Wave Theory [21] developed in MATLAB. Further description of the model can be found in [8,22,23]. The efficiency of each diffraction order L is given by the coupled differential equations

$$c'_{Lz}\frac{dA_L}{dz} + j\vartheta_L A_L + j\frac{\pi n_1}{\lambda}\left[A_{L+1}\left(\vec{p}_{L+1}\cdot\vec{p}_L\right) + A_{L-1}\left(\vec{p}_{L-1}\cdot\vec{p}_L\right)\right] = 0 \quad (1)$$

where c'_{Lz} is the directional cosine in z-direction of the L-diffraction order, A_L is the amplitude of the L-diffraction order wave, ϑ_L is the dephasing parameter of the L-order (that quantifies the deviation of the reconstruction conditions from the optimal ones of the recorded grating), n_1 the index modulation, λ the reconstruction (or illumination) wavelength and $\vec{p}_L$ the polarization vector of the L-order.

The coupled differential equations (1) are numerically solved for each diffraction order L, reconstruction wavelength and angle of incidence at each point of the HOE ("local grating" approach). Since sunlight is depolarized the coupled differential equations are solved for two perpendicular polarizations (one perpendicular to the recording plane and one contained in it, whose behavior is independent of one another) and the resulting efficiency of each one is averaged to obtain the final efficiency.

The optical concentration yielded by HOEs is different for each wavelength, so the concentrated spectral irradiance curve has a different shape from that of the incident solar spectrum. Since each wavelength produces a different current intensity response at the PV cell a global ratio of

the optical concentration is not an appropriate value to describe the system's concentration. Thus, the concentration of generated electrical current for each wavelength is defined instead, given by

$$CC_{current,\,\lambda} = \frac{I_{SC,\,HOEs,\,\lambda}}{I_{SC,\,no\,HOEs,\,\lambda}} \tag{2}$$

It is the ratio of the electrical current generated with the concentrating system over the one without the concentrating system for each wavelength [8]. The overall concentration of electrical current is calculated by integrating the electrical current,

$$CC_{current} = \frac{I_{SC,\,HOEs}}{I_{SC,\,no\,HOEs}} = \frac{\int I_{SC,\,HOEs,\,\lambda}\,d\lambda}{\int I_{SC,\,no\,HOEs,\,\lambda}\,d\lambda} \tag{3}$$

Sunlight on the Earth's surface is composed by direct and diffuse radiation. The reliability of this ray-tracing modeling is limited by the percentage of direct radiation, which depends on the clearness of the atmosphere at each location.

The *y*-distance between the two HOEs and the (*y*,*z*) position of the PV cell were optimized so that the PV cell would generate maximal current density averaged over the range $-60° < \phi < 60°$. It was chosen to optimize those parameters over a range of incidence angles in order to consider the variation of the Sun position in the sky throughout the day. Otherwise, if the optimization was carried out with $\phi = 0°$, at solar midday, the performance at that moment would be the best, but the overall performance of the day would be worse. The angular range $-60° < \phi < 60°$ corresponds to a time period of roughly 4 hours during the summer solstice, 9 hours during the winter solstice (the whole day) and 6.5 hours during the spring and autumn equinoxes for a location with 42°N latitude. The dimensions of the system resulting from the optimization and marked in Figure 1(a) are presented in Table 1. The geometrical concentration is equal to 11.5x, since the *y*-dimension of each HOE is 5.5 times larger than the one of the cell, as shown in Figure 1(a), and the *y*-separation between the lenses is half of the *y*-dimension of the PV cell. The theoretical current concentration $CC_{current}$ obtained with perpendicular incidence is 3.8, considering the standard AM1.5D spectrum as the incident one on the system.

Table 1. Geometry of the concentrating system depicted in figure 1(a).

y-separation HOEs (mm)	$y_{\text{cell center}}$ (mm)	$z_{\text{cell center}}$ (mm)
5.0	30.0	60.6

Since tracking is only carried out in the solar altitude movement direction, at solar noon the illumination of the HOEs will be perpendicular, but not during the rest of the day. The direction with no tracking (azimuth direction) is matched with the direction of low angular selectivity, as mentioned in the introduction, but if the angle of incidence is rather far away from $\phi = 0°$ then several factors (such as the decrease in efficiency, the increase in dispersion, total internal reflection, etc) will cause a remarkable overall loss in the generated current. In order to quantify this, the ϕ-acceptance is defined as the angular ϕ range for which the generated current is above 90% of the maximal. Simulations were carried out with incident angles in the range $0° \leq \phi \leq 60°$, with a step size of 2°, and the resulting normalized current concentration values are

presented in Figure 2(a). The behavior with negative values of ϕ is the same as with positive values, therefore the horizontal axis shows absolute values of ϕ.

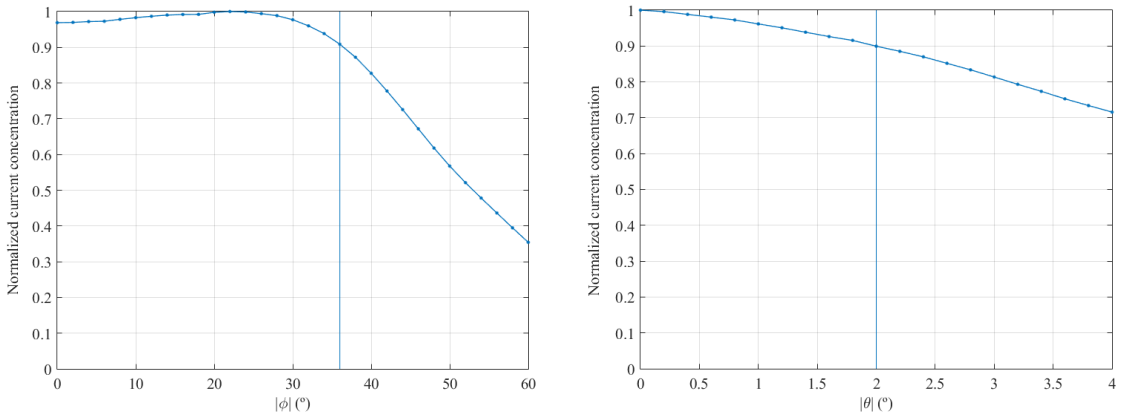

(a) (b)

Figure 2 (a) ϕ-acceptance, (b) θ-acceptance.

The optimal performance is not found with perpendicular incidence, but at ϕ=22º, with a current intensity approximately 3% higher, because the position of the PV cell and the distance between the lenses was optimized taking an angular range into account, as mentioned before. The ϕ-acceptance of this system is 72º (-36º< ϕ <36º), which corresponds to a time period of roughly 2 hours during the summer solstice, 5 hours during the winter solstice and 3.5 hours during the spring and autumn equinoxes for a location with 42°N latitude. The electrical current is higher with the concentrating system in place than without it for the whole considered angular range.

Even though tracking is carried out in the solar altitude direction, the tracking systems are not perfect and the tilt is corrected every certain amount of time. Simulations were also carried out in order to find out the θ-acceptance of the system when ϕ=0°, which gives an idea of how accurate the tracking must be. The results are presented in Figure 2(b), showing a θ-acceptance of 4º (-2º< θ <2º) while keeping ϕ=0°. This allows the use of less demanding, low-cost trackers, since their tracking errors are within that range [24]. Again, absolute values of θ are plotted because the system's behavior is symmetrical with θ (although not the behavior of a single HOE).

2.2. Fabrication of the holographic lenses

The recording parameters of the HOEs are presented in table 2 and marked in figure 3(a). They were all selected so that the HOE would provide maximal efficiency in the 1st diffracted order (shown in figure 3(b) with the paraxial approximation) when reconstructing with 800 nm rays at perpendicular incidence. The exposure dosage was such that provided index modulation at each point of the lens given by $n_1 = 2.469 \cdot 10^{-5} SF + 0.0126$, optimized with the experimental procedure explained in [8], where SF is the spatial frequency of each point expressed in lines/mm. Of course, if the illumination wavelength is different from 800 nm then the direction of the diffracted rays is different, as illustrated in figure 3(c), and their efficiency will be lower.

Table 2. Recording parameters of the cylindrical holographic lenses, marked in figure 3(a).

$\theta_{c,\,center}$ (º)	θ_p (º)	z_{focus} (mm)	$\lambda_{recording}$ (nm)	Exposure dosage (mJ/cm^2)
19.1	3.8	105	532	14

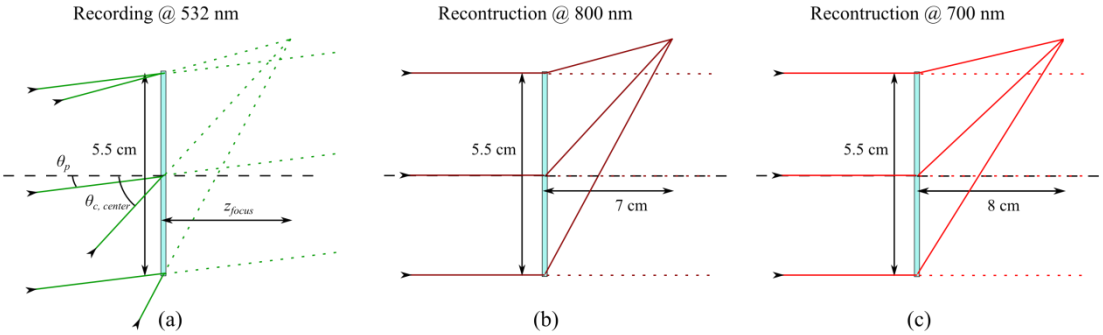

Figure 3. Recording scheme at 532 nm (a) and reconstruction with perpendicular incidence at 800 nm (b) and 700 nm (c) considering the paraxial approximation.

Holograms were recorded on Bayfol® HX 200, which is formed by a photopolymer layer and a cellulose triacetate substrate layer. Each Bayfol® HX 200 film sample was laminated on a glass slide by applying pressure with a soft roller, as indicated by the manufacturer [25] (with the photopolymer side of the sample in contact with the glass slide). A HOE was then recorded with the setup in figure 4 for the case of a cylindrical holographic lens. For the recording of holographic gratings that will be utilized in the temperature and the ageing studies (Sections 3.2 and 3.3), the cylindrical lens of the setup was removed. No post-processing was needed after the recording [10], only incoherent light photocuring, which was carried out as detailed in [11].

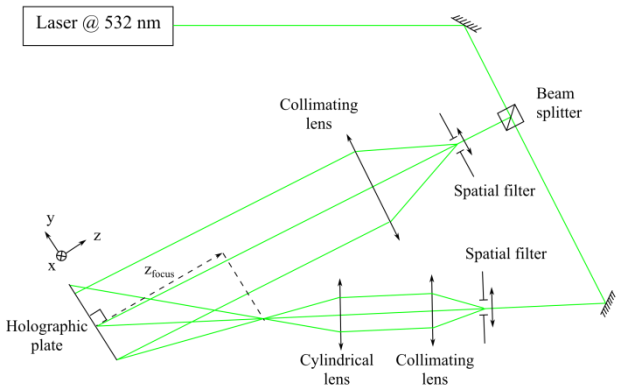

Figure 4: Recording setup of a cylindrical holographic lens [8].

3. Results and discussion

3.1. Sunlight illumination measurements

Experiments with the holographic concentrating system described in section 2 were carried out outdoors with solar illumination during the first week of August 2018 at the University of Lleida, Spain (41º37'N, 0º38'E).

A heliostat directed sun rays towards a testing unit. The holographic concentrating photovoltaic (CPV) system was placed inside in such a way that the incidence of the sun rays on the glass slides where the HOEs were laminated was perpendicular. A pyranometer (Kipp&Zonen CMP6) and a pyrheliometer (Kipp&Zonen CHP1) were fixed next to the CPV system and also

perpendicular to the incident sun rays to measure the global and direct irradiance, respectively. These data were sent to a Data Acquisition System DAQs (Campbell Sci. CR1000) and monitored throughout the whole experiment. The temperatures of the HOEs and the PV cell were measured by attaching T-type thermocouples to one of the corners of the HOE (shielded to prevent sunlight effects) and to the rear of the PV cell.

This experiment is divided in two parts: characterization of spectral irradiance and characterization of electrical performance. During the first part of the experiment the detector of a spectrometer (Ocean Optics USB4000, with a diameter of 3.9 mm and a sensitivity range from 350 to 1030 nm) was used to measure the incident solar spectrum. It is shown in figure 5 with a dot-dashed red line along with the standard spectrum normalized to the direct irradiance measured by the pyrheliometer during the experiment with a continuous blue line for comparison. Both curves include Fresnel reflection losses on the surface of the PV cell. It is noticed that the measured spectrum matches well the AM1.5D one.

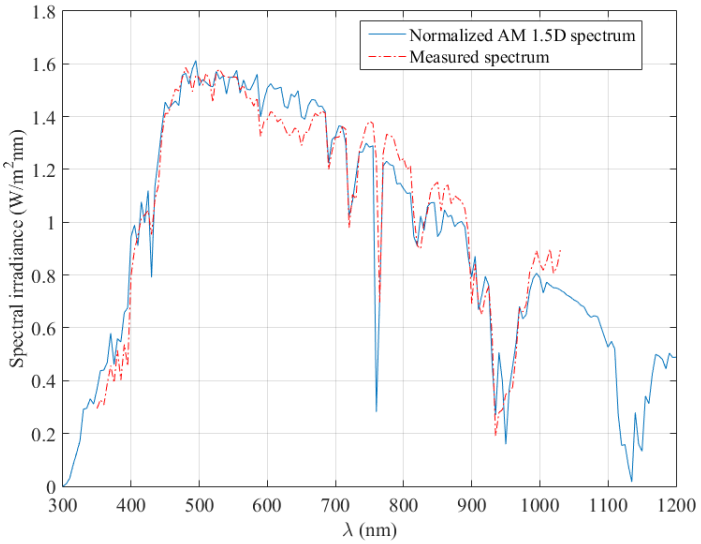

Figure 5: Standard solar spectrum AM1.5D normalized to the measured direct irradiance (continuous blue line), and measured spectrum (dot-dashed red line).

The detector was then placed at the center of the position where the PV cell would be located, characterizing the spectral irradiance produced by the holographic concentrator. The spectral irradiance measured at that location is plotted in figure 6(a) with markers. The noise at the limits of the measured data is due to the detector's sensitivity range. The spectral irradiance on the surface of the detector was modeled (using the measured solar spectrum as incident spectrum) and calculated as the addition of the contribution of the lower lens, the upper lens and the space between lenses and the resulting curve is plotted in figure 6(a) with a continuous line. Good agreement between the theoretical and experimental data is observed, with some differences between them, especially for wavelengths shorter than 700 nm. The peak centered on roughly 900 nm corresponds to rays of the 1st order of diffraction of both lenses, whereas the peak on approximately 450 nm, to the 2nd order of diffraction of both lenses as well.

This process was repeated for another position of the detector towards the edge of the PV cell's position and the results are plotted in figure 6(b), showing reasonably good agreement between the experimental and simulation data. The peaks at 800 nm and 400 nm correspond to the 1st and

2nd order of diffraction respectively of the lower lens. The peaks corresponding to the upper lens are not coincident in this case because the detector is not placed at a position symmetric with the HOEs.

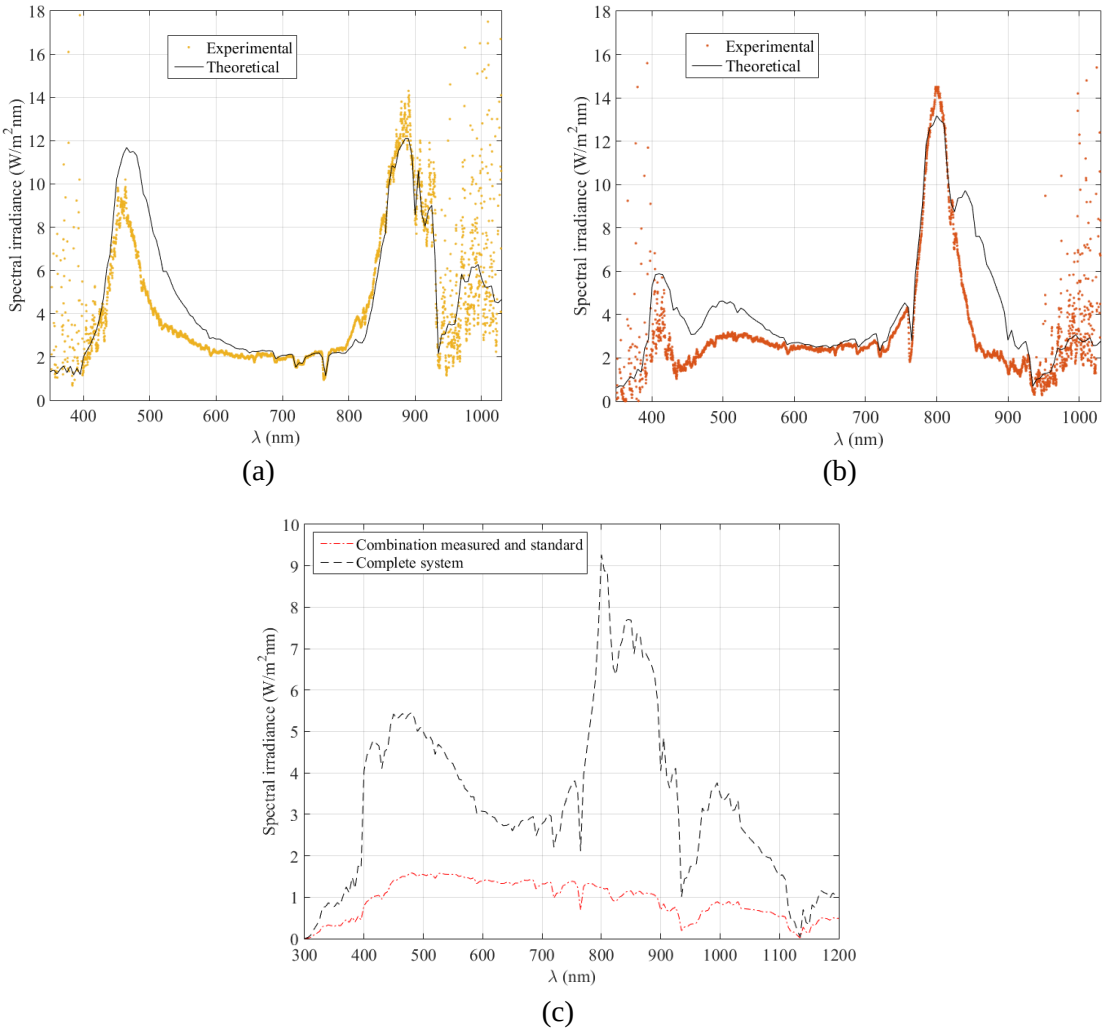

Figure 6: Experimental (markers) and simulated (continuous line) spectral irradiance received by the detector placed at the center of the position of the PV cell (a) and at a position towards its edge (b). Modelled spectrum received by the PV cell due to the concentrating system (dashed black line) and measured solar spectrum incident on the system, completed with standard spectrum (dot-dashed red line) (c).

These results confirm the validity of the modeling algorithm used in this study. The small differences observed between theoretical and experimental results are later addressed. The modelled spectral irradiance that would reach the whole surface of the PV cell is obtained by integration and it is illustrated in Figure 6 (c). In order to have data from 300 to 350 nm and from 1030 to 1200 nm, out of the spectrometer range, and extend the measured spectral range to the whole sensitivity range of the PV cell, the measured incident solar spectrum was completed with the standard AM1.5D spectrum. It can be seen that the obtained result is a partial combination of the two local spectra charted in Figs. 6 (a) and (b).

During the second part of the experiment a 1 cm x 1 cm PV cell was placed at the optimized position determined in section 2. The experiment was carried out with a PV cell of that size

instead of 1 cm x 5 cm (which are the design dimensions when using HOEs of 5 cm x 5 cm) for simplicity and avoidance of possible vignetting effects. This does not alter any result because there is no concentration in *x*-direction, so only a 1 cm-wide section in *x*-direction of the HOEs is considered instead of the whole surface. A picture of the system is shown in figure 7(a).

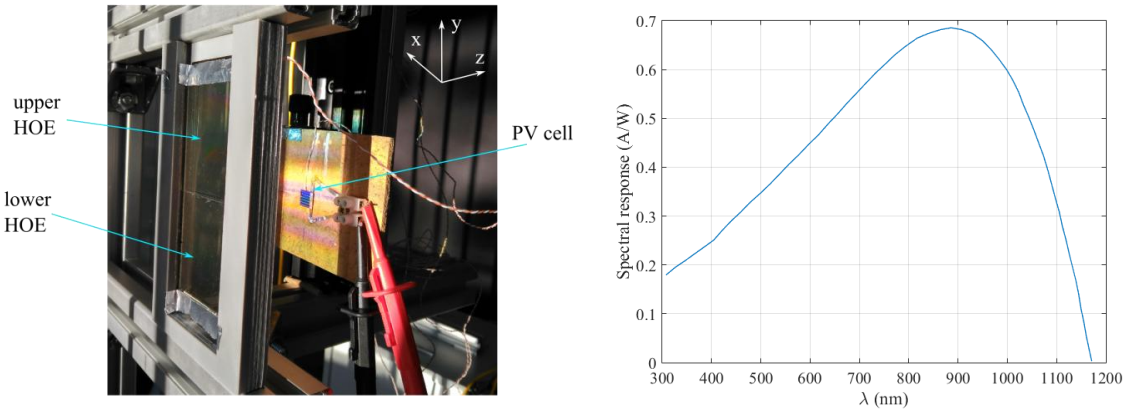

(a) (b)

Figure 7: (a) Picture of part of the setup for the measurement of the IV curves of the PV cell: two cylindrical holographic lenses on the left and a PV cell at the center of the picture; (b) Spectral response curve of the PV cell.

The PV cell was connected to a source meter (Keithley 2460) and a characteristic intensity-voltage (IV) curve without the HOEs was measured first, to determine the electrical performance of the PV cell under normal solar illumination. It is plotted in figure 8 with blue, non-filled markers. It should be noted that these values correspond to the contribution of both the direct and the diffuse irradiance that reaches the PV cell. Then the holographic concentrator was placed and the IV curve was measured again, presented in figure 8 as well, with red filled markers. The current generated at short-circuit conditions corresponding to the direct irradiance extracted from figure 8 is presented in table 3 for both cases.

The current density generated by the PV cell at short circuit conditions with and without the concentrating system was calculated from the spectral irradiance that the PV cell would receive (previously determined and shown in figure 6(c)) and the spectral response of the cell (figure 7(b)), obtaining the theoretical values in table 3. The calculated current density without the concentrating system (45 mA/cm^2) is lower than the measured one plotted in figure 8 (around 56 mA/cm^2) because in the simulations only the direct radiation is taken into account but in reality both direct and diffuse radiation contribute to the generation of electrical current. As mentioned in section 2, the ray-tracing algorithm developed to model HOEs is limited by the consideration of solely direct radiation.

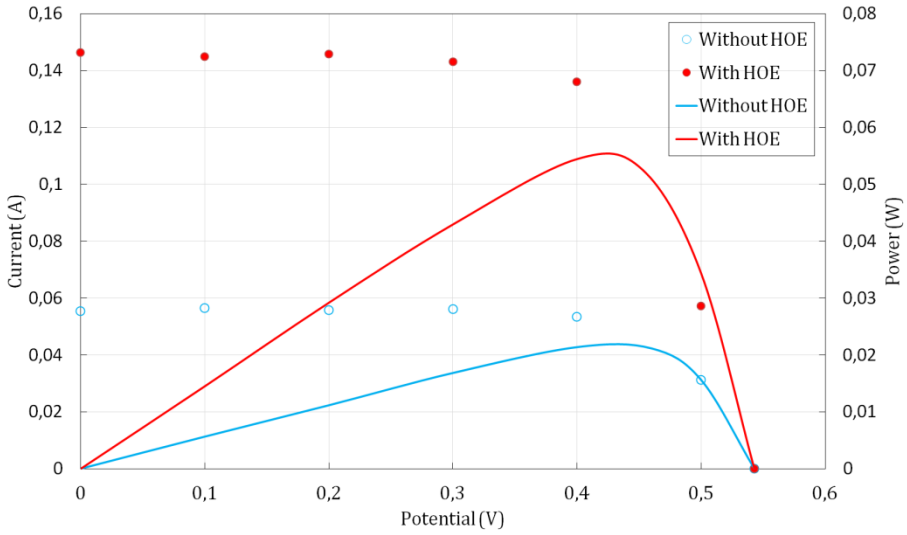

Figure 8: Experimental IV curves obtained with (red filled markers) and without the HOEs (blue non-filled markers) due to the direct and global irradiance, respectively. Calculated power-potential curves of the system with HOEs (continuous red line) and without (continuous blue line).

Table 3: Experimental and theoretical current density generated on the PV cell due to the direct irradiance.

	No concentrating elements	Holographic concentrating system	Current concentration
Experimental J_{sc} (mA/cm^2)	42	146	3.48
Theoretical J_{sc} (mA/cm^2)	45	172	3.81

The measured current density when the concentrating system is placed is 15% lower than the theoretical one. This difference can be attributed to some factors that may cause the performance of HOEs to worsen. One of them is the temperature of the HOEs during the experiment, which ranged between 37 and 49ºC, whereas the HOEs were designed to operate at room temperature. A study of the temperature dependence of HOEs recorded in Bayfol® HX 200 photopolymer is carried out in subsection 4.3 along with an estimation of the change in current.

In regard to the maximum power produced, the bare PV cell delivers 21.4 mW whereas the CPV system increases this value up to 55.2 mW. It can be appreciated that the power increases in a ratio of 2.58. This lower ratio related to the one obtained through the short-circuit current quotient is attributed to the fill factor. Fill factor of both curves takes almost the same value rounding 76% (74.5% -with concentrator - and 77.0% -without concentrator). On the other hand, as indicated previously, since the holographic concentrator only focus towards the PVs a certain bandwidth around the PV cell maximal spectral response, the temperature reached in both configurations does not differ substantially (4.94 ºC). Taking into account the temperature coefficient of crystalline silicon solar cells of around -0.3 %/ºC, the temperature difference registered would mean an open-circuit potential reduction of ~8 mV with respect to a value of 540 mW (see Fig. 8). Conversely, a logarithmic increase in the open-circuit potential is experienced due to the concentrated flux that counteracts the small potential decrease pointed

out. As a result, almost no variation over the open-circuit potential was measured, 544 mV for the bare PV and in 543 mV for the CPV.

Taking these considerations into account the concordance between theoretical and experimental results is reasonably good. Besides, in the next subsection a further analysis regarding temperature effects that could cause the small differences pointed out above is carried out. It is worth mentioning that the concentration ratio obtained for the present device is higher than that of other holographic concentrating systems found in the literature [3–6].

3.2. Study of the temperature dependence

An experiment was carried out to investigate the variation of the response of HOEs recorded in Bayfol® HX 200 at different temperatures. A slanted holographic grating was used for a more precise analysis. The advantage of using a slanted grating as opposed to an unslanted grating is that changes in the thickness of the photopolymer layer are more easily noticeable.

The HOE was illuminated perpendicularly with an unpolarized white light beam (Mikropack Halogen light source HL-2000) and the transmitted spectrum was measured with a spectrometer (Ocean Optics USB4000). The HOE was placed inside a plastic box with an open base and two holes to allow the incident beam to go through, as shown in the setup scheme in figure 9(a). An adjustable heater was placed underneath to increase the temperature in a controlled manner, with a honeycomb channels structure on top in order to avoid convection cycles. A T-type thermocouple was attached to the HOE to monitor the temperature with a Data Acquisition System DAQs (Campbell Sci. CR1000). The transmitted spectrum was measured at room temperature and while increasing it in steps of roughly 4°C up to 60°C, which is the highest temperature before Bayfol® HX 200's substrate may suffer deformation according to the manufacturer [25]. Then the temperature was decreased and measurements at the same temperature steps were taken.

When increasing the temperature, a shift of the transmitted spectrum towards shorter wavelengths, an increase of the minimum transmittance, i.e., a decrease of the efficiency of the 1st diffracted order, and a narrowing of the spectrum are noticed. The spectra measured when increasing the temperature did not match the ones measured when decreasing it (neither position nor transmittance of the minimum). The deviation from the initial central wavelength of the diffracted spectrum at different temperatures is presented in figure 9(b), showing maximal wavelength variations of 12 nm between the increase and decrease of the temperature. This is believed to be caused by a non-reversible thermal deformation of the photopolymer and/or the substrate layer. The experiment was repeated on different days and the same tendency was found.

In order to avoid this, another slanted holographic grating was encapsulated after the recording and bleaching. An optical adhesive, Norland NOA61 was extended on the substrate side of Bayfol® HX and another glass slide was placed on top. Some optical adhesive was also poured on all four glass borders in order to completely encapsulate the sample.

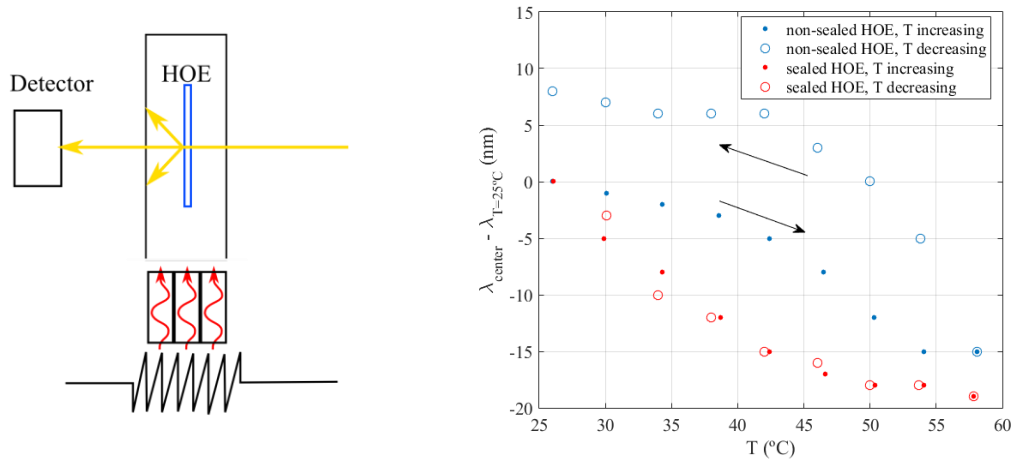

(a) (b)

Figure 9. (a) Experimental setup scheme for the temperature study; (b) Deviation from the central wavelength at room-temperature when varying the temperature for non-sealed (blue markers) and sealed (red markers) HOEs when increasing (filled markers) and decreasing (non-filled markers) the temperature.

The experiment was then carried out with the sealed holographic grating. Similar variations were observed when increasing the temperature, but in this case the measured spectra while decreasing it did match the spectra measured when increasing it, as shown in figure 9(b) as well, with maximal wavelength deviations of 2 nm between the increase and decrease of temperature. Therefore, sealing the HOE prevented irreversible thermal expansion from occurring at this stage. The measured spectra while increasing the temperature are presented in figure 10.

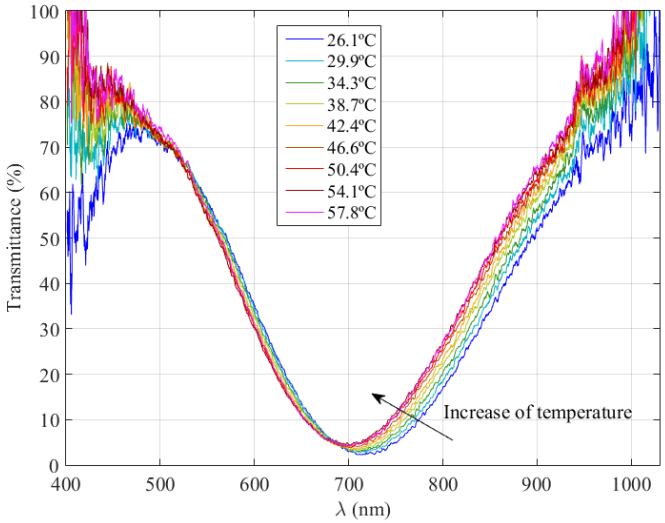

Figure 10: Transmission spectra when increasing the temperature.

The shift of the transmitted spectrum towards shorter wavelengths and simultaneous decrease in efficiency are consistent with two effects: thermal expansion of the photopolymer layer, which causes the slant of the grating to change increasing the spatial frequency, and a decrease of the index modulation. This was already suggested by other authors working with other photopolymer compositions (first effect by [14,15,17] and second effect by [14]).

Since the change in temperature causes a change in the response of the HOEs this should be included in the theoretical model as well in order to improve it so that the HOEs are optimized for the average operation temperature throughout the year, instead of at room temperature. However, the system is rather complex (a glass slide, photopolymer layer, substrate layer, optical adhesive and another glass slide, as well as optical adhesive on all four edges), and further research would be needed to obtain a mathematical model of all the thermal expansions and the resulting tensions among the different components and their effect on the refractive index, thickness and slant of the fringes.

A preliminary estimation resulting from this study was to consider a change of the slant of the fringes, compatible with an expansion of the photopolymer layer at high temperatures. The theoretical simulations of subsection 3.1 were repeated assuming a 1.3º tilt of the slant and the spectral irradiance that would be received by the detector is then plotted in figure 11(a) and (b). The agreement between experimental and theoretical data is better in this case than in figure 6.

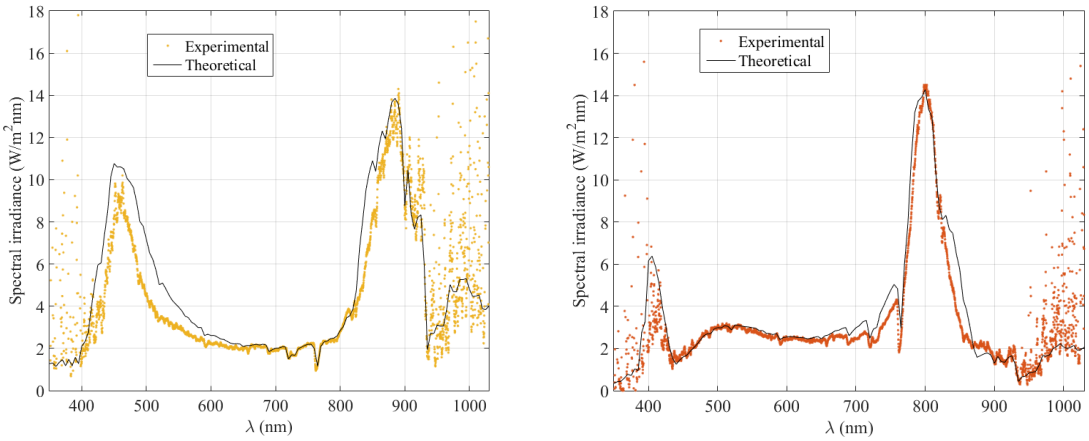

(a) (b)

Figure 11: Experimental (markers) and simulated (continuous line) spectral irradiance received by the detector placed at the center of the position of the PV cell (a) and at a position towards its edge (b).

The electrical current density obtained with this assumption is 155 mA/cm^2 and the current concentration, 3.43. These values are closer to the experimentally obtained ones in the previous subsection.

3.3. Study of ageing

A study of the possible degradation due to environmental conditions of HOEs recorded in Bayfol® HX photopolymer was carried out outdoors. Six cylindrical holographic lenses (named samples L1-L6), two samples of bleached unrecorded Bayfol® HX 200 (named samples B1 and B2), and one sample of the substrate of Bayfol® HX 200 (named sample S1 and obtained by mechanically removing the photopolymer layer) were used. Some of them were encapsulated and others simply laminated on glass, as specified in table 4.

Lenses L5 and L6 were kept in the laboratory as control samples. The rest of samples were placed on the South-oriented façade of a testing unit outdoors at the University of Lleida's facilities, Spain (41º37'N, 0º38'E), during summer 2018. Lenses L1 and L2 were simply placed

on a metallic structure, indicated in table 4 as "Testing unit outdoors". Samples L3, L4, B1, B2 and S1 were integrated as a box lid, in order to imitate the conditions of the solar shading louver where the concentrating system would be placed [7], which imply higher temperatures.

Table 4: Characteristics of holographic lenses and samples of bleached unrecorded Bayfol® HX 200 and substrate used during the degradation experiment.

Placement	Sample	Preparation	Outcome
Testing unit outdoors	L1	Laminated on glass	Deteriorated and detached
	L2	Encapsulated	No changes*
Testing unit outdoors, in box	L3	Laminated on glass	Deteriorated and detached
	L4	Encapsulated	No changes*
	B1	Laminated on glass	Detached
	B2	Encapsulated	No changes
	S1	Encapsulated	No changes
Laboratory	L5	Laminated on glass	No changes
	L6	Encapsulated	No changes*

* Indicates that a small increase of index modulation was observed after the sealing and encapsulation with the optical adhesive, but it stabilized after a few days.

Three T-type thermocouples were connected to a Data Acquisition Systems DAQs (Campbell Sci. CR1000) to monitor the temperature of the HOEs and samples placed inside the box, outside the box, and the ambient temperature. A pyranometer (Kipp&Zonen CMP6) was also placed on the façade to monitor the global irradiance. Temperature and irradiance data were stored every minute.

Figure 12 shows the recorded parameters on four summer days: two sunny days during a heat wave (figure 12(a)) and two cloudy days (figure 12(b)), to show different conditions. HOEs placed inside the box reached temperatures higher than 45ºC every day and higher than 50ºC during the hottest weeks of the summer. The maximal temperatures reached by the HOEs outside the box were approximately 5ºC lower, but remarkably higher than the air temperature during the central hours of the day. Since the whole setup was fixed at the South-oriented façade and tracking of the sun's movement was not carried out, the global irradiance recorded by the pyranometer was lower on days closer to the summer solstice than at the end of the summer. The "side lobes" of the global irradiance curve shown in figure 12(a) are due to reflections on the opposite building's windows, which reached the pyranometer at the start and end of the day around the summer solstice because of the large azimuth angles.

Every few days the samples were removed and characterized in the laboratory and then placed again on the testing unit. They were illuminated with an unpolarized white light source (Ocean Optics LS-1) and their spectral transmittance was measured with a spectrometer (Ocean Optics USB2000). They were also illuminated with an 800 nm laser (ThorLabs Laser Diode CPS808A, emitting 4.4 mW) while scanning the incidence angle and the transmitted beam was measured (with Newport Power Meter Model 1815-C with detector Model 818-SL, with an uncertainty of 5 μW). In the case of characterizing HOEs the first measurement provided their chromatic selectivity and the second one the angular selectivity. These measurements were carried out at three different points of the HOEs in order to study the behavior of different spatial frequencies and index modulations.

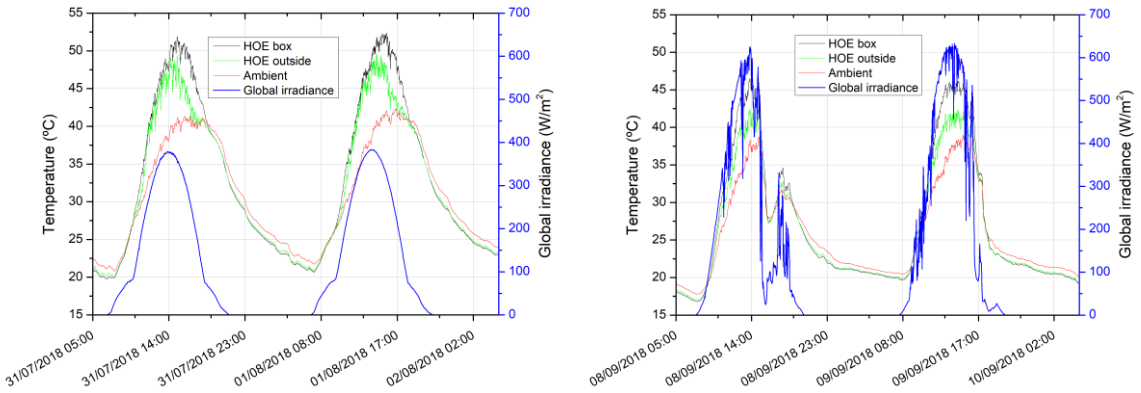

(a) (b)

Figure 12. Sample of the data recorded by the datalogger on four different days of the summer (two sunny days during a heat wave (a) and two cloudy days (b)): the temperature of HOEs inside the box (black line), outside the box (green line) and ambient temperature (red line), left *y*-axis, and the global irradiance measured in South-direction (blue line), right *y*-axis.

The following conclusions are extracted from the results of the measurements and summarized in table 4:

- Non-encapsulated lenses and samples detach from the glass where they are laminated and suffer deterioration due to the outdoor environmental conditions. Some of the angular selectivity measurements of L1 that illustrate the progression of the observed changes are represented in figure 13 (a). Two distinct stages are observed (which are not correlated with the first appearance of the detachment of the film from the glass slide). During the first phase (first 13 days of outdoor exposure) the position of the peaks does not change, and the efficiency of the 0 order decreases, while the efficiency of the 1st order increases. This corresponds to an increase in index modulation of approximately 11% from $n_1 = 0.0190$ to $n_1 = 0.0210$, while the grating vector $\vec{K}$ remains constant. Afterwards, a substantial shift in the position of the peaks occurs, meaning that the grating vector $\vec{K}$ has changed. These two behaviors were observed in the three points of the lens that were studied. They were also confirmed with the measurement of the chromatic selectivity. The first stage of this behavior is in agreement with the results of the temperature response of the non-sealed HOEs presented in section 3.3: after the heating and cooling cycle an increase of the index modulation of the grating is observed.
- Encapsulating Bayfol® HX photopolymer samples prevents them from detaching from the glass slide and preserves the material at least during the studied time period. Angular and chromatic selectivity measurements of the encapsulated HOEs L2, L4 and L6 only showed a slight difference between the first measurement (taken right after sealing) and the rest of the measurements. This corresponds to an increase in index modulation of approximately 2% and is associated with the optical adhesive, since no changes were observed in L5. Again, this behavior was confirmed in three different points of the sealed HOEs. Some representative angular selectivity curves of L4 are presented in figure 13 (b). Since the maximal efficiency of this HOE at 800 nm is approximately 100% this change is not perceptible at the peak itself but the change at the side lobes' efficiency is more noticeable. This corresponds to a change in index modulation from approximately $n_1 = 0.0231$ to $n_1 = 0.0236$. During the rest of the

experiment (37 days of exposure to outdoor ambient conditions) no further changes are observed. This is again in agreement with the results of the temperature response of the sealed HOEs presented in section 4.3: no changes are observed after the heating and cooling cycle.

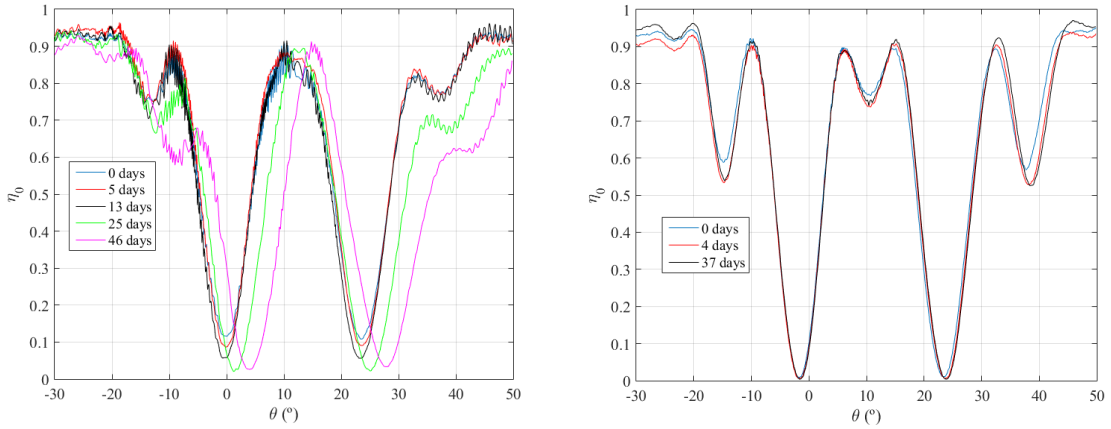

(a) (b)

Figure 13. Angular selectivity curves of a point of L1 (a) and a point of L4 (b) after several days of outdoor exposure.

It is concluded that although non-sealed HOEs recorded in Bayfol® HX 200 photopolymer are not suitable for outdoor applications, sealed HOEs have remained stable during the course of the study (except from the slight initial variation of index modulation) and seem to be appropriate for solar concentration applications. Although the results have been positive during the summer, when outdoor conditions are more extreme in this location, it is still necessary to continue this study for a longer period of time to verify the suitability of this material.

This does not contradict the results presented by Chrysler et al. [20], who also tested encapsulated gratings and samples of Bayfol® HX. They reported substantial changes both in the gratings (detected by measuring angular and chromatic selectivity) and in the material itself (by measuring the spectral transmittance of unrecorded samples) already after 4 weeks of outdoor exposure. Two factors are believed to cause this difference between the two studies. First, the recording material used by Chrysler et al was Bayfol® HX 102, which was substituted by Covestro Deutschland AG by Bayfol® HX 200 (the one used in the present study), so they are not exactly the same material and may have different properties. The substrate layer is indeed different: the substrate in Bayfol® HX 102 is made of polycarbonate [26], whereas the substrate in Bayfol® HX 200 is made of triacetate cellulose [25]. Second, Chrysler et al directly attached the HOEs to the PV cells, which may reach high temperatures (up to 80ºC [20]), while the manufacturer states that temperatures higher than 60ºC can lead to deformation of the substrate [26]. In the configuration considered in this study the HOEs are separated a certain distance from the PV cell, thus the temperature that they reach in our case would not be so heavily intensified by the temperature of the PV cell. The samples placed in the testing unit as a lid of a box (see table 4) imitate the conditions that the HOEs would experience when integrated as part of a double pane solar louver shading system, with higher temperatures than the ones of the samples outside the box (but still below 55ºC on the hottest days).

4. Conclusions

A holographic concentrating system comprising two cylindrical holographic lenses and a mono-crystalline Si PV cell was designed and optimized for building façade-integration on the blinds of a solar shading louver, which track the solar altitude movement. No tracking is needed in the azimuth direction, since the acceptance in that direction is 72º. The system was theoretically modeled with a ray-tracing algorithm based on Coupled Wave Theory, providing a current density value of 172 mA/cm^2 and current concentration ratio of 3.81 at perpendicular incidence. The HOEs, partially operating in the transition regime, were recorded on Bayfol® HX photopolymer and the system was assembled. Outdoor measurements of the diffracted spectrum with solar illumination yielded a current density value of 146 mA/cm^2 and a current concentration ratio of 3.48, somewhat lower than the simulated results but validating the theoretical model. The maximum power produced is increased in a ratio of 2.58, with a fill factor of 76% for both cases.

The difference between the theoretical and experimental current values is believed to be caused by a change in the holograms' internal structure due to the outdoor temperature, higher than room temperature, at which the HOEs had been designed and characterized. The temperature effect on HOEs recorded in Bayfol® HX photopolymer was studied, showing indeed variations when increasing the temperature, which are reversible if the HOE is encapsulated. Assuming a 1.3º tilt of the fringes in the holograms due to the outdoor temperature, better fits of the diffracted spectral curves and a theoretical current density of 155 mA/cm^2 and current concentration ratio of 3.43 were obtained, closer to the experimental ones.

A preliminary study of another important aspect for solar concentration, ageing of HOEs recorded in Bayfol® HX photopolymer, was carried out, showing that the recording material is suitable for solar concentration applications as long as the samples are sealed and encapsulated.

Future work is needed in order to analyze more thoroughly these two features: a model of the temperature response (which could allow the optimization of HOEs for higher temperatures) and an ageing study over a longer period of time.

Acknowledgements

The authors would like to thank Dr. Enrico Orselli (Covestro Deutschland AG) for supplying the recording photopolymer material. This research has been supported by the Spanish Ministerio de Economía y Competitividad (grants ENE2016-81040-R and FIS2015-71933-REDT), the Diputación General de Aragón-Fondo Social Europeo (TOL research group, E44_17R), the Universidad de Zaragoza (UZ2018-CIE-07) and the Generalitat de Catalunya (grants 2017 SGR 1276 and 2017FI_B2_00127).

References:

[1] Lamnatou C, Chemisana D. Concentrating solar systems: Life Cycle Assessment (LCA) and environmental issues. Renew Sustain Energy Rev 2017;78:916–32. doi:10.1016/j.rser.2017.04.065.

[2] Collados MV, Chemisana D, Atencia J. Holographic solar energy systems: The role of

optical elements. Renew Sustain Energy Rev 2016;59:130–40. doi:10.1016/j.rser.2015.12.260.

[3] Chemisana D, Collados MV, Quintanilla M, Atencia J. Holographic lenses for building integrated concentrating photovoltaics. Appl Energy 2013;110:227–35. doi:10.1016/j.apenergy.2013.04.049.

[4] Akbari H, Naydenova I, Ahmed H, McCormack S, Martin S. Development and testing of low spatial frequency holographic concentrator elements for collection of solar energy. Sol Energy 2017;155:103–9. doi:10.1016/j.solener.2017.04.067.

[5] Sreebha AB, Suresh S, Sreekala CO, Mahadevan Pillai VP. Volume holographic gratings in acrylamide-based photopolymer to provide selective light as an added input for improving the performance of dye-sensitized solar cells. Curr Sci 2018;114:2267–72. doi:10.18520/cs/v114/i11/2267-2272.

[6] Aswathy G, Rajesh CS, Sreejith MS, Vijayakumar KP, Sudha Kartha C. Designing photovoltaic concentrators using holographic lens recorded in nickel ion doped photopolymer material. Sol Energy 2018;163:70–7. doi:10.1016/j.solener.2018.01.017.

[7] Marín-Sáez J, Chemisana D, Moreno Á, Riverola A, Atencia J, Collados M-V. Energy Simulation of a Holographic PVT Concentrating System for Building Integration Applications. Energies 2016;9:577. doi:10.3390/en9080577.

[8] Marín-Sáez J, Atencia J, Chemisana D, Collados M-V. Full modeling and experimental validation of cylindrical holographic lenses recorded in Bayfol HX photopolymer and partly operating in the transition regime for solar concentration. Opt Express 2018;26:A398. doi:10.1364/OE.26.00A398.

[9] Marín-Sáez J, Collados MV, Chemisana D, Atencia J. Energy analysis of holographic lenses for solar concentration. In: Hrabovský M, Sheridan JT, Fimia A, editors. Proc. SPIE, 2017, p. 1023317. doi:10.1117/12.2265816.

[10] Jurbergs D, Bruder F-K, Deuber F, Facke T, Hagen R, Hönel D, et al. New recording materials for the holographic industry. Proc SPIE 2009;7233:72330K–72330K–10. doi:10.1117/12.809579.

[11] Marín-Sáez J, Atencia J, Chemisana D, Collados M-V. Characterization of volume holographic optical elements recorded in Bayfol HX photopolymer for solar photovoltaic applications. Opt Express 2016;24:A720. doi:10.1364/OE.24.00A720.

[12] Bruder F-K, Fäcke T, Grote F, Hagen R, Hönel D, Koch E, et al. Performance optimization in mass production of volume holographic optical elements (vHOEs) using Bayfol HX photopolymer film. In: Hrabovský M, Sheridan JT, Fimia A, editors. Proc. SPIE, 2017, p. 102330G. doi:10.1117/12.2265022.

[13] Cody D, Gul S, Mikulchyk T, Irfan M, Kharchenko A, Goldyn K, et al. Self-processing photopolymer materials for versatile design and fabrication of holographic sensors and interactive holograms. Appl Opt 2018;57:E173. doi:10.1364/AO.57.00E173.

[14] Liu H, Yu D, Zhou K, Wang S, Luo S, Wang W, et al. Improvement of temperature-induced spectrum characterization in a holographic sensor based on N-isopropylacrylamide photopolymer hydrogel. Appl Opt 2017;56:9006. doi:10.1364/AO.56.009006.

[15] Tomita Y, Nakamura T, Tago A. Improved thermal stability of volume holograms recorded in nanoparticle–polymer composite films. Opt Lett 2008;33:1750. doi:10.1364/OL.33.001750.

[16] Russo JM, Kostuk RK. Temperature dependence properties of holographic gratings in phenanthrenquinone doped poly(methyl methacrylate) photopolymers. Appl Opt 2007;46:7494. doi:10.1364/AO.46.007494.

[17] Dhar L, Schnoes MG, Wysocki TL, Bair H, Schilling M, Boyd C. Temperature-induced changes in photopolymer volume holograms. Appl Phys Lett 1998;73:1337–9. doi:10.1063/1.122375.

[18] Zanutta A, Bianco A, Insausti M, Garzón F. Volume phase holographic gratings for astronomy based on solid photopolymers. In: Navarro R, Cunningham CR, Barto AA, editors. Proc. SPIE, 2014, p. 91515X. doi:10.1117/12.2055743.

[19] Felder TC, Stevenson SH, O'Connor PJ, Yohannan, Jr. RM. Environmental Performance of Photopolymer Holographic Optical Elements. In: Benton SA, Stevenson SH, Trout TJ, editors. Proc. SPIE, 2000, p. 314–23. doi:10.1117/12.380011.

[20] Chrysler BD, Ayala Pelaez S, Wu Y, Vorndran SD, Kostuk RK. Environmental stability study of holographic solar spectrum splitting materials. In: Sulima O V., Conibeer G, editors. Proc. SPIE, 2016, p. 99370N. doi:10.1117/12.2237071.

[21] Syms R. Practical Volume Holography. Oxford University Press; 1990.

[22] Marín-Sáez J, Collados MV, Atencia J, Chemisana D. Optical and Energetic Performance of Volume Holographic Optical Elements for Solar Energy Applications. Adv. Energy Res., NOVA; 2017.

[23] Bañares-Palacios P, Álvarez-Álvarez S, Marín-Sáez J, Collados M-V, Chemisana D, Atencia J. Broadband behavior of transmission volume holographic optical elements for solar concentration. Opt Express 2015;23:A671–81. doi:10.1364/OE.23.00A671.

[24] Sallaberry F, Pujol R, Garcia de Jalón A. Direct Tracking Error Estimation on a 1-Axis Solar Tracker. Proc. EuroSun 2014 Conf., Freiburg, Germany: International Solar Energy Society; 2015, p. 1–8. doi:10.18086/eurosun.2014.16.20.

[25] Covestro Deutschland AG. Bayfol HX200 Datasheet. 2016.

[26] MaterialScience B. Bayfol HX102 Datasheet. 2014.

Chapter 8

Global discussion of the results

During the course of this PhD thesis both experimental and theoretical work has been simultaneously carried out. Modeling the behavior of HOEs and the whole concentrating system has allowed their understanding and the achievement of an optimized design. On the other hand, the realization of experimental work has validated the simulations and provided additional information.

Regarding the specific objectives of the thesis that were presented in chapter 1:

- *Experimental characterization of the recording material, Bayfol HX photopolymer.*

Three different photopolymeric materials provided by Covestro AG (formerly Bayer MaterialScience) have been tested: Bayfol HX 104, HX TP, and HX 200, depending on their availability. Although all of them had similar compositions, a complete characterization of each material was needed due to the existing differences.

Testing was initially carried out with the unrecorded material in order to determine the best bleaching procedure. Although this type of photopolymer is self-developing and does not need thermal or chemical post-processing, photocuring is nevertheless required after the recording to stop the photopolymerization process and remove the remaining dye (sensitive to the visible spectral range). In solar applications, this is of great importance because the existence of remaining dye in the photopolymer implies the absorption of light, which will cause an increase of the temperature of the material and will also involve a loss of efficiency because that radiation will not be diffracted toward the receiver. The optimum bleaching procedure was presented in chapter 5 and consisted of two steps: a 25 minutes exposure to a white light LED source, emitting in the visible range, with a dosage of 240 J/cm^2, and then a 35 minutes exposure to a metal halide lamp (Philips HPA 400 SD) that emits visible and UV light, with a dosage of 60 J/cm^2.

Bayfol HX film is formed by two layers: the active photopolymer layer and a substrate layer (polycarbonate, polyamide and cellulose triacetate in the case of Bayfol HX 104, HX TP and HX 200, respectively). The thickness and refractive index of each layer was provided by the manufacturer, except for the refractive index of Bayfol HX TP, which was measured with an Abbe refractometer. Some of the known magnitudes (refractive index of Bayfol HX 104 and thickness of Bayfol HX 104 and TP) were also measured and showed agreement with the provided values. These results are also presented in chapter 5.

Unslanted and slanted holographic transmission gratings were then recorded on all three materials. For a fixed spatial frequency of the grating (that is, fixed angle between the recording beams), the variation of the recording intensity on the holographic plate and the variation of the recording time, and therefore, the recording exposure, allows the achievement of different index modulation values. The gratings were characterized by measuring the efficiency of all existing

diffraction orders when illuminating at the reconstruction stage with different wavelengths and angles of incidence. The angular selectivity was obtained by measuring the efficiency of the transmitted order for a scan of incidence angles, and the chromatic selectivity, for a broadband continuous spectrum.

The agreement of the angular selectivity curves with the theoretically predicted ones ensured that no noticeable change in the thickness, and therefore, in the grating structure for the case of slanted holographic gratings, occurred. This is a great advantage of Bayfol HX photopolymer as opposed to other recording materials (as the commercial dichromated gelatin used in chapter 3, where swelling was observed due to the wet post-processing).

The characterization of the recorded gratings enables the determination of the refractive index modulation of each grating; thus the needed recording parameters (intensity and exposure) to obtain the desired index modulation for each spatial frequency. High enough modulation values were reached to achieve 100% efficiencies at 800 nm under certain conditions.

In addition, the dependency of the index modulation with the spatial frequency was empirically deduced for given recording intensity and exposure values: $n_1 = 1.31 \cdot 10^{-5} SF + 0.0114$ (for Bayfol HX TP with recording intensity 1.4 mW/cm^2 and exposure dosage 16 mJ/cm^2) and $n_1 = 2.47 \cdot 10^{-5} SF + 0.0126$ (for Bayfol HX 200 with recording intensity 0.18 mW/cm^2 and exposure dosage 14 mJ/cm^2), where the spatial frequency SF is expressed in lines/mm. This was necessary for the later modeling of holographic lenses. The first set of recording conditions provided 100% efficiency at the center of lens A in chapter 6, performing in the volume regime, when reconstructing with 800 nm and perpendicular incidence; whereas the second one provided maximal efficiency at the center of the lens studied in chapter 7, partly performing in the transition regime, also when reconstructing with 800 nm and perpendicular incidence.

All this is presented in chapters 5, 6 and 7, showing the suitability of Bayfol HX photopolymer as a recording material for HOEs for solar concentration applications.

- *Ray-tracing modeling of HOEs and holographic concentrating systems.*

A ray-tracing algorithm that describes the geometric and energetic performance of HOEs has been developed and is described below.

The wavelength and incidence angle of the recording beams determine the direction and modulus of the grating vector $\vec{K}$, and therefore, the spatial frequency that is obtained. The holographic grating is completely defined with the grating vector and the index modulation, assuming the material's properties (thickness and refractive index) are known.

A local analysis of holographic gratings is performed for any wavelength and angle of incidence at the reconstruction stage. The directional cosines in each medium and the impact coordinates at each interface are calculated, using vectorial Snell law. The number of existing diffraction orders (if a HOE is operating in the transition regime or if the general case, HOEs operating in any regime, is considered) and their propagation direction are determined with the beta-value closure and Ewald sphere.

The efficiency of volume holograms is calculated with Kogelnik's analytical solution of the coupled wave equations, which was used in chapters 3, 4 and 5. However, if the general case, HOEs operating in any regime, is considered, the coupled differential equations are solved numerically, as carried out in chapters 6 and 7.

When dealing with holographic lenses recorded on photopolymers, the grating vector (and the index modulation as well, as shown in chapter 6) that is recorded is different at each point of the HOE due to the different angle between the recording beams along the holographic plate. A "local grating" treatment is carried out: each point of the holographic lens is independently analyzed as a distinct grating. Its index modulation is determined with the linear dependency with the spatial frequency that was empirically obtained.

A bunch of rays is launched onto the entrance pupil (the HOE) for a given angle of incidence and they are propagated through the whole system. The energy contribution of each one is considered on the receiver's plane.

In any case, the illumination conditions can be chosen to simulate the characterization of HOEs in the laboratory (with a linearly polarized laser, for example, so N-polarization of the coupled equations is considered) or solar illumination (using the standard solar spectrum and assigning each wavelength of the reconstruction rays its corresponding energy, and averaging the results of polarizations N and M to obtain unpolarized light).

Fresnel reflection losses are calculated at each interface and the possibility of total internal reflection is also addressed, in order to obtain results that are as accurate as possible.

With all these considerations, the local and spectral distribution of energy on the receiver's plane is calculated. Then the spectral irradiance received across the PV cell (in the case of chapters 3, 6 and 7) or the PV cell and the thermal absorber (in the case of the system of chapter 4) has been determined. Additionally, the irradiance received by a detector of any shape and size (such as the spectrometer detector used in chapter 7) can be estimated for easier comparison with experimental measurements.

The integration of the irradiance on the PV cell surface has allowed the calculation of the current generated in short-cut conditions and the electrical power, considering the parameters of commercial cells as in chapter 4.

Scans of the incidence direction have also been included in the performed local and global analyses. In chapter 4, the incidence direction and spectrum every minute of the day for a whole year have been considered for two specific locations.

Most of the results of the performed simulations have been compared with experimental results of holographic gratings and lenses, showing good agreement between them and validating the developed ray-tracing algorithm, as illustrated in chapters 3, 5, 6 and 7.

Furthermore, the algorithm has enabled the optimization of the design of HOEs attending any requirements.

- *Analysis of the transition regime and its convenience for solar concentration.*

The intermediate regime between the volume (or Bragg) regime and the thin (or Raman-Nath) regime has been studied. For this scope, simulations of HOEs partly operating in the transition regime under certain conditions have been carried out and validated with measurements of recorded HOEs.

A characteristic feature of HOEs operating in this regime is the existence of several diffraction orders, and the available energy at the entrance of the HOE must be distributed among them. However, the global analysis of the studied HOEs in chapter 6 revealed that the loss of efficiency in the first diffracted order is overly counterbalanced by the lower angular and chromatic selectivities and dispersion. These effects are very beneficial for concentrating photovoltaics, as explained throughout the whole thesis. Lower dispersion implies that a broader spectral range reaches the PV cell. Lower chromatic and angular selectivity imply that a deviation from the optimal reconstruction conditions (which is inevitable with a broad spectrum, such as the solar spectrum, and a holographic lens recorded with a wavelength different from the optimized one) does not cause a decrease in efficiency as abrupt as with volume holograms.

All of this results in a broader spectrum received by the PV cell, as shown in the comparative study of different lenses in chapter 6. The FWHM of the spectral irradiance curve corresponding to the first diffraction order was highest (approximately 130 nm) when using the holographic lens partly performing in the transition regime for the target wavelength, whereas it is lowest (80 nm) with the lens entirely operating in the volume regime for that wavelength. The resulting electrical current concentration value due to one lens also increased: it was 1.36 with the former lens and 0.61 with the latter.

Therefore, HOEs partially operating in the transition regime are very promising for concentrating photovoltaics due to the advantages they offer compared to volume HOEs.

- *Design of the holographic concentrating system.*

A holographic concentrating system that comprises two cylindrical holographic lenses and a mono-crystalline Si PV cell has been designed. The HOEs are identical and are placed symmetrically to enhance the concentration ratio when the incidence is perpendicular. The geometrical concentration of this device is 11x. This system was proposed in chapter 4 with an initial design of the HOEs (and a hybrid PV-thermal receiver) and then it has been optimized in chapter 6 with the aim of maximizing the electrical current concentration, i.e. the ratio of current density obtained by the considered PV cell with the holographic concentrating system over the one obtained without it. Due to the dependency of the performance of HOEs with the reconstruction wavelength, the spectral irradiance curve received by the PV cell is not proportional to the incident solar spectrum; thus the optical concentration differs for each wavelength and it is not a suitable parameter to be maximized.

Several parameters of the design of HOEs have been optimized in chapter 6. It has been found that the recording wavelength does not have a significant effect on the generated current (as long as the design ensures the same reconstruction behavior under the paraxial approximation). The analysis of three different holographic lenses, each one including a different range of spatial frequencies (and index modulation dependent on it), revealed that the one with lower spatial

frequencies was more convenient for concentrating photovoltaics. The reason was that part of the HOE performed in the transition regime, which presents very advantageous characteristics for this application, as previously stated.

The dimensions of the system (the separation between the holographic lenses and the distance between the HOEs plane and the receiver's plane) were also optimized in chapters 4, 6 and 7.

As mentioned in chapter 7, the theoretical current concentration value given there, 3.77 with perpendicular incidence, is higher than any other ratio found in the literature. This proves that a correct optimization of the design of the system is essential to obtain a system that yields positive results.

- *Construction of the holographic concentrating system*

A holographic concentrating system formed by two cylindrical holographic lenses and a mono-crystalline Si PV cell has been assembled, as shown in chapter 7. The HOEs have been recorded on Bayfol HX 200 with the parameters resulting from the optimization procedure and characterized in the laboratory. Maximal efficiency (97%) is obtained at the center of each lens when reconstructing with 800 nm and perpendicular incidence. It is lower than 100% because under those reconstruction conditions, this lens operates in the transition regime. At that point, the FWHM of the first diffracted order's spectral curve when reconstructing with white light and perpendicular incidence is approximately 500 nm centered around 800 nm, which is rather broad in comparison with volume HOEs. For example, the FWHM of the first diffracted order's spectral curve corresponding to the center of the lens entirely performing in the volume regime studied in chapter 6 (referred to as lens A), was roughly 160 nm.

- *Experimental analysis of the holographic concentrating system.*

The constructed holographic concentrating system was also experimentally characterized outdoors with sunlight illumination in chapter 7. The spectral irradiance on the receiver's plane was measured with a detector, showing good agreement with the theoretically obtained curves.

IV curves of the PV cell were measured as well, obtaining a short-cut current density value of 146 mA/cm^2 and a current concentration value of 3.48, lower than the theoretical ones. This difference is attributed to the temperature of operation of the HOEs during the experiment, quite elevated in comparison to room temperature. Nevertheless, as mentioned above, this value is higher than any other experimental or theoretical current concentration found in the literature. The maximal generated electrical power was 55.2 mW, which was 2.58 times higher than the one without the holographic concentrator. This concentration ratio is lower than the current concentration because of the fill factor of the PV cell, approximately 76%. The slight variation of the open-circuit voltage with and without the concentrator (543 mV and 544 mV, respectively) reveals that the temperature of the PV cell was not greatly enhanced. This is one of the advantages of using a holographic concentrator, as opposed to a refractive or reflective concentrator.

The experimental results validate the theoretical simulations and prove that the developed ray-tracing algorithm is a reliable tool, not only for local characterization of HOEs, but also for the global performance description of holographic systems.

- *Evaluation of the material's response under real conditions.*

Chapter 7 also dealt with another aspect that has to be considered in solar applications: the outdoor conditions that the HOEs are exposed to (such as temperature variations, solar radiation, etc).

Measurements of the chromatic selectivity of HOEs recorded on Bayfol HX 200 have been taken while being subjected to a temperature variation cycle ranging from room temperature to 58ºC. Irreversible thermal expansions that cause a change in the grating structure occur unless the HOE is encapsulated. Introducing a 1.3º tilt of the fringes of the cylindrical holographic lenses of the concentrating system in the theoretical simulations, quantifying the effect of the high temperature at which the experiment was carried out, provided a better fit of the calculated spectral irradiance received by the detector to the experimental results. The obtained current density and concentration values (155 mA/cm^2 and 3.43, respectively) were also closer to the measured ones.

A study of ageing of HOEs recorded on Bayfol HX 200 due to environmental conditions was also realized out during summer 2018. The HOEs were placed under sunlight radiation and reached temperatures higher than 45ºC every day and higher than 50ºC during the hottest weeks of the summer. The reached lowest temperatures ranged between 13 and 23ºC. Permanent damage was noticed in non-encapsulated samples, whereas no changes were observed in the encapsulated ones during the course of the study (37 days of summer), stating again the need of sealing HOEs for this application.

8.1. Future work

Although the proposed objectives of the thesis have been addressed, some future studies related to the results that have been presented could be carried out.

The design of the HOEs could be further optimized attending other criteria. For example, the dimensions of the cylindrical holographic lenses, the thickness of the photopolymer layer or the index modulation could be adjusted. Stacking [1] or multiplexing could also be considered, in order to increase the chromatic or the angular acceptance range of the system. In order to do this, HOEs with higher spatial frequencies would need to be used to avoid cross-coupling.

The developed ray-tracing algorithm allows the analysis of different kinds of holographic system configurations, so they could be explored with the aim of increasing the current density on the PV cell or obtaining other advantages, e.g. suppressing the need of tracking in both directions, placing two or more receivers instead of only one PV cell…

Modeling of the thermal response of HOEs recorded on Bayfol HX photopolymer should be carried out in order to completely describe the system's performance under real operation temperatures. This would allow the optimization of the HOEs for higher temperatures,

corresponding to the central hours of the day, when the solar irradiance is maximal, so that the maximal theoretical current concentration, 3.77, could be reached.

An ageing study during a longer period of time should also be carried out to complete the assessment of the suitability of Bayfol HX photopolymer as recording material for holographic concentrating photovoltaic systems.

The temperature of the PV cell of the system could also be studied in the future, specifically in comparison with a refractive concentrating system, to evaluate the effect of using HOEs to help to reduce the temperature.

References

1. J. Marín-Sáez, S. Keshri, J. Atencia, D. Chemisana, I. Naydenova, K. Murphy, M. V. Collados, S. Garner and S. Martin, "Stacked Holographic Optical Elements for solar concentration," contribution presented in Photonics Ireland Conference, 3-5 September 2018 in Cork, Ireland.

Chapter 9

Conclusions

The main conclusions deduced from the development of this PhD are the following:

- A reliable ray-tracing algorithm has been developed in Matlab, based on the beta-value closure for the geometric analysis and Coupled Wave Theory for the energetic analysis. It describes the performance of HOEs (either holographic gratings or lenses) with a local and global analysis (the latter based on the local grating treatment) for any reconstruction conditions. The energetic analysis can be carried out either with Kogelnik's analytical solution for volume holograms or by numerically solving the coupled differential equations for any operation regime (Bragg, transition, or Raman-Nath). The simulations are validated with the characterization of the experimentally recorded HOEs.
- HOEs partially operating in the transition regime have been considered, revealing that they are highly advantageous for concentrating photovoltaics and in general for broadband reconstruction spectrum applications. The maximal efficiencies they provide are somewhat lower, but that is overly counterbalanced by the significant decrease in angular and chromatic selectivity and chromatic dispersion. This results in enhanced spectral irradiance curves of the spectrum received by the PV cell (still contained in its spectral response range); thus, higher current density values.
- Bayfol HX photopolymer is a suitable photosensitive material for the recording of HOEs for solar concentration applications, providing the necessary dynamic range of index modulation and stability after the recording (no shrinkage and therefore, no detuning has been detected). A linear dependency of the index modulation with the spatial frequency of recorded HOEs with the same intensity and exposure dosage has been found, experimentally verified and included in the simulation algorithm.
- A holographic concentrating photovoltaic system has been designed and optimized. It comprises two cylindrical holographic lenses recorded on Bayfol HX photopolymer and partly operating in the transition regime and a mono-crystalline Si PV cell, with a geometrical concentration of 11x.
- The holographic concentrating system has been constructed (with HOEs recorded on Bayfol HX photopolymer) and characterized. Measurements have been taken both in the laboratory with controlled conditions and outdoors with solar illumination, validating the global system simulations. A current concentration of 3.48 has been obtained, in agreement with the calculated value.
- Regarding the response of the recording material under outdoor conditions, it has been determined that encapsulation is necessary in order to prevent irreversible thermal expansions with the daily variations of the temperature. The performance of the holographic concentrating system is affected by these variations, which can be included in the simulation algorithm as a change in the grating structure.